A study of the cone-pressuremeter test in sand

by

Fernando Schnaid

A thesis submitted for the
Degree of Doctor of Philosophy
at the University of Oxford

Magdalen College

Trinity Term, 1990

ABSTRACT

A STUDY OF THE CONE-PRESSUREMETER TEST IN SAND

A thesis submitted for the degree of Doctor of Philosophy

F. Schnaid
Magdalen College, Oxford
Trinity Term, 1990

The cone-pressuremeter is a new site investigation device which incorporates a pressuremeter behind a standard cone penetrometer tip. This dissertation is concerned with an understanding of the new device, and in particular the establishment of a detailed procedure to allow the test to be used to determine the engineering properties of cohesionless soils.

A series of 34 calibration tests was performed, in which three cone-pressuremeter prototypes with cross-sectional areas corresponding to 15 cm^2, 10 cm^2 and 5 cm^2 were used. The tests were carried out on cylindrical samples, enclosed in a chamber 1.0 m in diameter and 1.5 m in height. Stress controlled boundaries allowed independent control of vertical and horizontal stress in the range of 50 kPa to 300 kPa. A raining deposition technique was used to produce three sand densities, corresponding to loose, medium and dense samples.

A programme of calibration was designed to provide an examination of the influence of relative density, stress level and stress ratio on cone-pressuremeter test data. Soil properties were related to the values of the limit pressure obtained from the pressuremeter test and the cone resistance values from the cone test. Empirical relationships were proposed for deriving density, friction angle and horizontal stress.

Cone-pressuremeter tests were used for assessing directly the shear stiffness of the soil. A series of calibrations was needed to obtain the best possible estimation of the unload-reload shear modulus. Interpretation of the measured modulus was made by examining appropriate methods of calculating the modulus from unload-reload loops. Strain arm measurements and volume change measurements were compared. A method has been presented that allows the shear modulus values to be correlated to the relevant stress level acting around the pressuremeter during the test. The values of shear modulus obtained with the cone-pressuremeter were compatible with those obtained from the self-boring pressuremeter.

An assessment of chamber size effects yielded useful information regarding the applicability of test correlations derived from calibration chambers to field problems. An additional study identified experimentally the influence of length to diameter ratio on the pressuremeter pressure-expansion curve.

O investigator,
do not flatter yourself that you know
the things nature performs for herself,
but rejoice in knowing the purpose
of those things designed by your own mind

Leonardo da Vinci (1452-1519)

To
Bia and
Gabriela

Contents

ACKNOWLEDGEMENTS

The author was supported by the Brazilian government, through the combined sponsorship of Federal University of Rio Grande do Sul, UFRGS, and Coordenacao de Aperfeicoamento de Pessoal de Nivel Superior, CAPES.

The work reported in this thesis was supported by the Science and Engineering Research Council, UK. The cone-pressuremeter was supplied by Fugro-McClelland Ltd. and Cambridge Insitu.

A research programme is never an individual work and it is with gratitude that I wish to acknowledge the collaboration in this study of many friends and colleagues.

Firstly, I would like to thank my supervisor, Dr. Guy Houlsby, for his advice and guidance. His engineering judgement has been most valuable for the development of this work. I wish to extend my thanks to the other members of the Soil Mechanics group, in particular Professor Peter Wroth whose personality and experience creates a stimulating working environment.

I am indebted to Mr. Bob Earl and Mr. Chris Donnelly for their technical expertise and assistance in the construction of the laboratory equipment.

Special thanks are due to my graduate colleagues for their ideas and advice, and particularly for their friendship. I would like to mention Hai Sui Yu for stimulating discussions and his readiness to help. Working in this group has been most enjoyable.

On a more personal level, I would like to mention Bia, for sharing the most important moments of my life, for her friendship, her deep understanding and her involvement during difficult times.

NOTATION

A,B,C,D	experimental coefficients
B	Skempton's pore pressure parameter
CU	coefficient of uniformity
D	diameter of the expanding section of the pressuremeter probe
D_{50}	medium grain size
G	shear modulus
G^a	shear modulus calculated from strain arms measurements
G^c	corrected shear modulus
G_{ap}	apices shear modulus
G_i	initial shear modulus
G_{max}	shear modulus measured from shear wave velocities and resonant column tests
G_{ru}	reload-unload shear modulus
G_{sq}	least square fit shear modulus
G_{ur}	unload-reload shear modulus
G^v	shear modulus calculated from volume change measurements
I_r	relative dilatancy index
I_s	stiffness index
K	modulus number
K	ratio of chamber boundary stresses (σ'_h/σ'_v)
K	$(1+\sin\phi'_{cv})/(1-\sin\phi'_{cv})$
K_o	coefficient of lateral earth pressure at rest ($\sigma'_{ho}/\sigma'_{vo}$)
K_1,K_2	hyperbola parameters
L	length of the expanding section of the pressuremeter probe

N	$(1-\sin\phi')/(1+\sin\phi')$
Q	experimental coefficient
R	radius of pressuremeter probe
R_c	pressuremeter radius during contraction
R_e	pressuremeter radius at maximum expansion
R_d	relative density
R_o	initial pressuremeter radius
S	$\sin\phi'_{ps}$
S	(1-N)/(n+1)
s'	$(\sigma'_1+\sigma'_3)/2=(\sigma'_r+\sigma'_\theta)/2$
S_d	slope of unloading curve in logarithmic plot
a,b,c,	hyperbola parameters
e	voids ratio
n	$(1-\sin\nu)/(1+\sin\nu)$
n	modulus exponent
p'	mean effective stress
	$(\sigma'_1+\sigma'_2+\sigma'_3)/3=(\sigma'_r+\sigma'_z+\sigma'_\theta)/3$
p_a	atmospheric pressure
p_o	initial mean effective stress
q	deviator stress $(\sigma_1-\sigma_3)/2$
q_c	cone tip resistance
q_t	total cone tip resistance
r	radius to a point in soil
r_1	radius to the elastic-plastic boundary during expansion of cavity
r_2	radius to the elastic-plastic boundary during contraction of cavity
s_u	undrained shear strength

v	specific volume
v_λ	ordinate on a plot v against ln p'
γ	bulk modulus
γ_{UR}	shear strain amplitude
γ_w	density of water
ε	pressuremeter cavity strain
ε_c	pressuremeter cavity strain at start of unloading
ε_{max}	pressuremeter cavity strain at maximum expansion
ν	angle of dilation
σ_h	horizontal total stress
σ_v	vertical total stress
σ'_h	horizontal effective stress
σ'_v	vertical effective stress
$\sigma_1, \sigma_2, \sigma_3$	principal total stresses
$\sigma'_1, \sigma'_2, \sigma'_3$	principal effective stresses
$\sigma_\theta, \sigma_r, \sigma_z$	hoop, radial and axial stress
σ_{ro}	lift-off pressure
ϕ'	angle of internal friction
ϕ'_{cv}	critical state angle of friction
ϕ'_{ds}	direct shear angle of friction
ϕ'_p	peak angle of friction in triaxial compression

ϕ'_{ps}	plane strain angle of friction
ψ	state parameter
ψ	pressuremeter cavity pressure
ψ_c	pressuremeter cavity pressure at start of unloading
ψ_f	hyperbola parameter
ψ_l	pressuremeter limit pressure
Γ	ordinate of critical state line

CHAPTER 1

INTRODUCTION

1.1 - Introduction

A reliable assessment of stress-strain-time and strength characteristics of natural deposits, as well as evaluation of *in situ* stresses, is essential to engineering geotechnical design. Assessment of these quantities can be obtained from pressuremeter tests, which were introduced over 30 years ago by Louis Ménard in France[1]. Since its creation, various types of pressuremeter devices have been developed and are currently in use. The major difference between categories of pressuremeter tests lies in the method of installation of the instrument into the ground. Devices can be installed in preformed holes, self-bored into the ground, pushed into the ground from the base of boreholes and, most recently, driven into the soil behind a standard cone penetrometer tip.

The Ménard-type pressuremeter (MPT) was designed to be lowered into a preformed hole with the purpose of applying uniform pressure to the walls of the borehole by means of a flexible membrane. Characteristics of the ground can be deduced from measurements of the pressure and the change in volume of the expanding membrane. Soil disturbance, due to drilling and stress relief around the hole, usually slightly oversized, is significant, and interpretation of pressuremeter tests is made in an empirical fashion. A general review of empirical relationships to enable data from a Ménard-pressuremeter test to be interpreted is given by Baguelin *et al* (1978). Foundation design rules are based on direct correlations between the limit pressure and pressuremeter modulus and the actual performance of foundations. Assessment of fundamental soil parameters is made by comparison with other *in situ* tests or laboratory tests.

---

1 *The concept of lowering a ballon-like device down a borehole to measure soil properties in situ dates from the early 1930's as described by Kogler (reported by Baguelin et al, 1978)*

In order to minimize soil disturbance caused by insertion, self-boring pressuremeters (SBP) were developed simultaneously in France (Baguelin *et al*, 1972) and England (Wroth and Hughes, 1973). The self-boring technique consists essentially of pushing the instrument into the ground, while the soil displaced by a sharp cutting shoe is broken into pieces by a rotary cutter, then flushed to the surface (Clarke, 1981; Wroth, 1982). The SBP appears to be an ideal device for determining *in situ* the engineering properties of soils, as it offers the possibility of inserting a testing device into the ground with minimal initial disturbance. Soil parameters can be evaluated analytically using cavity expansion theories, and in addition, an assessment of the *in situ* horizontal stress can be made. Unfortunately, the ideal of minimal disturbance is, on occasion, difficult to achieve, and although high quality pressuremeter data can be obtained, disturbance associated with the self-boring technique in sand is described as important (Windle, 1976; Fahey, 1980; Clarke, 1981; Wroth, 1982, 1984; Fahey and Randolph, 1984).

To overcome some of the installation problems, the push-in pressuremeter was developed (Henderson *et al*, 1979, Reid *et al*, 1982). The instrument has the form of a hollow 78 mm cylinder, similar to a sampling tube. The soil displaced by the probe during insertion enters the body of the instrument, reducing the disturbance to the surrounding soil. However, as the instrument is a thick-walled cylinder, some disturbance inevitably occurs. Most of the experience with the push-in pressuremeter is limited to comparison with pre-bored and self-boring pressuremeter tests.

The cone-pressuremeter is a new site investigation device conceived as an alternative approach to pressuremeter testing, in which a pressuremeter probe is incorporated behind a standard 15 cm^2 cone penetrometer (Withers *et al*, 1986). The pressuremeter is of the same diameter as the cone, and is mounted on the penetrometer shaft a short distance behind the cone tip. It is a more complex device to interpret than the self-boring pressuremeter because the pressuremeter test is carried out in soil which has been displaced by the penetration of the

cone. Nevertheless, the new device has certain advantages, principally in the simplicity and economy of its installation. It is recognized that the cone penetration causes disturbance of the soil, but it is considered that this disturbance should be repeatable, and that the pressuremeter test should therefore be amenable to rational analysis.

Insertion of the pressuremeter into the ground is performed as part of the cone penetration test operation. The new *in situ* testing device can then combine some of the merits of the pressuremeter test with the operational convenience of the cone penetrometer test. A continuous cone profile is obtained during penetration. Friction ratio measurements, as well as pore pressures in the case of the piezocone, provide detailed and representative soil profiles. Absolute values of cone resistance are used to estimate strength parameters on either sands or clays. The pressuremeter in turn enables soil stiffness and strength parameters to be assessed. Measured stress-strain properties can be directly correlated to cone resistance profile at any depth, in order to obtain as broad a view as possible of the geotechnical properties of the soil.

1.2 - Methods of interpretation

The principal attraction of the pressuremeter is that, in theory, the boundary conditions are well defined, as are the stress and strain conditions in the soil surrounding the pressuremeter probe. Therefore the pressuremeter permits a more rigorous theoretical analysis than many *in situ* tests. Such analysis is based on the expansion of a cylindrical cavity.

The cone-pressuremeter has the disadvantage that the pressuremeter test is carried out in soil which has already been displaced by the penetration of the cone. If fundamental soil parameters need to be derived from the test, an analysis which accounts for the installation process is required, as is an understanding of the complete stress path followed by the soil during expansion and contraction of the pressuremeter probe.

Cone penetration, however, poses considerable difficulties in analysis, and bearing capacity or cavity expansion models do not accurately describe the distribution of stresses around the instrument penetrating sand. For clay, Baligh (1986) presented a theoretical explanation of the mechanism of cone penetration, showing a narrow zone adjacent to the instrument in which high levels of shear strain and shear stress were developed due to intense deformation (compression under the tip and shear along the shaft). Outside this zone less intense plastic deformation exists and far beyond only elastic deformation occurs. It is possible that an equivalent narrow zone of intense plastic deformation is also developed around a cone penetrating sand deposits.

Experimental measurements recorded during cone penetration can enhance the understanding of the stress distribution that exists on the boundary of the cone as it is pushed into sand, as discussed by Hughes and Robertson (1985). The magnitude of measured tip cone resistance q_c is always much higher than the magnitude of the measured friction stress along the sleeve of the cone (and therefore the effective lateral stress, estimated from the measured friction stress and predicted friction angle). It is then suggested that very high stresses are developed when the cone tip passes an element in sand, followed by a remarkable decrease of stresses when the sand element comes in contact with the sleeve. Hughes and Robertson (1985) also suggested that an arch of high mean effective stress may be generated at some radius from the instrument, probably between the elastic and intense deformation zones, which limits the lateral stresses that can act on the body of the cone. The stresses that exist in the soil surrounding the instrument before the expansion of the pressuremeter membrane will be non-uniform and indeterminate, as both the radial and hoop stresses will vary with radius in a complex manner.

An alternative interpretation of the mechanism of installation of the pressuremeter can be provided by cylindrical cavity expansion and contraction theory. By expanding a cavity from 0 to R_o, R_o being the initial radius of the cone-pressuremeter probe, the radial stress experiences

a large increase and becomes the major principal stress. A stress relief postulated by Hughes and Robertson (1985) could be understood as a small cavity contraction, which occurs after the cone tip passes an element in sand. Under this condition the radial stress decreases while the hoop stress increases, which would explain the reduction on the magnitude of the lateral stress observed on the instrument shaft.

The above discussion illustrates some important aspects of the interpretation of the cone-pressuremeter test. The initial part of the pressure-expansion curve is unlikely to be suitable for analysis using simple cavity expansion theories, due to the complex pattern of mean effective stress at different radii. At sufficiently large strains the difficulties in modelling the disturbance caused by the installation process may be overcome. This implies that the maximum previous mean effective yield stress of every soil element inside the elastic plastic boundary would need to be exceeded, with the radial effective stress re-established as the major principal stress.

The stress path during a cone-pressuremeter test has been schematically described by Withers *et al* (1989), and it is reproduced here to clarify some aspects of the present discussion. Test stages are presented in Figure 1.1, in which the position of several material points are traced. Point A is initially on the centre-line of the pressuremeter before installation (Figure 1.1.I). After installation A is at the radius R_o, the pressuremeter radius (Figure 1.1.II). The pressuremeter is then expanded to its maximum dimension so that point A is at R_e (Figure 1.1.III), and finally Figure (1.1.IV) shows A at R_c ($R_o < R_c < R_e$) during the contraction phase. Point E lies at the elastic plastic boundary at maximum expansion (Figure 1.1.III) and is then at r_1. Point C lies within the plastic region at the stage of maximum pressuremeter expansion, and lies on the elastic-plastic boundary at radius r_2 when the pressuremeter has been contracted to dimension R_c. The position of the stress points for different materials is also shown in Figure 1.1, in which radial stress σ_r is plotted against hoop stress σ_θ. During penetration, as

the cone tip moves to the vicinity of A, the stress path moves towards the failure line. When the tip reaches A the maximum stress state is reached, and a dramatically reduction of stress is observed when the tip moves further into the soil (Figure 1.1.II).

At the pressuremeter's maximum expansion (Figure 1.1.III) the material between A and E has been deformed plastically, whilst the material outside E is still elastic. After contraction (Figure 1.1.IV) the material outside E ($r > r_1$) has remained elastic, that between C and E ($r_2 > r > r_1$) has been loaded plastically and unloaded elastically, and the material between A and C ($R_c > r > r_2$) has been loaded plastically and then unloaded sufficiently so that reverse plasticity has occurred.

The analysis of the pressuremeter test was first developed assuming that the sand behaves as an isotropic linear elastic material until yield occurs when the Mohr-Coulomb condition is satisfied; shearing of the soil takes place under conditions of zero volume change (Gibson and Anderson, 1961). Several attempts have subsequently been made to include more realistic volume change laws in the solution of the expansion of a cylindrical cavity (e.g. Ladanyi, 1972; Vesic, 1972; Hughes *et al*, 1977).

A refinement of the analysis presented by Gibson and Anderson (1961) has been developed by Hughes *et al* (1977), in which, after yielding, the material flows plastically at a fixed angle of dilation. This assumption is supported by a large number of plane strain shear tests on Leighton Buzzard sand in the simple shear apparatus (Stroud, 1971). From this small strain loading analysis the shear modulus, angle of friction and angle of dilation can be determined. For a Mohr-Coulomb material it has been shown that the gradient in a plot of logarithm of the effective radial stress (i.e effective cavity pressure ψ) against logarithm of the strain ε is controlled by the soil strength parameters. The slope S in this plot is given by the expression:

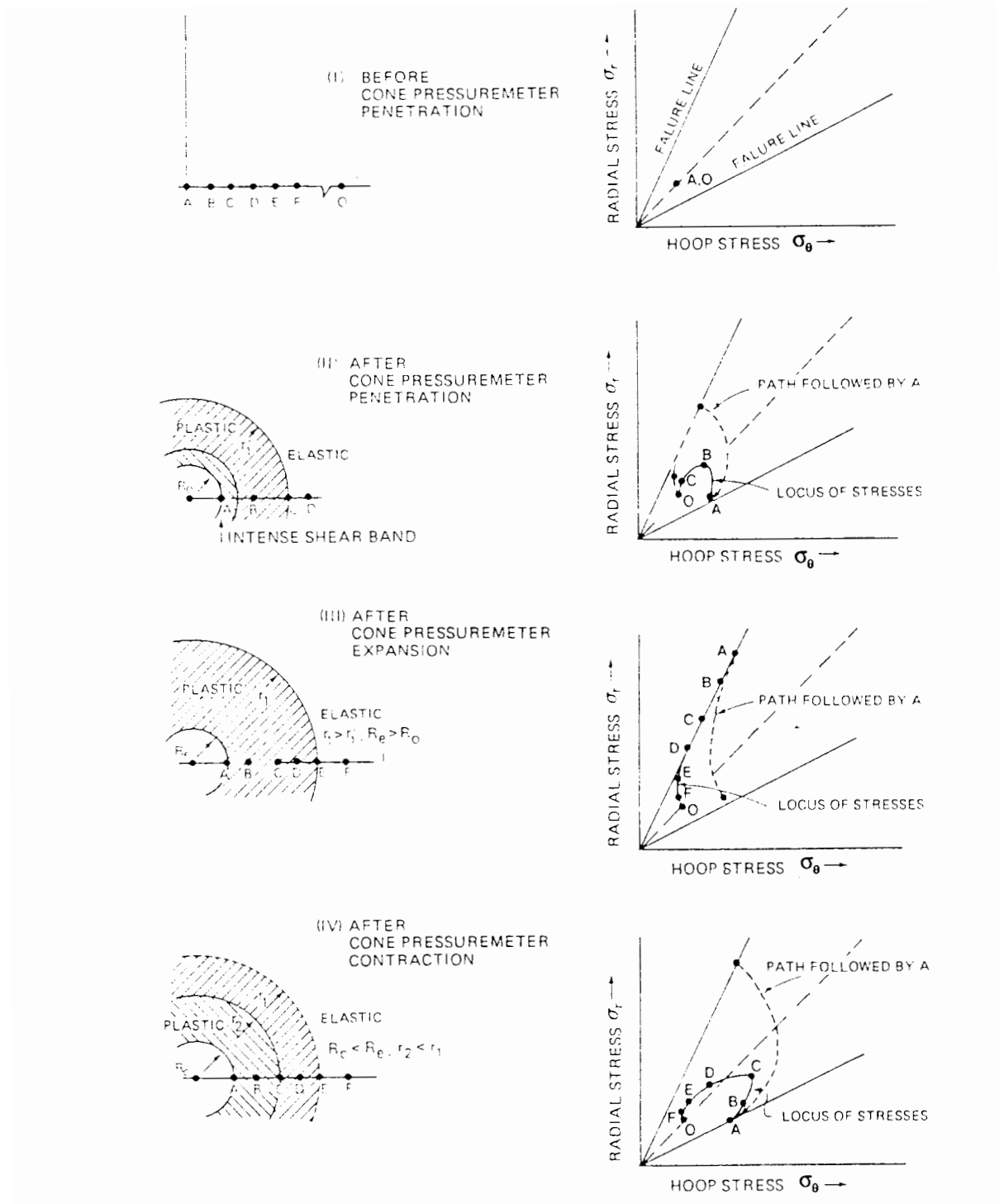

Figure 1.1 - Elastic-plastic boundaries and stress path during cone-pressuremeter test (after Withers *et al*, 1989)

$$S = \frac{1-N}{n+1} \qquad [1.1]$$

where $N = (1 - \sin\phi')/(1 + \sin\phi')$ and $n = (1 - \sin\nu)/(1 + \sin\nu)$, in which ϕ' and ν denote the plane strain friction angle and dilation angle respectively. Equation [1.1] has the inconvenience of being related to both friction and dilation angles. This problem can be eliminated by introducing a relationship between these angles using Rowe's stress dilatancy relationship (Rowe, 1962), expressed as:

$$\frac{1+\sin\phi'}{1-\sin\phi'} = \frac{1+\sin\phi'_{cv}}{1-\sin\phi'_{cv}} \frac{1+\sin\nu}{1-\sin\nu} \qquad [1.2]$$

where ϕ'_{cv} is the critical state friction angle, which can be easily determined by additional laboratory tests. By combining equations [1.1] and [1.2] and denoting $K = (1 + \sin\phi'_{cv})/(1 - \sin\phi'_{cv})$ the friction angle can be expressed as:

$$\sin\phi' = \frac{(K+1)S}{(K-1)S+2} \qquad [1.3]$$

Houlsby *et al* (1986) developed a small strain analysis of the unloading section of the test, using the same model as that used by Hughes *et al* (1977). It was suggested that there are certain advantages in making use of the pressure contraction data, as it is less sensitive to any initial disturbance caused by the installation of the pressuremeter. In this analysis it is necessary to account for the fact that the unloading takes place from an initially non-homogeneous stress state, which has been set up by the preceding expansion phase. Houlsby and Yu (1990) have shown that the unloading slope S_d in a plot of $-\ln\psi$ against $\ln(\varepsilon_{max} - \varepsilon)$ is primarily controlled

by the soil strength parameters and to a small extent by soil stiffness, where ψ is the cavity pressure and ε_{max} and ε denote the maximum and current cavity strain. The slope S_d can then be expressed as:

$$S_d = -\frac{N - \frac{1}{N}}{N + \frac{1}{N}} \qquad [1.4]$$

As for equation [1.1], S_d is related to both friction and dilation angles. By making use of equation [1.2] its possible to eliminate the dilation angle of equation [1.4], introducing instead the critical friction angle ϕ'_{cv}. The result is:

$$\sin\phi' = \left(\sin\phi'_{cv} + \frac{1+\sin\phi'_{cv}}{S_d}\right) - \sqrt{\left(\sin\phi'_{cv} + \frac{1+\sin\phi'_{cv}}{S_d}\right)^2 - 1} \qquad [1.5]$$

The suitability of small strain expansion-compression analysis for the interpretation of the cone-pressuremeter test can be examined using the methods described above. The examination consists of:

a) plotting pressure-expansion curves on logarithmic scales to investigate if asymptotes to straight lines can be found at high expansions. The slope of the fitting lines can then be converted to friction angles using equation [1.3], and compared to values obtained from other *in situ* tests or laboratory tests.

b) plotting pressure contraction curves also on logarithmic scales to convert the slope of asymptotic lines to friction angles using equation [1.5], and comparing these values with data obtained from other *in situ* tests or laboratory tests.

Data from calibration chamber tests performed with a prototype cone-pressuremeter were analysed using the above procedures. Results are discussed in Chapter 5 of this dissertation. A similar approach has been applied by Withers *et al* (1989) to cone-pressuremeter field tests. Equations for cylindrical cavity derived by Hughes *et al* (1977) and Houlsby *et al* (1986) were restated in a more general form to accommodate expansion and contraction of a spherical cavity. It is suggested that at large membrane expansions the boundary between the elastically and plastically deforming regions may have a diameter comparable to the length of the pressuremeter. Therefore, as the membrane expands, it is possible that the deforming pattern may progress from cylindrical to spherical shape. Spherical cavity expansion may then be more appropriate for modelling the later part of the expansion stage, as well as the contraction stage.

Analysis of the cone-pressuremeter test using cylindrical model of expansion produced unacceptably high values of friction angle when compared with the values obtained from the self-boring pressuremeter and the cone resistances[1]. The spherical model of expansion produced unacceptably low values of friction angles, when compared with values obtained from the conventional cylindrical model of self-boring pressuremeter expansion and the cone resistances. Unrealistic values of friction angles were obtained from the contraction curves. It is suggested that small strain analysis is not applicable to cone-pressuremeter tests due to the increasing importance of creep deformations at large pressuremeter strains and pressures.

The shear modulus measured from small unload-reload loops from cone-pressuremeter tests in sand produced values in good agreement with those from self-boring pressuremeters (Hughes and Robertson, 1985; Withers *et al*, 1989). This finding is consistent with previous experience on different pressuremeter probes, which suggests that the shear modulus obtained from

---

1 *The Robertson and Campanella (1983) correlation between peak friction angle and cone resistance was used in these comparisons.*

unload-reload loops is almost completely independent of the initial disturbance due to the installation process (Hughes, 1982; Wroth, 1982; Powell and Uglow, 1985; Houlsby and Withers, 1988; Lacasse *et al*, 1990; Powell, 1990).

Preliminary field data, as well as calibration chamber tests, have indicated that small strain cavity expansion and contraction analysis are not suitable to determine strength parameters from cone-pressuremeter tests. More realistic models of large strain analysis need to be developed, before derivation of reliable friction and dilation angles from loading and unloading curves becomes possible.

A new analysis of the cone-pressuremeter test in clay was presented by Houlsby and Withers (1988) and was applied successfully to derive values of undrained strength and shear modulus. The initial installation of the cone-pressuremeter was modelled theoretically as the expansion of a cylindrical cavity within the soil. The expansion phase of the pressuremeter test was modelled as a continuous expansion of the same cylindrical cavity, and the contraction phase as a cylindrical contraction. It is recognized that this modelling of installation is an approximate solution, as the penetration of a 60° cone tip follows a different stress path to that of cavity expansion. However, this approach is supported by theoretical work (Teh, 1987; Teh and Houlsby, 1988), in which the stress distribution far behind the cone tip predicted from Baligh's stress path method (Baligh, 1986) was found to be similar to the distribution created by the expansion of a cylindrical cavity from zero initial radius. In the analysis, the clay was modelled as an incompressible linear elastic, perfectly plastic (Tresca) material. A combination of large strain analysis in the plastically deforming region with small strain in the elastic region was used (similar to Gibson and Anderson, 1961). Soil parameters were obtained from the unloading section of the pressuremeter curve, as well as the loading section, to overcome the difficulties in modelling the disturbance caused by the installation of the cone-pressuremeter. Both cylindrical and spherical cases were presented so that the two interpretations were compared.

The strength and stiffness values obtained from cylindrical cavity contraction theory are in good agreement with other *in situ* test measurements. The horizontal stresses for cylindrical expansion theory imply rather high K_o values. Estimating the *in situ* vertical stress σ_v from the bulk unit weight results in $(\sigma_h - \sigma_v)$ values greater that $2s_u$, which is therefore impossible. It is suggested that cylindrical expansion theory is in error and that spherical expansion theory may be more appropriate in this case. Length to diameter ratio effects may also contribute to the large values observed in cylindrical model of expansion.

An equivalent approach for test interpretation of the cone-pressuremeter in sand has been presented by Houlsby and Yu (1990) and Yu (1990). A numerical analysis (i.e. finite element analysis) has been used, due to the difficulties of obtaining a simple analytical solution for modelling large strain cavity expansion in frictional material with dilation. The soil is idealised as an elastic, perfectly plastic Mohr-Coulomb material. This large strain finite element analysis provides a reasonable estimate of the cone-pressuremeter limit pressure ψ_l. Experimental results obtained by Schnaid and Houlsby (1990) were analysed by Houlsby and Yu (1990), using the measured values of shear modulus (as reported in Chapter 6 of this dissertation) and friction and dilation angles estimated from Bolton's formulation (Bolton, 1986). The predicted values of ψ_l agreed reasonably well with observed values obtained experimentally with the cone-pressuremeter.

Results of the finite element analysis suggest that the slope of a plot $\ln\psi$ against $-\ln(\varepsilon_{max} - \varepsilon)$ is primarily controlled by the soil strength parameters and to a small extent by soil stiffness. The same results were found for the small strain unloading analysis of a pressuremeter in sand (Houlsby *et al*, 1986). This dependency can be quantitatively expressed in the same way as the small strain solution, by making use of equations [1.3] and [1.5]. A typical experimental cone-pressuremeter expansion and contraction curve is shown in Figure 1.2. A linear unloading curve is clearly defined, which was found generally to be the case for tests on loose sand. For

medium and dense sands the slope of the unloading curve on this plot is much less well defined, and values of friction angles derived from the slope of unloading curves are not realistic. In general the calculated S_d values are significantly higher than those measured, and in any case there is a significant scatter in the observed S_d values for medium and dense sand.

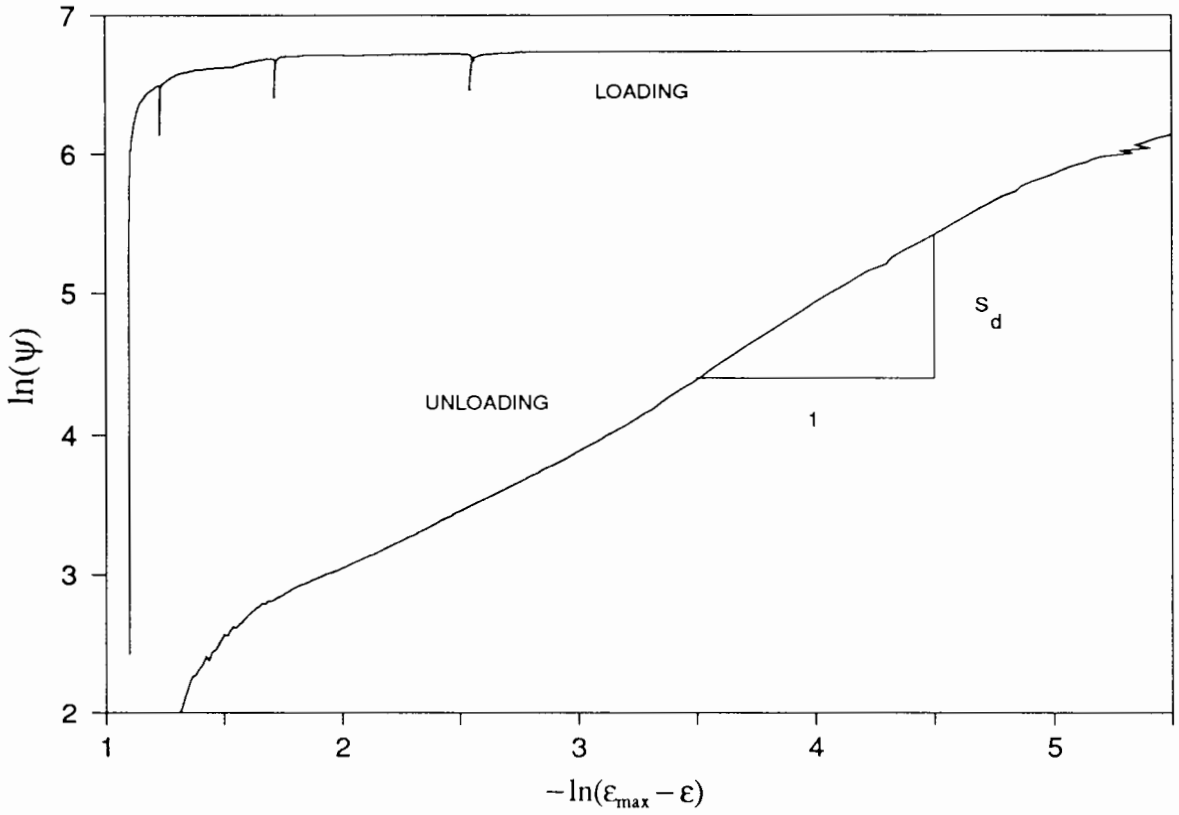

Figure 1.2 - Example of a loading-unloading curve from a cone-pressuremeter test (after Houlsby and Yu, 1990).

An analytical solution to obtain the entire pressuremeter pressure-expansion curve in sand is currently being developed by Yu (1990), but its ability to provide information on the shear strength and *in situ* stresses is still subject to further investigation. A two dimensional finite

element analysis is also being developed (Yu, 1990), which intends to provide a more general understanding of length to diameter ratio effects in clay and sand for self-boring and cone-pressuremeter probes.

As an alternative to the above approach, the results of cone-pressuremeter tests can be used directly for design purposes, by means of empirical correlations. This approach consists of obtaining information on two parameters, namely limit pressure (a failure parameter for verifying stability) and pressuremeter modulus (a stiffness parameter for estimating settlements). Direct correlations are then established between these parameters and the observed behaviour of structures. A prototype cone-pressuremeter developed in France by the Laboratoire Central des Ponts et Chaussées is currently being analysed in this way (e.g. Baguelin and Jezequel, 1986). Preliminary tests were carried out in sand, silt, clay, gravel and chalk. Results of cone-pressuremeter tests were compared with values obtained from Ménard-pressuremeter tests to investigate their similarities, and, therefore, the suitability of using Ménard-type correlations on the interpretation of the cone-pressuremeter test. This approach may prove to be a sensible way to use cone-pressuremeter results. However, it is felt necessary first to explore fully the potential of this new device to provide information on fundamental properties of the soil, allowing more rigorous theories to be used for engineering design.

1.3 - Outline of the research

In this introductory chapter it has been stated that results of *in situ* tests can be used in engineering design problems by means of empirical correlations. The pressuremeter has established its reputation as a reliable field technique under this philosophy, in which results of pressure-expansion tests have been used to determine directly the design of foundations (e.g. Baguelin *et al*, 1978, Frank, 1985).

Alternatively, results of *in situ* tests can be used to determine the values of engineering design parameters such as strength, stiffness and permeability. Engineering parameters can be also obtained from purely empirical correlations, but it is preferable to interpret *in situ* tests by use of either analysis or of correlations established from calibration chamber tests.

The pressuremeter has long been recognized as a test which works with well-defined boundary conditions and therefore permits a more rigorous theoretical analysis than many other *in situ* tests. As a result, empirical design approaches have been gradually replaced or improved by the use of soundly based theoretical ideas. It is believed that the cone-pressuremeter test, like the self-boring pressuremeter, can be analysed using cavity expansion theory. An interpretation of the tests in clay has already been proposed (Houlsby and Withers, 1988). Analytical and numerical methods of interpretation in sand are currently being developed (Houlsby and Yu, 1990; Yu, 1990), but its ability for deriving reliable friction and dilation angles still requires further investigation.

Under these conditions, calibration chamber tests are an appropriate option to calibrate and evaluate *in situ* testing devices in sand. A sample of known material at a known density is prepared in the chamber and tested under strictly controlled boundary conditions. Results of calibration tests can be directly related to relative density and the engineering properties in turn defined as a function of relative density. Alternatively, laboratory tests (usually triaxial tests) can be carried out to determine the engineering properties of the sample in the chamber. Therefore, a distinction is made between correlations established in well defined programmes of calibration and those inferred from more disjointed sets of field results.

Calibration chamber testing is the approach used in the work described in this dissertation. The purpose of the research is to provide a proper understanding of the new device, and in particular to establish a basic procedure to allow the tests to be used to determine the engineering

properties of soils. Tests have been carried out at Oxford University in a large calibration chamber in sand, to examine the influence of stresses and density on the readings obtained with the cone-pressuremeter. Although information can be obtained from the complete pressure-displacement curve, the study concentrates on the values of limit pressure obtained from the pressuremeter test and the cone resistance values from cone test. The interpretation of the shear modulus obtained from unload-reload loops is discussed, as is the influence of the method of installation on the measured shear modulus.

The organization of this dissertation is as follows. In Chapter 2 the design, construction and use of the laboratory equipment are described and specifications of the cone-pressuremeter testing device are given for three devices tested in the laboratory work (15 cm^2, 10 cm^2 and 5 cm^2 pressuremeter probes). In Chapter 3 sample preparation and testing procedures are described, together with a critical evaluation of the calibration chamber approach. The mechanical properties of the granular soil used in the experimental programme are investigated and certain aspects of the understanding of the behaviour of sand are discussed.

The main variables which influence the results of calibration chamber tests in sand are introduced in Chapter 4, and a testing methodology is established. Experimental results are presented which illustrate the effects of relative density, vertical stress and horizontal stress on results of cone-pressuremeter tests. In Chapter 5 a basic procedure for the interpretation of cone-pressuremeter tests is described, based on calibration chamber tests carried out with the 10 cm^2 prototype. It is shown that assessment of soil properties depends on the relationship between values of cone resistance obtained from cone tests and values of limit pressure obtained from pressuremeter tests. A procedure for deducing strength parameters and *in situ* horizontal stress is presented.

One of the most common uses of pressuremeter tests is for the evaluation of the shear modulus. The interpretation of the "elastic" shear modulus measured from unload-reload loops using the cone-pressuremeter is presented in Chapter 6. Comparisons are made between the shear moduli calculated from strain arm measurements and the shear moduli calculated from volume change measurements. The necessity of calibrations to account for compliance effects and corrections to account for the finite length of the pressuremeter is emphasised. A method that allows the moduli to be normalised with respect to stress level is examined and the values of moduli obtained from the cone-pressuremeter are compared with those obtained from the self-boring pressuremeter.

An assessment of the research programme is made in Chapter 7, and the main conclusions are restated. Recommendations for future work are made.

Additional work has been carried out on the 15 cm^2 and 5 cm^2 cone-pressuremeter prototypes. Results are described and discussed in Appendix I and II. An assessment of chamber size effects on calibration chamber tests in sands is presented in Appendix I. A large database of chamber tests carried out with the cone penetrometer in Norway, Italy and U.K. is examined. A numerical approach based on cavity expansion theory is used to highlight some of the problems regarding the validity of the calibration chamber approach to assess engineering properties of sand in the field. In Appendix II, a study of length to diameter ratio effects on the 5 cm^2 pressuremeter probe is presented. In both Appendix I and Appendix II the discussion confirms the difficulties of dealing with complex boundary problems in a purely empirical fashion. Clearly, further research is required before results of chamber size effects and length to diameter ratio effects can be used with confidence.

CHAPTER 2

EXPERIMENTAL EQUIPMENT

In this chapter the mechanical details of the design and construction of the calibration chamber are presented. Specifications of the cone-pressuremeter testing device are given. Reference is made to three prototype devices tested in the calibration chamber. Finally the experimental techniques, instrumentation and electronic data logging system are described.

2.1 - Introduction

The current practice for calibration of *in situ* testing devices in cohesive soils is mainly conducted with reference to field vane tests or laboratory triaxial tests carried out on undisturbed samples. In cohesionless materials, laboratory testing of undisturbed samples is still difficult and does not provide as suitable an approach as it does for clays. There is also no equivalent of the field vane test for sands to determine *in situ* strength characteristics directly. As an alternative a soil sample similar to natural deposits is simulated in the laboratory, in which *in situ* testing devices are calibrated under strictly controlled conditions.

Laboratory chamber testing is a well established technique to calibrate *in situ* testing devices in cohesionless materials. In the last two decades the use of calibration chambers for sands has increased, and chambers have been built in the USA (Holden, 1971; Villet and Mitchell, 1981), Australia (Chapman, 1974), U.K. (Fahey, 1980), Norway (Parkin and Lunne, 1982) and Italy (Bellotti *et al*, 1982). The experience acquired in the use and interpretation of calibration chamber testing has been widely addressed by researchers at informal meetings in

Southampton (1983), Milan (1986), Oslo (1988) and Grenoble (1990), in which data from different testing programmes were reported. The general acceptance of this technique can be explained by the inherent merits of calibration chambers, summarised as follows:

(i) capability of reproducing samples which, to some extent, are similar in structure to natural deposits formed by sedimentation.

(ii) homogeneity and repeatability of the samples under a wide range of relative densities.

(iii) ability to control accurately vertical and horizontal stresses applied to the samples.

(iv) possibility of simulating stress and strain history of the samples.

Against these advantages is the problem of the limited size of the chamber, resulting in the important influence of boundary conditions (as discussed in Appendix I).

A large triaxial chamber was designed and constructed to calibrate the cone-pressuremeter testing device. The general characteristics of the chamber have been described by Schnaid (1988); the lay-out of the equipment and a general view of the laboratory set up are presented in Figures 2.1 and 2.2. Three prototype cone-pressuremeter devices have been tested in the calibration chamber, two of which were designed and constructed for the work described in this dissertation. Details of the instruments, laboratory apparatus and its operation will now be discussed.

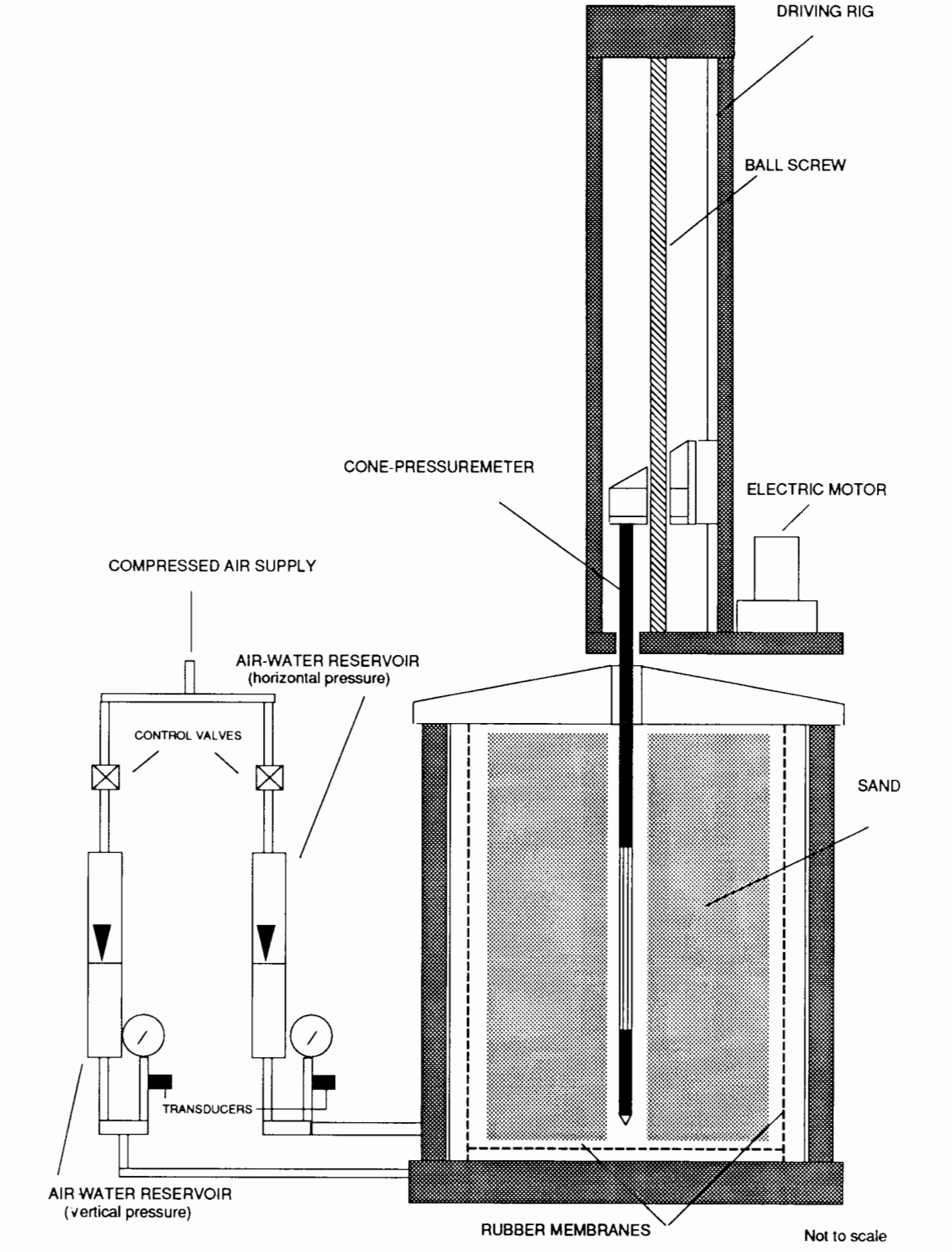

Figure 2.1 - Schematic diagram of calibration testing chamber

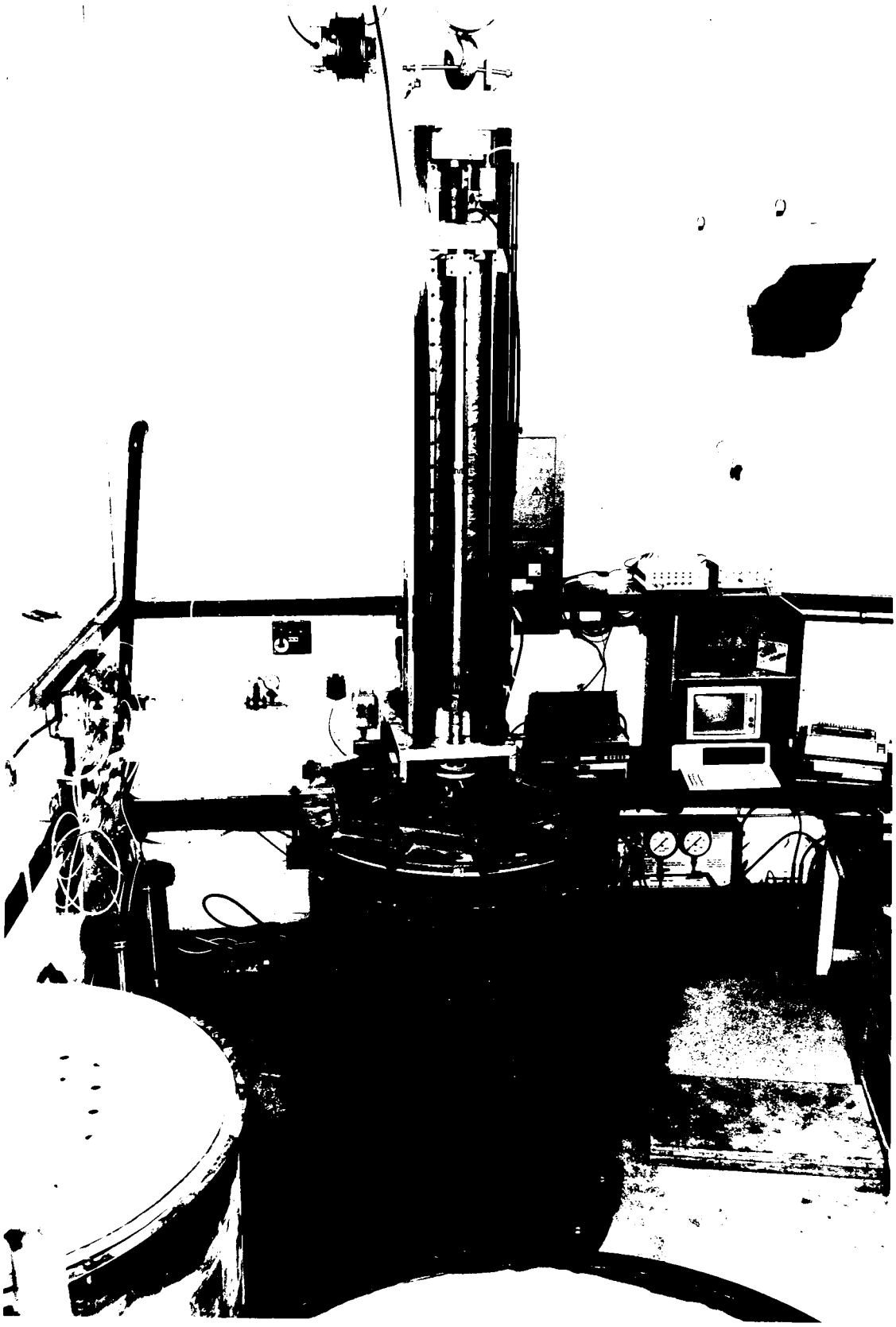

Figure 2.2 - General view of Oxford University calibration chamber

2.2 - Cone-pressuremeter testing device

The cone-pressuremeter is a new *in situ* testing device which incorporates a pressuremeter probe behind a standard cone penetrometer tip. The instrument is shown in Figures 2.3 and 2.4, and a detailed description is given by Withers *et al* (1986). A standard 60°, 15 cm^2 electric cone penetrometer is used to measure tip cone resistance. Sleeve friction measurements, as well as pore pressure measurements in the case of a piezocone, can also be monitored whenever required. The pressuremeter probe is of the same diameter as the cone and is mounted on the penetrometer shaft. This probe has a differential pressure capacity of 10 MPa and a radial expansion limit of 50%. This type of pressuremeter is often described as a "full-displacement" pressuremeter.

The overall length of the membrane is 450 mm which corresponds to a length to diameter ratio of approximately 10. During penetration an outer flexible protective membrane with stainless steel strips (the "Chinese lantern") is placed over the pressuremeter membrane. The radial expansion of the pressuremeter is measured at the probe midheight by three displacement transducers placed at 120° separation around the circumference. A system of pivoted arms and strain gauged springs similar to that used in the Cambridge self-boring pressuremeter has been fitted in the instrument (see Wroth and Hughes, 1973). Inflation is achieved by Nitrogen gas and inflation pressure is measured by a pressure transducer in the pressuremeter.

Above the pressuremeter is a module which amplifies the electrical signals from the strain gauged arms and the pressure transducer. Electrical signals from the cone are passed independently through the pressuremeter module on separate wires.

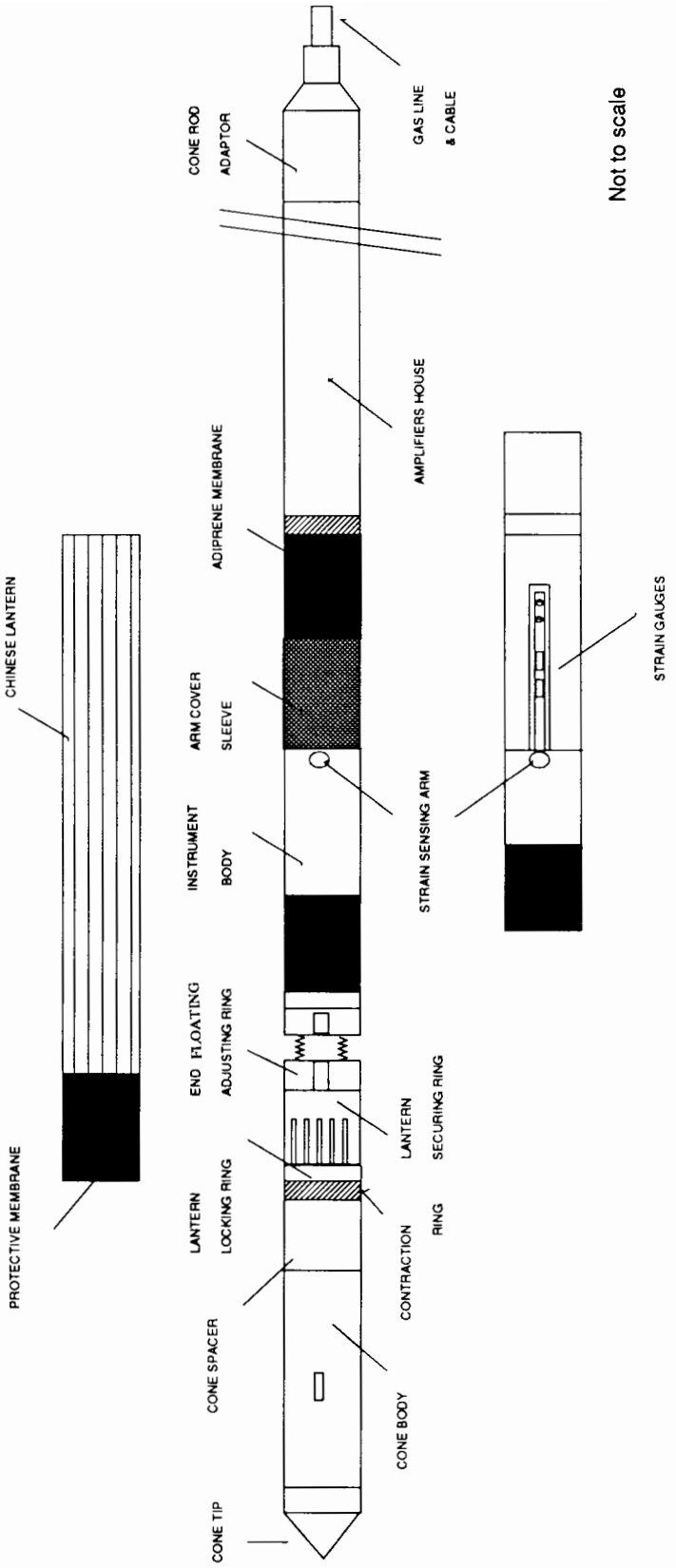

Figure 2.3 - Details of the cone-pressuremeter testing device

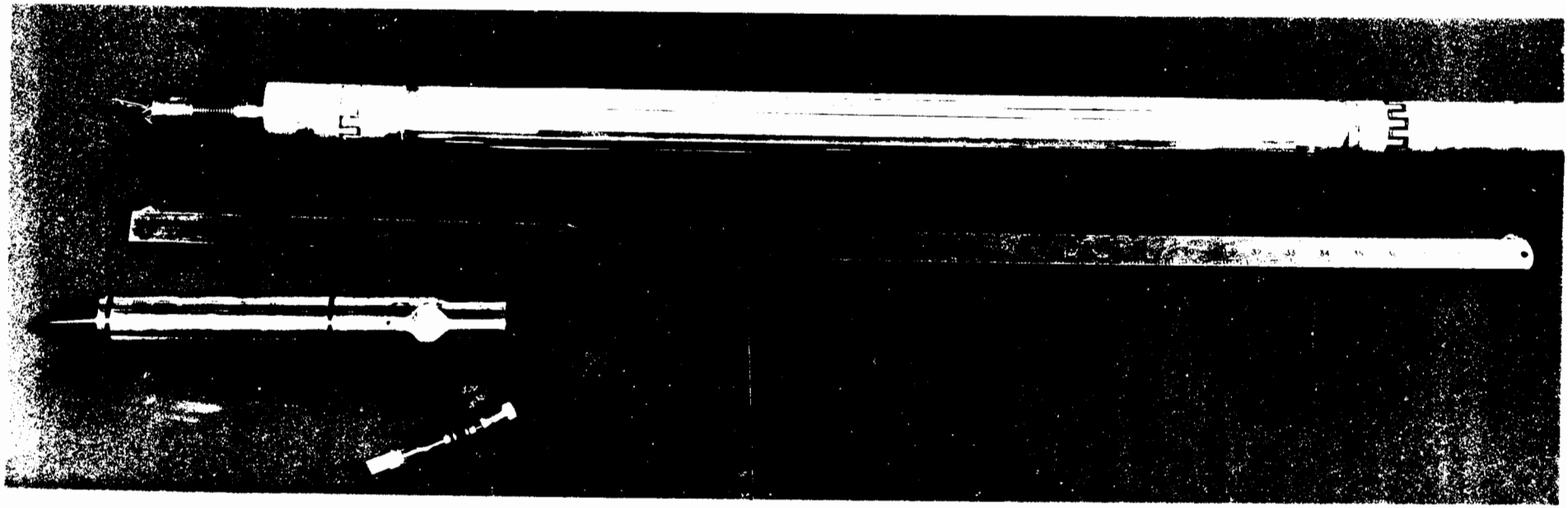

Figure 2.4 - Pressuremeter probe for attachment behind a 43.7 mm diameter cone tip

In the present research programme three cone-pressuremeter devices with cross-sectional areas corresponding to 15 cm^2, 10 cm^2 and 5 cm^2 were tested. Dimensions were selected to investigate boundary condition effects in the calibration chamber. The 15 cm^2 device was supplied by Fugro-McClelland Ltd. This instrument has been previously tested in the field in clay deposits, as reported by Withers *et al* (1986) and Houlsby and Withers (1988). The 10 cm^2 and 5 cm^2 devices were designed and constructed by Cambridge Insitu to specifications prepared by Oxford University and Fugro-McClelland Ltd. after joint discussions. The features of each instrument are now briefly described.

(i) 15 cm^2 device- The overall length of the device is approximately 2.2 m, and even if the shortest possible cone spacer was used to connect the cone penetrometer to the pressuremeter module the instrument could not fit in the calibration chamber (1.5 m height). As a result, the cone penetrometer had to be replaced with a dummy cone positioned immediately below the pressuremeter probe. Tip cone resistance, q_c, was not recorded during penetration.

(ii) 10 cm^2 device- An active 10 cm^2 cone penetrometer has been connected to a pressuremeter probe of the same diameter allowing tip cone resistance q_c to be measured during penetration. The pressuremeter module is similar to the 15 cm^2 instrument, except for a few modifications performed to overcome the constraints imposed by the small diameter. Membrane expansion is monitored by three equally spaced strain gauged cantilever springs. Inflation is achieved by silicone oil injected from a specially designed pressuremeter pressurisation system (see section 2.2.1 for details), with pressure being recorded from a pressure transducer in the oil supply line. The pressurisation system enables variations of volume of the pressuremeter to be

accurately monitored throughout the test. As a result, the pressure-expansion curve can be calculated both from strain arm measurements and from volume change measurements. An attempt was made to protect the membrane using a double layer sheath of stainless steel strips. The outer sheath severed twice during penetration and a standard "Chinese lantern" similar to the one used in the 15 cm^2 device had to be used.

(iii) 5 cm^2 device- The pressuremeter is inflated by silicone oil driven from the same pressurisation system used for the 10 cm^2 device. Due to limitations in diameter the instrument has no strain gauged arms and membrane expansion is only monitored by the change of volume of the pressuremeter probe. An active 5 cm^2 cone penetrometer is used for measuring cone resistance during penetration. The pressuremeter is provided with various adaptors enabling length to diameter ratios of 5, 10 and 20 to be tested.

2.2.1 - Pressuremeter pressurisation system

A pressurisation system was supplied by Cambridge Insitu, which allows stress controlled or strain controlled tests to be performed. The system has a maximum pressure capacity of 10 MPa and pressure is applied by means of Nitrogen gas. A pressure control panel, a strain control unit and an electronic box are the main components of the system, as illustrated in Figure 2.5. The provision of safety valves ensures that the unit cannot accidentally become pressurised inside.

Stress controlled tests can be carried out by operating the pressure control panel. A quick release coupling is connected to the bottle gas supply line and pressure is controlled by a

pressure regulator valve. Inflation pressure is monitored by means of two gauges, one that has a pressure capability of 4 MPa and, when the pressure exceeds that value, a second that works to a maximum pressure of 10 MPa.

Strain controlled tests can be carried out by operating a strain control unit. Magnetic valves were designed to work in response to the strain signal returning from the instrument in the ground. Ten constant rates of strain can be selected between 0.1% radial displacement ($R - R_o$) per hour to 2.0% per minute, operating for both loading and unloading. In addition the unit is able of holding the strain to a constant value to perform holding tests (e. g. Clarke *et al*, 1979). Inflation pressure, individual and average readings of the strain arms are displayed on the front panel of a readout box which is connected to the strain control unit. Test carried out with the 15 cm^2 prototype were all strain controlled, performed by operating the strain unit described above.

Unlike the 15 cm^2 prototype, the 10 cm^2 and 5 cm^2 cone-pressuremeter prototypes were inflated by silicone oil in order to monitor the volume change of the expanding membrane. A pressurisation system was designed and constructed at Oxford University to control the pressuremeter tests in the laboratory. The mechanism is illustrated in Figure 2.6 and is shown in Figure 2.7. A piston is driven inside a cylinder by a ball screw mechanically connected to a geared DC tacho motor. The ball screw nut is fixed to the piston and to a precision linear bearing so that it cannot rotate, thus providing linear movement. The volume of oil displaced from the cylinder by the movement of the piston is injected into the pressuremeter, inflating the membrane in a constant strain rate. A DC servo motor system controls the tacho motor to provide a constant motor speed proportional to the input voltage. In this mode the system detects any difference between motor speed and input command voltage. Power is then supplied by an amplifier until this difference is sensibly zero. The mechanism provides inflation or deflation rates in a range up to 1.5% radial displacement per minute. Full speed start, stop time

and speed selection is achieved in 30 milliseconds allowing any combination of strain rates to be selected during the test procedure. The pressure capability of the system is 10 MPa. A displacement transducer (potentiometer) is used to monitor the displacements of the piston, and the measurements are used to compute the variation in volume of the pressuremeter probe.

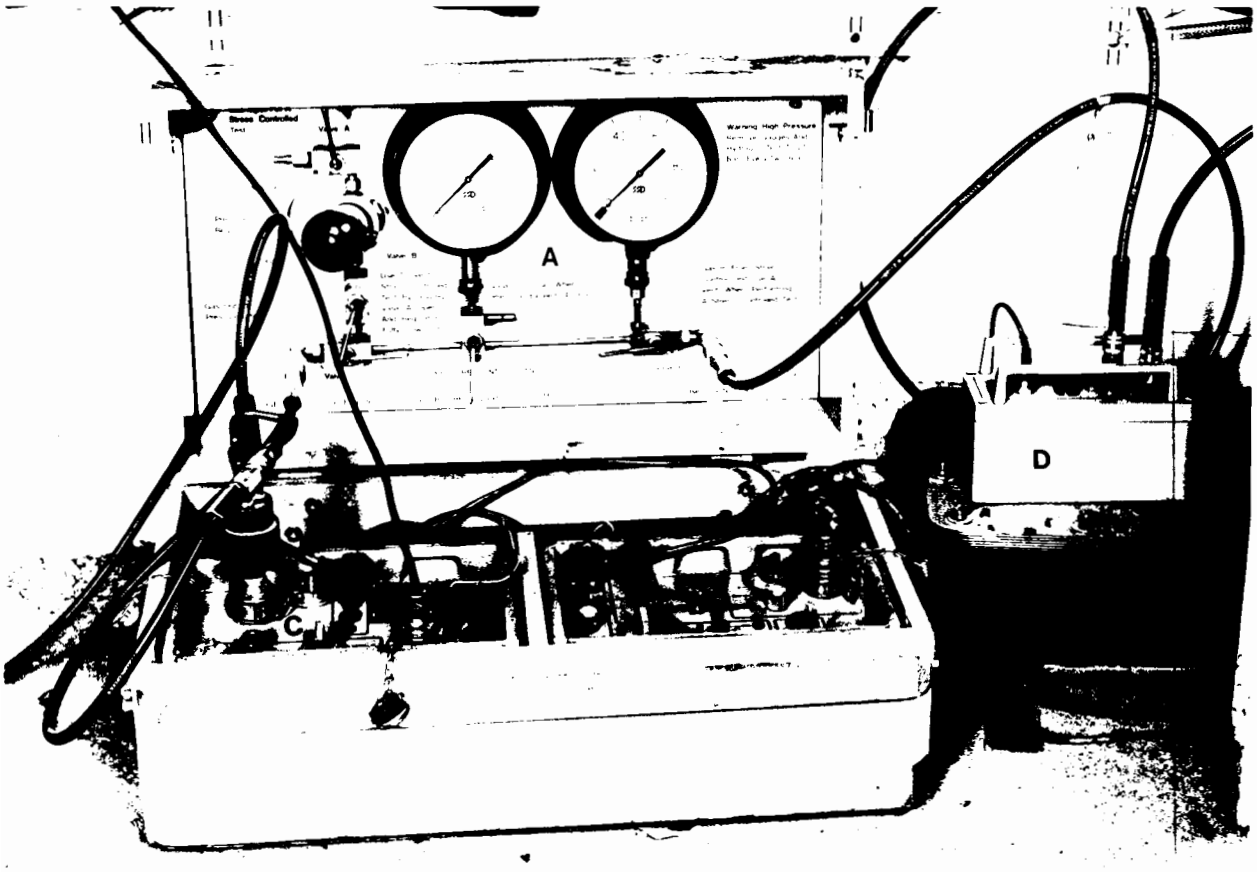

A - Pressure control panel
B - Strain control unit
C - Electronic box (output and display signals)
D - Safety valves unit

Figure 2.5 - Cambridge Insitu pressuremeter pressurisation system (pressure applied by means of nitrogen gas)

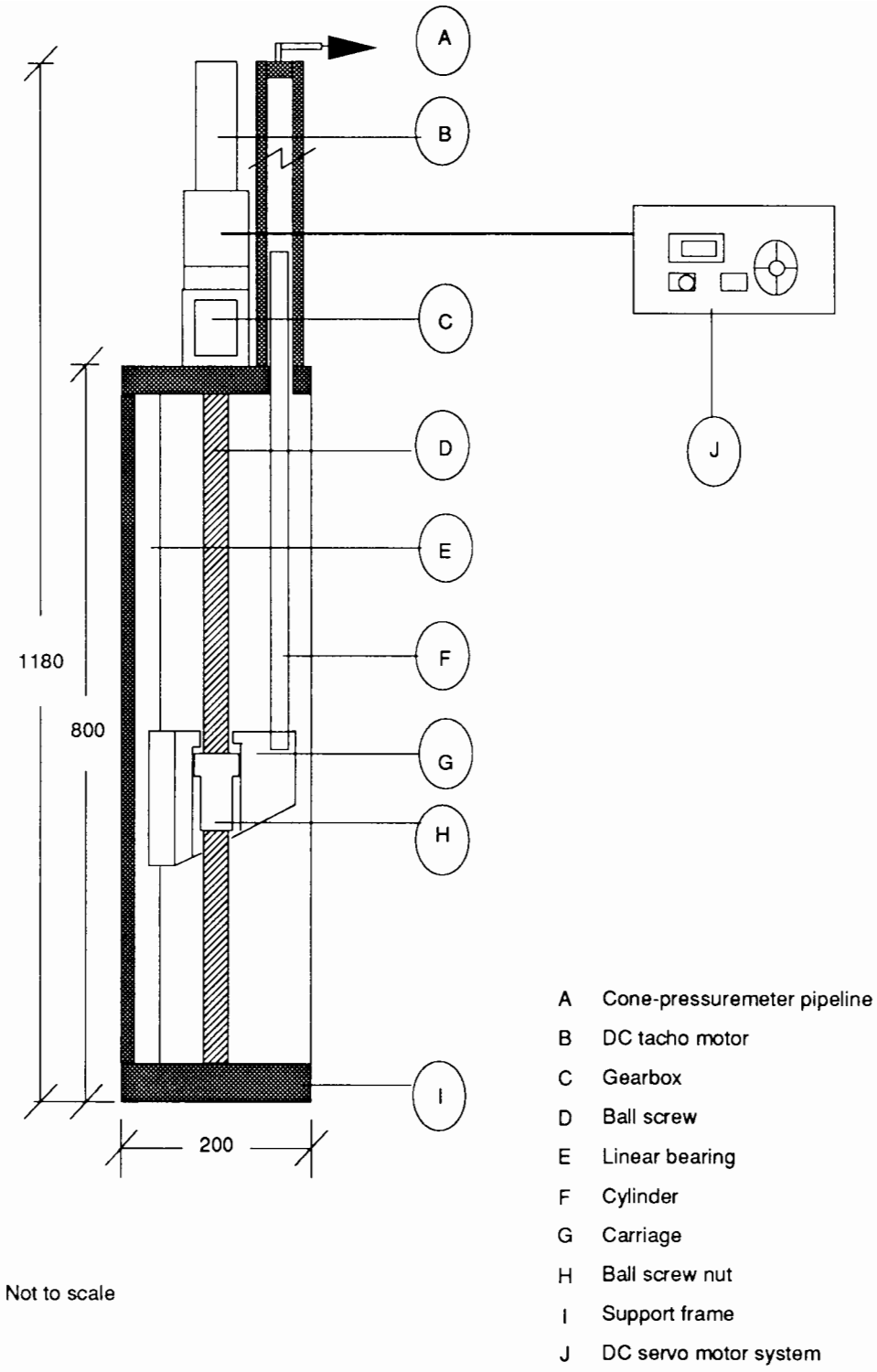

Figure 2.6 - Schematic diagram of pressurisation system developed at Oxford University

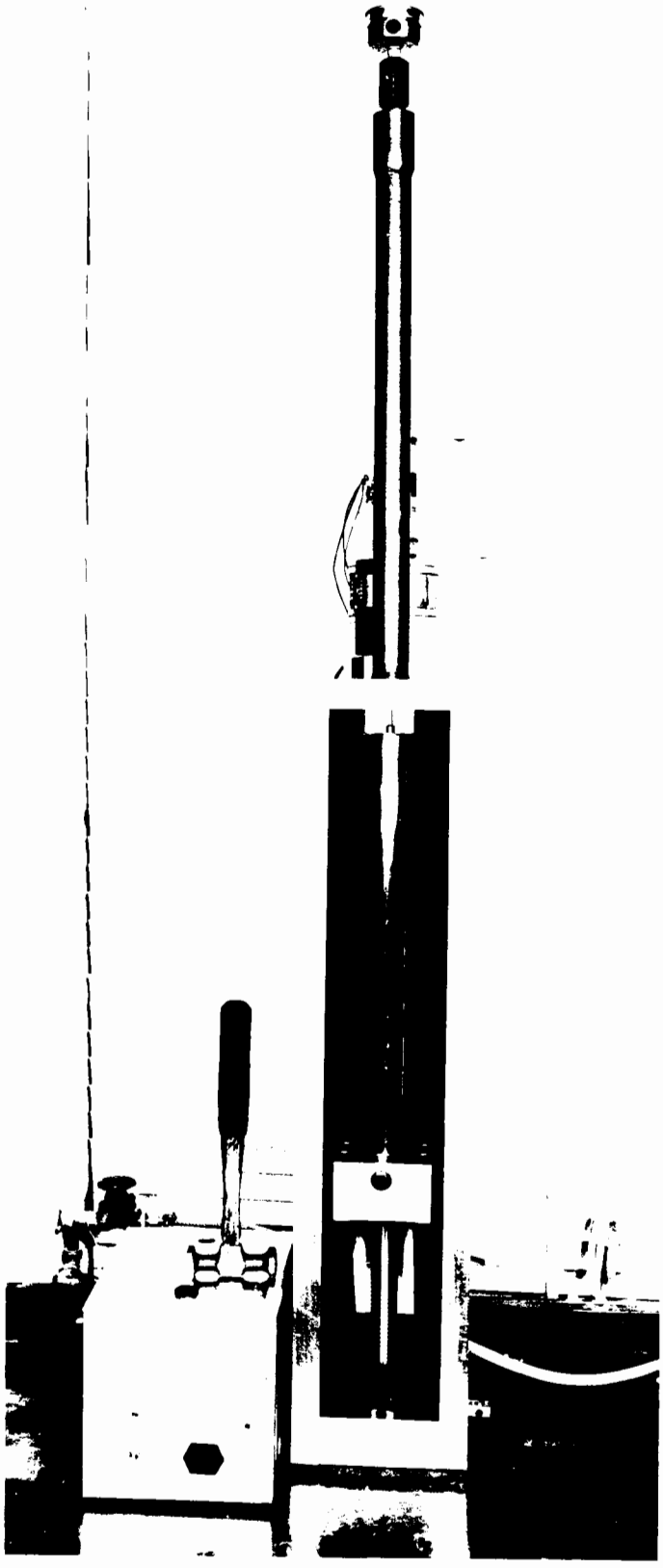

Figure 2.7 - Pressuremeter pressurisation system

(pressure applied by means of silicone oil)

2.3 - Calibration chamber

A triaxial calibration chamber was designed as a new version of that used at Cambridge University (Fahey, 1980) and later re-assembled at Oxford University (Houlsby and Hitchman, 1988). A general view of the chamber is shown in Figure 2.8. The chamber can test a cylindrical sample of sand 1.0 m in diameter and 1.5 m in height. The sample is confined laterally by a flexible rubber membrane, which is used to apply the horizontal stress by means of water pressure. The same principle is adopted at the bottom surface, where a rubber membrane is used to apply the required vertical stress (also by water pressure). The top of the sample is confined by a rigid top plate.

The main problem in chamber design centres around a system for sealing the edges of the membranes to avoid leaks during testing. A simple system has been designed and details are schematically shown in Figure 2.9. Each membrane was fixed between two metal faces, by means of circular clamping rings. The bottom membrane was cut from sheets of 3.0 mm thick "shotblasters" rubber. The lateral membrane was cut from 3.0 mm thick neoprene membrane, especially vulcanised in a cylindrical shape without lap joints. The procedure of fixing the membranes was conducted by disconnecting the body of the chamber from the base plate (see Figure 2.8). First the bottom membrane was clamped to the base plate and then the edges of the lateral membrane were independently fixed in position at the top and bottom flanges of the body of the chamber.

A laboratory test programme was planned to evaluate the influence of horizontal and vertical stress independently on either cone resistance and pressuremeter limit pressure. Two independent and identical pressurisation systems were designed, one for the horizontal pressure and one for the vertical pressure, to measure and control pressures during testing.

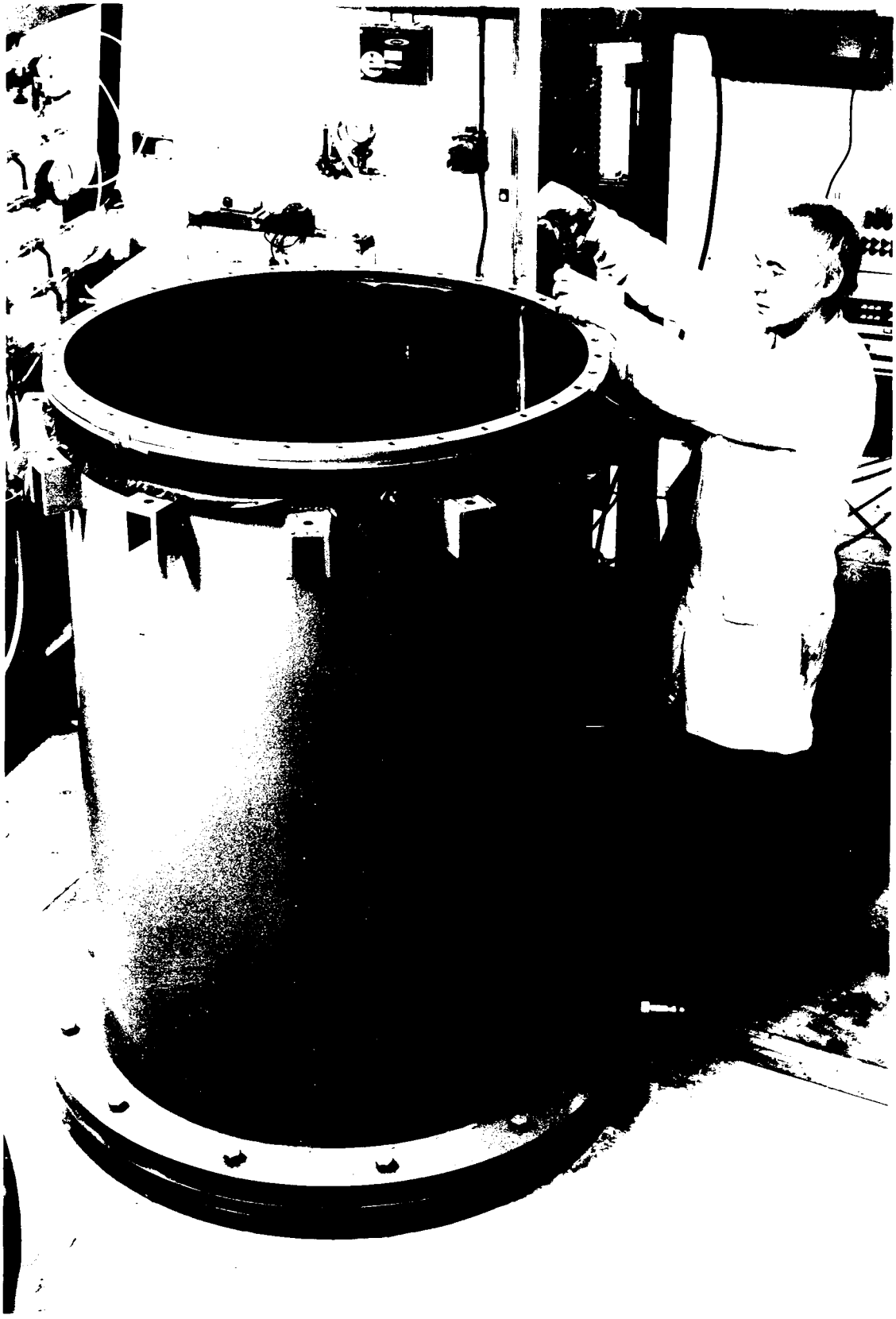

Figure 2.8 - Testing chamber (lateral membrane being fixed in position)

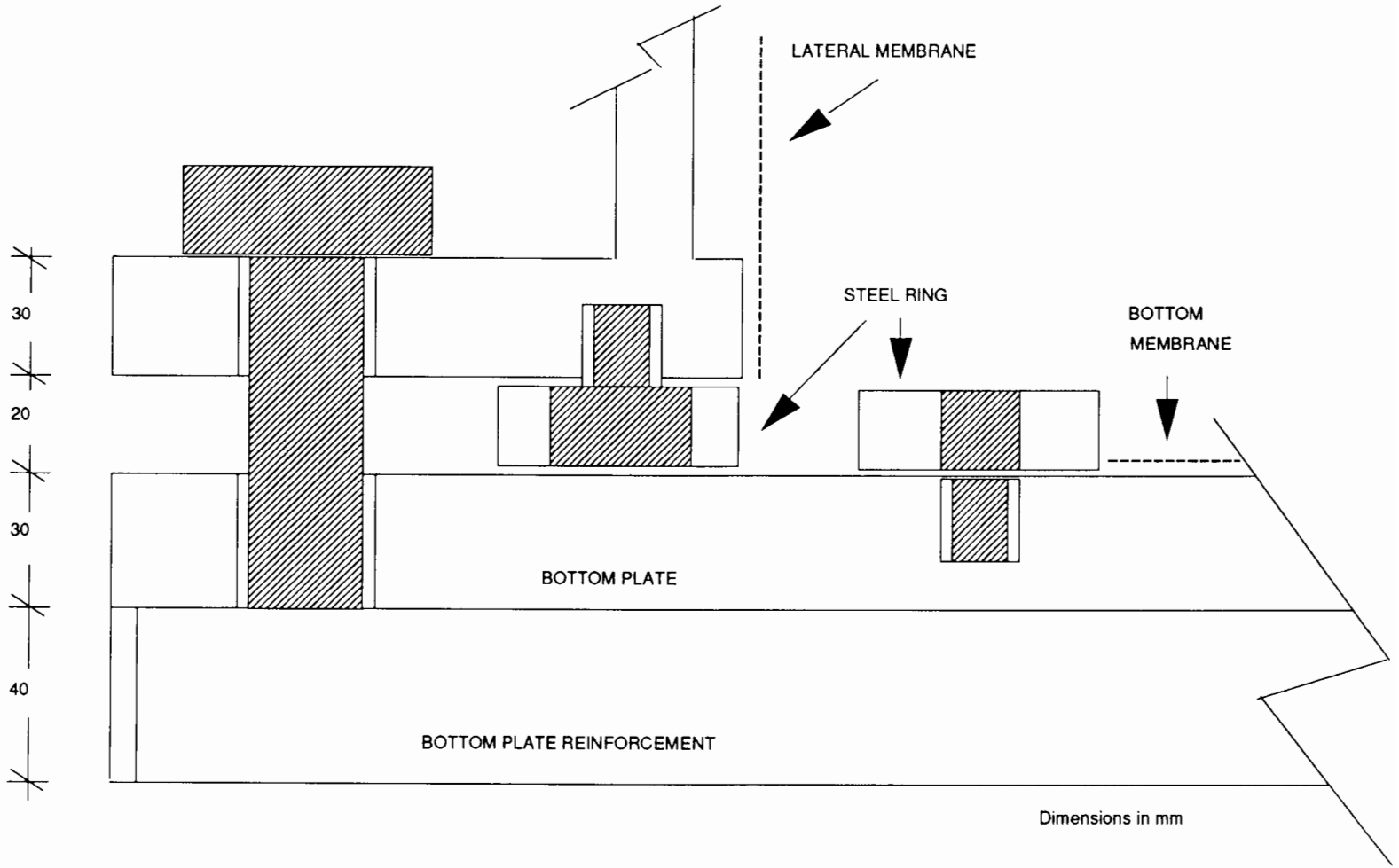

Figure 2.9 - Illustration of circular clamping rings for sealing the edges of lateral and bottom membranes

The change in pressure is produced by regulating air pressure using a self-relieving valve driving an air-water interface system. The interface allows water to be used to apply stresses to the soil sample and stabilises pressure fluctuation due to variations in volume experienced by the sample during test.

2.3.1 - Driving mechanism

A driving mechanism was designed according to the following criteria:

(i) to provide a linear speed of 20 mm/sec, with a tolerance of ± 5 mm/sec, as recommended by the ISSMFE Technical Committee on Penetration Testing (De Beer *et al*, 1988).

(ii) to give a load capacity up to 100 kN. The load capacity was assessed from penetration tests performed in calibration chambers reported by Baldi *et al* (1986), Last *et al* (1987) and Houlsby and Hitchman (1988).

The driving mechanism is illustrated in Figure 2.10 and is shown in Figure 2.11. A load transmission plate is driven by a ball screw mechanically connected to a geared 3 kW DC motor. A thrust ball bearing and a single row radial bearing hold each extremity of the ball screw to the loading frame. The screw nut is fixed to two precision linear bearings supported by four ball slide guides so that it cannot rotate, thus providing linear movement. The moments generated on the ball screw by the pushing forces required to drive the device into the chamber are supported by the linear bearings and guides.

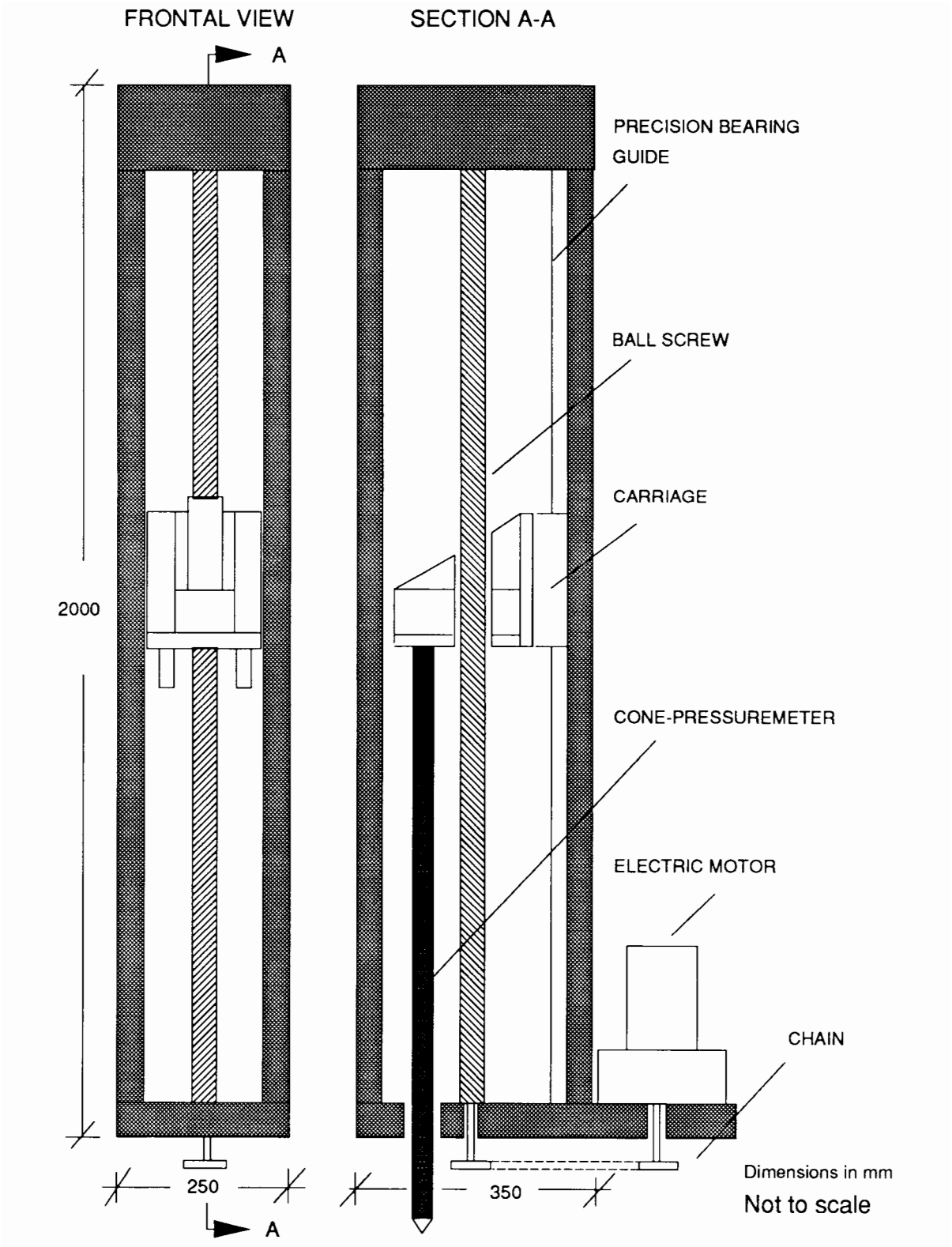

Figure 2.10 - Illustration of the driving mechanism

LATERAL VIEW

FRONTAL VIEW

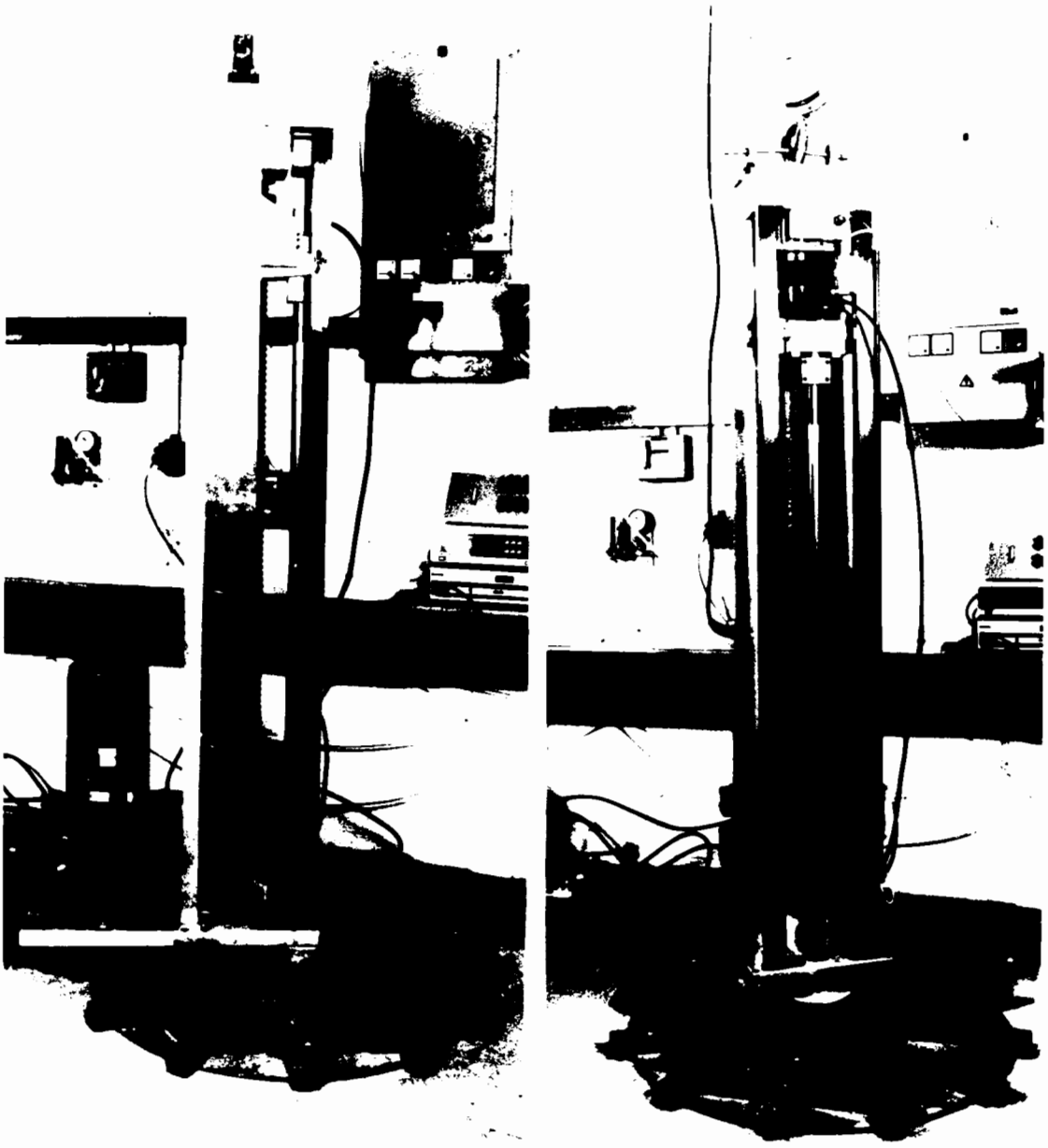

Figure 2.11 - Driving mechanism

The motor is positioned on the frame beside the ball screw and the drive is transmitted through a system of chains and sprockets. A pushing speed of 20 mm/sec with a tolerance of ± 2 mm/sec was measured during driving. The system gives a maximum displacement of 1.6 m, monitored continuously by a displacement transducer (potentiometer).

2.3.2 - Testing procedure

Chamber testing has become a routine operation at Oxford University, to be performed by one man and requiring two to three days per test, excluding maintenance. A complete description of the chamber has been given in previous sections and the operating procedures adopted in this research is now briefly discussed.

A sand sample was prepared by a raining deposition technique using a single hopper over the whole area of the sample. A critical review on sample preparation methods, densities tested and soil properties is presented in Chapter 3. In order to form a cylindrical sample inside a membrane walled chamber, a rigid cylindrical former was used. Prior to testing, the former was positioned inside the chamber, into which a closed bottomed cylindrical latex membrane of the same size of the sample to be prepared was placed. Sand was poured continuously into the chamber from a hopper through perforated plates and diffuser sieves, until the chamber was slightly overfilled. The sand rain was then halted and the hopper and sieves removed. The sand surface was roughly levelled and the inner latex membrane was gathered and connected to a vacuum supply. A vacuum pressure of 10 kPa (±5 kPa) was applied on the sample, keeping it in a cylindrical shape. A slight vacuum was applied to the annular space between the lateral flexible membrane and the chamber wall. This caused the rubber membrane to pull back to the chamber wall and the rigid former was thus easily removed. The annular space behind the lateral membrane was then filled with water. The sample vacuum was released and the boundary of the cylindrical sample became water supported.

The top plate was lowered and fixed to the chamber body after having the top surface of the sample accurately levelled. By opening the chamber valves and controlling the self relieving valves on the pressurisation panel the sample was confined independently horizontally and vertically, following any pre-selected K (σ'_h/σ'_v) path. Cone-pressuremeter tests were carried out at constant vertical and horizontal stresses.

The driving system was permanently fixed to the chamber lid and the cone-pressuremeter testing device attached to its pushing plate. The device was positioned immediately above the sand surface in a central hole in the chamber lid. At this stage the instrument was pushed into the chamber and continuous recordings taken of tip cone resistance, device penetration, horizontal stress and vertical stress. Insertion was stopped when the centre of the pressuremeter was at the midheight of the chamber. A strain controlled pressuremeter test was then performed in which inflation pressure, ψ , and radial displacements of the membrane were recorded.

Once the test was finished the lateral and vertical stresses were released, the motor on the driving mechanism was reversed and the device was pulled out from the chamber. The sand in the chamber was weighed in order to calculate the overall sand density. Finally the sand was removed from the chamber by pouring it straight into the hopper or using a powerful vacuum machine to remove dust.

2.4 - Instrumentation and data acquisition

Instrumentation was required to monitor the cone-pressuremeter testing device, chamber confining pressures, pressuremeter pressurisation system and driving mechanism.

The cone-pressuremeter testing device has been described in Section 2.2. The radial displacement of the pressuremeter membrane was measured by three displacement transducers

strain gauges in a 'full bridge' configuration. Cone tip resistance was measured by a strain gauged load cell. A 5V DC power supply was used to energise the transducers, and amplifiers were connected to both the load cell and displacement transducers to provide the necessary amplification of the output signals. Inflation pressure was monitored by a pressure transducer. The 15 cm^2 prototype has a differential pressure capacity of 10 MPa and pressure was measured by a pressure transducer mounted in the instrument. The 10 cm^2 and 5 cm^2 prototypes were inflated by silicone oil and pressure was recorded on the oil supply line by a 7 MPa pressure transducer. The accuracy of the transducers was 0.5% of full scale capacity.

Penetration of the cone-pressuremeter testing device into the chamber was monitored by a displacement transducer (potentiometer). A stainless steel cable was attached to the device and the transducer body was fixed to the driving frame. An electrical signal proportional to the linear extension of the cable was recorded and an internal spring motor maintained constant tension on cable for retraction. The potentiometer measured displacements in the range of 2.0 m with an accuracy of 0.1% full range to an excitation voltage of 5V DC. An identical transducer with a short range (1.0 m) was used to measure displacement of the driving piston in the pressuremeter pressurisation system.

Chamber confining pressures were continuously monitored during a test using a portable digital pressure indicator (DPI) placed on the air supply line. The DPI capacity was 700 kPa to 0.1% of full scale accuracy.

All transducers were regularly calibrated to check their calibration constants and accuracy. The term accuracy has been used here to represent the combined effects of linearity, hysteresis and repeatability. It was observed that calibrations remained practically the same over the duration of the research.

The data logging system consisted of an IBM-XT computer connected to a digital voltmeter (Solartron 7060) equipped with an analog scanner (Minate 7010) to provide 16 input channels. Communication between computer and voltmeter was provided by an IEEE 488 interface, also referred to as GPIB (General Purpose Interface Bus). The IBM Computer GPIB Programming Support was used for programming the interface in BASICA, receiving and sending interface messages (for bus management) and device dependent messages (for communication via the interface). Using this facility several programs were written in BASICA to monitor the tests and to store channel voltages read in each scanning operation.

CHAPTER 3

SAMPLE PREPARATION AND SOIL PROPERTIES

A detailed description of the Oxford calibration chamber set up has been presented in Chapter 2. The raining deposition technique of producing samples in the large chamber is now described in order to assess the adequacy of this technique in preparing reconstituted samples that reflect *in situ* properties (such as relative density and soil fabric). The mechanical properties of the granular material used in the experimental testing programme are investigated. Drained triaxial tests were carried out and certain aspects of sand behaviour are discussed.

3.1 - Sample Preparation

Chamber testing has become a routine laboratory operation in which a uniform sand sample is prepared. Different deposition techniques are in common use to produce homogeneous, repeatable samples of dry sand at specified densities. These techniques involve one of the following procedures: the sand is poured in layers and vibrated, the sand is poured from a longitudinal slit using a single hopper (Laier *et al*, 1975) and the sample is rained continuously using a single hopper over the whole area of the sample (Kolbuszewski and Jones, 1961; Cole, 1967; Battaglio *et al*, 1979; Bellotti *et al*, 1982; Miura and Toki, 1983; Rad and Tumay, 1987).

The sand specimen prepared by raining deposition appears to be the most satisfactory technique as it provides not only reasonably homogeneous samples with desired densities but simulates a soil fabric similar to the one found in natural deposits formed by sedimentation (Oda *et al*, 1978; Bellotti *et al*, 1982). The method consists of raining sand continuously from a single cylindrical hopper which holds the amount of sand necessary for sample preparation and is

placed above the chamber. At the base of the hopper there are two shutter plates perforated in exactly the same way. Sand will pour through the holes when the plates are correctly aligned and jets issuing from the holes are dispersed into a uniform rain by diffusor sieves.

The voids ratio of a sample poured from a hopper is dependent on the intensity of flow and on the height of fall of the sand (Kolbuszewski, 1948). The standard laboratory procedure to produce different voids ratios is to vary the intensity of flow. If the height of fall is to be controlled, some mechanism for lifting the hopper as the sample is being poured has to be constructed. As this would be difficult, especially for a 1.5 m height sample, the distance between the diffusor sieves and the top of the chamber was fixed at a minimum falling height of sand of about 600 mm. This relies on the assumption that there is a critical height of fall above which any increase in height has no further effect on sand density (Kolbuszewski and Jones, 1961; Rad and Tumay, 1987). Once this critical height of fall has been exceeded, the sample density can be controlled solely by varying the intensity of sand flow. The homogeneity of sands prepared by raining deposition was validated by Cole (1967) after radiographic examination of samples prepared in the Simple Shear Apparatus.

The raining deposition technique was used in the calibration chamber to produce three sand densities, corresponding to dense, medium and loose samples. The required densities were achieved by using a combination of different shutter plate sizes and diffusor sieves. Dense samples were prepared using perforated plates having 6 mm diameter holes on a 80 mm triangular grid, and passing through two sieves of apertures sizes 3.02 mm and 2.26 mm located at 150 mm and 250 mm respectively from the base of the hopper. Samples of medium density were obtained using 20 mm diameter holes in the shutter plates, also on a 80 mm triangular grid and passing through a 3.02 mm sieve located 150 mm below the hopper. Loose samples were prepared by pouring sand through the same shutter plates as for medium samples but omitting the diffusor sieves.

Three sand samples were prepared with the specific intention of density measurement and repeatibility checks at different locations inside the tank. As radiography examinations are not possible in a large steel walled tank, densities were measured by direct sampling experiments. Thin walled containers of 100 mm diameter and 200 mm height were placed inside the chamber at three vertical levels - top, middle and bottom, and two radial positions in each level - centre and boundary. Sand was poured from the hopper into the containers placed inside the chamber. The containers were then carefully removed from the chamber and weighed to determine sand density. Density variations of about 2% were observed for dense and loose samples, whereas for medium samples density variations of up to 4% were observed. Variations of density with depth was within the scatter of the results and no tendency was observed towards higher density at the bottom. The values of density compared very well with values obtained by Houlsby and Hitchman (1988) using a similar arrangement.

A similar technique to produce sand samples in large chambers has been widely used in Italy during the last decade (Battaglio *et al*, 1979; Bellotti *et al*, 1982; Baldi *et al*, 1986; Ghionna *et al*, 1990). The experience is described as giving specimens with satisfactory homogeneity and good repeatibility, with variations on relative density of the same order of magnitude as described here.

A total of 34 calibration chamber tests were carried out in the present research programme. The density of each sample was determined at the end of each test by weighing the sand in the chamber and dividing by the volume of the sample. The results, expressed in terms of voids ratio and relative density, are presented in Table 3.1. A good repeatibility of the values of relative density (or voids ratio) was observed for the ranges of density tested.

DENSITY	AVERAGE VALUES		MAXIMUM DENSITY VALUES		MINIMUM DENSITY VALUES		NUMBER OF TESTS
	Rd(%)	e	Rd (%)	e	Rd (%)	e	
LOOSE	23	0.705	27	0.694	16	0.728	9
MEDIUM	63	0.588	68	0.573	60	0.597	15
DENSE	86	0.519	89	0.511	83	0.529	10

TABLE 3.1 - Relative density and voids ratio determined from calibration chamber tests.

As noted previously, the raining deposition technique may produce a soil fabric similar to natural deposits. The application of calibration chamber derived correlations is, however, limited to clean quartz sands, as sample preparation techniques clearly cannot model important environmental factors such as aging and cementation. The main advantage of the raining technique is to produce reasonably homogeneous samples with the desired relative densities. Measured quantities from *in situ* tests can then be directly related to relative density, as well as stresses applied to the boundary of the sample. Since strength parameters are primarily defined as a function of the same quantities (i.e. density and stress level), the results of *in situ* tests carried out in the calibration chamber can be used to determine engineering properties of soils such as friction angle.

The strength parameters of the sample in the chamber were investigated. Drained triaxial compression tests were carried out, and triaxial peak friction angles determined. Certain aspects of sand behaviour are now briefly discussed, as are their effects on the interpretation of calibration chamber tests.

3.2 - Soil Properties

Leighton Buzzard sand was used as the standard granular soil for the experiments. The mechanical behaviour of this sand is well documented by high quality experimental data from tests performed under conditions of plane strain (Cole, 1967; Stroud, 1971; Bhudu, 1979) and direct shear (Jewell, 1980; Palmeira, 1987). However, different consignments of this sand can exhibit slightly different strength and dilatancy behaviour (Jewell, 1980; Sladen *et al*, 1985; Arthur and Dunstan, 1988). Direct shear box data on dense sand showed variations of friction angle of up to 3° from batch to batch of the same type of Leighton Buzzard sand, as reported by Arthur and Dunstan (1988).

Two separate batches of Leighton Buzzard sand have been used in model tests at the Oxford Soil Mechanics laboratory. The first discernible difference between these two sands is a yellow colouration of one, due to traces of ferric oxide, compared to the whitish colour of the other. The properties of the yellow sand were studied by Palmeira (1987) and its mechanical behaviour is described as being similar to the sand tested by Stroud (1971). A group of Casagrande direct shear tests was carried out as part of an investigation programme to determine the properties of the white Leighton Buzzard sand. Test results on dense samples (R_d from 86% to 96%) are presented in Figure 3.1, in which direct shear friction angles ϕ'_{ds} are plotted against mean effective stress S'. Also plotted in Figure 3.1 are results obtained from Casagrande direct shear tests on the yellow sand (Palmeira, 1987) and direct shear tests carried out on white and yellow sands using a medium size (253 x 152 x 152mm) shear box (Pedley, 1990). The yellow sand exhibits considerably higher peak friction angles ϕ'_{ds} at low confining pressures (up to 100 kPa). Differences between ϕ'_{ds} values measured on the yellow and white sands decrease with increasing mean effective stress. The same tests seem to indicate that the critical state line of the two sands is approximately the same. Therefore variations on the peak friction angles are related to the rate of dilation during shear, which is thought to be due to differences in angularity of the individual grains.

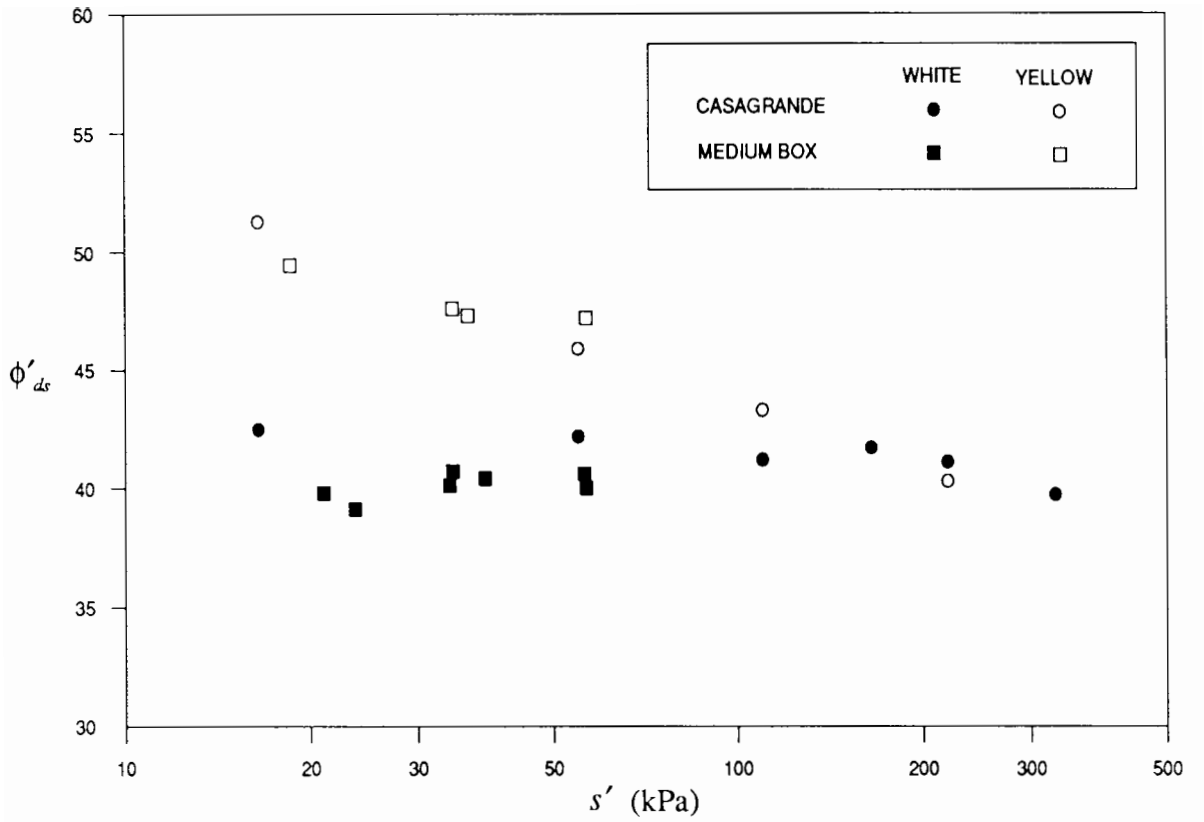

Figure 3.1 - Results of direct shear tests carried out on dense Leighton Buzzard sand

Since variations of strength and dilatancy behaviour were clearly observed, a comprehensive investigation on the mechanical behaviour of the white Leighton Buzzard sand was performed. First the index properties of the sand were determined. The specific gravity of the grains is 2.65 and the grading passing between the British Standard No 14 and No 25 sieves is shown in Figure 3.2. It is a very uniform sand (Coefficient of Uniformity CU = 1.3) and the mean grain size D_{50} is 0.8 mm. The individual grains are mostly quartz minerals with subangular to subrounded shapes. The limiting voids ratios are e_{min} = 0.479 and e_{max} = 0.774. Different procedures were used to measure the maximum and minimum voids ratio (Kolbuszewski, 1948; American Society for Testing Materials, 1982). The value of e_{min} was best estimated by a method that involves pouring oven-dried soil into a container (ASTM, 1982), while e_{max} was not significantly affected by test procedure.

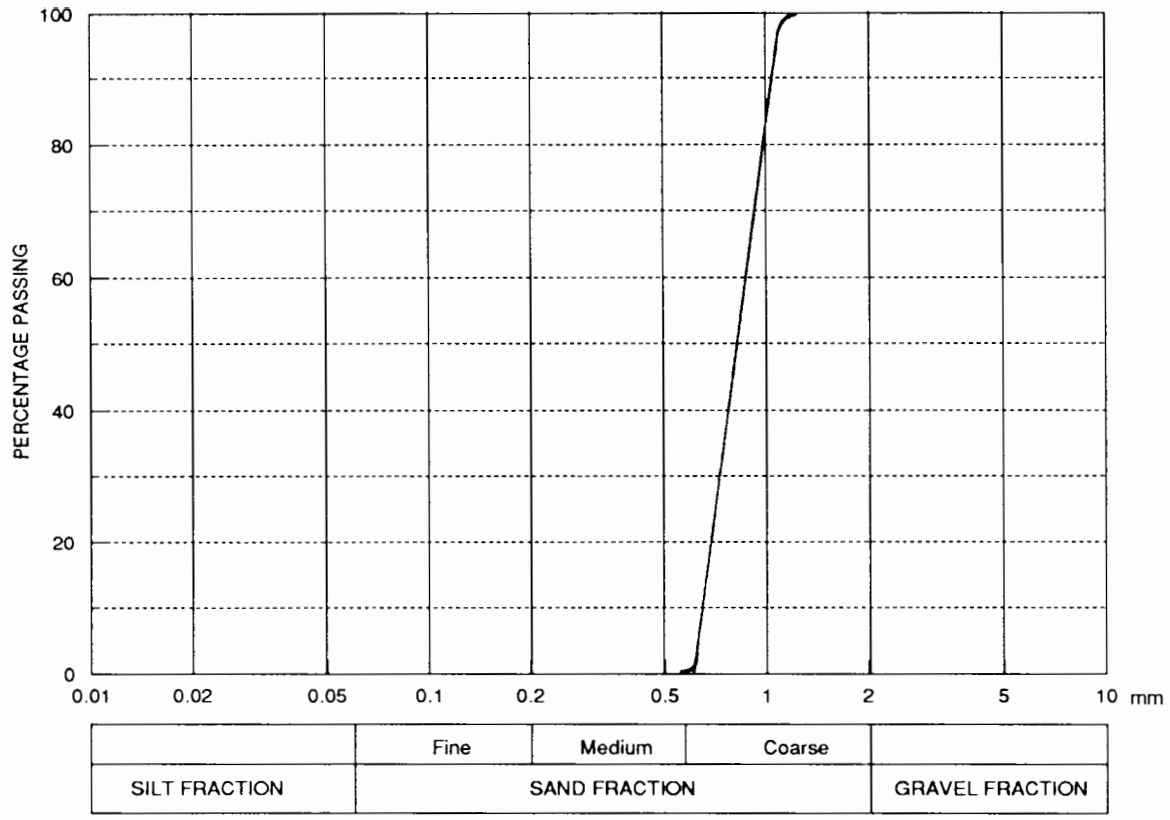

Figure 3.2 - Particle size distribution

The strength parameters of the sand were then determined by triaxial tests. Comparisons between triaxial friction angles and results of both cone penetration and pressuremeter limit pressure are a common practice in the interpretation of calibration chamber tests. This practice is basically adopted due to the extensive use of triaxial data in engineering design. Boundary conditions of *in situ* tests are often rather complex and an axi-symmetric test cannot be directly related to the mechanism of cone penetration. Pressuremeter expansion is more likely to be modelled by plane strain conditions.

A series of eleven drained triaxial compression tests was carried out on specimens which were initially 38 mm in diameter and 76 mm in height. Samples were prepared according to specifications described by Bishop and Henkel (1957). Sand was poured into a membrane vacuum-tensioned against a cylindrical former placed on the base of the triaxial cell. A cap

was placed on the specimen and secured to the membrane by an "O" ring. A small suction of approximate 5 kPa below the atmospheric pressure was then applied to the drainage line to give sufficient strength to the sample to stand while the split former was removed. The specimen was carefully measured and the cell body fitted and filled with de-aired water. The negative pressure was released and de-aired water was introduced through the bottom drainage line and allowed to seep slowly up through the sample, displacing most of the air to atmosphere through the top drainage line.

Cell pressure was applied in stages, each stage being held sufficiently long to allow variations in volume to occur. The last cell increment was applied under undrained conditions, and pore pressure was measured. The degree of saturation was checked by calculating the ratio between the increment of pore pressure and cell pressure (Skempton's parameter B). The value of B was found to be from 0.97 to 1.00 in most cases, indicating that specimens were virtually saturated. The excess of pore pressure was then released and a drained triaxial test carried out at a constant displacement rate (assuming 95% of equalization of pore pressure dissipation throughout the specimen, as suggested by Bishop and Henkel (1957)).

During consolidation and compression stages a volume gauge was connected to the back pressure line for measuring the volume of water moving into or out of the sample. The actual volume of the sample was known at any moment during test, as were the voids ratio and relative density.

Tests were performed on samples prepared to three initial densities: loose (R_d of about 30%), medium (R_d ~ 60%) and dense (R_d ~ 85%). Specific densities were achieved by a combination of flow rate and height of fall, using different sized funnels fixed at specific heights from the top of the former. The confining pressure σ_3 was selected in a range of 25 kPa to 400 kPa. The range of stresses and densities was chosen to enable soil properties measured in the triaxial

tests to be directly related to the properties of samples in the calibration chamber. Triaxial test results are presented in Table 3.2 and typical relationships between stress, strain and volume change are shown in Figures 3.3, 3.4 and 3.5 for loose, medium and dense sand respectively.

The results of triaxial tests clearly illustrate some basic aspects of the stress-dilatancy behaviour of granular materials. Dense samples tested under confining pressures in the range of 50 kPa to 400 kPa showed a peak in the stress-strain curve, followed by softening as the sand dilates. Loose samples reached a flat maximum stress after about 15% axial strain and a slight dilatancy was observed during shear for the range of stresses tested. Medium samples behaved somewhere in between the dense and loose states. It is clear that no ultimate state had been reached, since the samples were still expanding at the end of the tests. Nevertheless evidence exists that the soil in rupture zones will fully dilate to achieve a critical state, at which the soil deforms continuously at constant effective stress and voids ratio (Roscoe *et al*, 1958 and Schofield and Wroth, 1968).

Rd (%)	e_i	σ_3	$\sigma_{1failure}$	$p'_{failure}$	ϕ'_p	ψ_{max}
29	0.694	25.0	101.0	50.3	37.1	4.5
35	0.675	50.0	190.0	96.7	35.7	4.0
25	0.702	100.0	374.0	191.3	35.3	3.0
59	0.601	50.0	210.0	103.3	38.0	7.3
59	0.599	100.0	422.0	207.3	38.1	7.0
59	0.601	200.0	808.0	402.7	37.1	5.9
56	0.614	400.0	1540.0	780.0	36.0	6.0
90	0.513	50.0	248.0	116.0	41.6	12.6
86	0.519	100.0	506.0	235.3	42.1	12.6
84	0.532	200.0	1014.0	471.3	42.1	12.5
83	0.537	400.0	1800.0	866.7	39.5	10.5

Table 3.2 - Drained triaxial compression tests

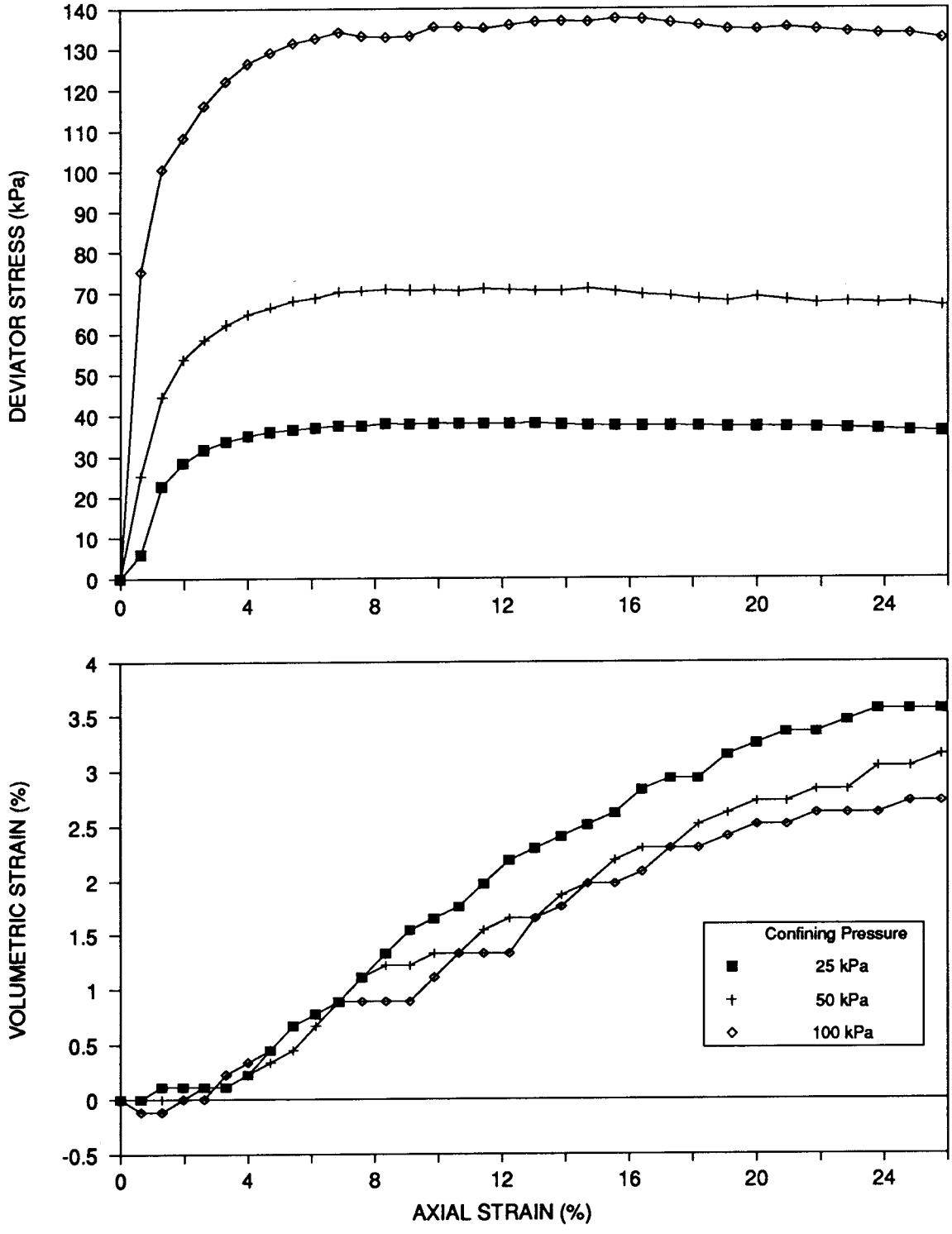

Figure 3.3 - Typical relationships between stress, strain, and volume change for loose sand

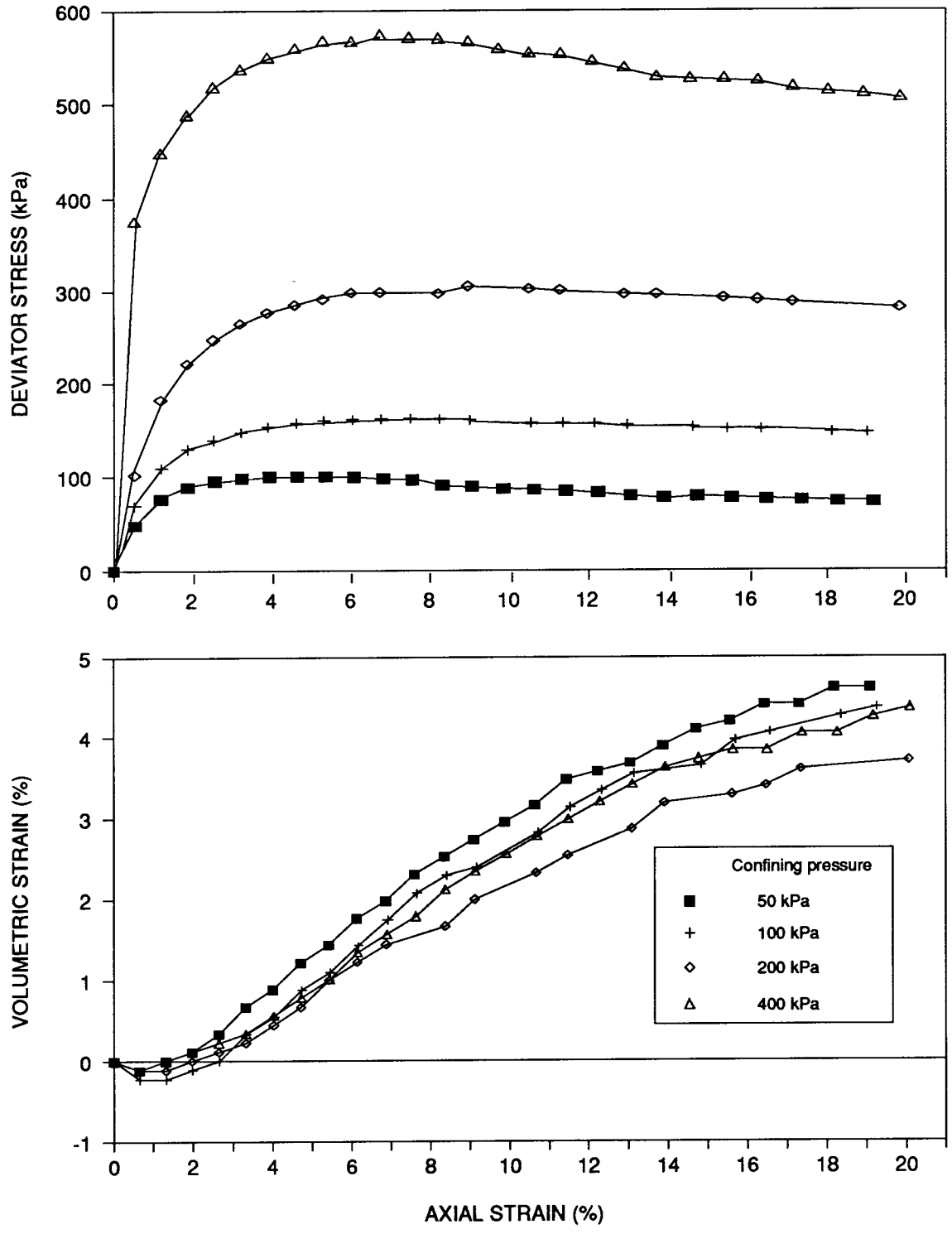

Figure 3.4 - Typical relationships between stress, strain, and volume change for medium sand

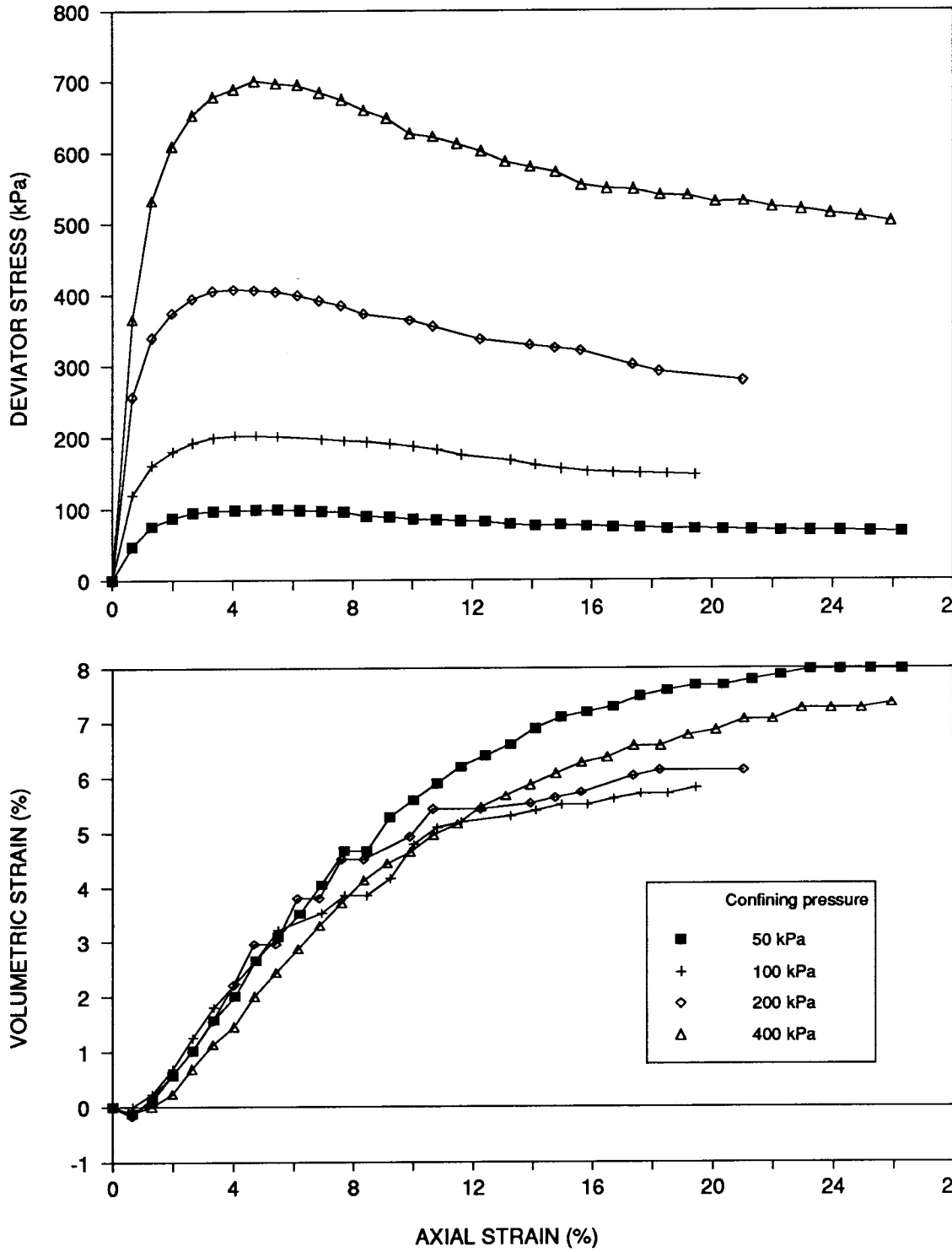

Figure 3.5 - Typical relationships between stress, strain, and volume change for dense sand

The most important consideration of the shear strength behaviour of cohesionless soils is the non-linearity of the failure envelope (e.g. De Beer, 1965; Vesic and Clough, 1968). The angle of friction of a given sand is not uniquely defined but depends on the magnitude of the effective normal stress on the failure plane at failure. This behaviour is illustrated by the values of peak secant friction angles ϕ'_p presented in Table 3.2, in which for a given sand density ϕ'_p decreases with increasing mean effective stress.

Two recent methods have been developed for describing sand behaviour (Been and Jefferies, 1985; Bolton, 1986), in which density and stress level are combined in a unique way for each sand. These approaches were validated by a large laboratory database and were later extended for the interpretation of cone penetration tests (Houlsby and Hitchman, 1988; Jamiolkowski *et al*, 1988). The two methods are now examined to investigate their application on the interpretation of triaxial data, and their potential use to support correlations with cone-pressuremeter test results.

A simple semi-empirical formulation has been proposed by Bolton (1986, 1987), which approximates Rowe's stress-dilatancy theory (Rowe, 1962). The shear strength of cohesionless soils is related to the critical state angle of shearing resistance and to the rate of dilatancy at failure, which in turn depends on relative density, level of mean effective stress and soil compressibility. Based on extensive laboratory data, the triaxial peak secant friction angle ϕ'_p was estimated as:

$$\phi'_p = \phi'_{cv} + 3I_r \qquad [3.1]$$

where ϕ'_{cv} is the critical friction angle and I_r is a "relative dilatancy index" given by:

$$I_r = R_d\left[\left(Q - \ln\frac{p'}{kPa}\right) - 1\right] \qquad [3.2]$$

where R_d is the relative density, p' the mean effective stress at failure and Q a constant depending on the compressibility and mineralogy of the sand. Bolton (1986) suggested a general value of Q= 10 for most silica sands.

Results of triaxial tests carried out on Leighton Buzzard sand were used to validate Bolton's theory. The value of the critical friction angle ϕ'_{cv} was determined from the relationship between measured peak triaxial friction angles ϕ'_p and the corresponding rate of dilation at failure, so that a value consistent with zero dilation could be assessed (Figure 3.6). A value of ϕ'_{cv} of approximately 33° was obtained. However, the empirical relationship between peak friction angle and dilation angle proposed by Bolton (1986)

$$\phi'_p - \phi'_{cv} = 0.8\psi \qquad [3.3]$$

overestimates $(\phi'_p - \phi'_{cv})$ by about 10% (see Figure 3.6).

The values of peak friction angle for each test were then predicted from the combination of equations [3.1] and [3.2], adopting $\phi'_{cv} = 33°$. A comparison between measured and predicted triaxial friction angles is presented in Figure 3.7. On average, Bolton's formula underpredicts ϕ'_p by about 1.1°, which may be explained by the differences on the values of $(\phi'_p - \phi'_{cv})$ obtained from triaxial tests and suggested by equation [3.3]. The scatter observed on the measured values of ϕ'_p is attributed to the natural difficulties of carrying out triaxial tests in sand (Bishop and Henkel, 1957; Lee and Seed, 1967; Head, 1986).

A non-linear regression analysis was performed using a combination of equations [3.1] and [3.2] to determine the coefficients that produce the best-fitting line for the relationship between measured triaxial friction angles ϕ'_p and relative density and stress level. Values of $\phi'_{cv} = 34.3°$

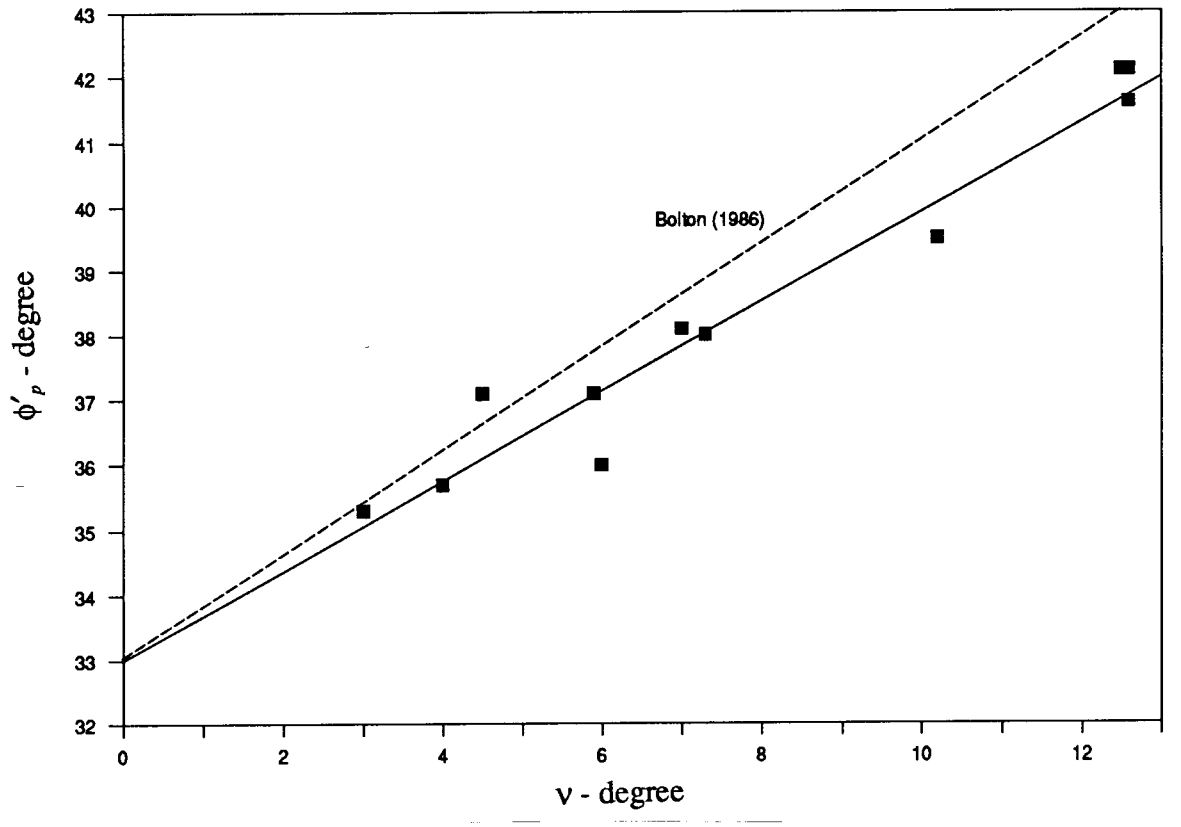

Figure 3.6 - Stress-dilatancy relationship

and Q = 9.9 produced such a result and will be used later in this work to support relationships between cone-pressuremeter testing data and peak friction angles. On average the best-fitting analysis predicts the values of ϕ'_p within approximately 1°.

The critical friction angle obtained from the regression analysis is similar to that determined from Figure 3.6 (with a difference of 1.3°). For Leighton Buzzard sand the empirical parameter Q was found to be very similar to 10, as proposed by Bolton (1986). Jamiolkowski and Robertson (1988) presented a similar study for Hokksund sand. Although Hokksund sand is a predominantly silica sand, Bolton's formulation underpredicts friction angles by about 2° to 3°. It is thus suggested that there is a need to define the empirical constant Q in relation to mineralogy and compressibility for a more general and accurate use of the formulation.

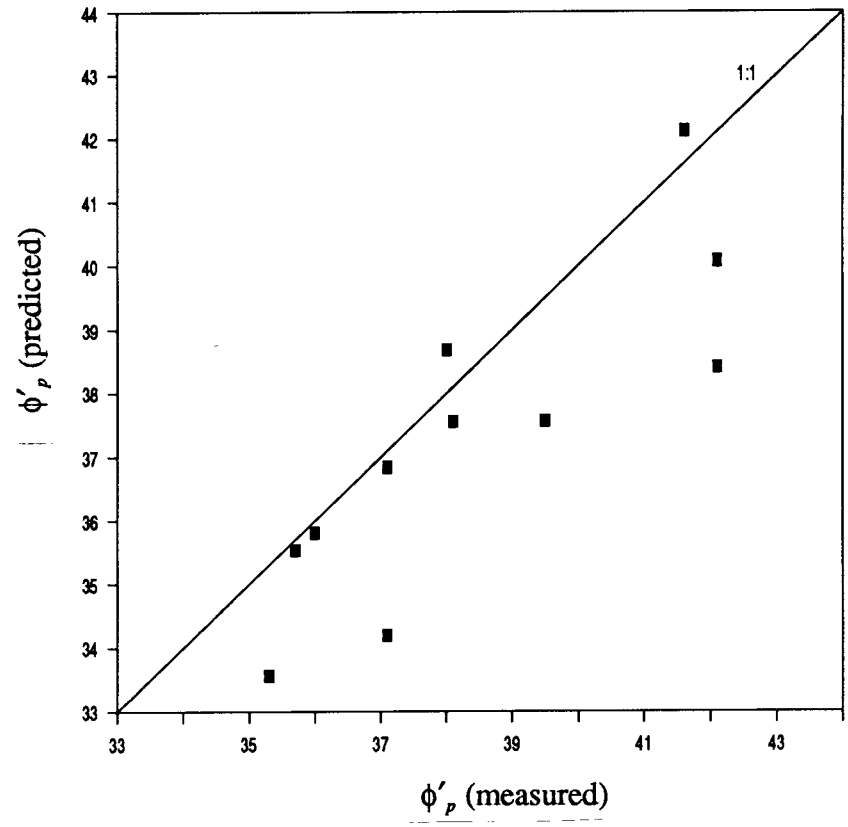

Figure 3.7 - Evaluation of peak triaxial friction angles for Leighton Buzzard sand using Bolton's stress dilatancy theory

Another method for predicting triaxial friction angles has been suggested by Been and Jefferies (1985) and Been *et al* (1986, 1987) using the concept of the state parameter ψ to describe the condition of a sand. The state parameter is defined as the difference between the voids ratio e of the sand and its void ratio e_{ss} at the "steady line" at the same mean effective stress p'and is in concept embodied in critical state theory (the parameter ψ is the same as $(v_\lambda - \Gamma)$ as defined by Schofield and Wroth (1968)). This approach requires the independent measurement (or estimation) of the *in situ* horizontal stress σ'_h and laboratory tests to determine the slope of the steady state line (plotted as voids ratio e against $\log_{10}$ p'). For a broad class of sands comprising subrounded to subangular particles a relationship between peak friction angle and state parameter has been developed and is expressed as:

$$\phi'_p = 32\left(1 - \frac{5}{3}\psi\right) \qquad [3.4]$$

Triaxial tests on Leighton Buzzard sand failed to produce a plot of the critical state line, because samples were still expanding at the end of tests (axial strains of about 20%). In order to estimate the state parameter for these tests, the critical state line determined from plane strain tests was used (Stroud, 1971)

$$e_{ss} = 0.88 - 0.06 \log_{10}[p'/kPa] \qquad [3.5]$$

A comparison between triaxial tests on Leighton Buzzard sand and the critical state line reported by Stroud (1971) has been presented by Sladen *et al* (1985). Although some scatter is observed, the triaxial data obtained at critical state conditions generally fall within the range of Stroud's data. This evidence suggested that plane strain and triaxial conditions at critical state may be similar, which support the use of equation [3.5] to determine the state parameter from triaxial test data. It is recognized that stress path and small differences in material properties may affect the location of the critical state line, and therefore state values cannot be used with complete confidence.

Figure 3.8 shows a plot between friction angles measured from triaxial tests and friction angles predicted from equation [3.4]. The predicted values are consistently higher than the measured values of friction angle (with two exceptions), and on average this approach tends to overestimate the friction angle by about 3°.

Triaxial data and its interpretation indicated that it is no longer adequate practice to express sand behaviour as a function of relative density only. The concepts of critical state theory (Schofield and Wroth, 1968) redefined as the "state parameter" by Been and Jefferies (1985) and the concept of "dilatancy index" proposed by Bolton (1986), in which density and stress

level are combined in a unique way for each sand, are more appropriate. This argument has important effects on the applicability of chamber tests to *in situ* conditions. Calibration tests are usually not carried out on the sand actually encountered in the field and an assumption has to be made that different clean quartz sands will have a similar response to field tests. The methods proposed by Been and Jefferies (1985) and Bolton (1986) have been successfully applied to predict sand behaviour for a wide range of subangular to subrounded sands and they both produced satisfactory results in determining strength parameters for Leighton Buzzard sand. If a calibration chamber derived correlation is to be used in the field, then a normalizing variable such as the state parameter or the dilatancy index should be used to link *in situ* tests to engineering properties of soils. This approach is addressed in Chapter 5 for the interpretation of cone-pressuremeter test results.

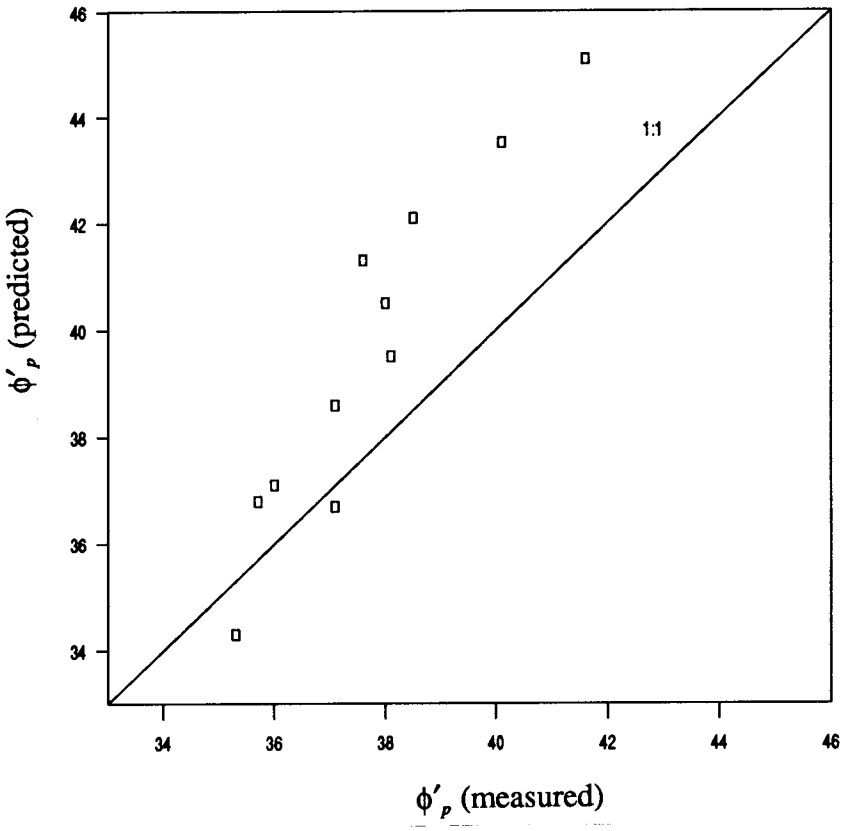

Figure 3. 8 Evaluation of peak triaxial friction angles for Leighton Buzzard sand using state parameter

CHAPTER 4

TEST PROGRAMME AND EXPERIMENTAL RESULTS

The parameters that affect the test results in the calibration chamber are examined, and a test programme to assess the influence of relative density, horizontal stress and vertical stress on the cone-pressuremeter testing data is established. Essential features of the progress of a test are presented and certain quantities extracted from the results are given.

4.1 - Test programme

This chapter presents a detailed discussion of the methodology adopted to establish a laboratory testing programme to study the cone-pressuremeter test in sand. Since the results of *in situ* tests depend on the strength, stiffness and permeability of the ground, as well as the *in situ* stresses, a well defined programme of calibration should consider the influence of these parameters on test data.

Chamber tests provide an opportunity for a systematic examination of testing results by controlling most of the variables that affect the parameters listed above. In the chamber a sample of a known material is tested under strictly controlled boundary conditions. Relative density, effective stresses, stress history and degree of saturation of the sample are the variables selected and controlled in the chamber. These variables (except degree of saturation) were examined in order to assess their independent effect on the cone-pressuremeter data, to enable correlations to engineering properties in granular soils to be established.

In granular materials *in situ* tests are often carried out to evaluate the drained shear strength expressed as the friction angle, ϕ'. The friction angle depends on relative density, level of mean effective stress, and soil compressibility (see for example Rowe, 1962), as discussed in Chapter 3. Tests were therefore primarily designed to investigate the effects of stresses and density on the results obtained with the cone-pressuremeter. Tests were carried out at three densities, with the density being controlled by adjusting the rate of flow at which the sand was rained from a hopper into the chamber (see Chapter 2). The densities achieved were loose (R_d of 16% to 30%), medium (60% to 68%) and dense (83 to 89%). For each density a range of stress states was studied. In order to separate the effects of stress level and stress ratio, tests were carried out at three mean effective stresses of 50 kPa, 100 kPa and 200 kPa and at three stress ratios, $K = \sigma'_h/\sigma'_v$, corresponding to 0.5, 1.0 and 2.0. The stress points tested are shown in Figure 4.1 and detailed in Table 4.1. Seven combination of stresses were selected, but there was no attempt to fulfil all the possible combinations using the three cone-pressuremeter devices. Instead a main series of tests was performed using the 10 cm^2 device and complementary tests were carried out with the 15 cm^2 and 5 cm^2 pressuremeters. A maximum mean effective stress of 200 kPa was used in the tests due to the limited thrust and inflation pressure capacity of the cone-pressuremeter (as discussed in Chapter 2). The combination of stresses applied to the samples corresponds to field tests carried out to depths up to approximately 20 m.

The stress history of a sand deposit is simulated in the calibration chamber by means of mechanical overconsolidation of samples stressed under conditions of zero lateral strain (c.f. Bellotti *et al*, 1982). Recent work on the dilatometer (Bellotti *et al*, 1986; Houlsby, 1988) and cone penetrometer (Bellotti *et al*, 1986) has shown that a cycle of overconsolidation was found to have a negligible effect on test results. In addition a limited range of values of the ratio σ'_h/σ'_v is observed at the end of the cycles. With the purpose of assessing the influence of horizontal and vertical stresses independently on cone resistance and pressuremeter limit

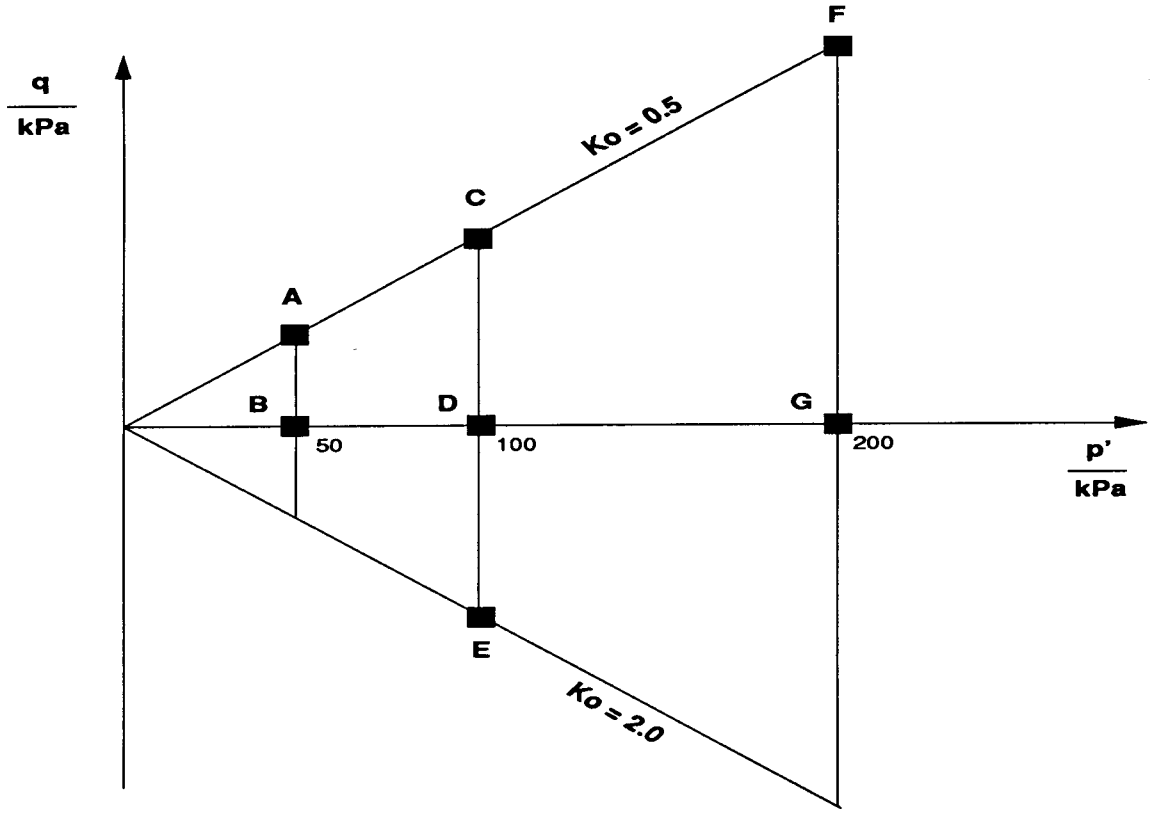

Figure 4.1 - Nominal stress states used in sand tests

POINTS	σ'_v kPa	σ'_h kPa	p' kPa	q kPa	Ko
A	75.0	37.5	50.0	37.5	0.5
B	50.0	50.0	50.0	0	1.0
C	150.0	75.0	100.0	75.0	0.5
D	100.0	100.0	100.0	0	1.0
E	60.0	120.0	100.0	-60.0	2.0
F	300.0	150.0	200.0	150.0	0.5
G	200.0	200.0	200.0	0	1.0

Table 4.1 - Nominal stress states

pressure, an alternative approach was adopted, in which samples were stressed to a wide range of K values. The term K is here simply used to denote the ratio of σ'_h/σ'_v , and there is no implication intended that there was no lateral strain during the stressing of the sample. In practice high K values are associated with the cycle of overconsolidation, but this was not modelled in the tests, in all of which the stresses were equal to their past maximum values at the time of the test. The values of K in the range of 0.5 to 2.0 were chosen to cover the range of the coefficient of earth pressure at rest, K_o, measured in natural sand deposits. The measured values of K_o observed in normally consolidated deposits seem to agree well with the simplified Jaky equation (after Jaky, 1944)

$$K_o = 1 - \sin\phi' \qquad [4.1]$$

as reported by Schmidt (1966), Sherif *et al* (1974), Al-Hussaini and Townsend (1975), Al-Hussaini (1980) and Mayne and Kulhawy (1982). In overconsolidated deposits the authors reported values of K_o greater than unity, mainly in the range between 1 and 2.

Interpretation of *in situ* test results has always been made referring to either fully undrained (saturated cohesive deposits) or fully drained (cohesionless deposits) conditions. All tests reported in the present research work were performed on dry sand, hypothesizing that results can be applied to field deposits, usually saturated, considering that testing takes place under fully drained conditions. A limited number of comparative cone penetrometer tests carried out on dry and saturated samples on Ticino sand (Baldi *et al*, 1986; Bellotti *et al*, 1988) and Monterey sand (Villet and Mitchell, 1981) indicate a negligible effect due to full saturation on test results. As expected, no excess pore pressures are observed during penetration in saturated granular deposits, justifying the performance of laboratory test on dry samples.

The proposed methodology will allow a direct assessment of the influence of relative density, vertical effective stress and horizontal effective stress on results obtained with the cone-pressuremeter tested under drained conditions. Having established such a methodology it is important to mention the uncertainties involved in calibration chamber interpretation.

A first obstacle to the accurate interpretation of tests is the impossibility of adjusting the stiffness of the sand in the chamber independently to assess its influence on test data. The effect of stiffness on *in situ* test results has been theoretically demonstrated using cavity expansion theory (e.g. Teh, 1987; Yu, 1990). Since pressuremeter tests, as well as cone tests, may be understood at least partially as the expansion of a cavity in the soil, cone and pressuremeter test data are expected to vary with stiffness in the same way as the cavity expansion limit pressure.

Another uncertainty for the rational interpretation of tests is associated with the validity of the chamber testing approach. Chamber size effects, boundary conditions for stresses or strains imposed on the sample and sand type (tests are rarely, if ever, carried out in sands identical to those encountered *in situ*) are factors to be considered when establishing correlations to be applied to field conditions. Factors related to sand type were examined in Chapter 3 whereas boundary conditions and chamber size effects are discussed in Appendix 1.

4.2 - Experimental results

A total of 34 cone-pressuremeter tests has been carried out in the large calibration chamber. Only one test was carried out on each sample. Test results will be presented in this section using a combination of curves and tables. The former are intended to show essential features of test progress and the latter to indicate the values of certain quantities extracted from the results, as well as the relevant information associated with each test.

A simple system was adopted to identify each test, in which the instrument size, followed by the initial **CPMT**, to indicate a cone-pressuremeter test, and the test number, described in chronological sequence are indicated. Thus, for example, 10CPTM4 is the fourth cone-pressuremeter test carried out with the 10 cm^2 prototype. The general information related to each test is given in additional tables.

Note that the vertical and horizontal stresses shown earlier in Table 4.1 are nominal values for a reference position. The vertical pressure is applied to the base of the sample and therefore varies linearly from σ_v at the base to $\sigma_v - \gamma h$ at any height h above the base. For a unit weight of the sand, γ, of about 16 kN/m^3, and the height of the sample of 1.5 m, the vertical stress varies by approximately 24 kPa from top to bottom. The horizontal stress is applied through an air-water interface placed about 300 mm above the base of the chamber. Since the chamber is confined laterally with a flexible rubber membrane which is water supported, the horizontal stress therefore varies according to a column of water, from σ_h at the interface level to $\sigma_h \pm \gamma_w z$ at any height z above or below the interface level.

A detailed description of the experimental results is now presented. As far as the tests are concerned, the study is divided into two sections: cone penetrometer testing results and pressuremeter testing results.

4.2.1 - Cone penetrometer testing results

The test procedure adopted in this research has already been described in Chapter 3. After the sand had been stressed to the appropriate condition, the cone-pressuremeter was driven into the sample at a standard penetration rate of 20 mm/s. Cone resistance, q_c, and penetration depth were measured every half second to produce profiles of q_c against depth. Insertion was stopped when the centre of the pressuremeter module was at the midheight of the chamber. As dry

sand was used, total and effective stresses were therefore identical in the calibration chamber and no distinction is necessary between the measured cone resistance q_c and the total cone resistance q_t.

At the end of each test, the file containing the raw data (i.e. the voltages corresponding to every channel for every scan) were stored on a $5\frac{1}{4}$" floppy disk. These data were then processed on a spreadsheet (Lotus 123). The voltage corresponding to each transducer and its respective calibration coefficients were used to calculate tip cone resistance and displacements throughout the test.

A typical example of two profiles of q_c against depth is shown in Figure 4.2, in which two identical tests carried out under the same stress conditions (p'= 100 kPa, K_o= 1.0) and approximately the same density are presented. The results illustrate the high degree of experimental control and the excellent repeatability of tests which could be achieved in the calibration chamber. The typical characteristics that may be noted from the profile are: an initial section, in which resistance increases with depth (and is probably influenced by the proximity of the top plate); a central section in which resistance is essentially constant or experiences a small variation with local stresses; and a final section, in which readings are affected by the proximity of the bottom plate. However, in the central section, cone resistance is not as constant as theoretically expected and the cone profiles are found to have characteristic shapes that reflect density, boundary conditions (Parkin and Lunne, 1982; Houlsby and Hitchman, 1988) and stress ratio. From the cone profile the value of q_c measured at the midheight of the chamber had to be extracted for correlations with pressuremeter limit pressure and soil parameters. This particular depth corresponds to the position of the centre of the pressuremeter in the chamber after penetration, so that cone resistance and pressuremeter limit pressure can be directly correlated under the same stress conditions. Two criteria were adopted to calculate cone resistance: to average the values of q_c measured 250 mm above and below

the midheight of the chamber and to choose a single value corresponding to q_c at the chamber midheight (750 mm from the top plate). Values reported in this chapter are defined by the first criterion, although the two criteria led to virtually the same results.

A testing methodology was established in the previous section to investigate the influence of relative density, stress level and stress ratio on the cone-pressuremeter testing data. Results presented in Figures 4.3 to 4.5 show the independent effect of each of these quantities on cone results. Consistent behavioural patterns are evident, although some characteristic shapes can be observed as noted earlier in this section. Figure 4.3 shows the influence of relative density on q_c for tests carried out under the same stress conditions (p'= 100 kPa and K_o = 1.0), whereas Figure 4.4 shows the influence of mean effective stress on q_c for tests performed at the same stress ratio (K_o = 0.5) and about the same density (from 62% to 68%). A trend of increasing tip cone resistance with increasing density and increasing mean effective stress is clearly observed. This behaviour has been addressed by researchers several times and results of a large number of tests in calibration chambers showed that relative density and mean effective stress are the most important variables influencing the tip cone resistance (Schmertmann, 1976; Villet and Mitchell, 1981; Baldi *et al*, 1982, 1986).

The influence of the stress ratio on cone resistance is presented in Figure 4.5, for tests carried out on dense samples at a mean effective stress of 100 kPa. The value of q_c increases with increasing stress ratio, even for tests carried out at the same mean effective stress. Recent developments on *in situ* testing interpretation (e.g Been *et al*, 1986; Wroth, 1988), as well as classical works on pile foundations (e.g Vesic, 1972,1977), suggest that point resistance is governed not by the vertical stress in the ground, but by the mean effective ground stress. The data shown in Figure 4.5 raises the question of which is the most suitable parameter with which to normalise the q_c values: the horizontal stress or the mean effective stress, in which

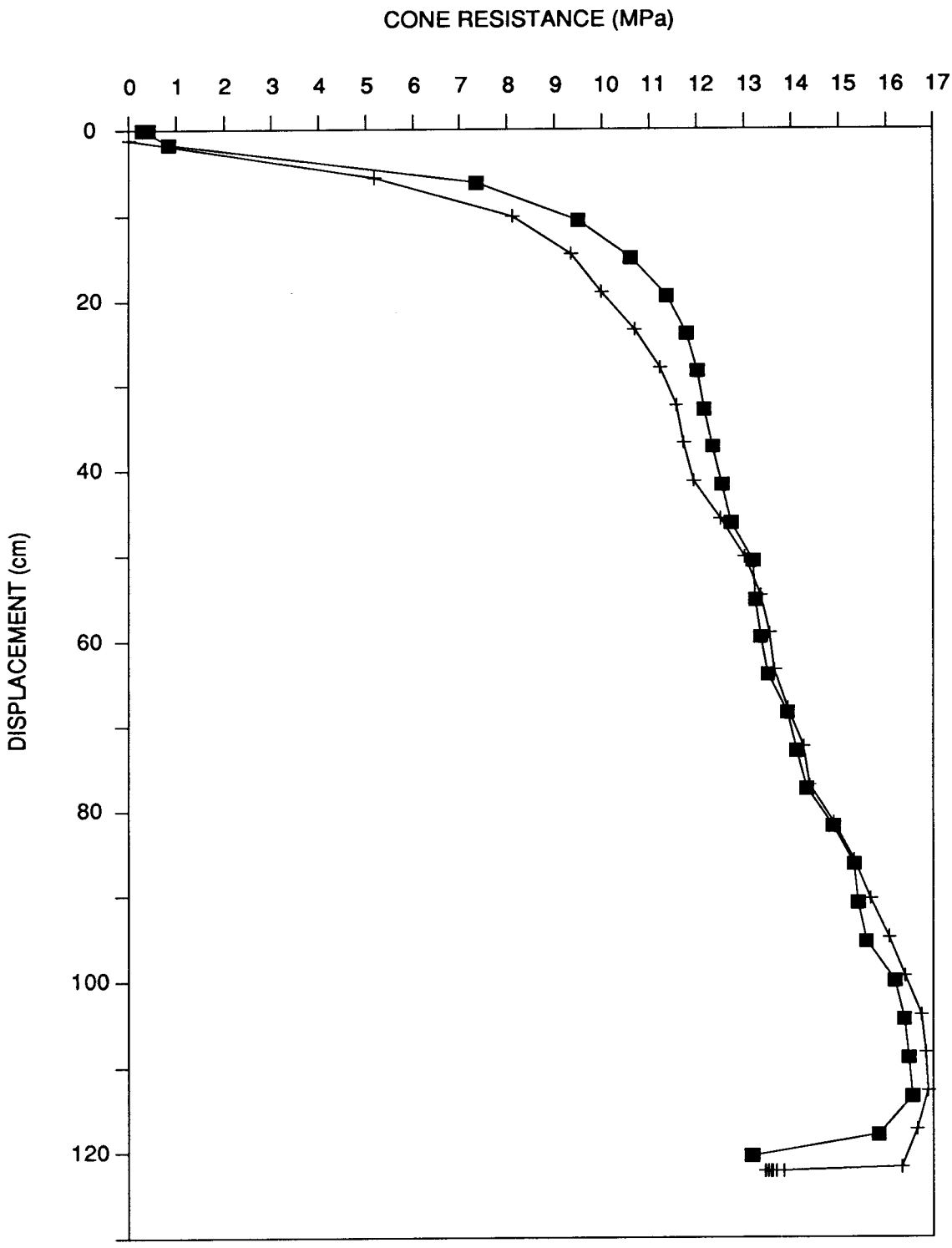

Figure 4.2 - Typical examples of profiles of tip cone resistance against depth (two identical tests carried out under approximately the same density and the same stress conditions - p'= 100 kPa and K_o= 1.0).

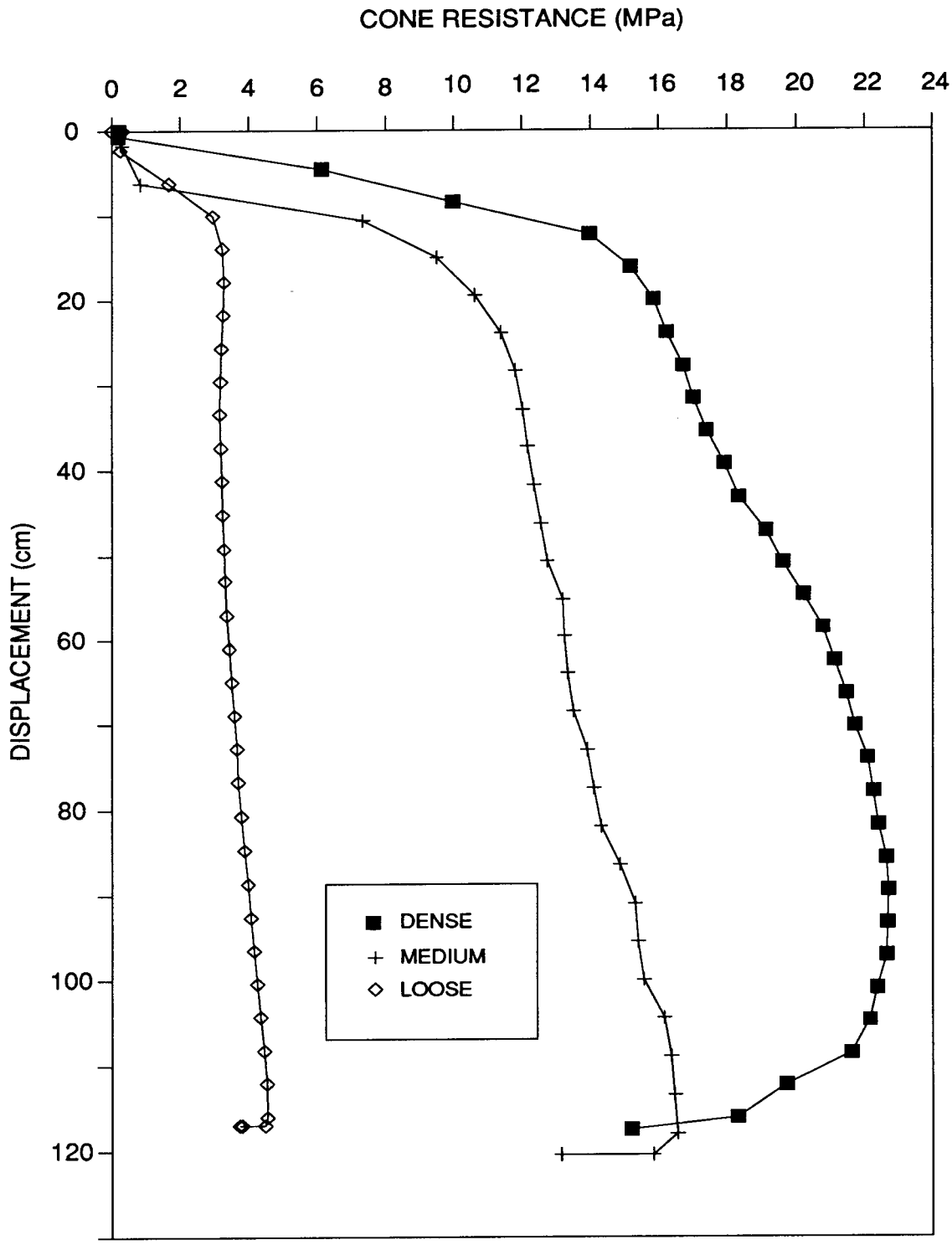

Figure 4.3 - Influence of relative density on a profile of tip cone resistance against depth.

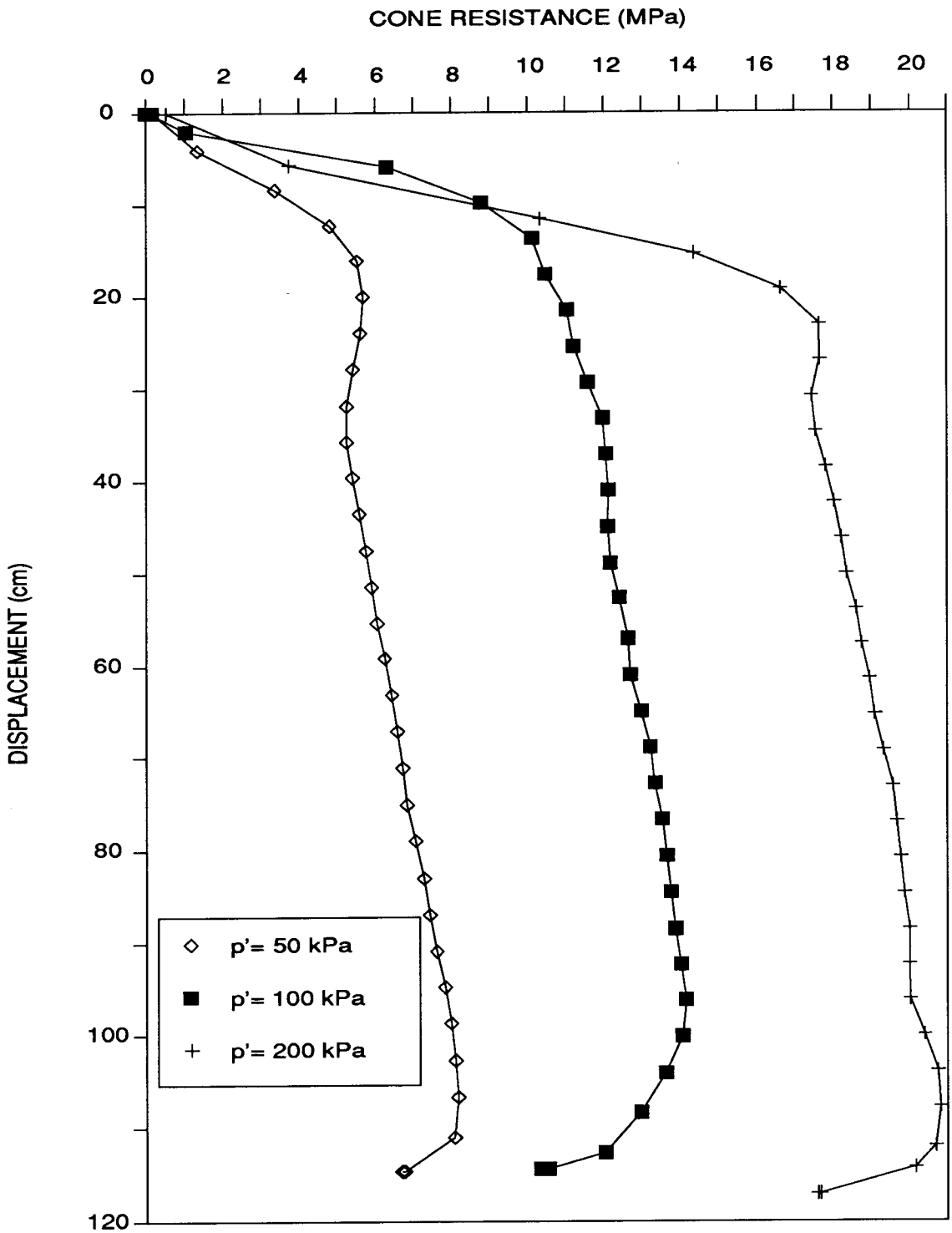

Figure 4.4 - Influence of mean effective stress on a profile of tip cone resistance against depth.

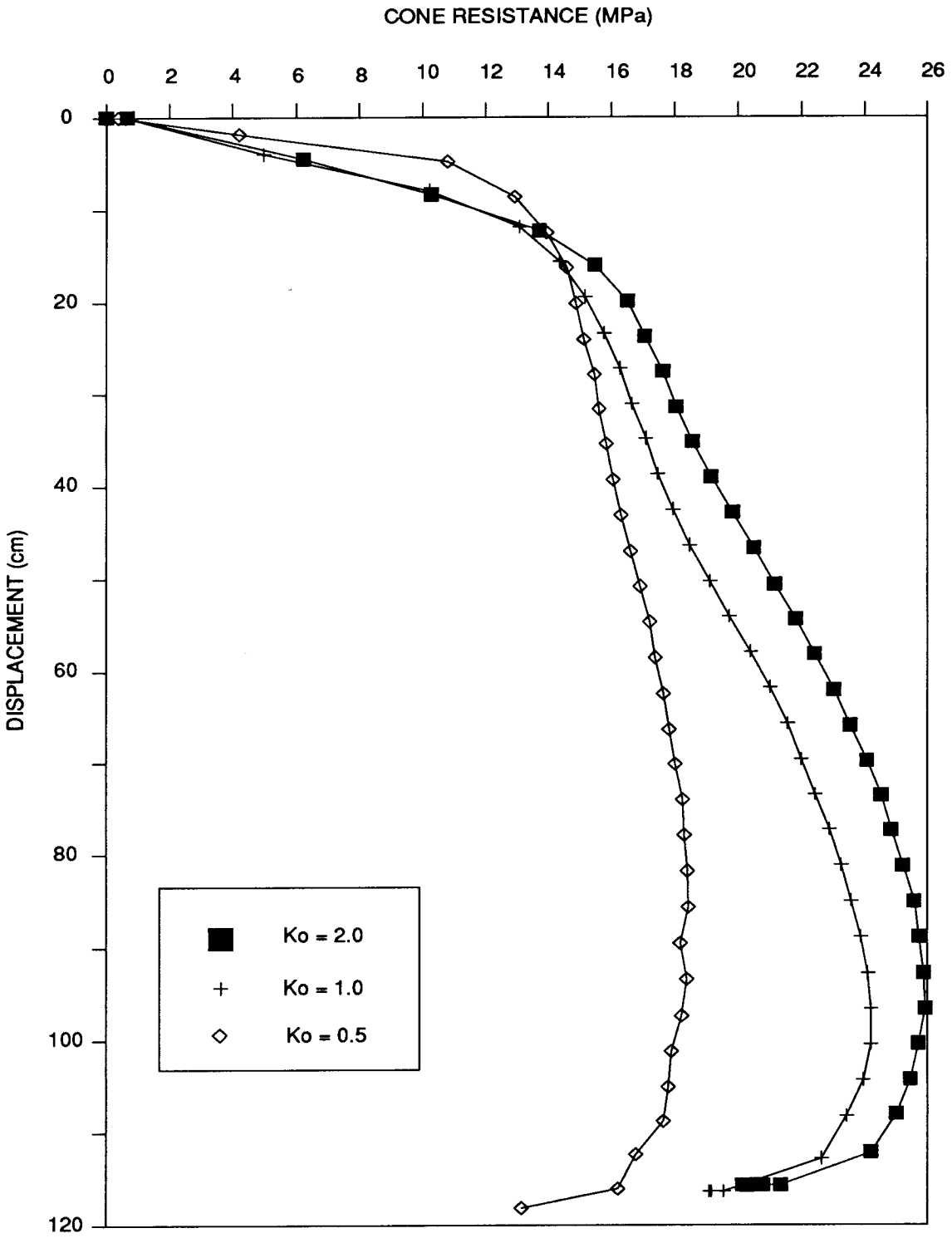

Figure 4.5 - Influence of stress ratio on a profile of tip cone resistance against depth.

effectively the horizontal stress is made twice as important as the vertical stress. This problem has been recently addressed by Houlsby and Hitchman (1988, 1989) and Been *et al* (1989). Houlsby and Hitchman (1988) carried out cone penetrometer tests in a large calibration chamber, in which cone resistance was normalized with respect to σ_h'. Normalizing with respect to p' produced reasonably consistent results, but not as clear as a result plotted in respect to the horizontal stress. Analysis of the pressuremeter data seems to confirm this evidence.

The values of q_c extracted from the calibration chamber tests are presented later in this chapter in Tables 4.4 and 4.5 together with the pressuremeter testing data.

4.2.2 - Pressuremeter testing results

The cone-pressuremeter device was pushed into the calibration chamber at a constant speed of 20 mm/s and cone resistance was measured during penetration. When the centre of the pressuremeter module was at the midheight of the chamber, insertion was stopped and a pressuremeter test was performed. The time between the end of cone penetration and the start of the pressuremeter test varied from 15 to 20 minutes.

Pressuremeter tests were performed under strain controlled conditions. Inflation pressure ψ was measured, as were the radial displacements ($R-R_o$) of the centre of the membrane and the variation of volume of the pressuremeter probe. Inflation and deflation rates of about 0.4% radial displacement per minute were selected for the tests. Since no constrains of time were imposed on laboratory tests, a low strain rate was chosen to reduce the effect of creep strains on the pressuremeter data (as discussed in Chapter 6). Generally, tests were interrupted three times during inflation to carry out small unload-reload loops and once during contraction to perform a reload-unload loop. Before carrying out a loop, cavity pressure was held constant until the cavity strain rate gradually reduced to zero. Loops were then carried out at very low

strains rates, of about ± 0.025%/min. The purpose of this was to minimize apparent large hysteresis of the loop, allowing most potential creep strains to occur before unloading and allowing a more accurate determination of shear modulus.

The pressuremeter membrane was usually inflated to 30% linear hoop strain $\varepsilon = \Delta R/R_o$, where ΔR was taken as the average readings of the three strain gauged arms. At this stage a well-defined plateau in the pressure-expansion curve had always been reached, corresponding to the limit pressure ψ_l.

At the end of each test, files containing raw data (i.e. voltages corresponding to every channel in every scan) were stored on a $5\frac{1}{4}$" floppy disk. These data were then processed through FORTRAN programs written by Dr. G.T. Houlsby to operate on IBM compatible micro-computers. The software calculated the pressuremeter pressure-expansion curve and the shear modulus taken from individual unload-reload loops, introducing the necessary corrections for membrane stiffness. The processing programs are summarized as follows:

Program VTOENG: Processed raw data (voltages) to convert them to engineering units. Inflation pressure, cavity strain (from individual and average readings of the three strain gauged arms) and cavity strain (from volume readings) were calculated. Cone-pressuremeter tests, as well as calibrations for membrane stiffness, were processed by the program.

Program SUBSET and CALUNL: These programs were used in association with a non-linear regression analysis to produce the best fit line of each calibration curve for correction of membrane stiffness. A complete description of this procedure is given later in this section.

Program SUBCAL: Subtracted the curve fitting analysis produced by CALUNL to account for membrane stiffness from the pressuremeter testing data to obtain a corrected pressure-expansion curve.

Program MODCAL: Input the corrected pressure-expansion curve produced by SUBCAL to calculate the values of shear modulus from the slope of unload-reload loops. A detailed description of the program, the criteria adopted to calculate the slope of loops and the interpretation of the shear modulus are presented in Chapter 6.

Calibrations of the pressuremeter were considered an essential operation to obtain a correct pressure-expansion curve. Periodically (every two to three tests) the device was calibrated to take account of errors from the instrument's accuracy, pressure losses and membrane corrections, as recommended by Windle (1976), Baguelin *et al* (1978) and Mair and Wood (1987). Calibrations for compliance of the instrument were found to be an essential operation for the correct interpretation of the shear modulus and are described in Chapter 6. As far as membrane corrections is concerned, calibration tests were made as a simulation of a real test, obtained by inflating the membrane in air with the "chinese lantern" fitted. Figure 4.6 shows a typical example of one such a calibration, in which it is possible to observe that the loading and unloading sections are approximately parallel curves. For a computer manipulation of these data the following procedure was adopted.

Program SUBSET obtained a subset of data for analysis of the loading section of the calibration curve. A curve fitting of the loading section was performed using a non-linear regression analysis. The model which was found to represent best the results was a three-parameter hyperbola

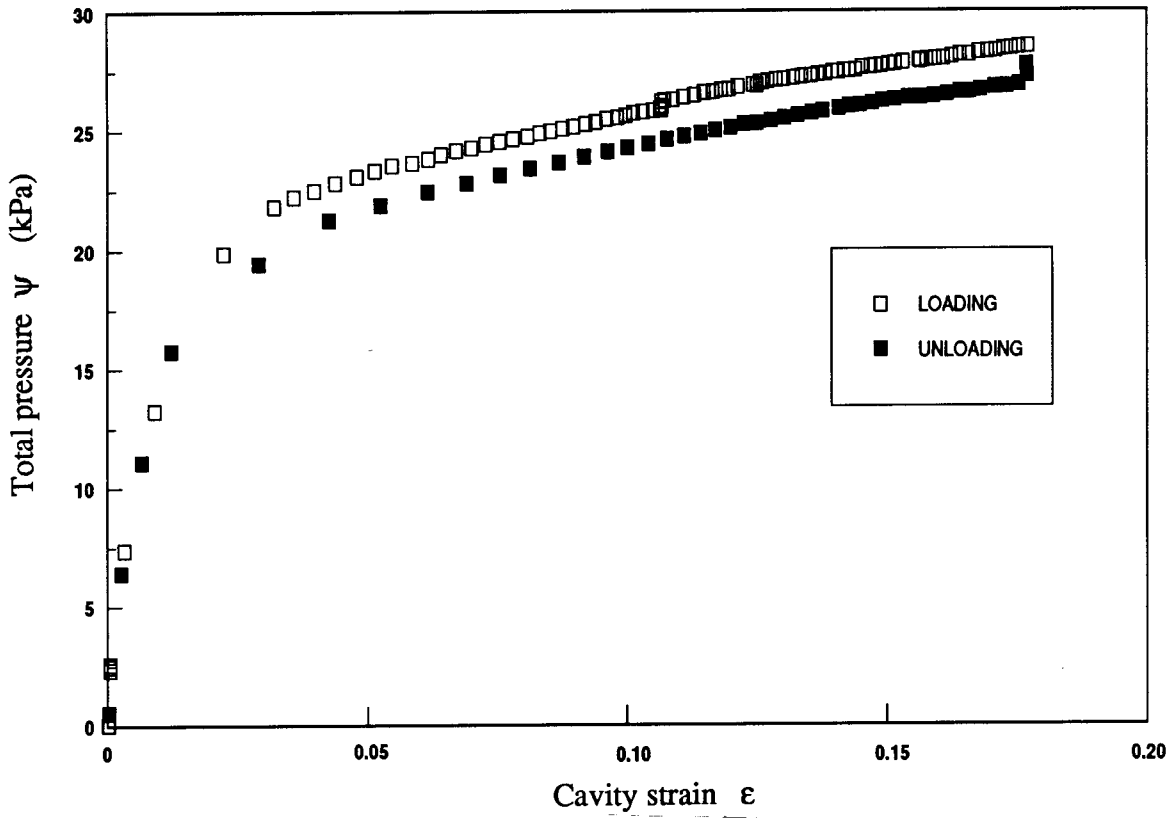

Figure 4.6 - Typical calibration curve for correction of membrane stiffness.

$$\psi = \frac{\varepsilon}{\frac{1}{a} + \frac{\varepsilon}{b + c\varepsilon}} \qquad [4.2]$$

passing through the origin and having one asymptote parallel to the vertical axis and the other inclined with a slope K_2 with respect to the horizontal axis, as illustrated in Figure 4.7. The vertical asymptote intercepts the horizontal axis at $\varepsilon = -b/(a+c)$ and the other intercepts the vertical axis at $\psi = a^2 b/(a+c)^2$. The slope of the tangent to the origin is

$$K_1 = \left[\frac{d\psi}{d\varepsilon}\right]_{\varepsilon=0} = a \qquad [4.3]$$

and at $\varepsilon \rightarrow \infty$ (inclined asymptote)

$$K_2 = \left[\frac{d\psi}{d\varepsilon}\right]_{\varepsilon\to\infty} = \frac{ac}{a+c} \qquad [4.4]$$

The tangent at the origin intercepts the inclined asymptote at point F, with coordinates

$$\varepsilon_f = \frac{b}{a+c} \quad \text{and} \quad \psi_f = \frac{ab}{a+c} \qquad [4.5 \text{ and } 4.6]$$

Equation [4.2] can also be written as a direct function of K_1, K_2 and ψ_f

$$\psi = K_1\varepsilon\left[\frac{\psi_f + K_2\varepsilon}{\psi_f + K_1\varepsilon}\right] \qquad [4.7]$$

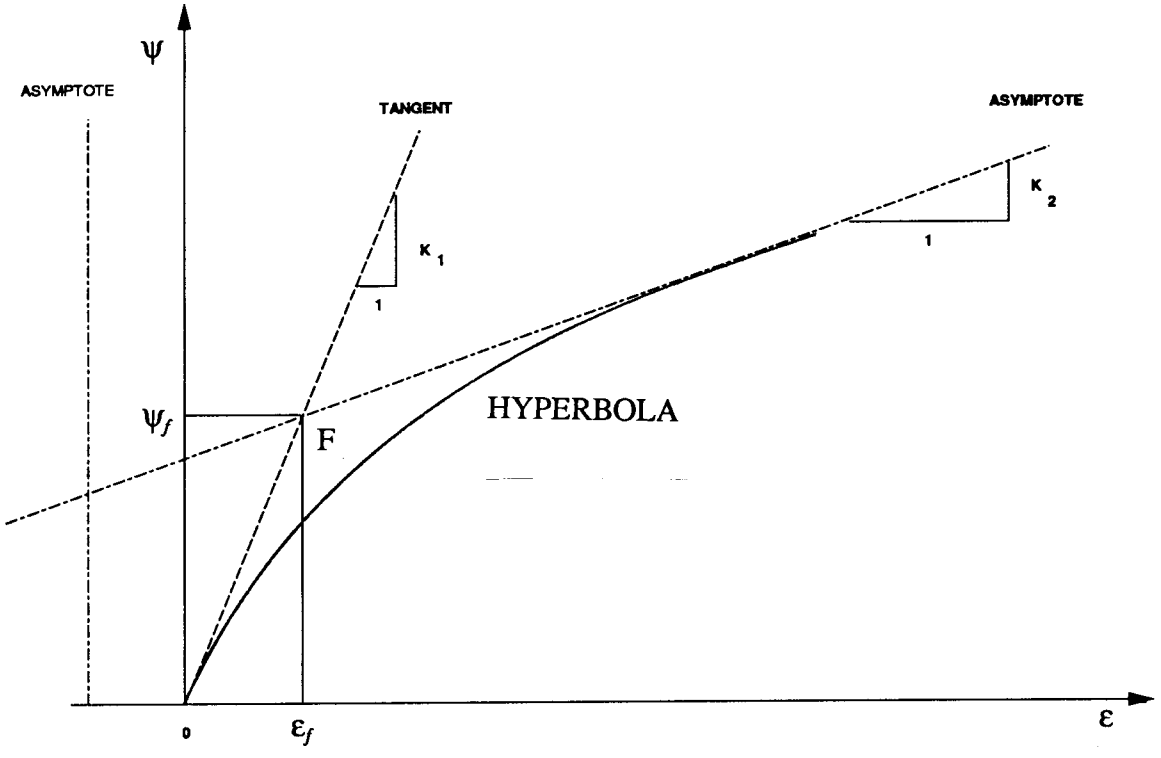

Figure 4.7 - Three-parameter hyperbola

Figure 4.8 shows one example of the fitted loading curve together with the actual points obtained from the calibration. The values of the coefficients K_1, K_2 and ψ_f obtained in each regression are listed in Table 4.2. Also listed in the table is the correlation coefficient squared r^2 obtained in each fitting. The values of r^2 indicate that the behaviour of the calibration curve for membrane stiffness correction can be very well represented by a three-parameter hyperbola. Finally program CALUNL calculated the unloading off-set of the calibration curve, using the parameters from the curve fitting analysis and assuming that the loading and unloading sections of the calibration curve were parallel lines. The curve fitting analysis was then completed and pressure-expansion curves from cone-pressuremeter tests were corrected for the stiffness of the membrane.

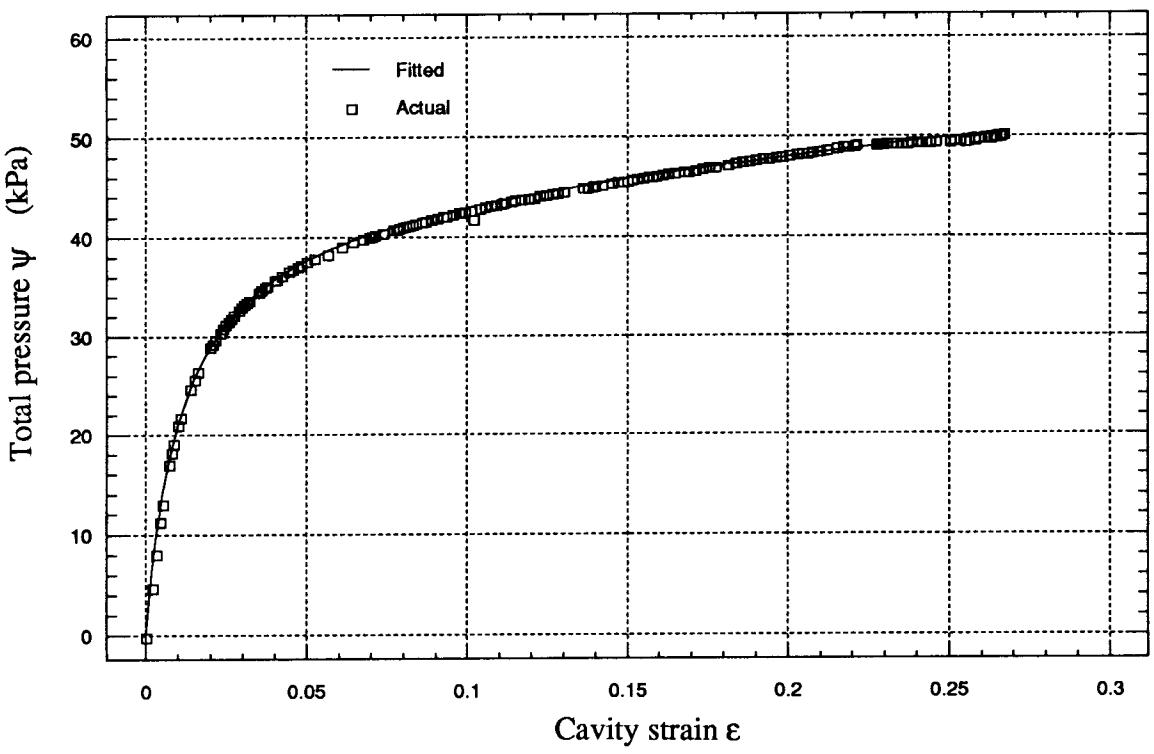

Figure 4.8 - Fitted hyperbola compared with actual points obtained from calibration of membrane stiffness

Pressuremeter results are usually presented as a plot of inflation pressure ψ against either the change of volume of the pressuremeter or the hoop strain at the pressuremeter surface ε. In this work the hoop strain definition was adopted. In small strain analysis it is not necessary to distinguish between the various definitions of strain - e.g. Cauchy strain $(R-R_o)/R_o$; or Hencky strains $\ln (R/R_o)$, as they produce indistinguishable values for small strains. The strains imposed by the pressuremeter on the surrounding soil are large, since cavity strains up to 50% were applied to cone-pressuremeter tests. In large strain analysis a distinction on the definition of strains is necessary and Hencky strain was chosen.

$$\varepsilon = \ln(R/R_o) \qquad [4.8]$$

This definition has been previously applied to the analysis of cone-pressuremeter tests, as it simplifies the mathematical treatment of cavity expansion theory (Houlsby and Withers, 1988). The radius R was taken from the central deflection of the membrane measured by strain gauged arms and was calculated from volume change measurements assuming that the membrane expands as a right cylinder.

A typical pressuremeter testing result is shown in Figure 4.9, in which inflation pressure ψ is plotted against hoop strain ε. The pressure measurements have already been corrected for the stiffness of the membrane. As illustrated in the figure, a highly non-linear pressure-expansion curve is observed, until pressure eventually approached a maximum value that corresponds to the limit pressure ψ_l. During initial phase of cavity contraction pressure dropped rapidly with displacement and, on further unloading, cavity pressure tended to zero (note that dry sand was tested and ambient pore pressure was equal to atmospheric pressure). Three unload-reload loops and one reload-unload loop have been performed to compute the shear modulus of the sand.

CALIBRATION	DEVICE cm^2	K_1	K_2	OFFSET kPa	ψ_f kPa	r^2
CALCP01	15	7139.9	304.7	1.3	49.9	0.972
CALCP02	10	3717.9	29.7	0.5	24.9	0.999
CALCP03	10	3802.1	22.5	0.6	26.7	0.998
CALCP04	10	6360.6	9.32	0.6	26.5	0.992
CALCP05	10	4088.9	35.8	1.3	43.0	0.999
CALCP06	10	4844.9	36.8	1.8	36.8	0.998
CALCP07	10	4271.2	42.4	1.3	42.4	0.999
CALCP08	10	4276.6	41.6	3.1	44.3	0.999
CALCP09	10	3895.4	29.1	1.4	44.9	0.999
CALCP10	10	3795.0	7.02	0.2	29.3	0.998
CALCP11	10	6118.9	62.41	1.2	43.4	0.999
CALCP12	5(L/D=20)	5767.6	223.9	1.1	19.2	0.981
CALCP13	5(L/D=10)	14511.8	173.2	1.1	49.53	0.977
CALCP14	5(L/D=5)	4275.3	457.4	0.2	58.23	0.998

NOTES

1- K_1, K_2 and ψ_f = hyperbola parameters

2- Offset = distance between loading and unloading segments

3- r^2 = correlation coefficient squared

Table 4.2 - Results of curve-fitting analysis to account to membrane stiffness corrections.

The measured values of the "elastic" shear modulus G and its interpretation are presented in Chapter 6. Calibration to account for compliance of the equipment and corrections for the finite length of the pressuremeter probe are discussed there. Possible effects of installation disturbance on the measured G values are examined. A method that allows the shear modulus to be normalised with respect to the stress level is discussed and the moduli obtained with the cone-pressuremeter tests are compared with those obtained from the self-bored test. In this chapter only general comments are presented to clarify the testing procedure adopted in the calibration chamber tests.

A set of pressuremeter results is now presented. As established in the testing methodology, the influence of relative density, stress level and stress ratio on pressuremeter data is investigated. Whenever necessary, other parameters are also examined, such as the influence on test results of length to diameter ratio and boundary conditions. For the sake of simplicity, results are distributed in groups, divided according to the size of each device tested in the calibration chamber - 15 cm^2, 10 cm^2 and 5 cm^2 cross section area.

a) 15 cm^2 device

The primary objective of carrying out tests with the 15 cm^2 prototype was to check the operation of the instrument and to acquire experience in controlling the pressuremeter pressurisation system (see Chapter 2 for details). Test results should be considered with great care. The diameter of the calibration chamber is only 22 times the diameter of the prototype and results are highly affected by chamber size effects (as discussed in Appendix I). Furthermore, the overall length of the instrument was of about 2.2 m, using the shortest possible cone spacer to connect the cone penetrometer to the pressuremeter module. The whole instrument did not fit in a 1.5 m height tank. To allow penetration to be performed in such a way that the centre of the pressuremeter was at the midheight of the chamber after penetration,the cone penetrometer had to be replaced for a dummy cone placed immediately below the pressuremeter probe. In this series of tests tip cone resistance q_c was not recorded during penetration.

The quality of these trial tests was good, judged both by the resolution of the pressure-expansion curves, including unload-reload loops, and the repeatability of tests. Table 4.3 shows the results of calibration chamber tests carried out with the 15 cm^2 prototype and Figure 4.10 illustrates their progress. A combination of mean effective stress of 100 kPa and stress ratio 1.0 was used in all these tests. Three different densities corresponding to loose (Rd= 25%), medium (67%)

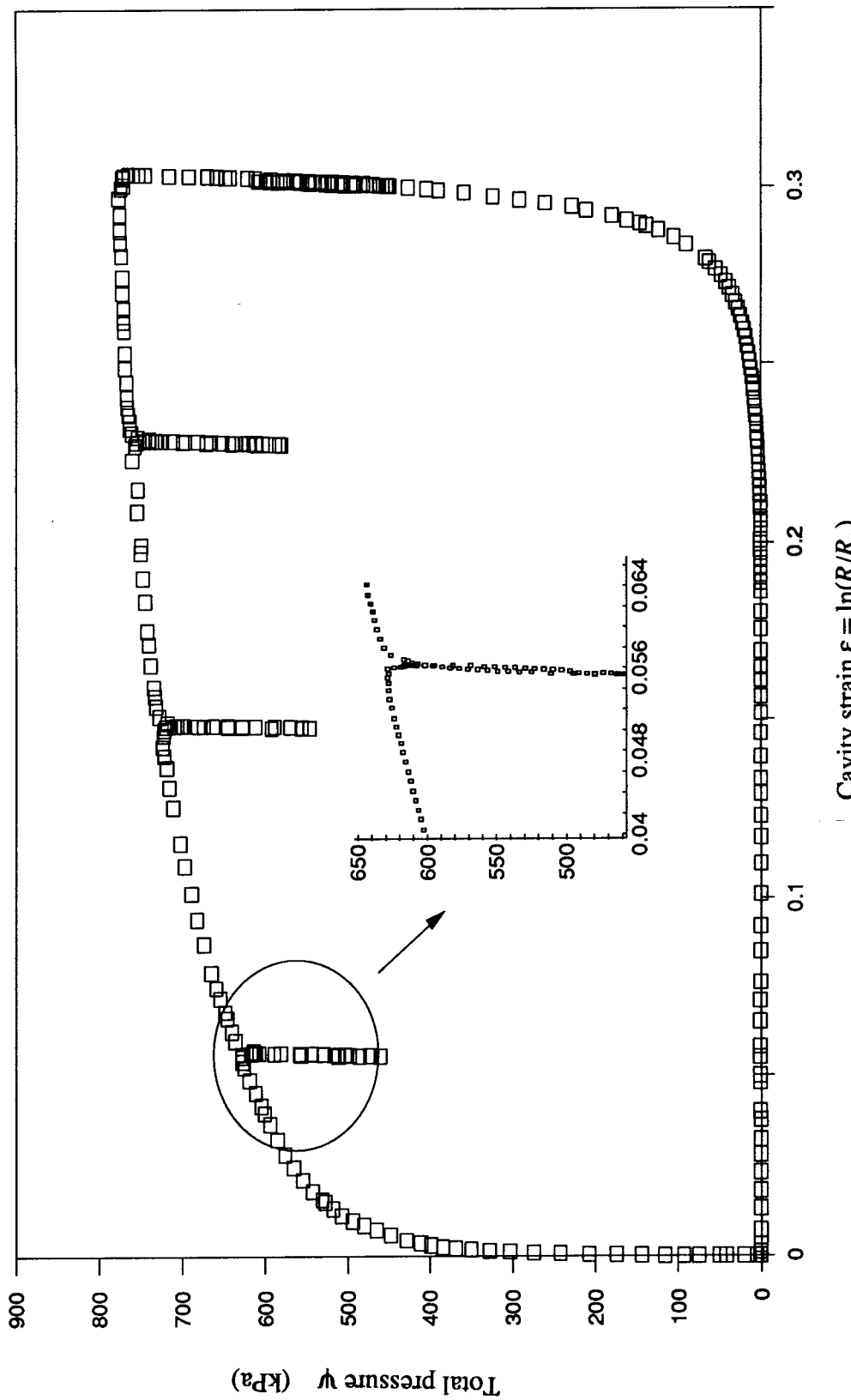

Figure 4.9 - Example of a pressuremeter pressure-expansion curve

and dense (86% and 88%) sand were tested to assess the influence of relative density on pressuremeter data. One test (15CPMT01) was lost due to pressure losses at the sealing system at the top of the pressuremeter probe.

In each of the tests, limit pressure was well defined by a plateau observed in the pressure-expansion curve. However, the shape of the pressure-expansion curve and the measured values of limit pressures are likely to be affected by the proximity of the boundaries of the chamber. The influence of relative density on pressuremeter data is similar to that observed for the cone tip resistance q_c, with a clear trend of increasing limit pressure ψ_l with increasing density.

Two small unload-reload loops were carried out in each test to measure the "elastic" shear modulus G of the soil. The first loop was performed at about 20% cavity strain and the second at about 30%. At 20% and 30% cavity strain possible effects of installation disturbance are expected to be minimised and the measured values of shear modulus can be compared to those obtained from other tests. The measured G values are presented in Chapter 6.

Tests 15CPMT02 and 15CPMT05 were intentionally carried out under the same stress conditions and at the same density to check repeatability. A good similarity is observed between the measured limit pressures, although test 15CPMT02 had an uncommon stiffening behaviour at the end of the expansion stage. The shape of the contraction stage is very similar in the two tests, suggesting that an analysis of cavity contraction in sand can be useful for a rational interpretation of test results. The values of the shear modulus measured from the two small unload-reload loops performed in each test show a remarkable agreement. However, a poor comparison was observed on the initial section of the two tests. Pressuremeter expansion was measured by three strain gauged arms and a systematically dissimilar behavioural pattern among the arms was observed at early stages of the tests. These anomalies are thought to be

a result of possible movements of the instrument in the soil mass at the beginning of membrane expansion. It is suggested that this has affected the calculated values of the initial shear modulus (taken as the tangent of the curve at the origin) and the measured values of lift-off pressure. This raises questions as to whether or not they can be useful for evaluating the *in situ* horizontal stress from a cone-pressuremeter test (as discussed in Chapter 5).

TEST	Rd	e	σ_v	σ_h	p'	K_o	ψ_l
	%		kPa	kPa	kPa		kPa
15CPMT01	85.0	0.523	88.1	96.6	93.8	1.10	
15CPMT02	88.0	0.515	88.1	96.6	93.8	1.10	1420.0
15CPMT03	67.0	0.576	88.8	96.6	94.0	1.09	1160.0
15CPMT04	23.0	0.706	89.8	96.6	94.3	1.08	615.0
15CPMT05	84.0	0.525	88.1	96.6	93.8	1.10	1460.0

NOTES

1- The values of σ_v and σ_h shown in Table 4.1 are nominal values for a reference position. In this table, values of σ_v and σ_h correspond to pressures at the midheight of the sample.

2- A dummy cone has been used in this series of tests. Tip cone resistance q_c was not recorded during penetration.

Table 4.3 - Results of calibration tests of the 15 cm^2 cone-pressuremeter

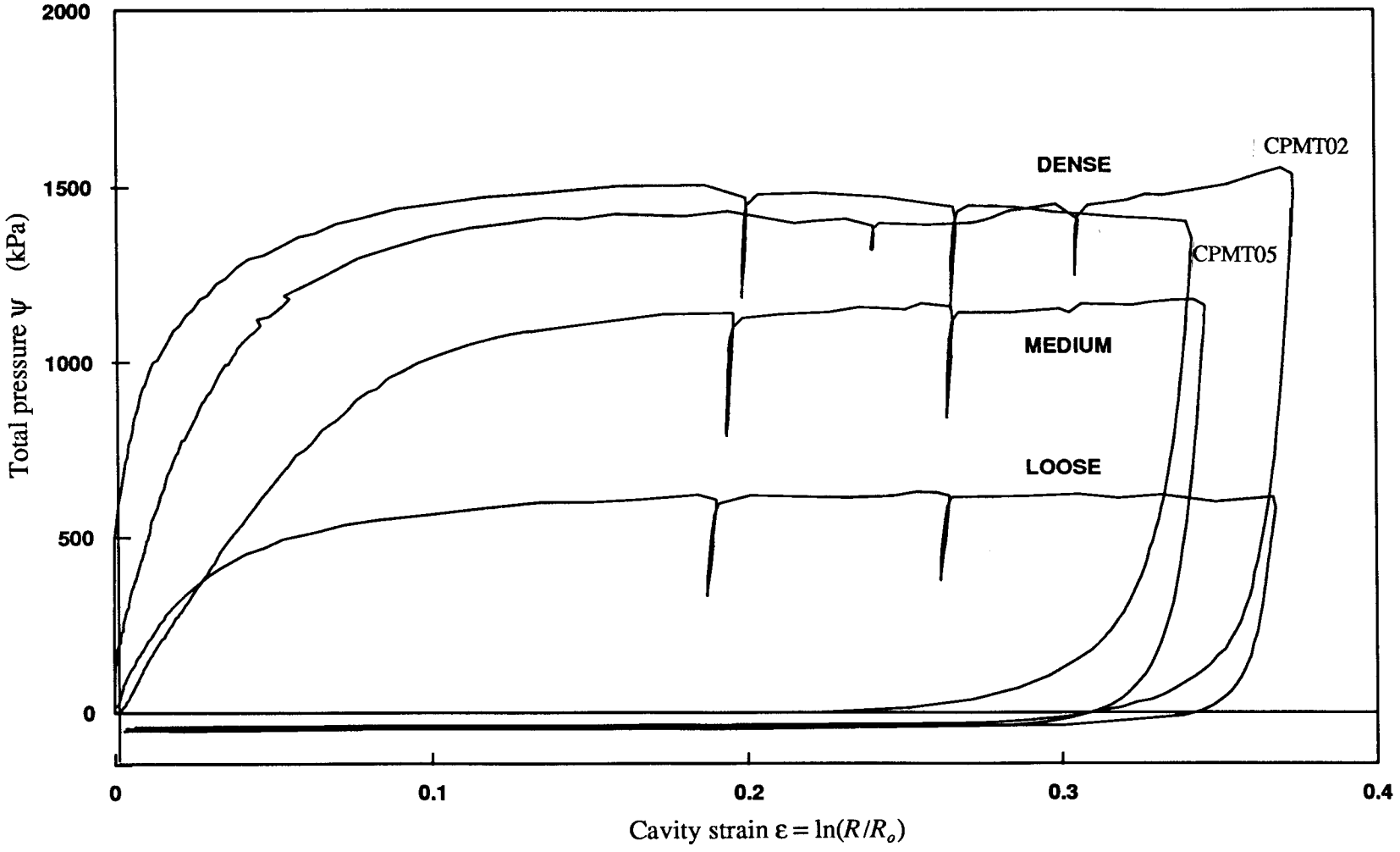

Figure 4.10 -Influence of relative density on pressuremeter pressure-expansion curves

b) 10 cm^2 prototype

A total of 21 cone-pressuremeter tests have been carried out in the large chamber using the 10 cm^2 prototype. Seven combinations of stresses and three densities were tested, as discussed in the testing methodology and detailed previously in Figure 4.1. This set of results consists of the main framework on which analysis is based to establish a basic procedure for a rational interpretation of cone-pressuremeter tests in cohesionless soils.

Results obtained with the 10 cm^2 prototype are presented in Table 4.4. The values of relative density, voids ratio, applied vertical and horizontal stresses and measured limit pressure ψ_l are listed in the table, as well as the values of cone resistance q_c (measured at the same stress levels as ψ_l). The ratio $(q_c - \sigma_h)/(\psi_l - \sigma_h)$ is also given although its application to the interpretation of cone-pressuremeter tests is discussed in Chapter 5.

In this series of tests the membrane expansion was monitored by both volume changes of the pressuremeter probe and central deflections of the membrane measured by strain gauged arms. Pressuremeter testing results can then be presented as a plot of inflation pressure ψ_l against both cavity strain calculated from strain arm measurements $\varepsilon_{(arms)}$ and cavity strain calculated from volume change measurements $\varepsilon_{(volume)}$. Comparisons between volume changes and strain arm measurements are presented in Figure 4.11, in which $\varepsilon_{(arms)}$ is plotted against the ratio $\varepsilon_{(volume)}/\varepsilon_{(arms)}$. Three tests corresponding to dense, medium and loose samples are presented in the figure. For cavity strains $\varepsilon_{(arms)}$ up to about 10% the ratio gradually reduces from about 1 to approximately 0.85; for cavity strains $\varepsilon_{(arms)}$ greater than 10% a well defined plateau is observed, in which the ratio $\varepsilon_{(volume)}/\varepsilon_{(arms)}$ remains constant without being affected by the strain magnitude and relative density.

TEST	Rd	e	σ_v	σ_h	K_o	ψ_l	q_c	$\frac{q_c - \sigma_h}{\psi_l - \sigma_h}$
	%		kPa	kPa		kPa	MPa	
10CPMT01	24.0	0.703	39.6	46.6	1.18		2.11	
10CPMT02	27.0	0.694	39.6	46.6	1.18	410.0	1.96	5.3
10CPMT03	16.0	0.728	64.8	34.1	0.52	325.0	1.57	5.3
10CPMT04	17.0	0.723	89.8	96.6	0.93	750.0	3.80	5.7
10CPMT05	26.0	0.698	139.6	71.6	0.51	630.0	3.14	5.5
10CPMT06	21.0	0.712	189.8	196.6	1.04	1400.0	6.75	5.5
10CPMT07	26.0	0.698	49.6	116.6	2.35	830.0	4.29	5.9
10CPMT08	24	0.704	289.7	146.6	0.51	1090.0	5.77	6.0
10CPMT09	60.0	0.597	88.8	96.6	1.09	1490.0	14.4	10.3
10CPMT10	62.0	0.590	138.7	71.6	0.52	1310.0	13.5	10.8
10CPMT11	61.0	0.593	88.8	96.6	1.09	1500.0	14.3	10.1
10CPMT12	63.0	0.588	138.7	71.6	0.52	1310.0	13.4	10.8
10CPMT13	62.0	0.591	48.7	116.6	2.39	1600.0	16.0	10.7
10CPMT14	63.0	0.587	288.7	146.6	0.51	2080.0	19.6	10.1
10CPMT15	68.0	0.573	63.7	34.1	0.54	640.0	6.90	11.3
10CPMT16	60.0	0.597	188.7	196.6	1.05	2450.0	22.2	9.76
10CPMT17	89.0	0.511	63.1	34.1	0.54	790.0	9.96	13.1
10CPMT18	83.0	0.529	138.1	71.6	0.52	1540.0	18.2	12.4
10CPMT19	86.0	0.519	88.1	96.6	1.10	1890.0	22.0	12.2
10CPMT20	85.0	0.523	89.1	96.6	1.08	1930.0	22.4	12.2
10CPMT21	84.0	0.525	48.1	116.6	2.42	2120.0	24.4	12.1

NOTES

1- The values of σ_v and σ_h shown in Table 4.1 are nominal values for a reference position. In this table, values of σ_v and σ_h correspond to pressures at the midheight of the sample.

2- Values of ψ_l listed in this table are slightly different form those reported by Schnaid and Houlsby (1990). A more accurate calculation of ψ_l was obtained after introducing the use of a FORTRAN program to account for membrane stiffness.

Table 4.4 - Results of calibration tests of the 10 cm² cone-pressuremeter

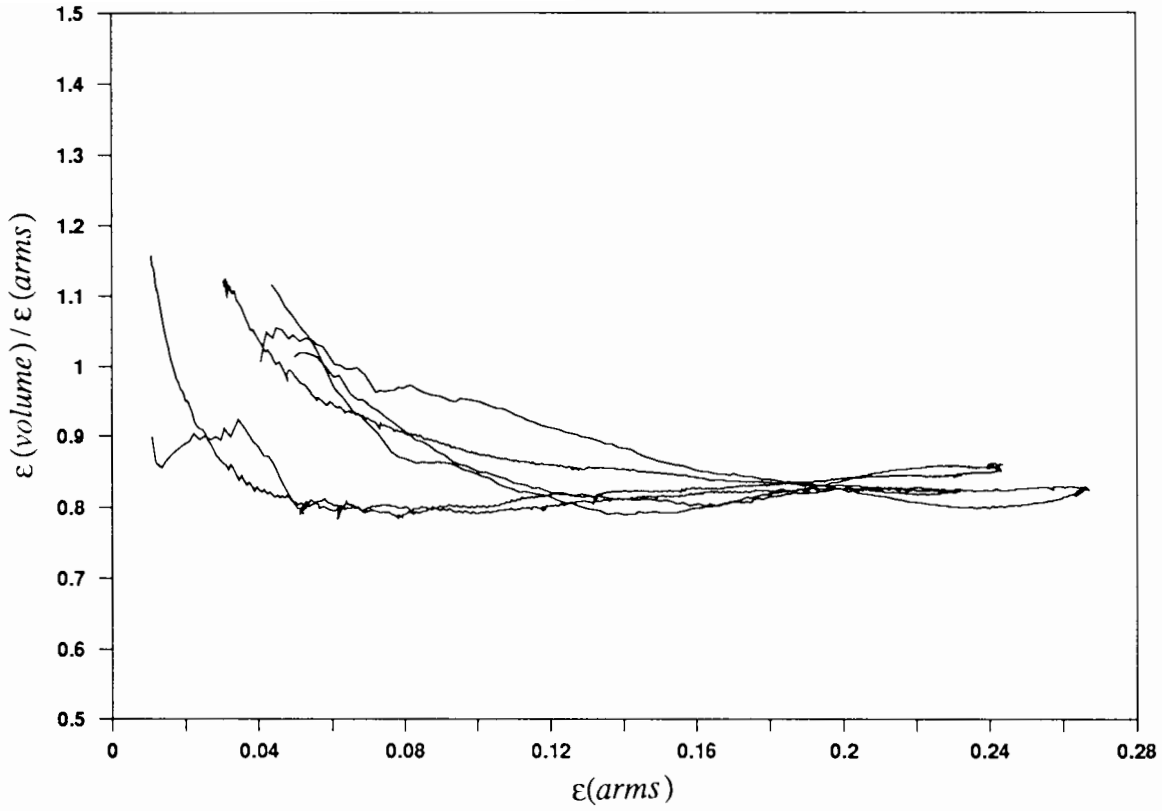

Figure 4.11 - Comparison between volume change and strain arms measurements for loose, medium and dense sands.

For tests carried out with the 10 cm^2 device attention has been given to the measurement of the shear modulus of the sand. Three unload-reload loops and one reload-unload loop were performed on each test. The unload-reload loops were carried out at about 5%, 15% and 20% cavity strain, followed by a final loop performed during the contraction phase of the pressuremeter test. For each loop the modulus was calculated based on both strain arm and volume change measurements.

The influence of relative density on pressuremeter tests has already been shown in Figure 4.10 for results obtained with the 15 cm^2 prototype. The effect of stresses on pressure-expansion curves from the 10 cm^2 device is presented in Figures 4.12 and 4.13. The figures illustrate test results obtained on loose samples, although the same patterns are observed for medium and

dense sands. In Figure 4.12 three tests carried out under the same stress ratio (K_o= 0.5) and about the same density (Rd= 60% to 68%) are plotted to show the influence of the mean effective stress p' on the pressure-expansion curve. A trend of increasing limit pressure ψ_l with increasing p' was clearly observed, for tests carried out in the range of 50 kPa to 200 kPa. The influence of stress ratio on the pressure-expansion curve is shown in Figure 4.13, in which three tests carried out under the same mean effective stress (p'= 100 kPa) and about the same density (Rd= 60% to 68%) are presented. Small increases in limit pressure with increasing stress ratio are observed, suggesting that mean effective stress may not the most suitable parameter with which to normalise the ψ_l values. The pattern observed for variations of ψ_l with mean effective stress and stress ratio is similar to that obtained from measurements of cone resistance q_c.

c) 5 cm^2 prototype

The characteristics of the 5 cm^2 cone-pressuremeter prototype have been described in Chapter 2. The instrument has no strain gauged arms, due to limitations in diameter. The membrane was inflated by oil and expansion was monitored by the change in volume of the pressuremeter probe. The pressuremeter module was provided with various adapters enabling length to diameter ratios of 5, 10 and 20 to be tested. The main aim of this series of tests was:

a) to investigate the effect of the finite length of the pressuremeter module on the pressure-expansion curve. For "full-displacement" probes, i.e. large strains, the elastic-plastic boundary of the deforming soil surrounding the probe has a diameter comparable to length of the pressuremeter and, under these conditions it is debatable whether spherical or cylindrical cavity expansion theory should be used for modelling the test.

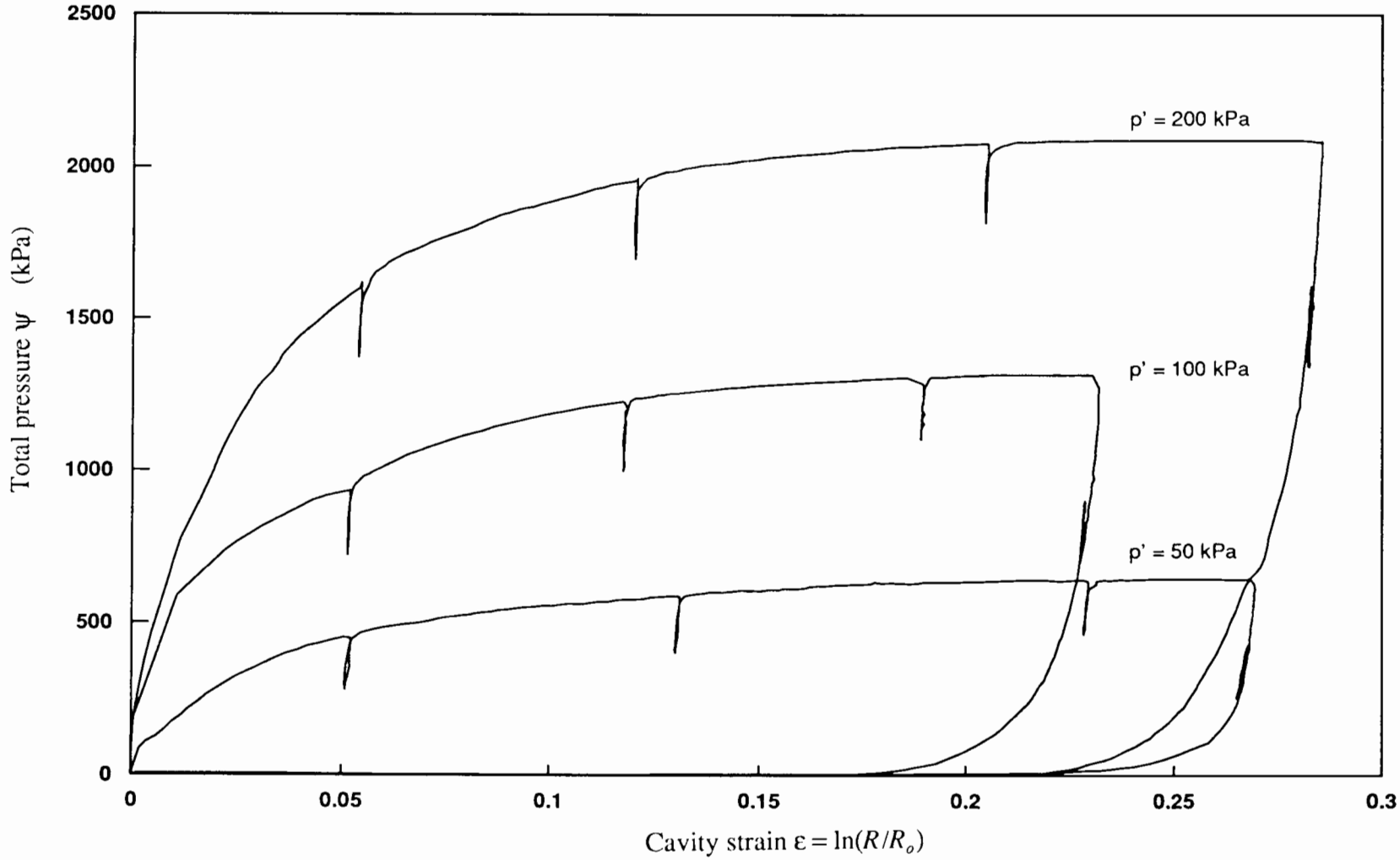

Figure 4.12 -Influence of mean effective stress on pressuremeter pressure-expansion curves

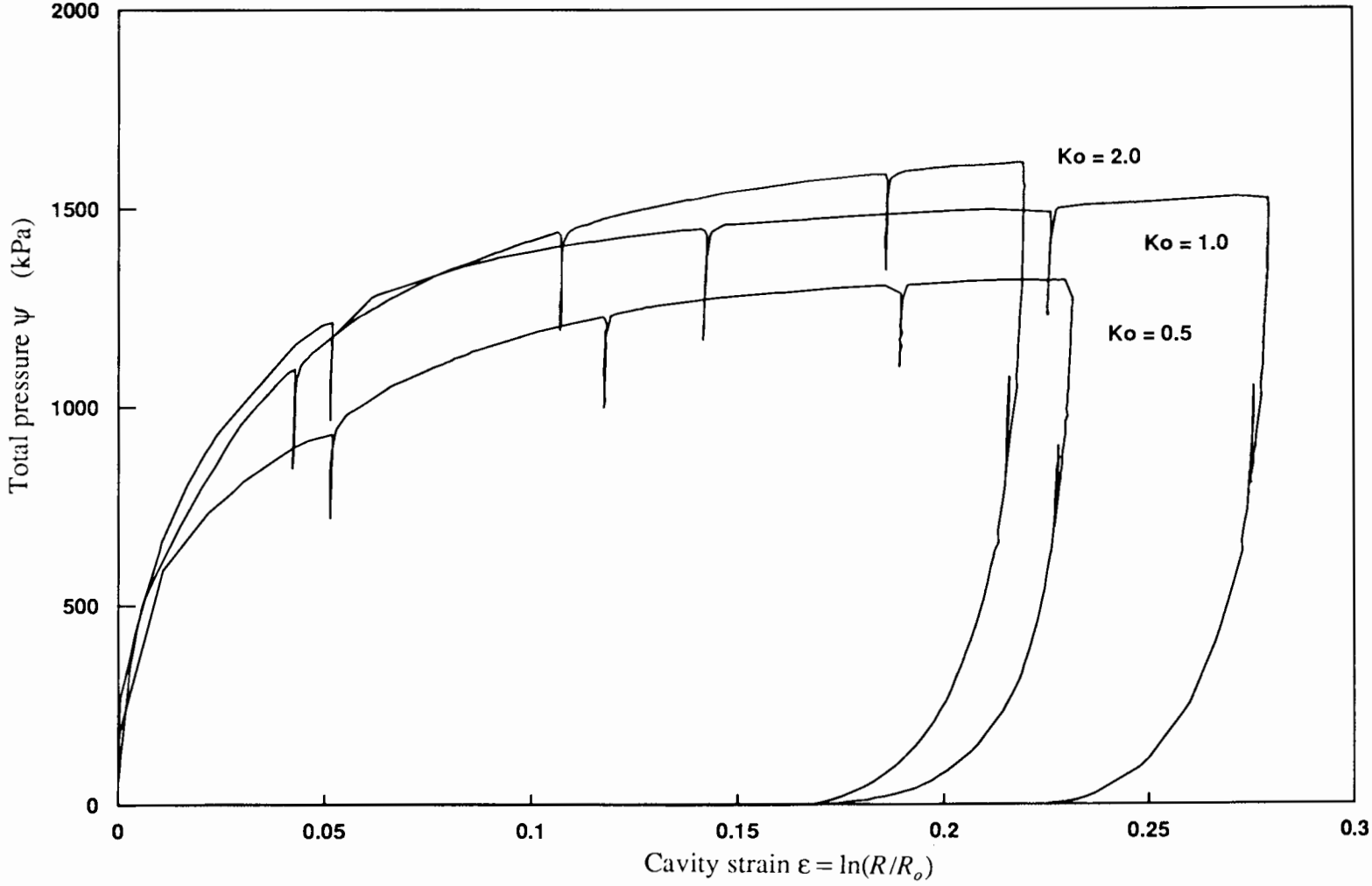

Figure 4.13 -Influence of stress ratio on pressuremeter pressure-expansion curves

b) to assess the influence of chamber size effects on cone-pressuremeter testing results. This issue is addressed in Appendix I, in which the 15 cm^2, 10 cm^2 and 5 cm^2 testing data are compared.

A total of 8 tests was carried out using the 5 cm^2 prototype. Test data are presented in Table 4.5. The measured values of limit pressure and cone resistance and the values of relative density, voids ratio, vertical stress and horizontal stress are listed in the table, as well as the length to diameter ratio used in each test.

TEST	L/D	R_d %	e	σ_v kPa	σ_h kPa	K_o kPa	ψ_l	q_c MPa
05CPMT01	10	84.0	0.525	63.1	34.1	0.54	1120.0	13.7
05CPMT02	10	87.0	0.518	138.1	71.6	0.52	1930.0	25.9
05CPMT03	10	64.0	0.585	138.7	71.6	0.52	1460.0	14.5
05CPMT04	10	65.0	0.583	88.8	96.6	1.09	2050.0	16.1
05CPMT05	5	67.0	0.576	138.1	71.6	0.52	1940.0	13.7
05CPMT06	5	63.0	0.588	88.8	96.6	1.09	2200.0	16.0
05CPMT07	20	61.0	0.593	138.1	71.6	0.52	1140.0	14.3
05CPMT08	20	62.0	0.590	88.8	96.6	1.09	1490.0	15.3

NOTES

1- The values of σ_v and σ_h shown in Table 4.1 are nominal values for a reference position. In this table, values of σ_v and σ_h correspond to pressures at the midheight of the sample.

2- L/D represents the length to diameter ratio of the pressuremeter probe. For L/D = 5 the pressure-expansion curves did not reach a well defined plateau (i.e. limit pressure). Values listed in this table correspond to the maximum pressure observed within the range of strains tested.

Table 4.5 - Results of calibration tests of the 5 cm^2 cone-pressuremeter

Typical results are presented in Figure 4.14, in which the influence of the length to diameter ratio, L/D, on the pressure-expansion curve is illustrated. A significant increasing of limit pressure with decreasing L/D ratio is clearly observed. A discussion of the influence of the ratio L/D on limit pressure is presented in Appendix II.

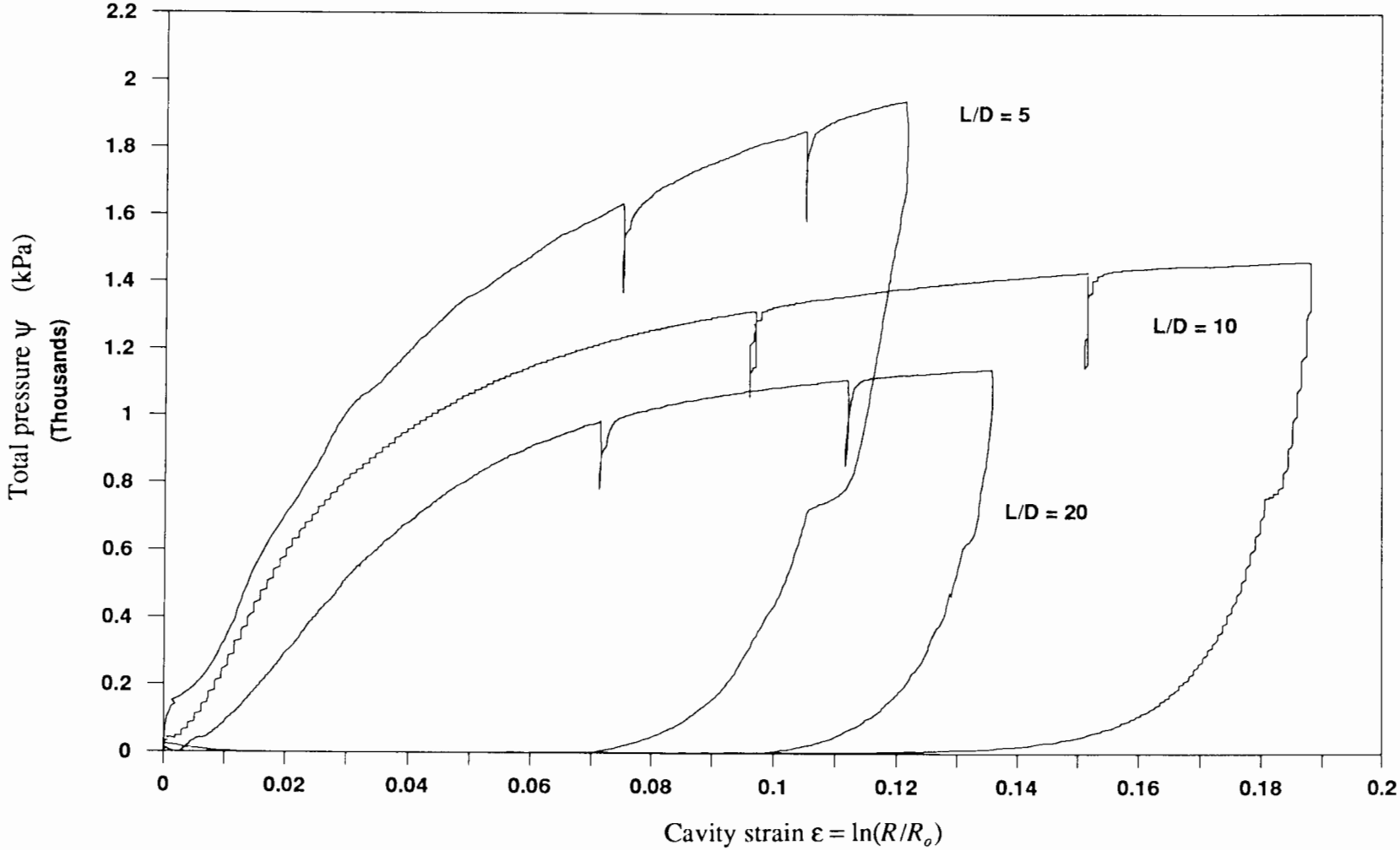

Figure 4.14 -Influence of length to diameter ratios on pressuremeter pressure-expansion curves

CHAPTER 5

INTERPRETATION OF CALIBRATION CHAMBER TESTS

The interpretation of the cone-pressuremeter tests carried out in the calibration chamber is presented. The observed limit pressures, as well as the cone resistance values, are found to be related primarily to the *in situ* horizontal stress and density. The ratio of cone resistance to limit pressure is found to be primarily determined by the sand density. A procedure for deducing the *in situ* horizontal stress, density and friction angle from the results of the cone-pressuremeter test is described, and is shown to give reasonable values when used to back-analyse the tests.

5.1 - Introduction

In previous chapters the basic features of the cone-pressuremeter testing device have been given and the testing programme has been discussed. It is felt that at this stage the characteristics of the test have been clearly illustrated. It is a more complex device to interpret than the self-boring pressuremeter because the pressuremeter test is carried out in soil which has been displaced by the penetration of the cone. It is recognized that the cone penetration causes disturbance of the soil, but it is considered that this disturbance should be repeatable, and that the pressuremeter test should therefore be amenable to rational analysis.

An analysis of the cone-pressuremeter in clay was presented by Houlsby and Withers (1988), and applied quite successfully to the results of field tests. An equivalent analysis for deriving soil parameters in sands is not yet fully developed, although interpretation methods for the

cone-pressuremeter test in sands based on large strain analysis of cavity expansion have been presented by Yu and Houlsby (1989) and Yu (1990). Since a limited amount of field data is available for cone-pressuremeter tests in sand (Hughes and Robertson, 1985; Withers *et al*, 1989), interpretation of the test in sand must be based on the results of calibration tests. The purpose of this chapter is to examine the results of a set of tests in a large calibration chamber, which were designed to investigate possible methods of interpretation of the cone-pressuremeter. Although information can be obtained from the complete pressure-displacement curve from the pressuremeter test, including the unload-reload loops for modulus measurement, this chapter will concentrate on the values of the limit pressure obtained from the pressuremeter test and the cone resistance values from the cone test. The main conclusions taken from this approach have been presented by Schnaid and Houlsby (1990).

The data presented in this chapter were obtained from tests carried out using the 10 cm^2 cone-pressuremeter prototype. This series of tests is believed to form a basic body of data which enables a comprehensive understanding of the test to be obtained, and allows relationships for measuring soil parameters to be established. It also allows tip cone resistance measured in the chamber to be compared to results of previous studies carried out at Oxford University. Comparisons of results obtained from the 15 cm^2, 10 cm^2 and 5 cm^2 prototypes are presented in Appendix I, in which corrections for scale effects due to influence of chamber to probe size ratios are discussed.

5.2 - Analysis of results

The calibration chamber tests on the cone-pressuremeter give measurements of limit pressure ψ_l and cone resistance q_c under conditions of controlled density, vertical stress and horizontal stress. Interpretation of the test depends on understanding of the influence of each of these variables on q_c and ψ_l.

Houlsby and Hitchman (1988) showed from calibration chamber tests of the cone penetrometer in sand that, for a given density of sand, the tip cone resistance q_c depends on the *in situ* horizontal stress, and only to a small extent on the vertical stress. Figure 5.1 illustrates such a correlation, which shows q_c against horizontal effective stress. The original figure presented by Houlsby and Hitchman (1988) has been modified to include results obtained with the cone-pressuremeter testing device. Based on this set of data the following observations can be made:

a) for each of the three densities tested there is an almost unique relationship between q_c and horizontal stress, in spite of the factor of 4 covering the range of σ'_h/σ'_v. The relationship can be well fitted by a power expression (Houlsby and Hitchman, 1988). The non-linearity that represents a considerable reduction of values of the ratio q_c/σ'_h with increasing stress level is thought to be a result of the reduction of peak friction angle with increasing stress level.

b) a remarkable agreement was obtained between the values of tip cone resistance measured by Houlsby and Hitchman (1988) and in the present work. Since the first group of tests was carried out in yellow Leighton Buzzard sand, whereas the second was performed in a batch of white sand, minor discrepancies are entirely explained by differences on the measured peak friction angle observed for the two batches of sand (q_c values measured in the yellow sand showed consistently higher values than those measured in the white sand, as discussed in Chapter 3).[1]

By comparison, values of tip cone resistance plotted against vertical effective stress showed no reasonable relationship for any of the densities tested. This set of tests was carried out

---

1 *The good agreement observed between these two sets of data provides further support for the approach of calibrating in situ testing devices in large laboratory chambers, as a very similar pattern with almost no scatter was observed for tests performed in different tanks using two different cone penetrometer probes.*

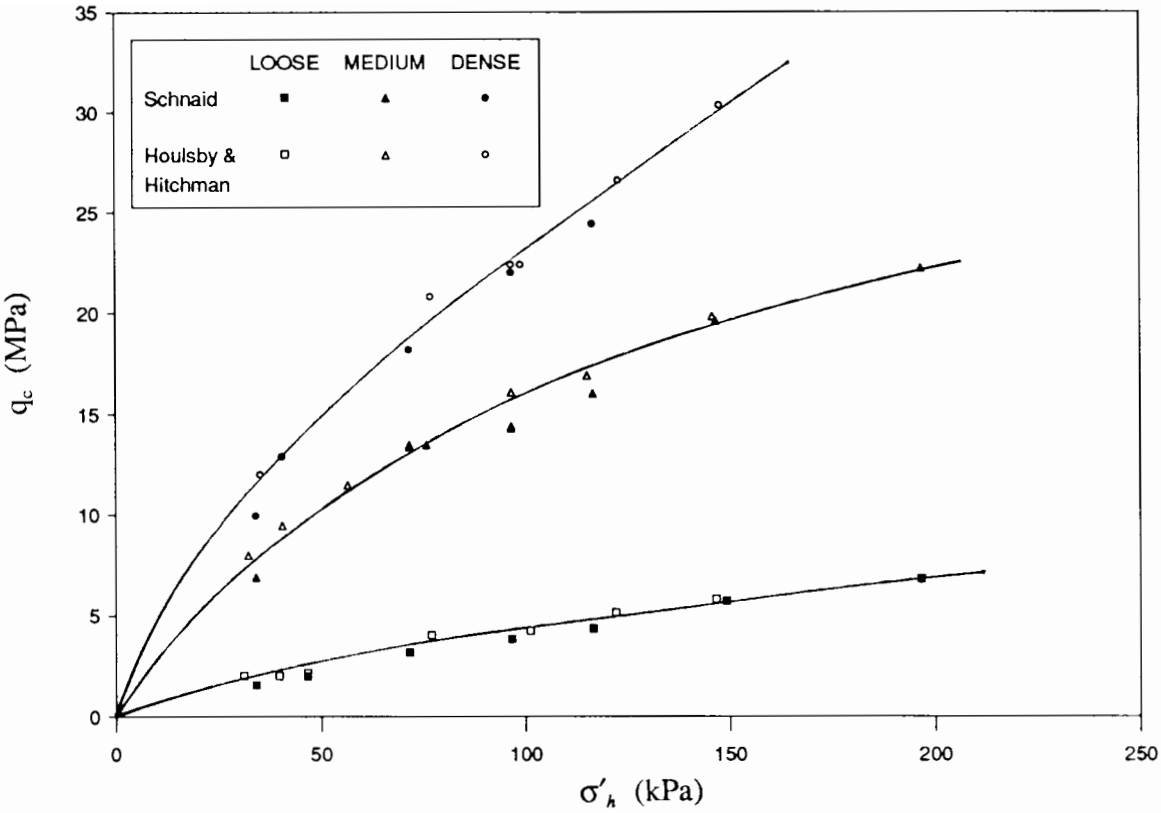

Figure 5.1 - Tip cone resistance against horizontal stress (modified from Houlsby and Hitchman, 1988)

specifically to evaluate the independent influence of horizontal stress and vertical stress on cone resistance. However, the dominant influence of σ'_h on q_c has long been recognized from an extensive number of calibration chamber tests (Holden, 1971; Veismanis, 1974; Schmertmann, 1978; Baldi *et al*; 1986; Houlsby and Hitchman, 1988).

The same approach has been applied to the pressuremeter test data. Figure 5.2 shows measured limit pressure ψ_l against applied horizontal effective stress σ'_h. A unique relationship is clearly observed between ψ_l and σ'_h for each of the three densities tested. Like the relationship presented in Figure 5.1 for tip cone resistance, a reduction on the ratio ψ_l/σ'_h with increasing stress level is observed and is thought to be a result of the reduction of peak friction angle with increasing stress level. A similar plot shows limit pressure against vertical stress (Figure 5.3),

showing no connection between these quantities. These observations suggest that both the cone resistance and the limit pressure depend primarily on the same variables, i.e. density and horizontal stress.

It is therefore useful to explore the relationship between q_c and ψ_l, which is shown in Figure 5.4. The horizontal stress has been subtracted from both quantities for consistency with the analysis of tests in clay (Wroth, 1988; Houlsby, 1988); this subtraction has only a small effect on the plot. Figure 5.4 shows that, for a given density, there is a constant ratio between limit pressure and cone resistance and this ratio is independent of stress level and stress ratio. The direct correlation between q_c and ψ_l suggests that the resistance to cone penetration, as well as the limit pressure in the pressuremeter test, is closely controlled by a cavity expansion process. The ratio $(q_c - \sigma_h)/(\psi_l - \sigma_h)$ may be a useful variable for deriving soil parameters, in particular the density. If a cavity expansion process controls both q_c and ψ_l then the ratio between them may not be as sensitive to the effects of boundary conditions in the calibration chamber as the independent measurements of cone resistance and limit pressure.

5.2.1 - Relative density

The first important application of the cone-pressuremeter test for measuring soil parameters is the estimation of density as a function of q_c and ψ_l. The density was obtained by weighing the sand in the chamber at the end of each test and dividing by the volume of the sample. Figure 5.5 shows the ratio of $(q_c - \sigma_h)/(\psi_l - \sigma_h)$ against relative density, R_d. The ratio is sensitive to the relative density and the results can be approximated by a linear equation:

$$R_d = 9.0\frac{(q_c - \sigma_h)}{(\psi_l - \sigma_h)} - 30 \qquad [5.1]$$

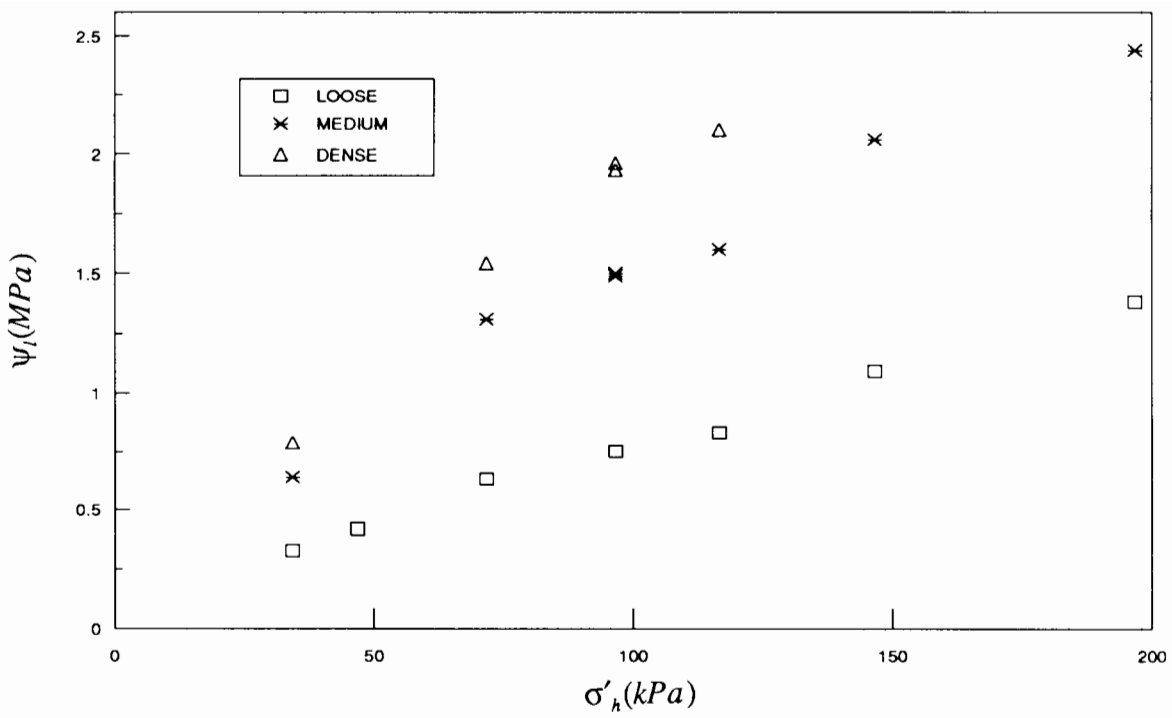

Figure 5.2 - Limit pressure against horizontal stress

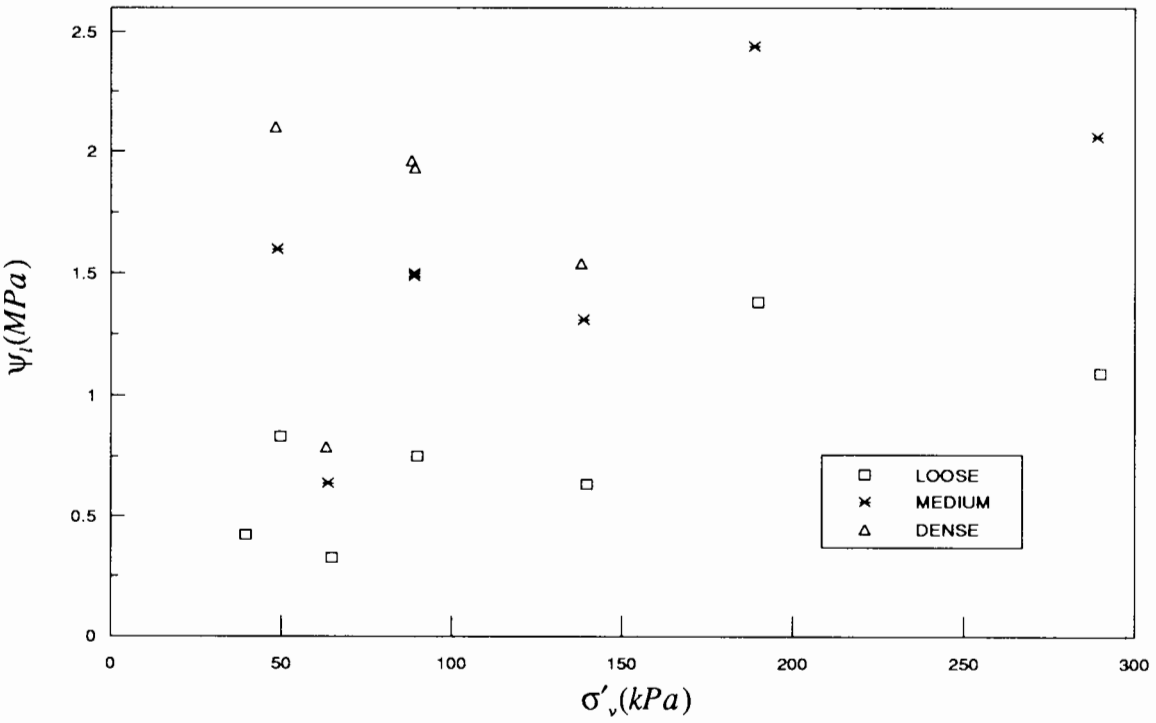

Figure 5.3 - Limit pressure against vertical stress

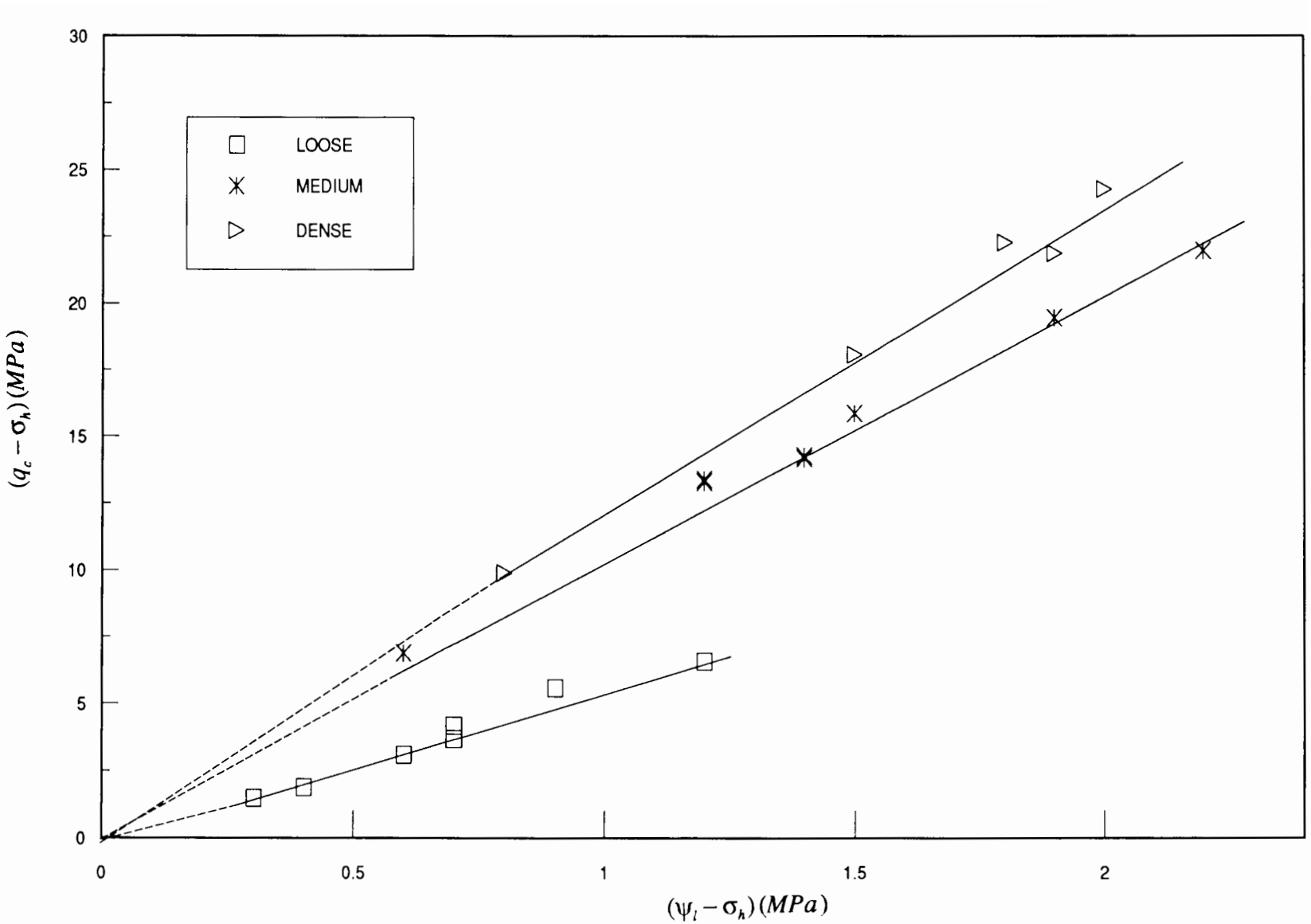

Figure 5.4 - Cone resistance against limit pressure

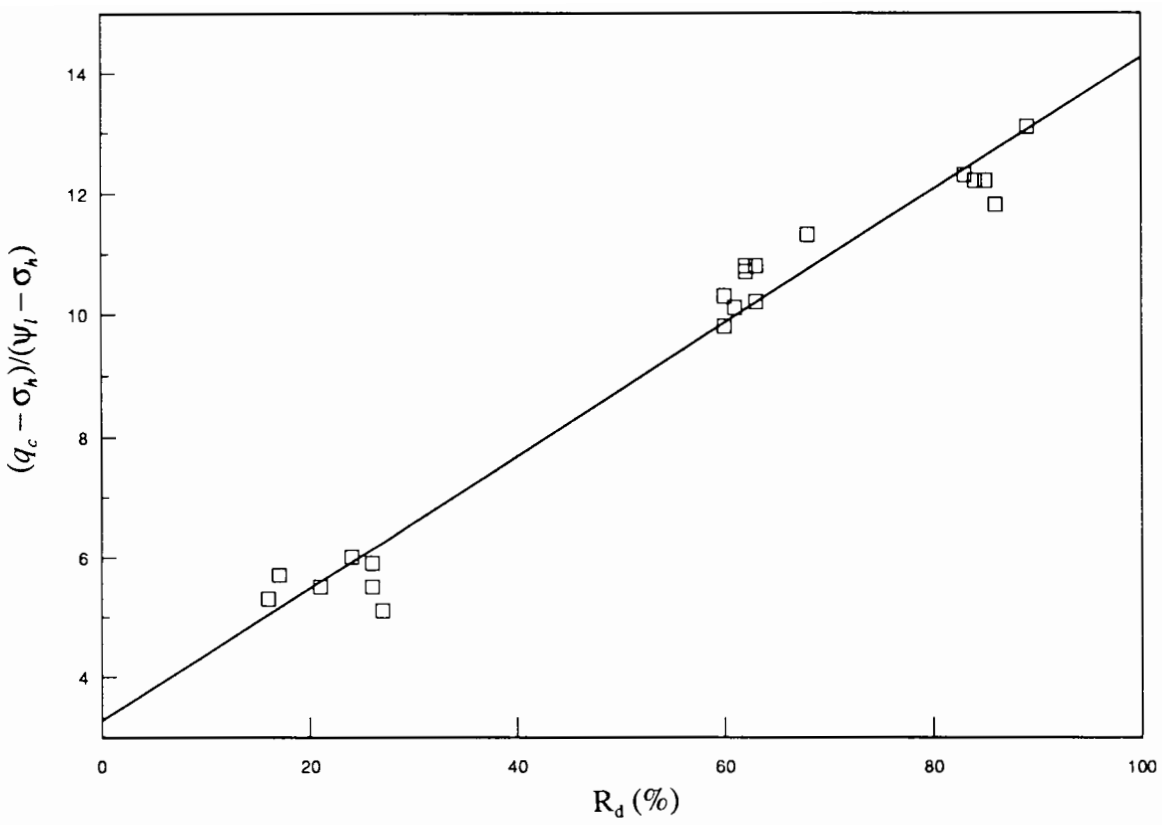

Figure 5.5 - Ratio of cone resistance to limit pressure against relative density

which is applicable for Leighton Buzzard sand with values of $(q_c - \sigma_h)/(\psi_l - \sigma_h)$ in the range of 6 to 14.

Calibration chamber data have in the past been extensively used to correlate relative density to cone resistance (Schmertmann, 1976; Lancellotta, 1983). For normally consolidated deposits R_d has been expressed as a function of q_c and σ'_v. As explained above, q_c is almost completely controlled by the horizontal stress and therefore, for overconsolidated sands, any relationship must take account of the value of σ'_h or p' since K_o varies with the overconsolidation ratio. The relationship based on the cone-pressuremeter testing results can be considered as a step forward in the prediction of density, as it depends only on the measured values of q_c and ψ_l (the subtraction of σ_h from both quantities represents a small correction for sands, and derived R_d values are insensitive to a poor estimate of σ_h). Note that the correlation of $(q_c - \sigma_h)/(\psi_l - \sigma_h)$

against R_d has been tested for a wide range of K values, but further research should be carried out to validate the correlation in different sands, in order to take into account the influence of other variables such as stiffness.

By making further use of the results of the cone test, however, it is possible to obtain information about both the in-situ horizontal stress and the density. Recalling that the cone resistance is primarily controlled by the horizontal stress and density, it is found that the results of the calibration chamber tests can be reasonably approximated by the expression:

$$R_d = \frac{1}{3}\frac{(q_c - \sigma_h)}{\sigma_h'} + 10 \qquad [5.2]$$

The relationship is illustrated in Figure 5.6. Similar correlations between cone resistance and stress level have been presented before. However, the mean effective stress p'_o or even the vertical stress σ'_v has usually been used to correlate with q_c (Schmertmann, 1976; Villet and Mitchell, 1981; Baldi *et al*, 1982; Lunne and Christoffersen, 1983; Been *et al*, 1986; Jamiolkowski *et al*, 1988). It is important to observe that equation [5.2], in contrast to equation [5.1], is expected to be influenced by chamber size effects (Parkin and Lunne, 1982; Parkin, 1988). Chamber tests in loose and medium sands represent field conditions reasonably well, but tests in dense sand are affected by the proximity of the chamber boundary. It is likely that the cone resistance for the dense tests is underestimated by a factor of approximately two by comparison with field tests. Neglecting the effects of chamber size leads to an overestimation of the density values in the field. An extensive database of approximately 400 tests has been analysed, in the context of cylindrical cavity expansion theory, to quantify these effects more precisely and is presented in Appendix I. It is emphasised that equation [5.2] therefore applies to calibration chamber results, and that the coefficients in the equation would change for field tests.

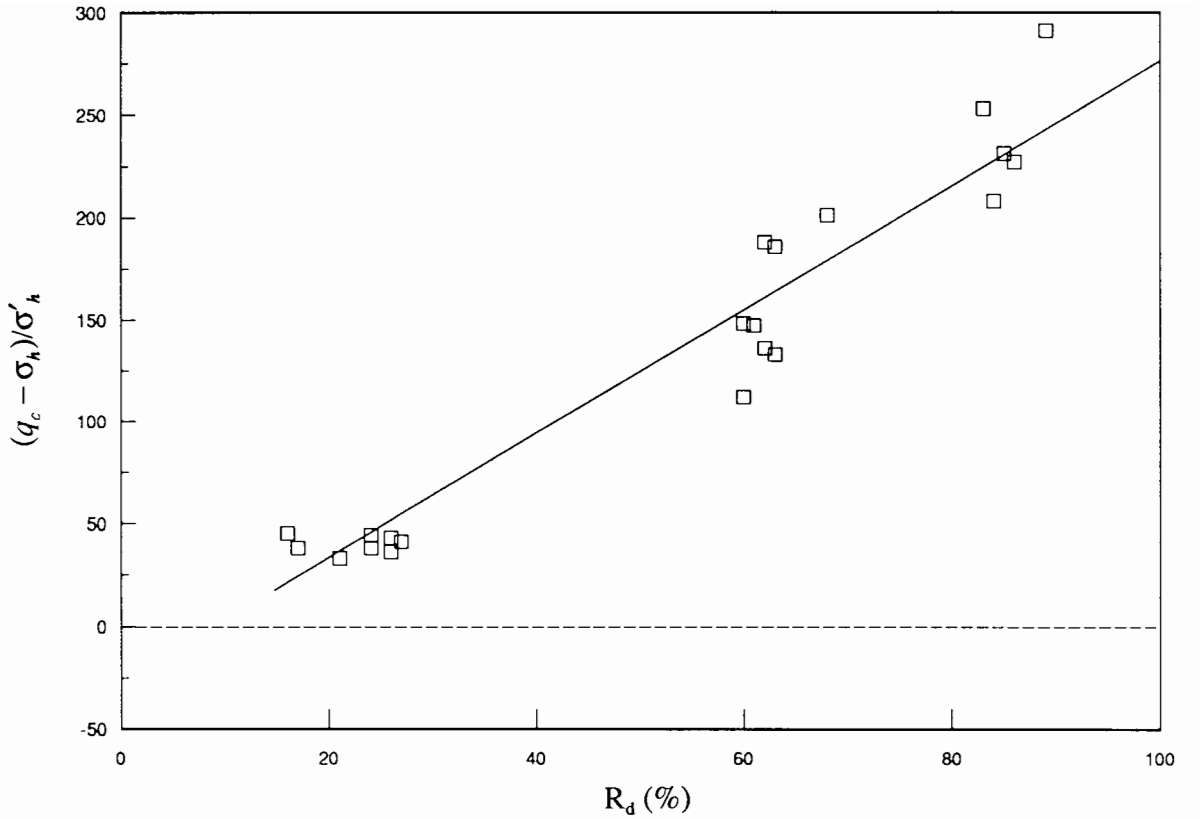

Figure 5.6 - Normalized cone resistance against relative density

5.2.2 - Friction angle

The interpretation of calibration chamber tests in this chapter has been made so far in terms of density rather than friction angle simply because more certainty can be attached to the former quantity in the tests. Density and friction angle are of course closely related. Once the relative density is known, it is then possible to make an estimate of the peak angle of friction, using for instance Bolton's empirical correlation (Bolton, 1986).

As an alternative to the above procedure, it is also possible to establish relationships in the form of equations [5.1] and [5.2] which give a direct relationship between the results of the cone-pressuremeter test and the angle of friction. For consistency with the analysis proposed for deriving relative density, the friction angle was here predicted as a function of the ratio

$(q_c - \sigma_h)/(\psi_l - \sigma_h)$. A triaxial test programme and its interpretation has been discussed in Chapter 3, and values of triaxial peak friction angles ϕ'_p were given. The measured values of ϕ'_p were related to the properties of each sand sample in the calibration chamber throughout relative density and stress level adopting Bolton's approach. The values of ϕ'_p were expressed as a combination of equations [3.1] and [3.2]

$$\phi'_p = \phi'_{cv} + 3\left[R_d\left(Q - \ln\frac{p'}{kPa}\right) - 1\right] \qquad [5.3]$$

in which ϕ'_{cv} and Q were obtained experimentally from triaxial test data. For Leighton Buzzard sand the values of $\phi'_{cv} = 34.3°$ and Q = 9.9 were found to give a best fitting line to relate ϕ'_p to relative density and stress level.

Figure 5.7 shows the relationship between the ratio $(q_c - \sigma_h)/(\psi_l - \sigma_h)$ and the triaxial peak friction angle, ϕ'_p, calculated from equation [5.3]. Due to the limited amount of experience using the cone-pressuremeter testing device it has been decided to present data in a natural scale and fit results through a linear equation:

$$\phi'_p = 1.45\frac{q_c - \sigma_h}{\psi_l - \sigma_h} + 26.5 \qquad [5.4]$$

although the figure suggests that a curved relationship would be more accurate. Equation [5.4] predicts the friction angle to within approximately 1° to 2°. Predictions are considered fairly good as they reflect the same degree of accuracy as that obtained in the laboratory triaxial tests.

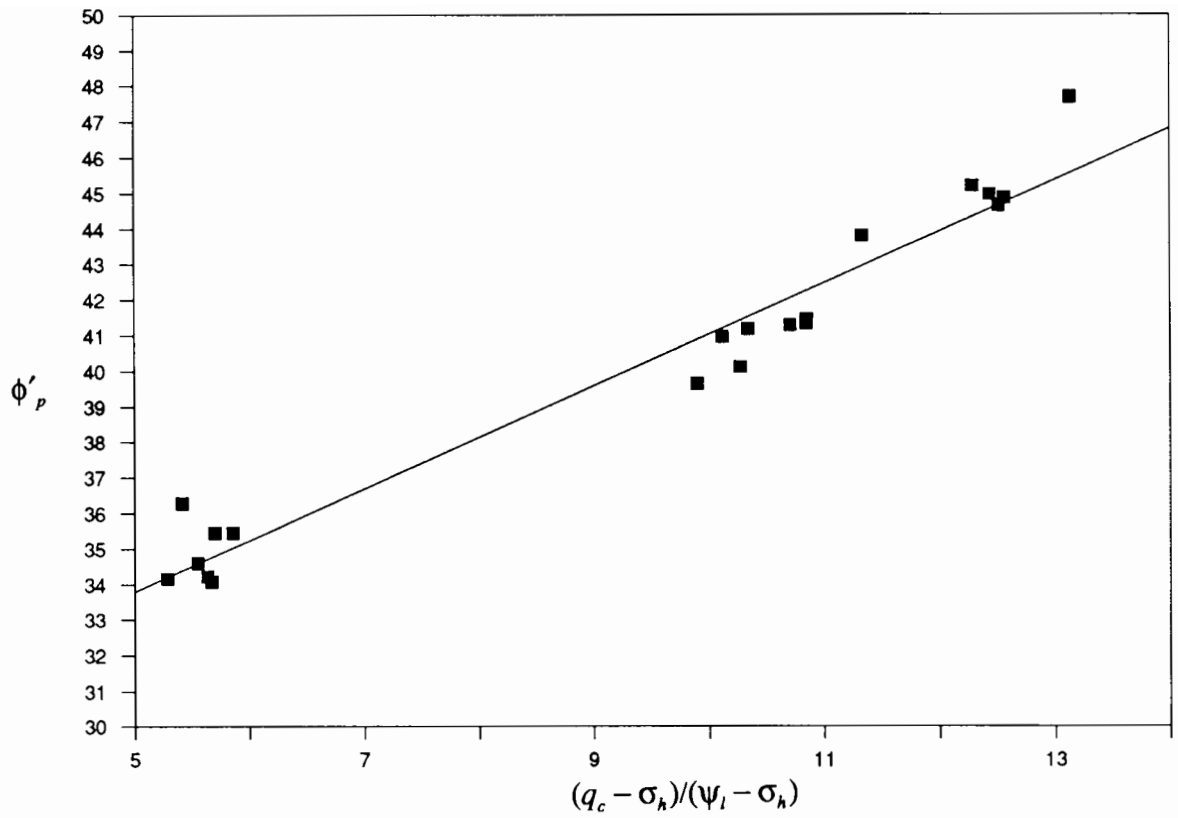

Figure 5.7 - Ratio of cone resistance to limit pressure against triaxial peak friction angle

5.2.3 - Horizontal effective stress

Calibration chamber data have clearly shown that, for a given density, tip cone resistance and limit pressure depend primarily on the *in situ* horizontal stress; therefore σ'_h or Ko (σ'_h/σ'_v) must be accounted for in a rational interpretation of field tests. Despite the various methods developed to predict the *in situ* state of stress, it is still not possible to determine with reasonable accuracy the value of the horizontal stress in most natural deposits because they have undergone a complex stress history of loading and unloading which is difficult to reconstruct.

The self-boring pressuremeter appears to be the most suitable technique for determining the *in situ* horizontal stress, as it offers the possibility of being able to insert a testing device into

the ground with very little disturbance to the surrounding soil. In sand only limited experience has been reported of the evaluation of σ'_h; experimental data are presented by Windle (1976), Fahey (1980), Wroth (1982, 1984), Fahey and Randolph (1984) and Mair and Wood (1987). Problems associated with the self-boring technique are extremely important, as even a small disturbance leads to measured lift-off pressures which closely match the ambient pore pressure.

The cone-pressuremeter has a disadvantage when compared to the self-boring pressuremeter as tests are carried out in soil which has already been displaced by the cone. The possibility of inferring σ'_h from test data is still to be validated, as the insertion of the instrument into the soil is likely to change the geostatic stress conditions prior to penetration (Hughes and Robertson, 1985; Houlsby and Withers, 1988; Withers *et al*, 1989). The same limitations are well recognized for other penetration tools, such as the cone penetrometer, standard penetrometer (SPT) and dilatometer (Schmertmann, 1978; Marchetti, 1985; Huntsman *et al*, 1986; Jamiolkowski *et al*, 1985, 1988; Jefferies and Jonsson, 1987).

An attempt to correlate the horizontal stress acting on the pressuremeter probe after penetration with the *in situ* horizontal stress has been presented by Hughes and Robertson (1985). The authors presented a qualitative description of the stress path followed by soil elements surrounding the cone-pressuremeter device, as discussed in Chapter 1. It has been suggested that high mean effective stresses are generated by cone tip penetration, and a stress relieved zone was formed along the shaft of the cone. The magnitude of the stress relief in this zone is so large that radial stress acting on a soil element adjacent to the probe would be reduced to a value which may be close to the initial stress state in the ground. This hypothesis is supported by experimental data reported by Hughes and Robertson (1985) and Withers *et al* (1989), in which some similarities between the measured lift-off pressure and the expected *in situ* horizontal stress have been observed.

In the cone-pressuremeter test, however, the use of the lift-off pressure as a measurement of the horizontal stress can be criticised. As previously discussed, the insertion of the instrument into the ground is likely to change the stress conditions from those existing prior to penetration. The change in stress is material dependent (i.e. grading, mineralogy etc) and fabric dependent (i.e. anisotropy, cementation etc), and, for a given sand, is expected to be a function of stress level and critical voids ratio (Robertson, 1982; Huntsman, 1985; Huntsman *et al*, 1986; Jamiolkowski *et al*, 1988). The theoretical evaluation of these effects is rather complex and consequently correlations with lift-off pressure are purely empirical. The mechanical performance of the instrument also contributes to this criticism. The three strain gauged arms were often observed to give different results during the initial stages of the test, so that lift-off pressure had to be taken as an average value of the three readings. This issue has been presented in Chapter 4 and has been informally addressed in the seminar on laboratory calibration in Oslo (1988). If the best interpretation of lift-off pressure is to be used to predict σ'_h, some scatter on the test data is expected. Variations on the ratio of lift-off pressure σ'_{ro} to horizontal stress σ'_h, with horizontal stress are shown in Figure 5.8. The ratio (σ'_{ro}/σ'_h)varied from 0.4 to 2.8 and no specific trend was observed with changing stresses. A poor repeatability was observed for tests carried out under the same conditions of density and stress level.

An alternative method to the conventional practice of assessing horizontal stress from lift-off pressure has been developed, based on the measured values of q_c and ψ_l. It has been previously shown that density can be estimated from $(q_c - \sigma_h)/(\psi_l - \sigma_h)$ or directly from q_c, if a reasonable estimate of the horizontal stress can be made. As both quantities q_c and ψ_l are controlled by the horizontal stress, an alternative approach is to reverse the process to estimate σ_h'. The combination of equations [5.1] and [5.2] gives σ_h' as a function of q_c and ψ_l, expressed as the root of a quadratic equation:

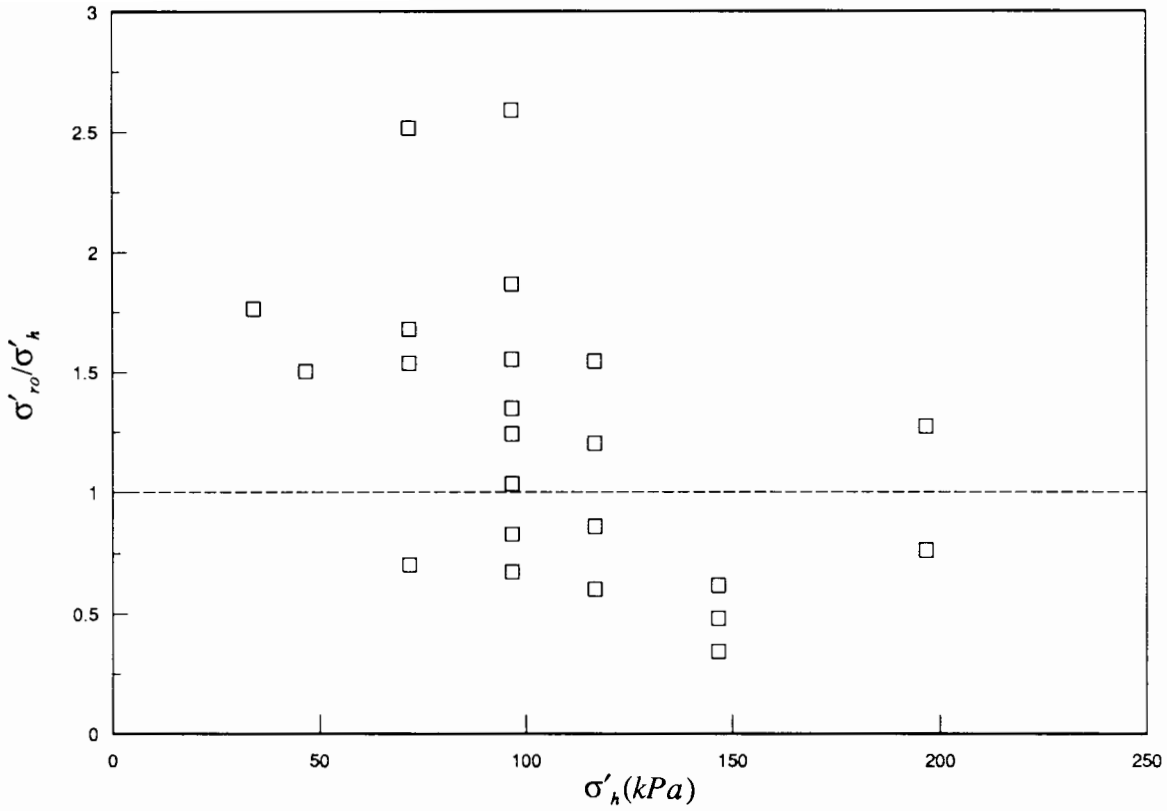

Figure 5.8 - Ratio of lift-off pressure to horizontal stress against horizontal stress

$$A\sigma'^{2}_{h} + (B\psi_l + Cq_c)\sigma'_h + Dq_c\psi_l = 0 \qquad [5.5]$$

which is applicable for Leighton Buzzard sand with A= 92.0, B= -119.0, C= 28.0 and D= -1.0. Figure 5.9 shows the comparison between σ_h' estimated from the measured values of q_c and ψ_l and σ_h' applied in the calibration chamber. The same data are replotted in Figure 5.10 in terms of the earth pressure coefficient K, defined as the ratio σ_h'/σ_v'. The vertical stress applied to the chamber was used, together with the estimated and applied horizontal stress to compute the K values. A generally good agreement is observed in the predictions for the range of conditions tested. The horizontal stress was estimated within a factor of 1.3 for every case but one, but with a tendency to underestimate the horizontal stress at high horizontal stress values.

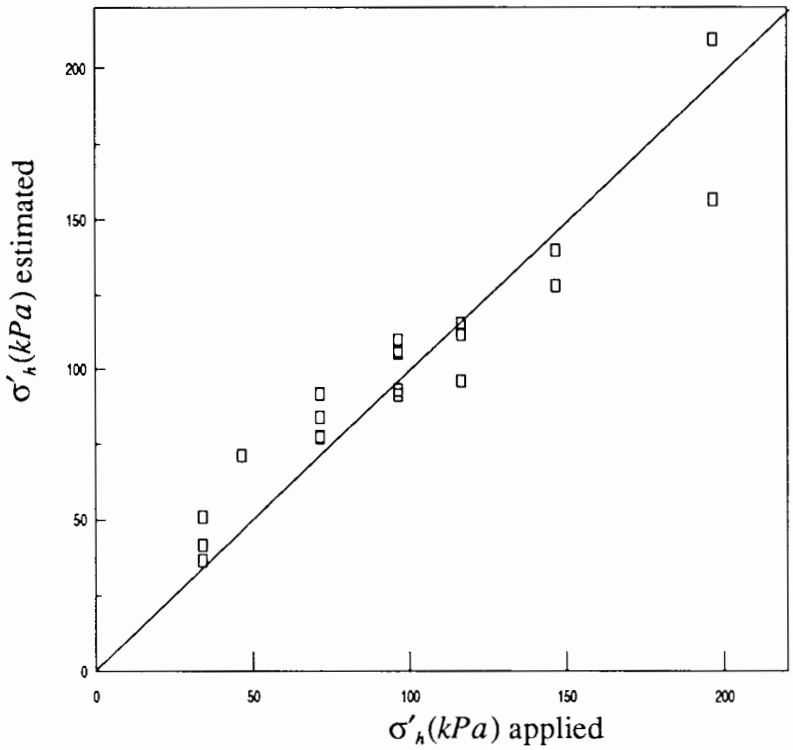

Figure 5.9 - Estimated and applied horizontal stress values

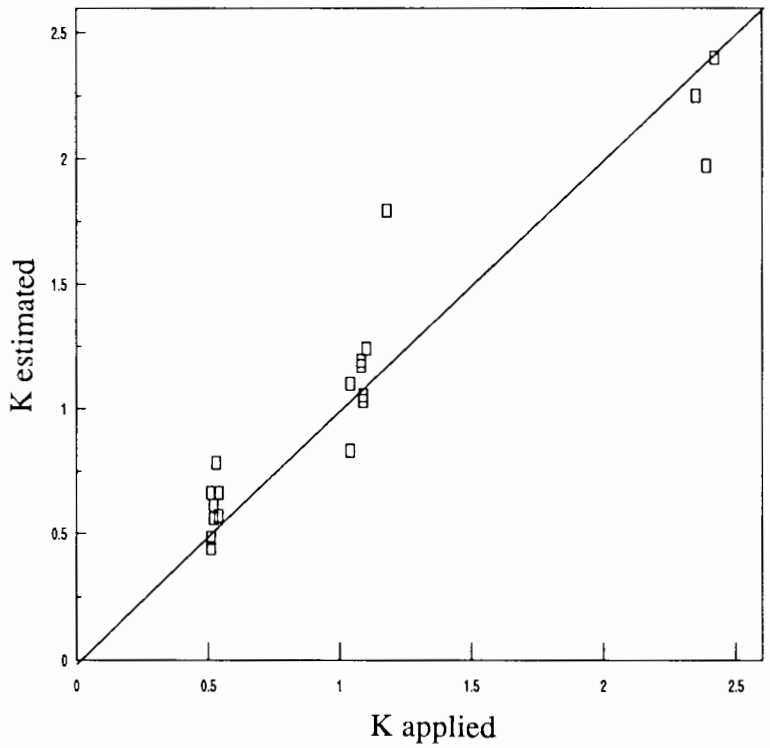

Figure 5.10 - Estimated and applied stress ratio values

5.3 - Final remarks

Calibration chamber tests have been carried out to establish a basic procedure for the interpretation of the cone-pressuremeter test in cohesionless soils. Assessment of soil properties depends on the relationship between cone resistance q_c and limit pressure ψ_l. The ratio $(q_c - \sigma_h)/(\psi_l - \sigma_h)$ is essentially dependent on relative density and not on stress level or stress ratio. An empirical relationship has been proposed for deriving density as a function of q_c and ψ_l.

Test results also show that, for a given density, both the cone resistance and the limit pressure are controlled by the horizontal effective stress. Based on this evidence, a method to estimate σ_h' as a function of the measured values of q_c and ψ_l has been proposed as an alternative to the conventional practice of assessing σ_h' from the lift-off pressure.

The horizontal stress estimated from equation [5.3] can then be used together with the measured values of q_c and ψ_l to back-calculate relative density. Relative density R_d was predicted as a function of the ratio $(q_c - \sigma_h)/(\psi_l - \sigma_h)$ from equation [5.1], as recommended for field testing interpretation. Figure 5.11 shows the comparison between R_d predicted from equation [5.1] and R_d measured in the calibration chamber in each test. A good agreement between measured and estimated values is observed and relative density can be estimated within an accuracy of about ±4%.

Finally the triaxial friction angles were evaluated by a procedure similar to that adopted for relative density. Friction angles were back-calculated by equation [5.5], using σ'_h estimated from equation [5.3] and the measured values of q_c and ψ_l. Figure 5.12 shows the comparison between ϕ'_p calculated from equation [5.5] and values measured in the triaxial tests. A generally good agreement is observed ; ϕ'_p was estimated within an accuracy of about 1°, except for two tests in which the correlation underestimates ϕ'_p by 2°.

Calibration chamber test derived correlations were established for the interpretation of the cone-pressuremeter test. However, the pressuremeter has been long recognized as an *in situ* device which works with well defined boundary conditions, as it simulates the expansion of a cylindrical cavity, and consequently permits a more rigorous theoretical analysis than many other *in situ* tests. It is therefore appropriate to examine the suitability of cavity expansion-contraction analyses for the interpretation of the cone-pressuremeter test in sand (as discussed in Chapter 1).

An attempt to apply small strain cavity expansion and contraction theories to interpret cone-pressuremeter tests was made by Withers *et al* (1989). The analyses developed by Hughes *et al* (1977) and Houlsby *et al* (1986) were examined, in which a value for the angle of friction ϕ' and a value for the angle of dilation ν were determined. Pressure-expansion curves were plotted on logarithmic scales to investigate if asymptotes to straight lines could be found at high expansions. A preliminary set of field data clearly showed that at higher pressuremeter strains the curve deviates below the theoretical straight line, which may suggest an increasing importance of creep deformations at large strains. The best fits to the slopes of those straight lines were converted to friction angles using cylindrical cavity expansion theory, and unacceptably high angles of friction were obtained from the full-displacement and cone-pressuremeter, when compared to values assessed from self-boring pressuremeter and cone resistances[2].

Equations for cylindrical expansion cavity derived by Hughes *et al* (1977) were restated in a more general form to accommodate expansion spherical cavity. The aim was to investigate if spherical rather than cylindrical cavity was more appropriate to model inflation at large strains.

---

2 *In the original paper, Withers et al (1989) make a distinction between cone-pressuremeter and full-displacement pressuremeter. According to the authors the cone-pressuremeter combines a* 60° *electric piezocone with a pressuremeter probe (as described by Withers et al, 1986). The full-displacement pressuremeter consists of a 74 mm diameter self-boring pressuremeter mounted directly behind a solid* 60° *tip which is pushed into the ground.*

The spherical model of expansion produced unacceptably low values of friction angles from cone-pressuremeter test data, when compared with values obtained from the conventional cylindrical model of self-boring pressuremeter expansion and the cone resistances.

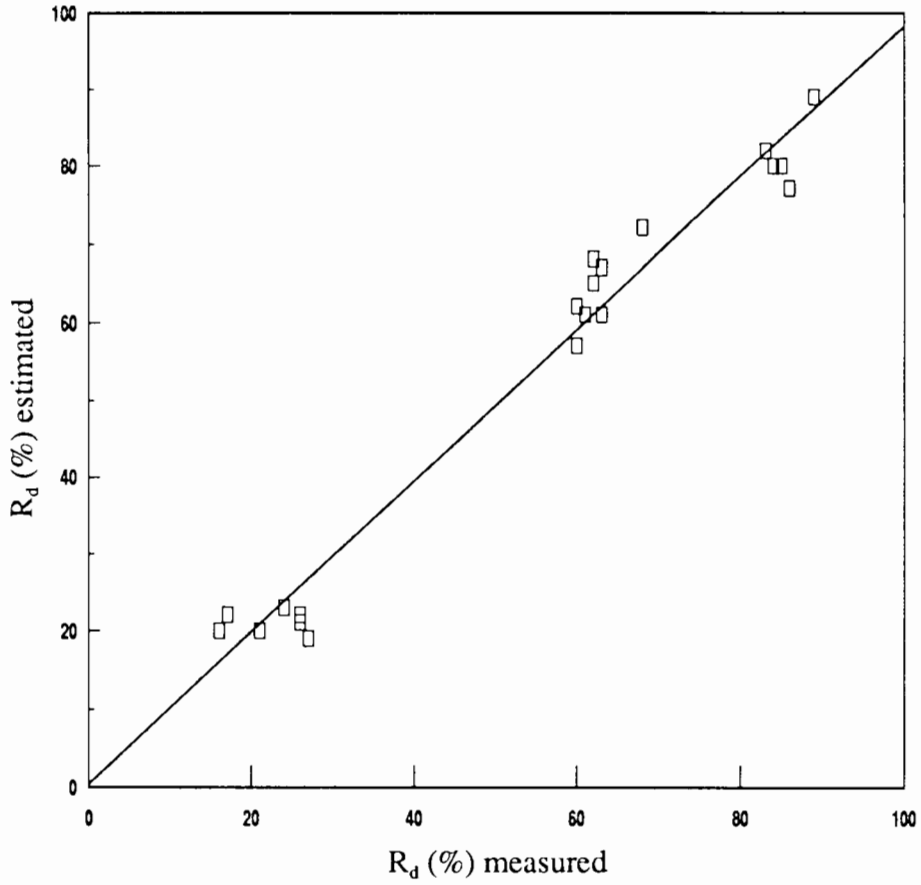

Figure 5.11 - Estimated and measured relative density values

The pressure-contraction curves were analysed using the cavity contraction theory developed by Houlsby *et al* (1986). This analysis produced unrealistic low values of friction angle from self-boring, full-displacement and cone-pressuremeter tests, when compared to values obtained from the cylindrical model of expansion and the cone resistances.

Analysis of cone-pressuremeter tests carried out in the calibration chamber produced similar unrealistic values. Like the results presented by Withers *et al* (1989), pressure-expansion and

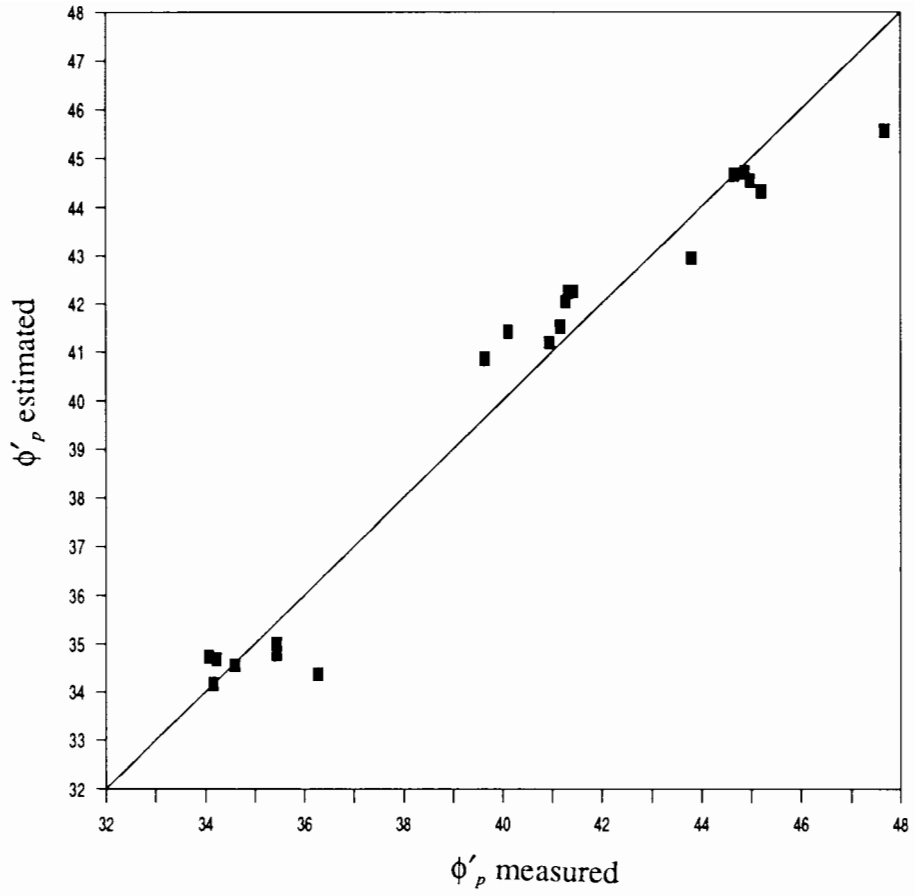

Figure 5.12 - Estimated and measured friction angle values

pressure-contraction curves indicated an increasing importance of creep deformations at large strains and pressures. For dense sand (tests 10CPMT17 to 10CPMT21) the analysis proposed by Hughes *et al* (1977) gave values of friction angle of more than 10° higher than the values obtained from the cone resistances (using equation 5.2) and the cone-pressuremeter approach using the ratio $(q_c - \sigma_h)/(\psi_l - \sigma_h)$ (equation 5.4). It is then suggested that cavity expansion-contraction theory using small strain analysis is not suitable to determine strength parameters from the cone-pressuremeter. More realistic models of large strains are necessary to produce reliable values of friction and dilation angles from loading and unloading curves.

A new analysis of the cone-pressuremeter test in clays was presented by Houlsby and Withers (1988) and was applied successfully to derive values of undrained strength and shear modulus.

The installation of the cone-pressuremeter was modelled theoretically as the expansion of a cylindrical cavity within the soil. The expansion phase of the pressuremeter test was modelled as a continued expansion of the same cylindrical cavity, and the contraction phase as a cylindrical contraction. The clay was modelled as an incompressible linear elastic, perfectly plastic (Tresca) material. A combination of large strain analysis in the plastically deforming region with small strains in the elastic region was used.

An equivalent approach for test interpretation in sand using one-dimensional finite element analysis has been presented by Houlsby and Yu (1990) and Yu (1990). The Mohr-Coulomb yield criterion was used to model the behaviour of sands. In this analysis, as well as that developed for cohesive materials, it is suggested that the difficulties in modelling the disturbance caused by the installation of the device into the ground may be overcome by using the plastic unloading curve from the pressuremeter test to derive soil parameters. Both cylindrical and spherical cases were presented so that the two interpretations were compared. In general this formulation provides a reasonable estimate of the limit of pressure. Experimental results obtained with the cone-pressuremeter (Schnaid and Houlsby, 1990) were analysed by Houlsby and Yu (1990), using the measured values of shear modulus (reported in Chapter 6), and friction and dilation angles estimated from Bolton's formulation (reported in Chapter 3). The predicted values of ψ_l agreed well with observed values in the chamber, except for dense sands, where a slight underprediction is observed. Cavity expansion large strain analysis, however, does not succeeded in deriving realistic values of strength parameters from the cone-pressuremeter test. At present it also does not give indication of horizontal stress.

An analytical solution to obtain the entire pressuremeter pressure-expansion curve in sand, as well as a two-dimentional finite element analysis, are currently being developed by Yu (1990), but its ability to provide information on the shear strength and *in situ* stresses is still subjected to further investigation. These methods outlined above must be checked by measurements of cone-pressuremeter tests carried out in the calibration chamber.

CHAPTER 6

SHEAR MODULUS

The interpretation of the "elastic" shear modulus obtained from cone-pressuremeter tests is discussed. Two procedures adopted to calculate the slope of unload-reload loops are presented, together with comparisons between the shear moduli calculated from strain arm measurements and the shear moduli calculated from volume change measurements. A method that allows the moduli to be normalised with respect to stress level is examined and the values of the moduli obtained from the cone-pressuremeter are compared with those obtained from the self-boring pressuremeter.

6.1 - Introduction

One of the most common uses of the pressuremeter test in sands is for the evaluation of soil moduli (Wroth, 1982). However, interpretation of soil moduli measured by the pressuremeter, and the application of these moduli in engineering design is far from simple, as the moduli vary with both stress level and strain amplitude (Wroth *et al*, 1979; Jamiolkowski *et al*, 1985; Bellotti *et al*, 1986, 1989; Robertson and Hughes, 1986).

In a discussion of the interpretation of the shear modulus measured by pressuremeter tests, it is assumed that the pressuremeter is a long cylindrical cavity expanding radially under plane strain conditions in the axial direction. From this, if a pressuremeter is expanded in a linear

isotropic elastic material the relationship between the change in cavity effective stresses and the change in cavity strains is well known, so that the shear modulus G can be calculated from the slope of the pressure-expansion curve as:

$$G = \frac{1}{2}\frac{d\psi}{d\varepsilon_c} \qquad [6.1]$$

which implies that the soil surrounding the probe is only subjected to shear, and the test measures the "elastic" shear modulus of soil G (Wroth, 1975; Wroth *et al*, 1979).

Ideally, three different shear moduli can be computed from a pressuremeter test as shown in Figure 6.1: the initial tangent modulus G_i, the unload-reload modulus G_{ur} and the reload-unload modulus G_{ru}. Use of a shear modulus defined over some percentage of the ultimate or yield strength (G_{30}, G_{50} etc) is not within the scope of the present work.

The initial tangent shear modulus G_i is estimated from the initial slope of the pressure-expansion curve. In sands the almost inevitable disturbance during installation makes G_i values extremely unreliable, even for the self-boring probe. For cone-pressuremeter tests expansion initially occurs in a soil that has already experienced plastic deformations due to cone penetration, and therefore G_i values are expected to be influenced by the high shear stress and shear strain levels developed in the soil surrounding the probe, as discussed in Chapter 4.

An alternative approach was proposed by Hughes (1982) and Wroth (1982), in which the elastic shear modulus is measured by performing small unload-reload loops during the test. This approach implies that any unload of the expanding cavity brings the surrounding soil below the currently expanded yield surface into a zone where strains are small and to a large

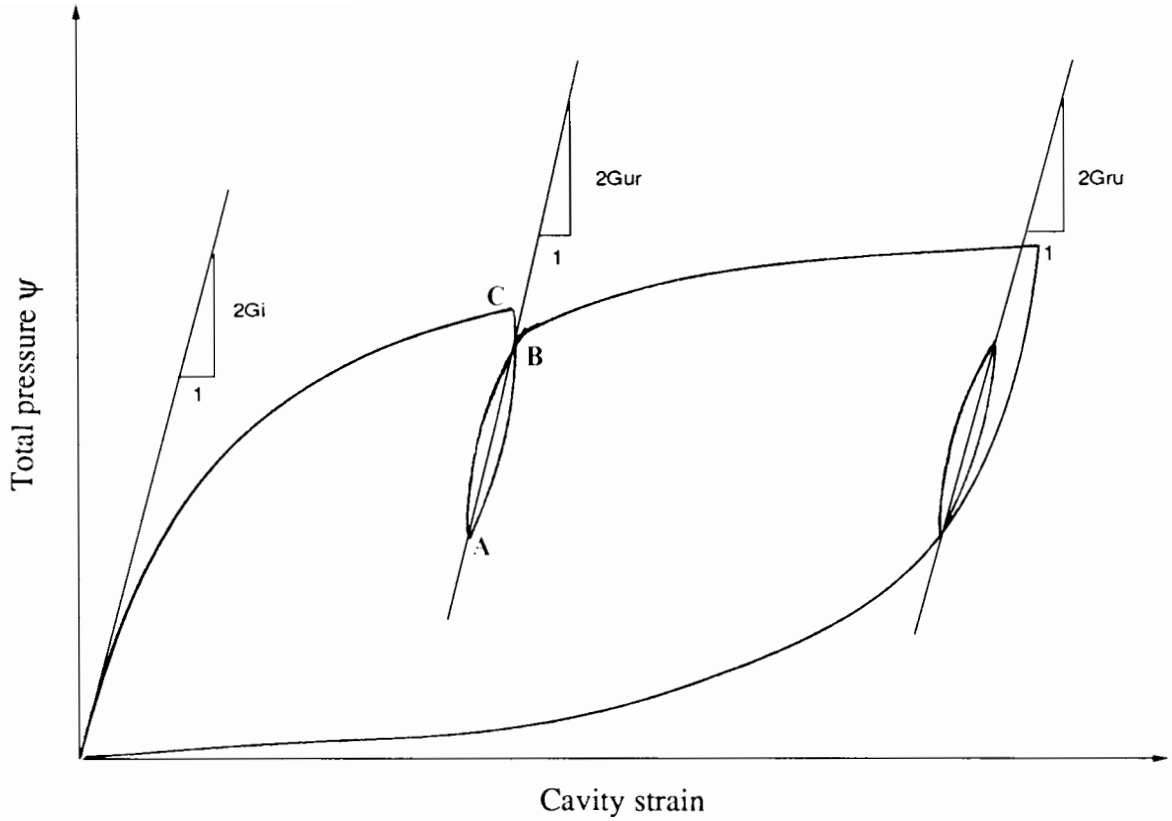

Figure 6.1 - Illustration of the determination of the three shear moduli from the cone-pressuremeter test

extent reversible. In carrying out small unload-reload loops it is necessary not to exceed the elastic limit of the soil during the unloading phase. Wroth (1982) suggested that the magnitude of the change in cavity effective stress during elastic unload should not exceed:

$$\Delta\psi' = \frac{2\sin\phi'_{ps}}{1+\sin\phi'_{ps}}\psi'_c \qquad [6.2]$$

where ψ'_c is the cavity effective stress at which unloading starts.

Previous experience with the self-boring pressuremeter test (Hughes, 1982; Wroth, 1982) has shown that G_{ur} and G_{ru} are almost completely independent of the initial disturbance due to the

installation process. Preliminary tests carried out with the cone-pressuremeter seem to confirm this finding (Hughes and Robertson, 1985; Withers *et al*, 1989). This chapter examines the methods adopted to calculate the slope of unload-reload loops. The shear moduli obtained from strain arm measurements and the shear moduli obtained from volume change measurements are compared. Possible effects of installation disturbance on the measured values of G_{ur} and G_{ru} are examined.

Finally there still exists the problem of how to apply the measured shear modulus to engineering problems in design. Wroth *et al* (1979), Robertson and Hughes (1986) and Bellotti *et al* (1989) suggested that G_{ur} and G_{ru} should be corrected to account for the average stress and strain levels existing around the probe. In this chapter a method that allows the shear modulus to be normalised with respect to stress level is examined. It is suggested that the unload-reload loop response is dominated by the maximum stresses generated at the soil-instrument interface. A method to calculated the mean stress level at the interface is proposed, in which a fully associated flow rule is used (i.e. $\phi' = \nu'$) to compute the intermediate principal stress from Matsuoka's plastic model (Matsuoka, 1976). The measured values of shear moduli are related to the mean effective stress by a power expression, similar to that suggested by Janbu (1963). It is also suggested that account should be taken of the variation of the shear moduli with the relevant shear strain amplitude observed in the loop. Within this framework, the values of G_{ur} and G_{ru} obtained form the cone-pressuremeter are compared with those obtained from the self-boring pressuremeter.

6.2 - Evaluation of the measured unload-reload shear modulus

Interpretation of the shear modulus was made using a data-base obtained from 34 cone-pressuremeter tests carried out in the Oxford calibration chamber, in which approximately 90 loops were performed. The shear modulus is computed from both radial deformation on

the mid-plane and volume variation.

Figures 6.2 and 6.3 show typical examples of expanded plots of unload-reload loops obtained from the cone-pressuremeter tests. Figure 6.2 shows two unload-reload loops in which the radial expansion of the membrane was measured by strain gauged arms. The loops were chosen to illustrate the best and the worst examples as far as resolution is concerned. Figure 6.3 presents a loop where membrane expansion was calculated by the change in volume of the pressuremeter probe.

The typical shear strain amplitude of loops in the cone-pressuremeter test is of about 0.1% to 0.2%, which for the 10 cm^2 prototype is equivalent to a variation in radius ΔR of approximately 0.02 mm to 0.04 mm. For the 5 cm^2 prototype ΔR can be as small as 0.01 mm. For each loop approximately 100 readings were recorded, so that cavity strain between two consecutive readings was of the order of 0.001% ($\Delta R = 2 \times 10^{-4}$ mm), which is equivalent to the resolution of the strain-measuring system. The electric signals from the strain gauged arms were amplified and filtered to achieve the necessary accuracy in the resolution of displacement measurements. However, in a few tests some occasional interference on the electronics was observed, and a few points deviated from the overall pattern of the loop (as illustrated in Figure 6.2b). In four tests one of the strain gauged arms showed an anomalous behaviour due to malfunction of the electronics, and the slope of the loops was calculated only from readings taken from the other two arms.

The resolution of the volume measuring system was of the order of 0.02%, although the system had been designed to produce an accuracy of the same order of magnitude as that obtained from the strain arms. As illustrated in the expanded loop shown in Figure 6.3, small steps were observed in cavity strain values recorded from volume measurements, reducing the accuracy of G values calculated from these loops.

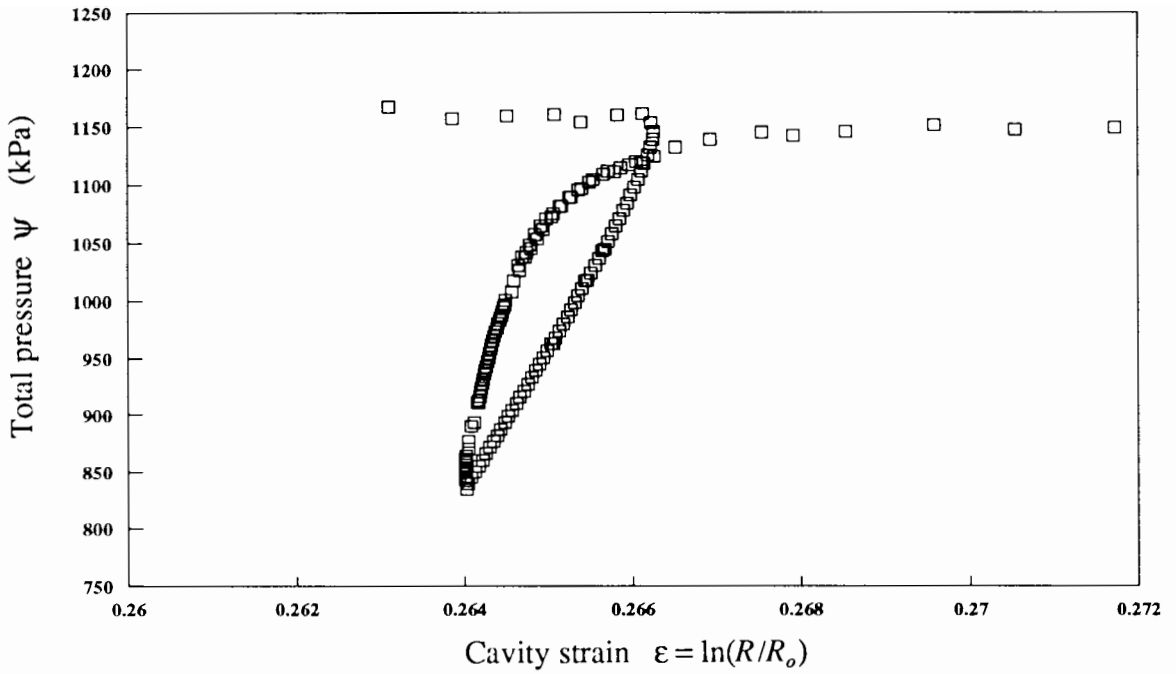

(a)

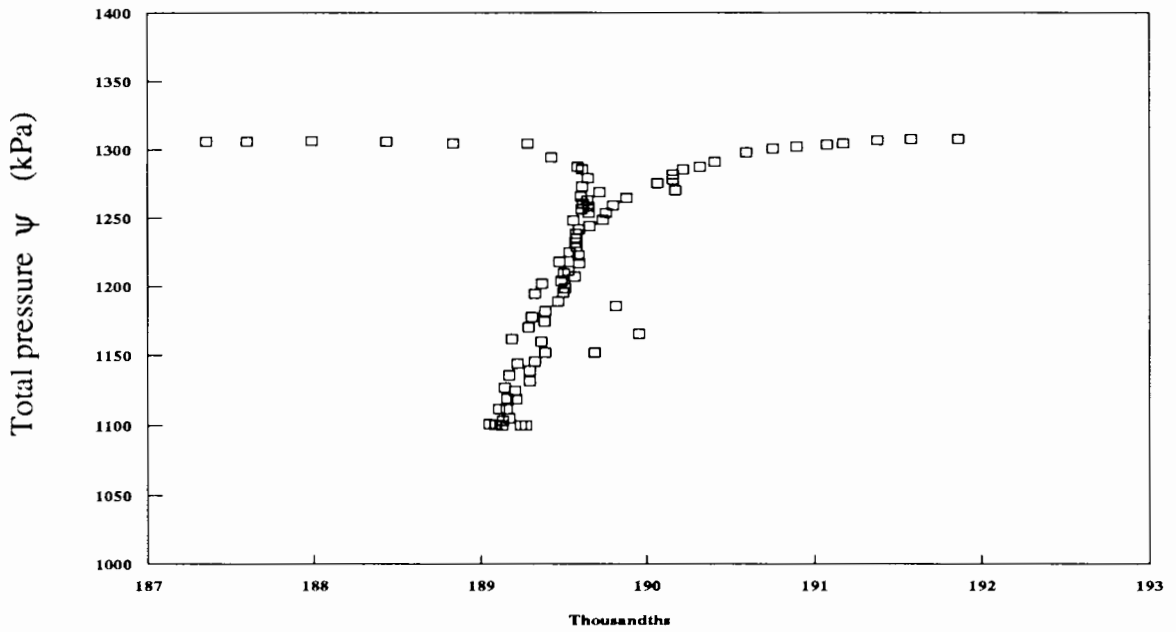

(b)

Figure 6.2 - Expanded plots of unload-reload loops measured by the central deflection of the membrane by strain gauged arms (best and worst examples as far as resolution is concerned are shown in plots (a) and (b) respectively)

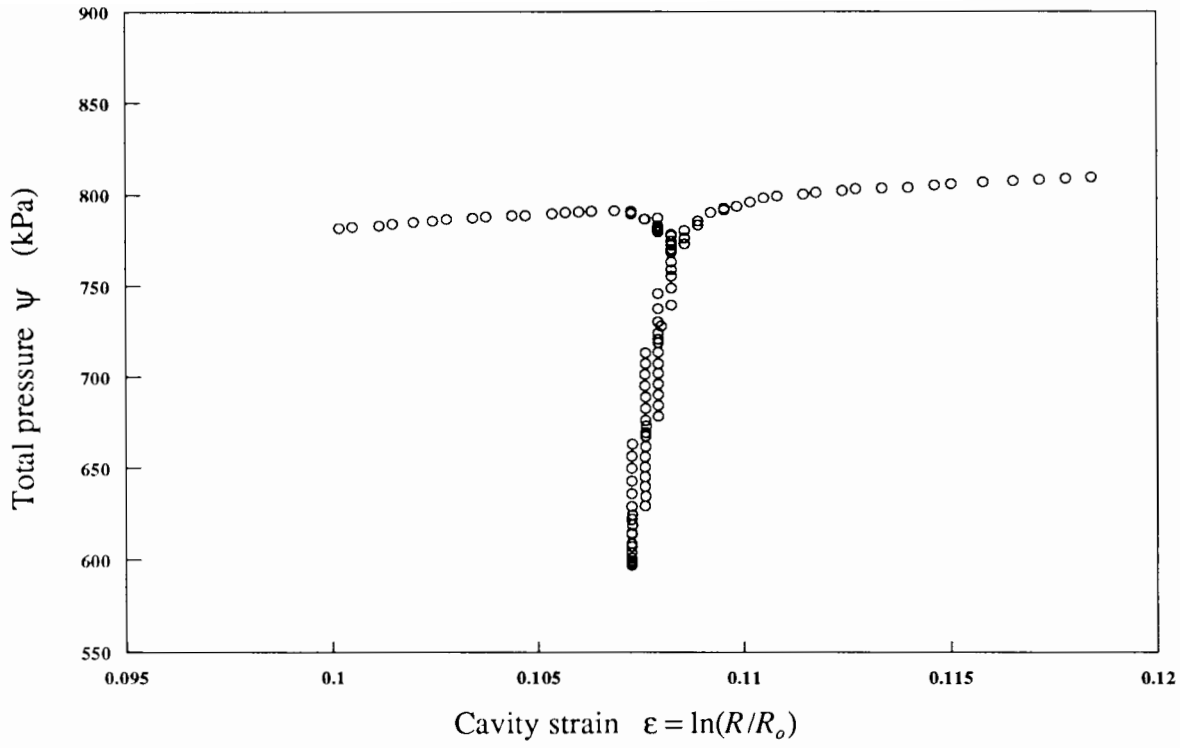

Figure 6.3 - Typical expanded plot of unload-reload loop calculated from volume change measurements

The characteristic shape of the unload-reload loops shown in Figures 6.2 and 6.3 can illustrate some important aspects to be considered in the evaluation of the shear modulus. Up to shear strain amplitudes of about 0.1% to 0.2% a non-linear hysteretic loop was formed, even if reduction in pressure was not sufficient to cause failure in extension (see equation 6.2). This hysteretic behaviour has been previously noted in laboratory and field tests (Hardin and Drnevich, 1972; Iwasaki *et al*, 1978; Hughes, 1982; Bellotti *et al*, 1989). Hysteresis in some field tests was thought to be a result of the excess of pore pressure generated during inflation and not dissipated before start of the loop, and also due to creep strains that occur during membrane expansion (Hughes, 1982). Since tests were carried out in a calibration chamber on dry sand, the accumulation of strains at constant cavity pressure was not associated with pore pressure dissipation. The possibility of creep cannot be totally eliminated, but the tests were carried out at very slow rates of shearing.

In a recent work carried out with the self-bored pressuremeter in sand, Bellotti *et al* (1989) suggested that typical shear strain amplitudes of unload-reload loops are greater than twice the elastic threshold strain of cohesionless soils (in the order of 10^{-3}%). During a loop the soil behaves as an elastic-plastic material and a non-linear hysteretic loop is formed. Resonant column tests support this hypothesis (Dobry *et al*, 1980; Lo Presti, 1987). In this work, the cone-pressuremeter is used to evaluated possible influences of non-linearity on the measured shear modulus. For this, shear strain amplitudes were kept in the range of approximately 0.1% to 0.2% and tests were carried out slowly to keep the effect of creep strains to a minimum.

The sensitivity of pressure-expansion curves to strain rates to account for creep deformation has been recently discussed by Withers *et al* (1989). The amount of creep deformation is known to increase as cavity pressure increases. To reduce the influence of creep deformation on small unload-reload loops a test procedure has been suggested by Withers *et al* (1989), in which cavity stress is held constant until an acceptably low rate of creep strain has been reached (about 0.1%/min) and then the loop is performed. An alternative approach was suggested by Bellotti *et al* (1989), in which an unload-reload loop is performed without any holding period. A hysteretic loop is then observed and the slope is calculated by drawing a line between the two apices of the loop.

In this research a test procedure was established in which the membrane was inflated at very slow rates to keep creep strains to a minimum. An inflation and deflation rate of about 0.4%/min was imposed to the tests. Before carrying out an unload-reload loop, the cavity pressure was held constant until the cavity strain rate gradually reduced to zero. Although strain increments were small, a strain controlled loop was then performed, in which the motor of the pressurisation system was driven at its minimum speed (about 0.025%/min). The time for carrying out a loop was about 10 minutes and a complete pressure-expansion curve was about 2.5 hours.

There was no intention to adopt a test procedure which would be appropriate for commercial tests, where constraints of time impose faster inflation rates, but to establish a procedure which would ideally minimise creep strain effects on pressuremeter testing data.

As presented in Chapter 4, a FORTRAN program has been developed to calculate automatically the slope of the loops. Two points were selected in the pressure-expansion curve, one immediately before and one immediately after the loop. Starting from the given points, the program searches for the two apices of the loop (points A and B in figure 6.1). First the program determines point A by searching for the lowest cavity pressure measured in the loop. Once point A is known, the program computes the cavity strains of the points in the vicinity of A and comparisons are made until the intersection of the unloading and reloading segments is found (point B). The slope of the loop and the corresponding shear modulus G are than easily calculated.

In the cone-pressuremeter tests carried out in the calibration chamber, membrane expansion was monitored by both strain gauged arms and volume changes. For each loop two values of G were then computed - the shear modulus calculated from strain arm measurements G^a and the shear modulus calculated from volume change measurements G^v.

The unload-reload loops showed a non-linear hysteretic behaviour even for a test procedure in which creep strains were allowed to occur before the loop was performed and no pore pressure was generated during inflation (see Figures 6.2 and 6.3). Under these conditions, two procedures to calculate the slope of the loops were examined:

a) to draw a single line between the two apices of the loop, and from the slope calculate the shear modulus G_{ap}.

b) to perform a simple linear regression analysis based on the least square fit of all points included between the two apices of loop, and from the slope calculate the shear modulus G_{sq}.

As a result, four shear moduli were computed from each unload-reload loop (or reload-unload loop): apices modulus values G^{a}_{ap} (arms) and G^{v}_{ap} (volume) and least square fit modulus values G^{a}_{sq} (arms) and G^{v}_{sq} (volume). Tables 6.1 to 6.3 summarize the values of shear modulus calculated from each unload-reload loop carried out using the cone-pressuremeter testing device, as well as the relevant data associated with each loop. Table 6.1 presents test results obtained with the 15 cm^2 device. In this series of tests the shear moduli measured from volume changes were not recorded, because the pressuremeter was inflated by nitrogen gas. Table 6.2 shows results obtained with the 10 cm^2 cone-pressuremeter prototype. Finally Table 6.3 presents tests carried out with the 5 cm^2 prototype, in which the shear modulus was computed from volume changes only.

6.2.1 - Calibrations and Corrections

Calibrations are an essential operation required to obtain the corrected pressure-expansion curve, and they can have an appreciable influence on the measurement of the unload-reload shear modulus. In stiff soils, the strain amplitude observed during an unload-reload loop is very small and inaccuracies in the strain arm measuring system or in the volume measuring system can result in large errors. To account for small volume or radius changes due to system compliance very careful calibrations were carried out.[1]

---

1 *The compliance of the strain arm system means any compression of the rubber membrane, together with the actual compliance of the strain arms. The compliance of the volume measuring system is understood as line and control unit flexibility.*

TEST	LOOP	ε_C	ψ_C	γ_{UR}	G^a_{ap}	G^a_{sq}
		%	kPa	%	MPa	MPa
15CPMT02	A	24.10	1381.5	0.081	76.1	28.8
	B	30.59	1426.6	0.254	73.8	66.3
15CPMT03	A	19.61	1100.8	0.500	63.7	61.8
	B	26.62	1120.4	0.427	66.9	51.2
15CPMT04	A	19.04	583.0	0.624	41.5	37.4
	B	26.47	602.8	0.600	39.0	34.8
15CPMT05	A	20.07	1448.5	0.352	75.5	56.1
	B	26.73	1418.0	0.408	67.4	45.2

Notes

(1) G = unload-reload shear modulus

(2) ψ_C = cavity pressure at start of unloading

(3) ε_C = pressuremeter cavity strain at start of unloading (calculated from strain arm measurements)

(4) γ_{UR} = average shear strain amplitude of unload-reload loop (calculated from strain arm measurements)

Table 6.1 - Shear moduli obtained from unload-reload loops using the 15 cm^2 cone-pressuremeter prototype

TEST	LOOP	ε_C %	ψ_C kPa	γ_{UR} %	G^a_{ap} MPa	G^a_{sq} MPa	G^v_{ap} MPa	G^v_{sq} MPa
10CPMT02	A	3.190	295.5	0.198	43.3	34.4	20.4	16.9
	B	13.77	375.1	0.106	74.4	55.4	44.7	33.4
	C	21.82	401.6	0.118	55.1	58.5	47.3	40.2
	D	27.31	249.6	0.154	52.0	44.1	23.8	19.2
10CPMT03	A	5.752	262.5	0.129	45.2	42.6	23.6	18.7
	B	14.43	295.9	0.152	53.4	28.1	60.8	34.5
	C	22.52	301.6	0.115	60.4	59.5	30.1	27.9
	D	29.40	186.7	0.200	41.6	28.8	20.4	18.9
10CPMT04	A	5.631	600.2	0.172	81.4	63.6	57.3	51.7
	B	14.84	692.7	0.135	109.3	95.1	71.3	71.0
	C	22.86	724.2	0.215	67.1	63.0	76.8	64.1
	D	30.04	462.6	0.268	55.8	44.6	70.7	60.0
10CPMT05	A	6.220	451.2	0.132	84.8	76.6	48.5	42.9
	B	15.25	558.8	0.225	72.7	55.0	54.1	44.7
	C	23.48	576.0	0.231	61.7	59.8	59.9	55.6
	D	30.60	329.6	0.262	59.1	49.3	39.6	40.5
10CPMT06	A	5.101	1172.0	0.198	111.7	91.5		
	B	14.50	1341.0	0.168	132.0	118.5		
	C	26.44	1407.0	0.209	126.7	68.3		
10CPMT07	A	4.079	618.0	0.182	82.5	60.9	91.5	56.3
	B	14.21	750.7	0.168	91.6	89.5	82.1	79.8
	C	22.43	763.8	0.138	92.2	104.7	82.2	86.6
	D	28.09	430.4	0.261	75.3	64.0	47.6	54.0
10CPMT08	A	5.292	817.4	0.117	142.5	111.5	101.8	82.4
	B	14.29	974.3	0.202	82.8	81.8	125.8	86.0
	C	22.37	1025.2	0.178	84.6	104.2	114.5	59.4
	D	27.33	662.8	0.191	100.7	77.1	113.9	55.2
10CPMT09	A	6.560	1117.9	0.090	195.2	151.7	121.0	90.1
	B	12.50	1332.5	0.087	193.4	163.4	119.7	91.6
10CPM10	A	6.922	1162.0	0.138	178.2	118.4	95.6	79.6
	B	15.74	1259.5	0.148	157.7	130.5	92.0	82.6
10CPMT11	A	5.185	1136.5	0.114	155.3	167.1		
	B	14.27	1383.1	0.172	126.4	119.7		
	C	22.63	1388.0	0.155	102.9	184.8		
	D	27.45	805.3	0.177	139.1	85.4		

Table 6.2 - Shear moduli obtained from unload-reload loops using the 10 cm² cone-pressuremeter prototype

TEST	LOOP	ε_C	ψ_C	γ_{UR}	G^a_{ap}	G^a_{sq}	G^v_{ap}	G^v_{sq}
		%	kPa	%	MPa	MPa	MPa	MPa
10CPMT12	A	5.193	906.9	0.125	149.0	130.4	118.5	99.4
	B	11.81	1166.1	0.195	176.2	118.3	105.1	75.5
	C	18.96	1238.7	0.091	152.0	159.6	112.9	91.5
	D	22.72	727.6	0.210	97.3	104.4	108.6	83.1
10CPMT13	A	4.301	1042.3	0.137	142.5	110.0	216.1	96.4
	B	10.74	1358.1	0.071	233.9	144.4	246.0	127.7
	C	18.64	1535.0	0.100	193.1	154.4	140.9	130.6
	D	21.53	832.6	0.173	142.6	103.9	111.7	94.2
10CPMT14	A	5.433	1543.9	0.078	222.5	186.9		
	B	12.08	1913.6	0.096	226.0	98.9		
	C	20.51	2031.4	0.116	186.5	185.2		
10CPMT15	A	5.035	433.4	0.291	52.6	41.5	57.5	48.4
	B	13.25	551.7	0.232	65.1	50.4	69.3	54.6
	C	23.51	593.1	0.234	56.8	51.1	54.3	46.6
	D	27.42	264.2				29.8	27.8
10CPMT16	A	10.20	2247.8	0.087	250.3	185.9	143.8	124.7
	B	12.15	2266.6	0.109	189.7	166.8	214.9	133.8
10CPMT17	A	6.233	629.8	0.165	115.6	88.1	64.1	56.5
	B	13.25	720.1	0.169	115.7	107.8	48.0	46.1
	C	23.18	742.6	0.272	66.7	58.9	52.5	44.8
	D	23.99	439.4	0.299	65.7	46.6		
10CPMT18	A	6.558	1184.5	0.103	264.3	206.0	123.1	95.2
	B	12.15	1365.8	0.095	239.1	171.0	110.9	82.6
10CPMT20	A	7.021	1580.7	0.075	278.8	228.6	209.5	186.4
	B	12.44	1762.4	0.078	263.8	175.3	172.9	148.8
	C	16.02	1828.5	0.077	273.3	227.0	128.4	79.4
	D	18.17	1358.8	0.125	231.8	228.2	160.6	107.9
10CPMT21	A	6.828	1719.0	0.082	291.9	198.3	210.6	99.8
	B	12.93	1976.6	0.068	277.3	151.5	250.3	124.3
	C	16.65	2028.6	0.122	193.9	182.5	175.1	120.3

Notes
(1) ψ_C = pressuremeter cavity pressure at start of unloading
(2) ε_C = pressuremeter cavity strain at start of unloading (calculated from strain arm measurements)
(3) γ_{UR} =average shear strain amplitude of an unload reload loop (calculated from strain arm measurements)

Table 6.2 (continued)- Shear moduli obtained from unload-reload loops using the 10 cm² cone-pressuremeter prototype

TEST	LOOP	ε_C %	ψ_C kPa	γ_{UR} %	G^v_{ap} MPa	G^v_{sq} MPa
5CPMT01	A	16.05	904.5	0.083	98.0	40.8
5CPMT02	A	7.820	1712.2	0.188	128.6	70.6
5CPMT03	A	9.684	1279.7	0.180	121.9	69.7
	B	15.15	1359.5	0.098	215.4	105.9
5CPMT04	A	9.850	1568.9	0.178	76.0	23.3
5CPMT05	A	7.515	1526.5	0.036	424.2	101.8
	B	10.51	1760.4	0.022	789.5	218.0
5CPMT06	A	6.800	1591.6	0.037	564.7	64.7
	B	9.322	1887.1	0.036	529.4	170.0
5CPMT07	A	7.136	865.7	0.051	163.0	94.4
	B	11.20	96.1	0.106	130.9	107.1
5CPMT08	A	7.400	1229.7	0.109	182.6	115.8
	B	12.53	1401.0	0.180	110.4	90.3

Notes

(1) ψ_C = pressuremeter cavity pressure at start of unloading

(2) ε_C = pressuremeter cavity strain at start of unloading (calculated from volume change measurements)

(3) γ_{UR} = average shear strain amplitude of an unload reload loop (calculated from volume change measurements)

Table 6.3 - Shear moduli obtained from unload-reload loops using the 5 cm² cone-pressuremeter prototype

The effect of pressuremeter compliance on the measured shear modulus has already been recognized (Mair and Wood, 1987; Fahey and Jewell, 1990). Fahey and Jewell (1990) suggested a calibration procedure to determine the compliance of the measuring system, which consists of expanding the pressuremeter inside a thick-walled steel cylinder until the membrane comes in contact with the inside wall of the cylinder, and then increasing the pressuremeter pressure in a manner which mimicked the procedure adopted in tests. A series of compliance tests was performed with the cone-pressuremeter testing device . The results of one such calibration are shown in Figure 6.4, in which cavity pressure is plotted against cavity strain calculated from both strain arm measurements and volume change measurements. Several unload-reload loops were performed to estimate the "system shear modulus" G_{system} at different levels of cavity pressure.[2] The compliance of the volume measuring system is significantly higher than that observed in the strain arm measuring system, but in both cases the stiffness of the system increases as cavity pressure increases. In both cases the relationship between shear modulus G_{system} and cavity pressure at the beginning of unloading ψ_c was well fitted by an exponential expression:

$$G_{system}/p_a = \exp(A + (\psi_c/p_a)B) \qquad [6.3]$$

with A = 6.460, B = 0.254 and a correlation coefficient squared r^2 = 89.67% for strain arm measurements; and A = 6.300, B = 0.142 and a correlation coefficient squared r^2 = 88.40% for volume measurements. In equation [6.3] shear modulus and stresses have been normalised by atmospheric pressure in order to make the expression dimensionless. By making use of equation [6.3] to determine G_{system}, the effect of compliance (i.e. the stiffness of the system) on the measured soil shear modulus was determined as:

---

2 *For this series of calibrations a high degree of precision was required, since the measurements of very small strains were necessary. The volume measuring system has been completely checked and by making improvements on the electronics a resolution of 0.001% has been achieved, which is equivalent to the resolution of the strain measuring system.*

$$\frac{1}{G_{corrected}} = \frac{1}{G_{measured}} - \frac{1}{G_{system}} \qquad [6.4]$$

As far as the strain arm measuring system is concerned, the apices shear moduli were corrected on average by a factor G^c_{ap}/G_{ap} of approximately 1.22, whereas the least square moduli were corrected by an average factor of G^c_{sq}/G_{sq} of 1.18. For the volume measuring system the corrections were even more significant. The apices shear moduli were corrected in average by a factor G^c_{ap}/G_{ap} of about 1.64, whereas the least square moduli were corrected by a factor G^c_{sq}/G_{sq} of 1.47. The magnitude of this correction on the shear modulus measured for every loop is given later in this chapter. Such a correction has a considerable influence on shear moduli, especially for volume change measurements, and was applied to test data with the specific purpose of comparing shear moduli calculated from the volume measuring system with shear moduli calculated from the strain arm measuring system. In four of the unload-reload loops, the measured soil shear modulus was roughly of the same order of magnitude as the system shear modulus, leading to unacceptably large correction factors. In these cases the volume measuring system was considered inadequate to measure the unload-reload shear modulus of the soil and the corrected values of G were not included in further correlations. One consolation is that the compliance observed in the volume measuring system, as well as the strain arm measuring system, is not as significant as that observed for probes currently used in engineering practice (as reported by Fahey and Jewell, 1990).

Small corrections to account for system compliance have an appreciable influence on the modulus obtained from unload-reload loops. To make a best estimate of the shear modulus another minor correction has to be applied to account for the finite length of the pressuremeter probe. This problem has been investigated by Houlsby and Carter (1990) using two dimensional finite element analysis. Volume changes and central deflections of the membrane were computed for probes of different length to diameter ratios. As far as elastic theory is concerned, corrections to the measured shear modulus were given to compensate for the constraints

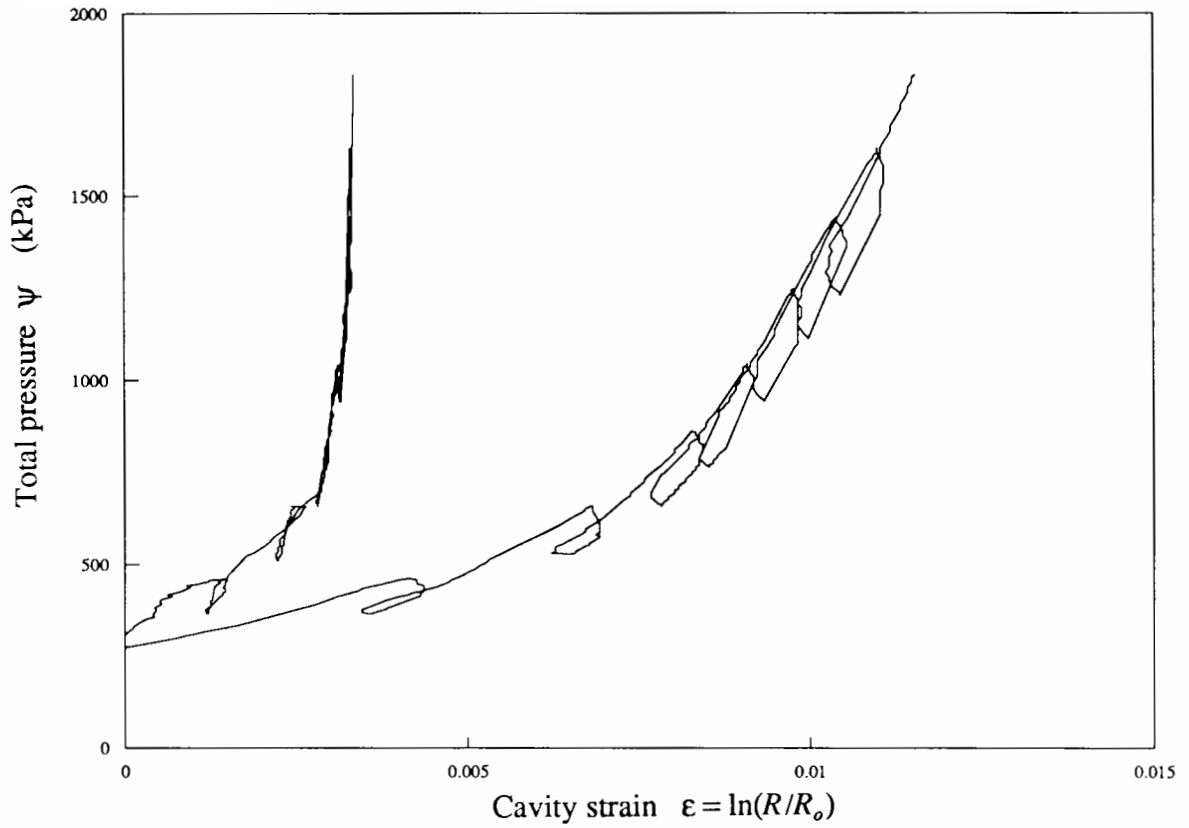

Figure 6.4 - Compliance tests in a thick-walled steel cylinder

imposed by the end of the membrane. The correction factors obtained for a 10:1 length to diameter probe were applied to the cone-pressuremeter data. The shear moduli calculated from measurements of the central deflection of the membrane were corrected by multiplying by a factor of 0.997, whereas the shear moduli calculated from volume change measurements were corrected by a factor of 0.907.

A block diagram is presented in Figure 6.5 to illustrate the correction procedure adopted to obtain the best possible estimate of the unload-reload shear modulus. The inflation pressure recorded during the test is first corrected by subtracting the "membrane correction", which is undertaken by inflating the pressuremeter in air to obtain the membrane stiffness (see Chapter 4 for details). The corrected pressure-expansion curve is then used for calculating the shear moduli G_{ap} and G_{sq}. As previously discussed, two other corrections are still necessary to

account for compliance effects and for the finite length of the pressuremeter probe. In order to quantify the magnitude of these corrections the apices moduli G_{ap} are presented in Table 6.4, in which the values of G_{ap} were corrected to account for compliance effects and then further corrected to account for the finite length of the probe . The values of G_{ap} (before corrections) and G^c_{ap} (after overall corrections) were used to calculate the correction factors G^c_{ap}/G_{ap} shown in Table 6.5. The average correction, as well as the maximum and minimum corrections recorded on a single loop, are presented in the table. The magnitude of the correction to account for compliance of the equipment has serious implications for the measured shear modulus obtained from unload-reload loops and the need for calibrations is emphasized. The adoption of corrected factors to account for the finite length of the pressuremeter probe is recommended, specially if volume measurements are to be used.

6.3 - Interpretation of shear modulus

The interpretation of the unload-reload (or reload-unload) shear modulus consisted of three parts. In the first, the two procedures to calculate the slope of the loops were examined and values of G_{ap} and G_{sq} were compared. Secondly, comparisons between the shear moduli calculated from strain arm measurements and the shear moduli calculated from volume change measurements were presented. In the third part, a method that allows the shear modulus to be normalised with respect to stress level is discussed. The unload-reload shear moduli presented in this section correspond to values obtained after corrections to account for compliance effects and pressuremeter finite length (see section 6.2).

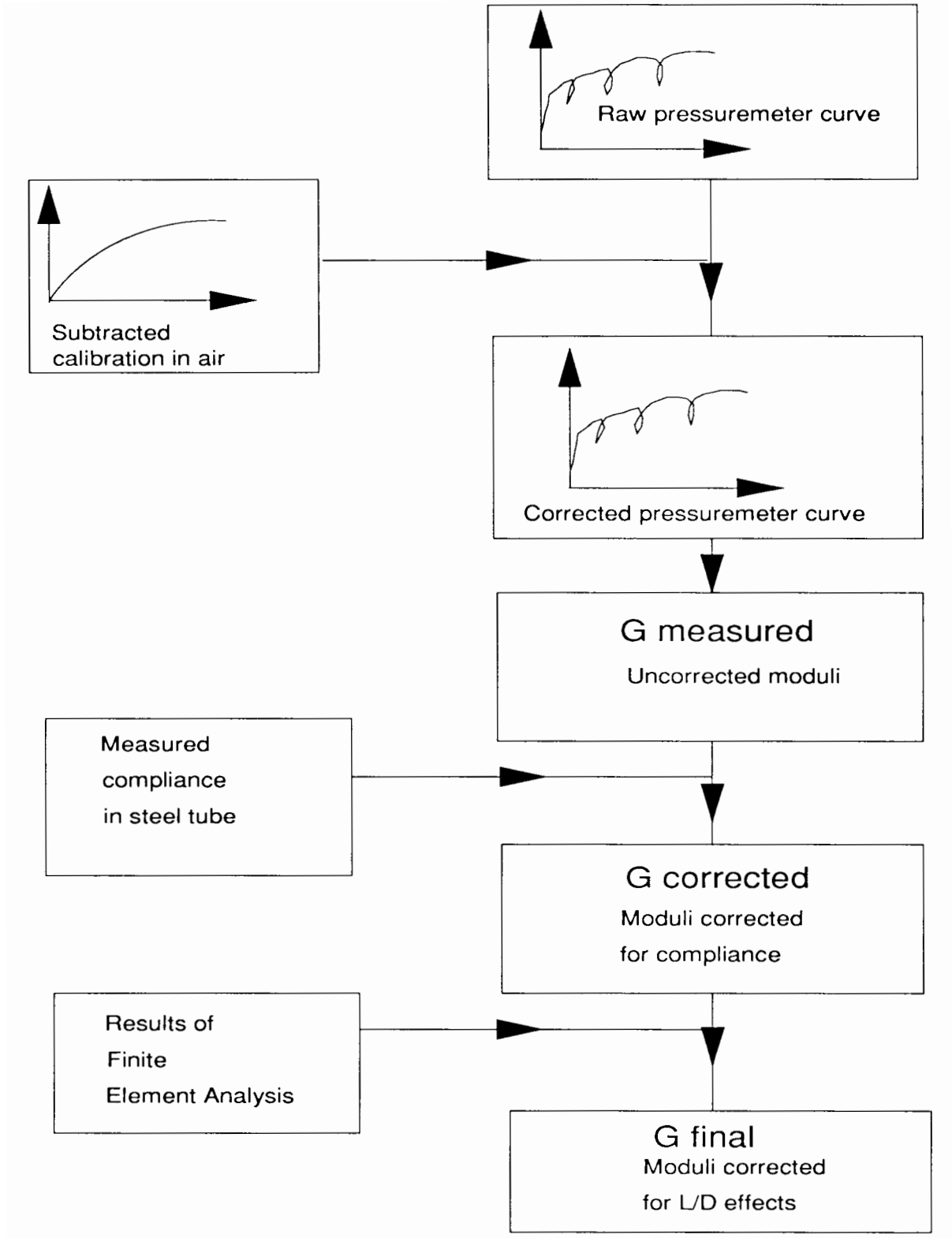

Figure 6.5 - Block diagram representing the corrections to the measured unload-reload shear modulus

RAW DATA		CORRECTION TO PROBE FINITE LENGTH		CORRECTION TO COMPLIANCE EFFECTS	
G^{a}_{pa} MPa	G^{v}_{ap} MPa	G^{a}_{pa} MPa	G^{v}_{ap} MPa	G^{a}_{pa} MPa	G^{v}_{ap} MPa
43.3	20.4	43.2	18.5	63.4	23.8
74.4	44.7	74.2	40.54	134.3	72.1
55.1	47.7	54.9	43.3	79.6	78.7
52.0	23.8	51.8	21.6	84.7	29.3
45.2	23.6	45.1	21.4	70.1	29.4
53.4	60.8	53.2	55.15	87.7	165.2*
60.4	30.1	60.2	27.3	107.2	40.6
41.6	20.4	41.5	48.5	60.3	23.9
84.1	57.3	81.2	52.0	112.2	87.8
109.3	71.3	109.0	64.7	154.3	116.6
67.1	76.8	66.9	69.7	80.3	128.7
59.1	49.3	58.9	44.7	60.5	88.9
84.9	48.5	84.7	44.0	146.3	76.7
72.7	54.1	72.5	49.1	99.9	82.9
61.7	59.9	61.5	54.3	79.2	97.2
59.1	39.6	58.9	35.9	79.0	52.9
117.2		116.9		128.9	
132.0		131.6		141.3	
126.7		126.3		133.7	
82.5	91.5	82.3	83.0	112.4	227.4*
91.6	82.1	91.3	74.5	116.0	141.1
92.2	82.2	91.9	74.5	115.9	139.1
75.3	47.6	75.1	43.2	98.7	64.1
142.5	101.8	142.1	92.3	197.1	197.7
82.8	125.8	82.6	114.1	92.6	241.3
84.6	114.5	84.4	103.9	93.5	187.6
100.7	113.9	100.4	103.3	123.8	247.2
195.2	121.0	194.6	109.8	236.9	187.3
193.4	119.7	192.8	108.6	214.8	155.5
178.2	95.6	177.7	86.7	207.9	125.1
157.7	92.0	157.2	83.4	174.8	112.4
155.3		154.8		179.0	
126.4		126.0		133.9	

* Values not included in any further correlation - ($G_{system} \sim G_{soil}$)

Table 6.4 - Shear moduli corrections to account for probe length and compliance effects

RAW DATA		CORRECTION TO PROBE FINITE LENGTH		CORRECTION TO COMPLIANCE EFFECTS	
G^{a}_{pa} MPa	G^{v}_{ap} MPa	G^{a}_{pa} MPa	G^{v}_{ap} MPa	G^{a}_{pa} MPa	G^{v}_{ap} MPa
102.9		102.6		107.7	
139.1		138.7		163.2	
149.0	118.5	148.6	107.5	193.5	236.8
176.2	105.1	175.7	95.3	204.8	143.5
152.0	112.9	151.5	102.4	168.8	151.8
97.3	93.6	97.0	84.9	114.5	149.6
142.5	216.1	142.1	196.0	168.6	1101.5*
233.9	246.7	233.2	223.8	263.8	559.4*
193.1	140.9	192.5	127.8	205.0	174.3
142.6	111.7	142.2	101.3	166.3	170.6
222.5		221.8		238.2	
226.0		225.3		231.7	
186.1		185.5		188.7	
52.6	57.5	52.4	52.2	72.1	108.3
65.1	69.5	64.9	63.0	86.6	134.1
56.8	54.3	56.6	49.3	70.5	80.8
	29.8		27.0		41.0
250.3	143.8	249.6	130.4	255.0	150.0
189.7	214.9	189.1	194.9	190.9	227.8
115.6	64.1	115.3	58.1	181.3	103.4
115.7	48.0	115.3	58.1	181.3	103.4
66.7	52.5	66.5	47.6	79.0	68.6
65.7		65.5		82.3	
264.3	123.1	263.5	111.7	330.9	180.9
239.1	110.9	238.4	100.6	269.7	137.2
278.8	209.5	278.0	190.0	301.7	302.4
263.8	172.9	263.0	156.8	275.9	205.6
273.3	128.4	272.5	116.5	284.1	138.7
231.8	160.6	231.1	145.7	244.8	197.1
291.9	210.3	291.0	190.7	308.9	275.1
277.3	250.3	276.5	227.0	284.6	304.1
193.9	175.1	193.3	158.8	196.8	190.1

* Values not included in any further correlation - ($G_{system} \sim G_{soil}$)

Table 6.4 (continued) - Shear moduli corrections to account for probe length and compliance effects

CORRECTION	ARMS MEASUREMENTS		VOLUME MEASUREMENTS	
	G^c_{ap}/G_{ap}	G^c_{sq}/G_{sq}	G^c_{ap}/G_{ap}	G^c_{sq}/G_{sq}
AVERAGE	1.22	1.18	1.40	1.28
MAXIMUM	1.81	1.75	2.17	1.79
MINIMUM	1.01	1.01	1.01	1.00

Table 6.5 - Summary of shear moduli corrections

6.3.1 - Apices modulus G_{ap} against least square fit modulus G_{sq}

Examples of unload-reload loops from cone-pressuremeter tests were presented earlier in this chapter in Figures 6.2 and 6.3. Although shear strain amplitudes of about 0.1% to 0.2% were recorded, the loops have shown a non-linear hysteretic behaviour even for a test procedure in which creep strains were allowed to occur before the loop was performed. To assess the influence of non-linearity of a loop on the measured shear modulus two procedures were examined to calculate the slope of the loops, and values of G_{ap} and G_{sq} were determined.

Note that if sand behaves as a perfectly elastic-plastic material then the unload-reload loop will be a straight line of gradient 2G, and identical values of G_{ap} and G_{sq} would be obtained. In practice a non-linear hysteretic unload-reload loop is formed. A procedure for calculating the slope from the two apices of the loop is then recommended (e.g. Bellotti *et al*, 1989), hypothesizing that a line drawn between the two apices corresponds approximately to the

rotational axis of symmetry of the loop. If this simplification is corrected any difference between G_{ap} and G_{sq} values will be negligible, and the choice of procedures would have no effect on the evaluation of the shear modulus.

A direct comparison between G_{ap} and G_{sq} obtained from strain arm measurements is shown in Figure 6.6, whereas the same comparison obtained from volume change measurements is shown in Figure 6.7. Although some scatter is observed, G_{sq} values are generally smaller than G_{ap} values. In average the ratio G_{sq}/G_{ap} is of about 0.80 for strain arm measurements and of about 0.70 for volume change measurements. The ratio G_{sq}/G_{ap} is not dependent on density, stress level or pressuremeter strain at the start of unloading.[3]

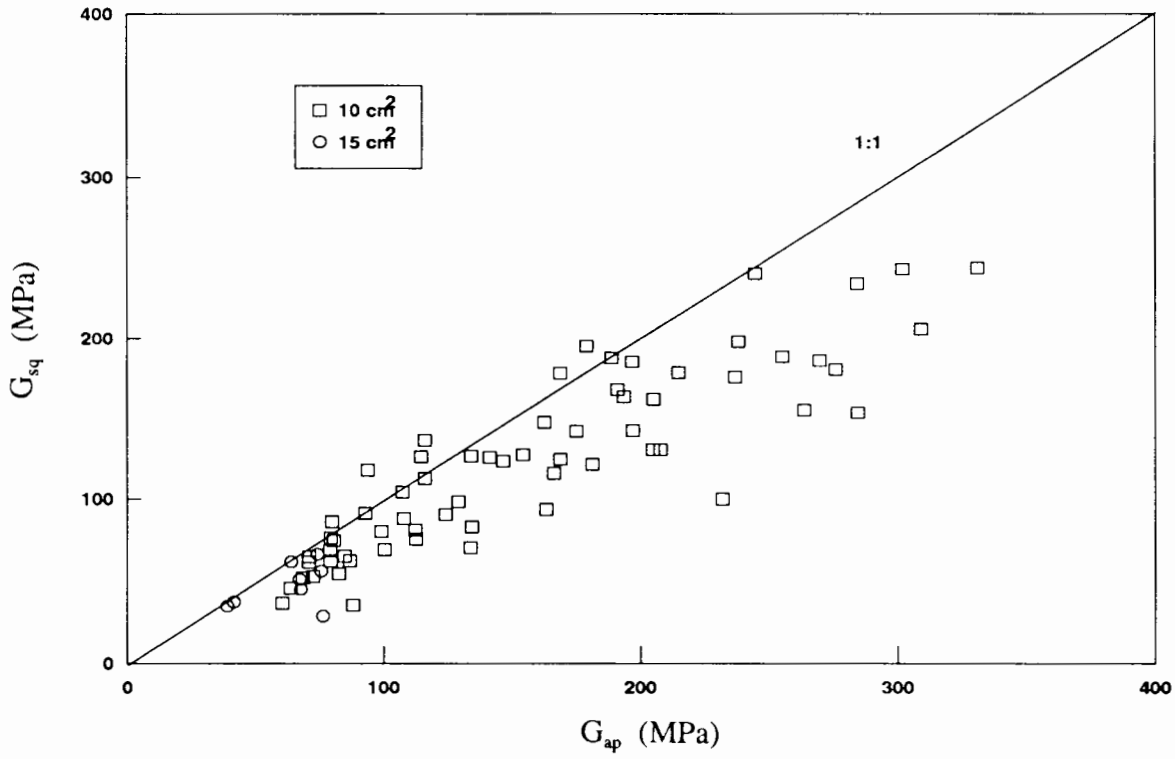

Figure 6.6 - Comparison between the apices moduli G_{ap} and the least square fit moduli G_{sq} obtained from strain arm measurements

---

3 *Although not corrected to account for compliance effects, the unload-reload shear moduli measured with the 15 cm² and 5 cm² prototypes were included in Figures 6.6 and 6.7. Such a correction would change the relative position of these values in the figures.*

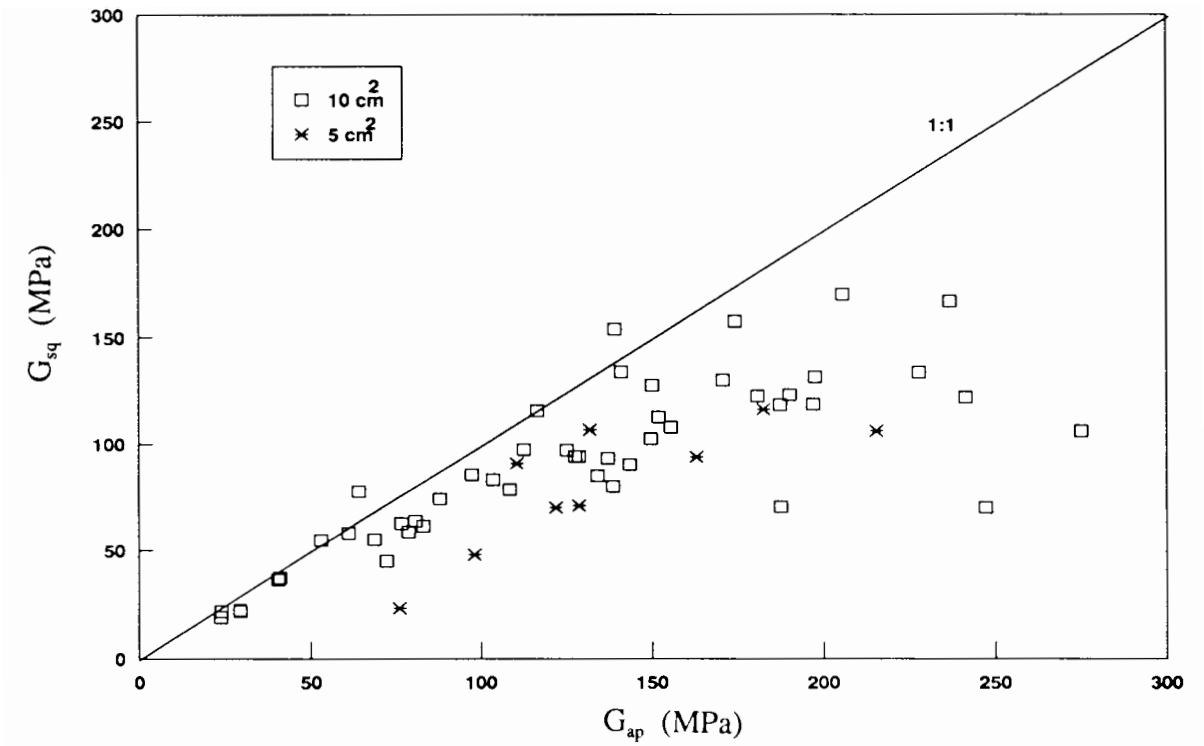

Figure 6.7 - Comparison between the apices moduli G_{ap} and the least square fit moduli G_{sq} obtained from volume change measurements

The pressuremeter has been designed primarily to measure the shear modulus of the soil. High precision is required in the measurements of strains for a reliable evaluation of the shear modulus, but a simple change in the definition used for G leads to average typical changes of 20% to 30% on G values calculated from small unload-reload loops. The understanding of the differences between G_{ap} and G_{sq} can only be addressed in a qualitative way. The unloading and reloading segments are non-linear but not symmetrical in respect to the slope $2G_{ap}$. A close observation of recorded unload-reload loops from cone-pressuremeter tests show that generally unloading remains sensibly linear, whereas reloading exhibits a markedly non-linear behaviour (this pattern is clearly illustrated in Figure 6.2). The shear modulus G_{ap} is dominated by the slope of unloading, whereas G_{sq} is influenced by measurements recorded in both unloading and reloading. Since reloading is highly non-linear G_{ap} values are usually stiffer than G_{sq} values.

The relationship between G_{ap} and G_{sq} (G_{sq}/G_{ap} from 0.7 to 0.8) was observed for tests carried out with the 15 cm^2, 10cm^2 and 5 cm^2 cone-pressuremeter testing devices in Leighton Buzzard sand, from strain arm measurements and volume change measurements. Loops were carried out under controlled conditions, in which the change in cavity effective stress did not exceeded the elastic limit of the sand during the unloading phase (variations in cavity effective stress were usually less than half the maximum value suggested by equation 6.2). Therefore, the ratio G_{ap}/G_{sq} is not associated with large plastic deformations or mechanical features of the displacements sensors.

Shear moduli G_{ap} and G_{sq} were calculated from unload-reload loops, in which creep strains were allowed to occur before the loop was carried out. The effect of creep deformations is known to increase the non-linear hysteretic behaviour of loops, but its influence on the measured shear modulus (and therefore the ratio G_{sq}/G_{ap}) is still to be investigated. Since a complete explanation of the effect of creep strains on the measured shear modulus is still needed, any test procedure should be designed to allow creep displacements to occur, before the unload-reload loop is carried out. The evaluation of the shear modulus from unload-reload loops should be made using the two procedures described in this chapter (to calculate G_{ap} and G_{sq}). The use of the ratio G_{sq}/G_{ap} can provide additional information on the accuracy of the strain-measuring system, as it is sensitive to occasional interferences on the electronics and to anomalous behaviour of the mechanical displacement sensors.

6.3.2 - Strain arm measurements against volume change measurements

On tests carried out with the 15 cm^2 prototype, membrane expansion was monitored by the central deflection of the membrane measured by strain gauged arms, whereas with the 5 cm^2 prototype membrane expansion was monitored only by measurements of volume change (due to limitations in diameter the instrument has no strain gauged arms). On tests carried out with

the 10 cm^2 prototype, membrane expansion was monitored by both strain arms and volume changes, which allows a direct correlation between strain arm measurements and volume change measurements. Cavity strain was calculated using equation [4.7] (see Chapter 4) based on Hencky's logarithmic strain definition, $\varepsilon_c = \ln(R/R_o)$, in which the radius R was measured at the midheight of the membrane by strain arms and calculated from volume changes assuming that the membrane expands as a right cylinder. Adopting Hencky's definition, the shear modulus was calculated from the slope of unload-reload loops using equation [6.1].

Comparisons between the shear moduli calculated from strain arm measurements and the shear moduli calculated from volume change measurements are plotted in Figures 6.8 and 6.9 for tests carried out with the 10 cm^2 prototype. A reasonably good agreement can be seen between the two moduli from both comparisons - G^v_{ap} against G^a_{ap} and G^v_{sq} against G^a_{sq}. The ratio G^v/G^a falls within a range of 0.5 to 2.0, suggesting that volume change measurements can produce G values of the same order of magnitude as G values calculated from measurements of the central deflection of the membrane (taken from strain gauged arms).

The compliance problem in the cone-pressuremeter measuring system has serious implications on the plots shown in Figures 6.8 and 6.9. As previously discussed, such a problem can result in corrections of more than 20% of the measured shear modulus. Since the compliance of the volume measuring system is significantly higher than that observed in the arm measuring system (see Figure 6.4), the ratio of G^v/G^a is also largely affected by these corrections.

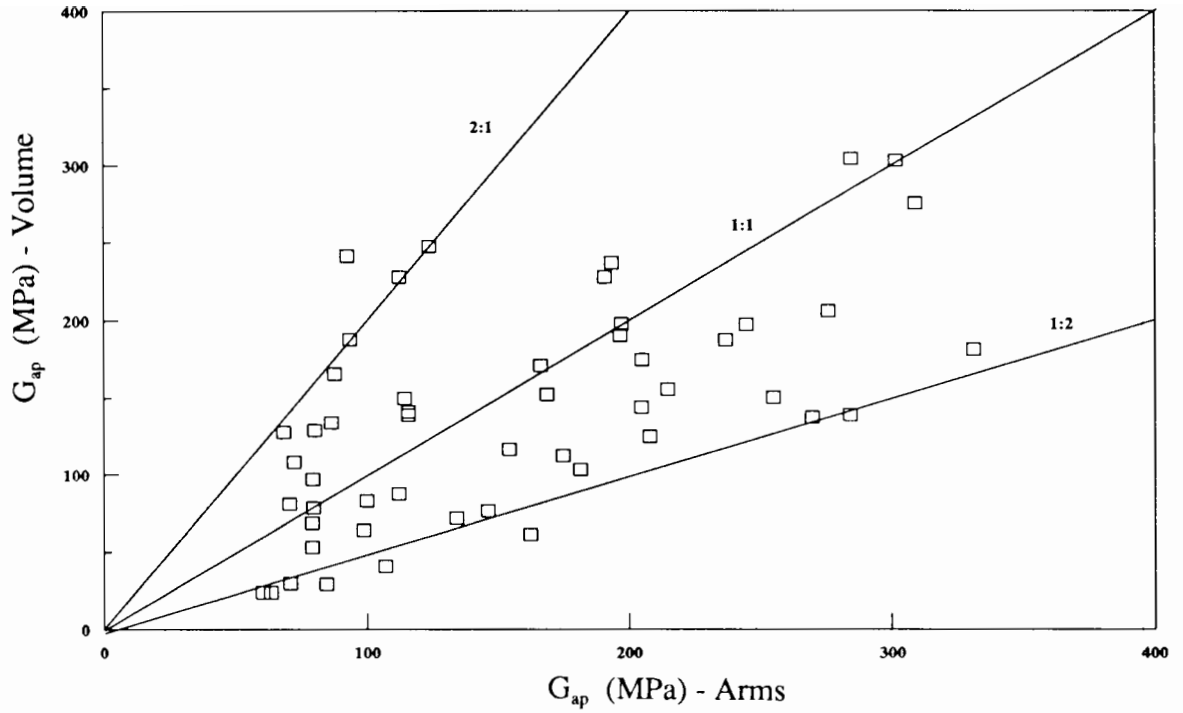

Figure 6.8 - Comparison of the apices moduli G_{ap} calculated from strain arm measurements and from volume change measurements

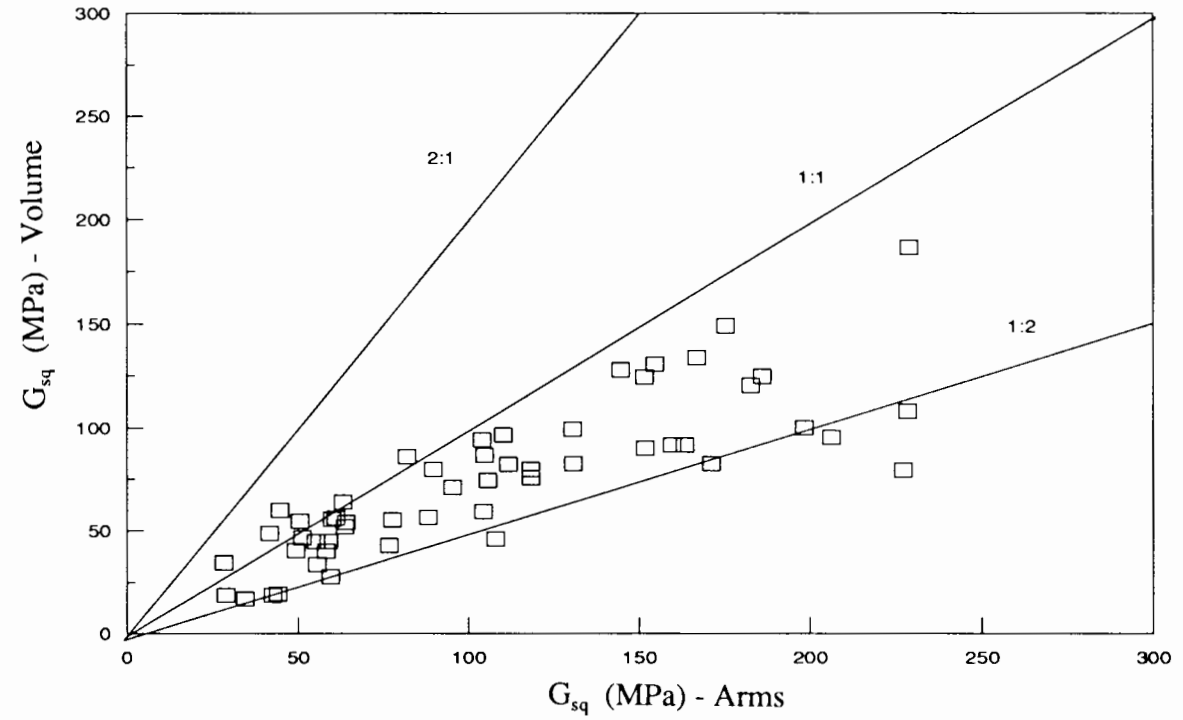

Figure 6.9 - Comparison of the least square fit moduli G_{sq} calculated from strain arm measurements and from volume change measurements

6.3.3 - Influence of stress level

Three unload-reload loops and one reload-unload loop were carried out in a typical pressure expansion-compression curve performed with the cone-pressuremeter in the calibration chamber. The variation of the moduli G_{ap} of one such a test is shown in Figure 6.10, in which G_{ap} is plotted against pressuremeter strain at the start of unloading ε. A trend of increasing moduli as a test progresses is clear, until a final reduction is observed for the shear modulus measured from the loop performed during the pressure-contraction curve. The first loop was carried out at ε of about 5.0%, to avoid the initial stages of the pressure-expansion curve, in which the pattern of mean effective stresses at different radii is probably influenced by cone penetration (unexpectedly high values of G obtained at early stages of test ($\varepsilon = 2\%$) were reported by Withers *et al* (1989)).

The pattern observed in Figure 6.10 can be understood within the framework of cavity expansion theory. At very early test stages an elastic deforming zone is formed and the mean effective stress remains unchanged. When the soil surrounding the probe reaches failure, the mean effective stress increases as a function of the effective radial stress. Therefore, an increase in the moduli as the position of the loop moves further from the start of the test reflects an increase in mean effective stress in plastic zones, when no excess pore pressure is observed (Wroth, 1982; Fahey and Randolph, 1984; Robertson and Hughes, 1986; Bellotti *et al*, 1989).

However, the mean effective stresses in the plastic zone decreases with increasing radius from the probe, becoming equal to the *in situ* stress at some distance from the expanding cavity (Fahey, 1980; Robertson and Hughes, 1986; Yu, 1990). Robertson and Hughes (1986) suggested that the unload-reload loop response is dominated by the maximum stresses generated at the soil-instrument interface, so that G values should be normalised by the maximum mean effective stresses. On the basis of this assumption, the mean effective stresses

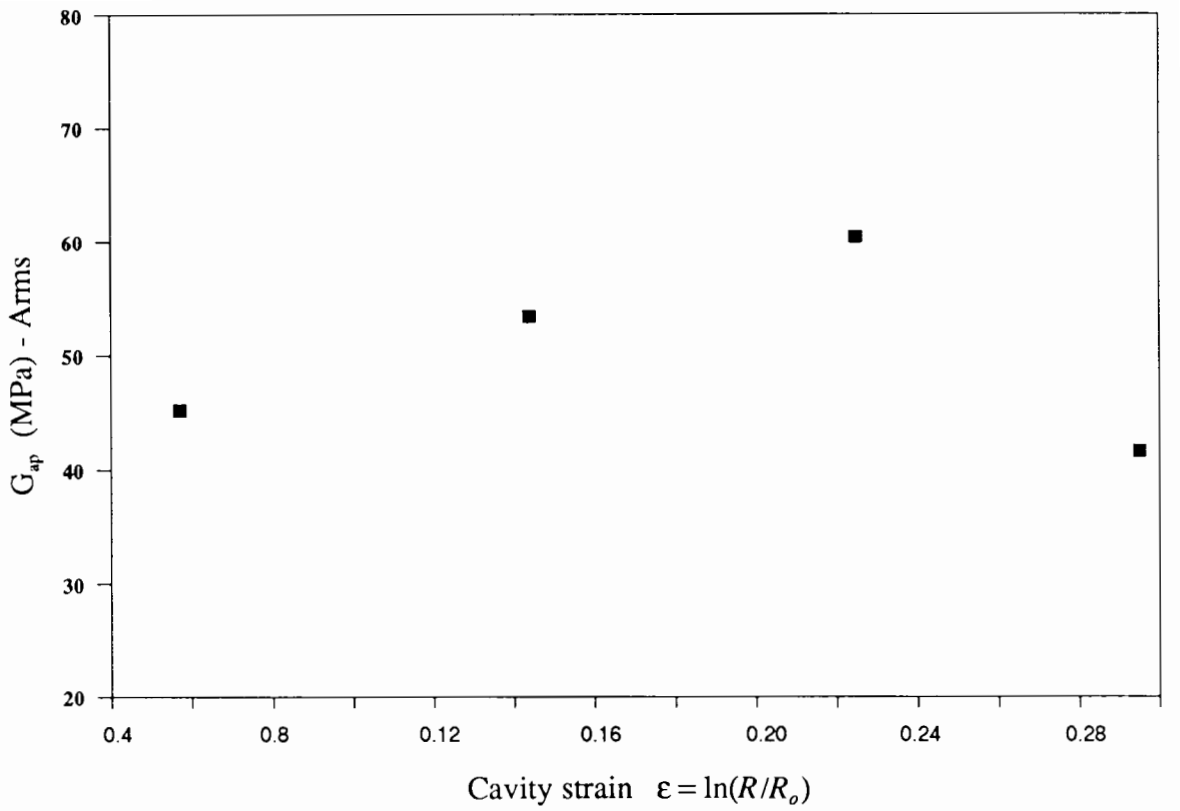

Figure 6.10 - Typical variation of shear modulus with pressuremeter strain before unloading

around the pressuremeter cavity can be taken as either the mean octahedral effective stress $p' = \frac{1}{3}(\sigma'_r + \sigma'_z + \sigma'_\theta)$ (Robertson, 1982) or the mean plane strain effective stress $s' = \frac{1}{2}(\sigma'_r + \sigma'_\theta)$ (Fahey and Randolph, 1985; Bellotti *et al* , 1989; Yu, 1990).

For the interpretation of the cone-pressuremeter data the following method is proposed. The sand surrounding the pressuremeter is assumed to be deformed under conditions of axial symmetry and plane strain. The mean effective stress is calculated at the soil-instrument interface at the start of the unload-reload loop, hypothesizing that during the loop the soil behaves as a perfect elastic material, so that the hoop stress decreases by the same amount as the radial stress increases and therefore the mean effective stress remains constant. A simplified

assumption of an elastic perfectly plastic material is made to define sand behaviour, in which a constant stress ratio is observed during failure. The ratio of the principal stress can then be expressed in cylindrical coordinates

$$\sigma'_{\theta} = \sigma'_{r}\left(\frac{1-S}{1+S}\right) \qquad [6.5]$$

where $S = \sin\phi'_{ps}$. A problem arises when computing the intermediate principal stress σ'_z, since there is no unique solution to determine σ'_z from σ'_r and σ'_{θ}. However, for a case in which a fully associated flow rule is used (i.e. $\phi' = \nu$) a relatively simple expression can be obtained from Matsuoka's plastic model (Matsuoka, 1976). Burd (1986) gives the equation, in which σ'_z can be expressed as

$$\sigma'_z = (\sigma'_r \sigma'_{\theta})^{\frac{1}{2}} \qquad [6.6]$$

assuming no plastic deformations in the vertical direction. This simple expression has been empirically validated by results of plane strain tests in sand in an independent stress control apparatus (Green and Bishop, 1969; Bishop, 1971; Green, 1971). Combining equations [6.5] and [6.6] the average mean effective stress at the edge of the expanding cavity at the start of the unload-reload loop can be given by

$$p' = \frac{\sigma'_r}{3}\left[1 + \frac{1-S}{1+S} + \left(\frac{1-S}{1+S}\right)^{\frac{1}{2}}\right] \qquad [6.7]$$

The expression relating mean effective stress at the face of the pressuremeter probe to effective radial stress is dependent upon the friction angle. To quantify this dependency, equation [6.7] can be written as:

$$p' = \alpha\sigma'_r \qquad [6.8]$$

where $\alpha = 0.61$ for $\phi'_{ps} = 34°$ (loose sand), $\alpha = 0.54$ for $\phi'_{ps} = 43°$ (medium sand) and $\alpha = 0.50$ for $\phi'_{ps} = 49°$ (dense sand). For dense sand the value of $\alpha = 0.50$ is the same as that proposed by Robertson and Hughes (1986), which is based on empirical evidences taken from a large number of field data.

During the initial phase of cavity contraction the whole of the soil behaves elastically, with elastic unloading of the previously plastic region. The elastic phase ends when:

$$\frac{\Delta\sigma'_r}{\sigma'_r} = \frac{2S}{1+S} \qquad [6.9]$$

where $\Delta\sigma'_r$ is the reduction in cavity pressure. In the elastic region there are no volumetric strains and no change in mean effective stress. Reverse plasticity then occurs, where stress are related by:

$$\sigma'_\theta = \sigma'_r\left(\frac{1+S}{1-S}\right) \qquad [6.10]$$

so that the mean effective stress can be expressed as:

$$p' = \frac{\sigma'_r}{3}\left[1 + \frac{1+S}{1-S} + \left(\frac{1+S}{1-S}\right)^{\frac{1}{2}}\right] \qquad [6.11]$$

For tests carried out in the calibration chamber using the cone-pressuremeter, the reload-unload loops were performed within the elastic zone (a zone in which the material has been loaded plastically and unloaded elastically). At the start of reloading, the cavity pressure was not reduced sufficiently to cause reverse plasticity, and equation [6.7] was used to calculate the mean effective stress.

For granular materials the relationship between the elastic moduli and the mean effective stress can be expressed in a similar way to that suggested by Janbu (1963)

$$G/p_a = K_G(p'/p_a)^n \qquad [6.12]$$

where K_G= modulus number
n = modulus exponent
p_a = atmospheric pressure
p'= mean effective stress

This approach has been used by several workers (Duncan and Chang, 1970; Lade and Duncan, 1975; Wroth *et a*l, 1979; Bellotti *et al*, 1986; Robertson and Hughes, 1986). The value of the exponent n is typically in the range 0.4 to 0.8 (Wroth *et al*, 1979; Bruzzi *et al*, 1986; Bellotti *et al*, 1986), and is dependent on the strain amplitude over which the modulus is measured (Wroth *et al*, 1979). In order to determine the modulus number K_G and the modulus exponent n from cone-pressuremeter data for Leighton Buzzard, the values of log G have been plotted against log p' for loose, medium and dense sand, as shown in Figures 6.11, 6.12 and 6.13 respectively. The examples illustrate the behaviour of the shear moduli G^a_{ap} obtained from

measurements of the central deflection of the membrane by strain gauged arms. A remarkably similar pattern was also obtained when plotting the corrected square fit moduli G^{a}_{sq} from strain arm measurements.

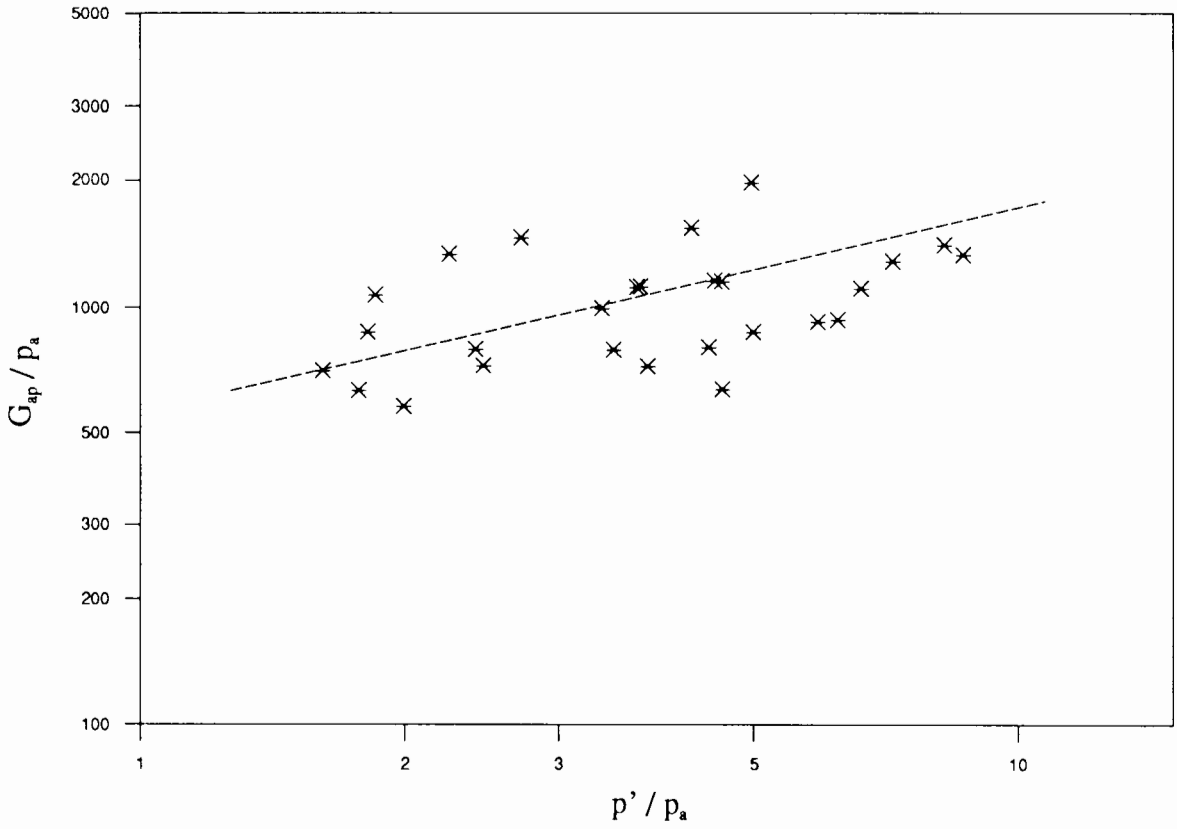

Figure 6.11 - Relationship between shear moduli and mean effective stress for loose sand

For each of the three densities there is an almost unique relationship between shear moduli and mean effective stresses. The modulus values K_G and n calculated from each plot are given in Table 6.6. Despite the scatter, relationships between G and p' produced consistent values, in which the modulus exponent n increases with increasing density (i.e. decreasing strain

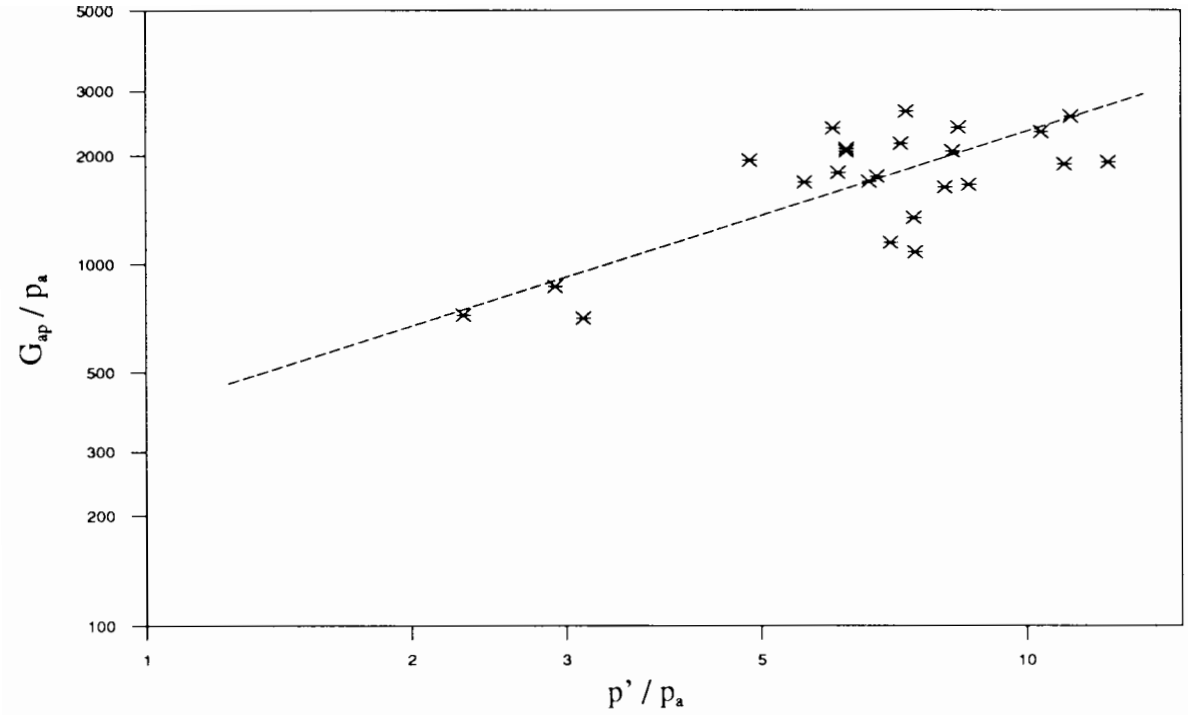

Figure 6.12 - Relationship between shear moduli and mean effective stress for medium sand

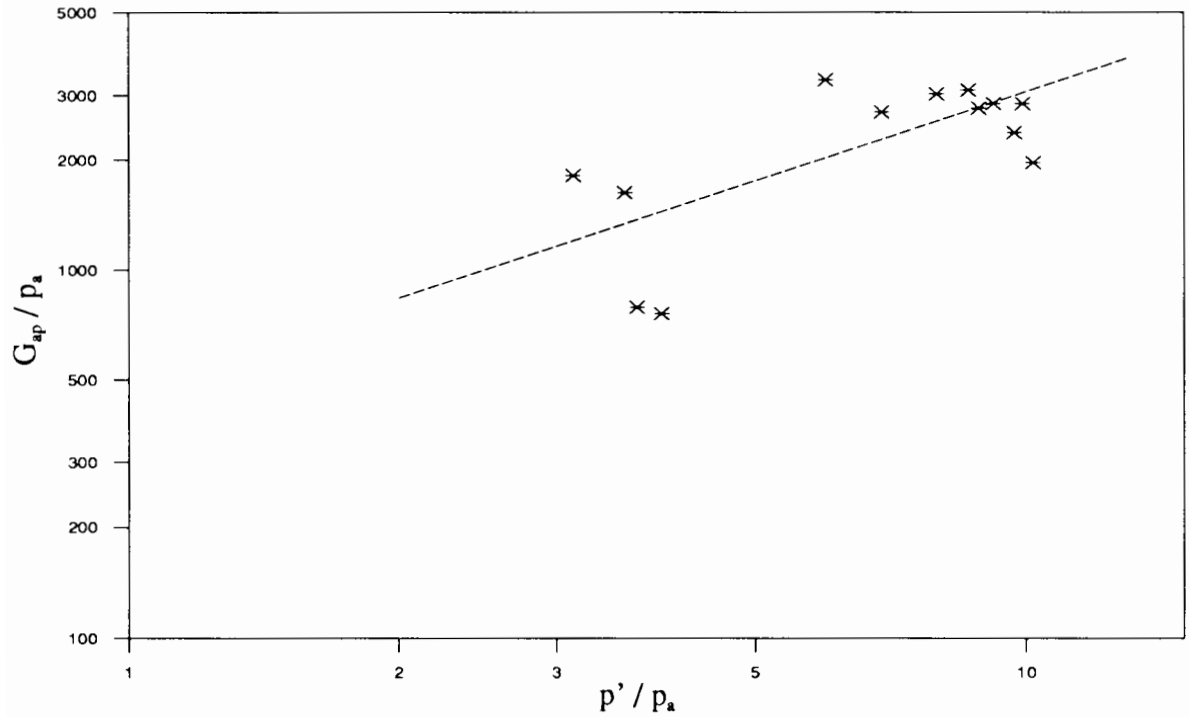

Figure 6.13 - Relationship between shear moduli and mean effective stress for dense sand

amplitude) in the range of 0.4 to 0.8, and the modulus number K_G remains approximately constant. For Leighton Buzzard sand the modulus number is about K_G = 480, whereas the modulus exponent varies with density approximately as:

$$n = 0.28 + 0.59R_d \qquad [6.13]$$

	G^a_{ap}			G^a_{sq}		
	LOOSE	MEDIUM	DENSE	LOOSE	MEDIUM	DENSE
K_G	682.0	455.8	493.7	478.7	370.2	378.8
n	0.346	0.700	0.790	0.477	0.676	0.781
r^2 (%)	32.0	58.2	56.8	38.7	53.0	55.3

Table 6.6 - Modulus number K_G and modulus exponent n for Leighton Buzzard sand.

The scatter observed in Figures 6.11 to 6.13 is thought to be a result of the influence of shear strain amplitude on shear modulus. To examined this problem, the shear modulus measured from each unload-reload loop G(measured) was normalised by the shear modulus calculated at the same mean stress by equation [6.12], G(calculated), using the values of K_G and n presented in Table 6.6. The shear strain amplitude recorded from each loop γ(measured) was normalised by the average shear strain amplitude γ(average), calculated by averaging the shear strain amplitude of all loops carried out at the same density. Results are presented in Figures 6.14 and 6.15, in which the ratio G(measured)/G(calculated) is plotted against the ratio γ(measured/γ(average). As a general trend, ratios of γ(measured/γ(average) < 1 are observed for G(measured)/G(calculated) > 1, i.e. the measured shear modulus is greater than the value calculated by the regression analysis whenever the shear strain amplitude recorded in the loop is smaller than the average amplitude calculated from all loops. Ratios of γ(measured/γ(average) > 1 are in turn observed for G(measured)/G(calculated) < 1. The pattern observed in the figures

confirms the assumption that scatter on the relationship between shear moduli and mean effective stresses is a result of variations on the shear strain amplitude recorded in unload-reload loops. Note that Figures 6.14 and 6.15 have shown results obtained from loose and medium sands respectively. For dense sand fewer loops were performed and the relationship between shear moduli and strain amplitude is not as clear as that obtained for loose and medium densities.

Equations [6.12] and [6.13] can be combined to express the dependence of the shear moduli on stress level and relative density, as presented in Figure 6.16. A review on Tables 6.1 to 6.3 shows that the shear modulus values were measured at mean effective stresses from approximately 150 kPa to 1500 kPa.[4] In this range the shear moduli increase with increasing mean effective stress and increasing density. As the mean effective stress increases, the effect of relative density is more significant.

The evaluation of the experimental coefficients K_G and n obtained from the relationship between log G and log p' from volume change measurements did not produce consistent values. The scatter observed in the relationship can be due to

a) lack of accuracy on the volume measurement system, since a resolution of only 0.02% has been achieved on the tests.

b) the excessively large correction factors applied to the measured shear moduli to account for the compliance of the system.

---

4 *Note that the modulus data were obtained from calibration chamber tests carried out at mean boundary stresses in the range of 50 kPa to 200 kPa. In these tests the mean effective stress at the face of the pressuremeter changed from approximately 150 kPa to 1500 kPa.*

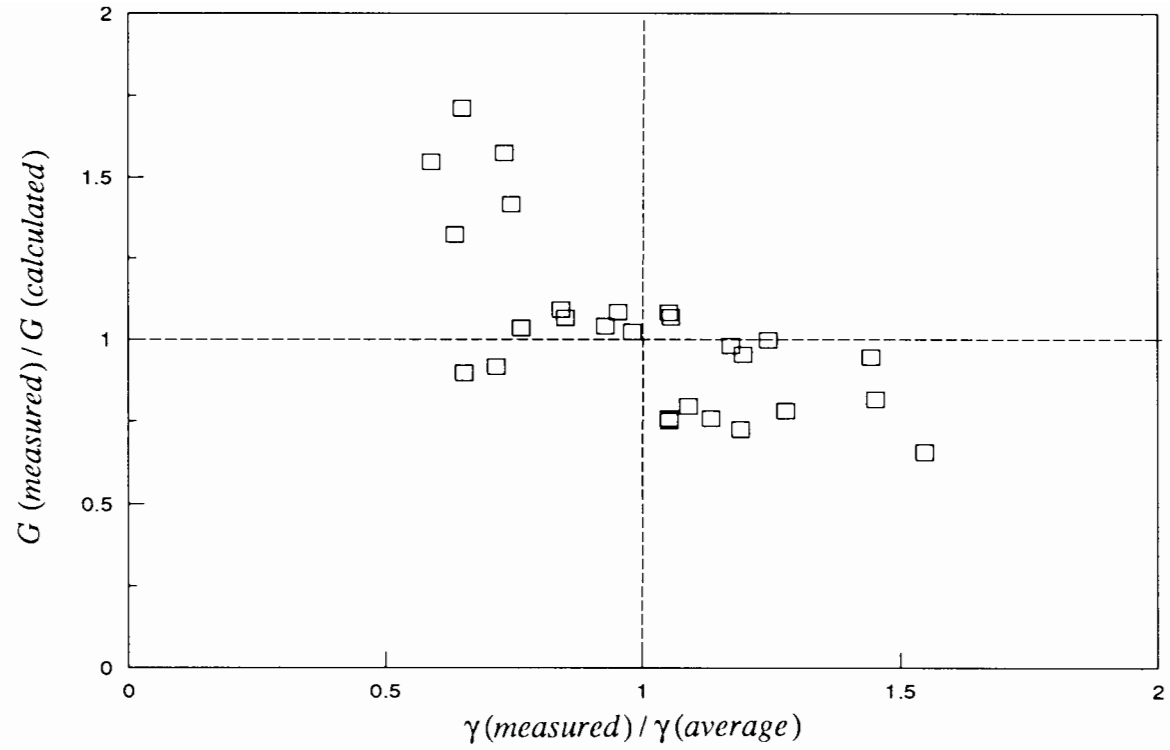

Figure 6.14 - Influence of shear strain amplitude on the shear modulus in loose sand

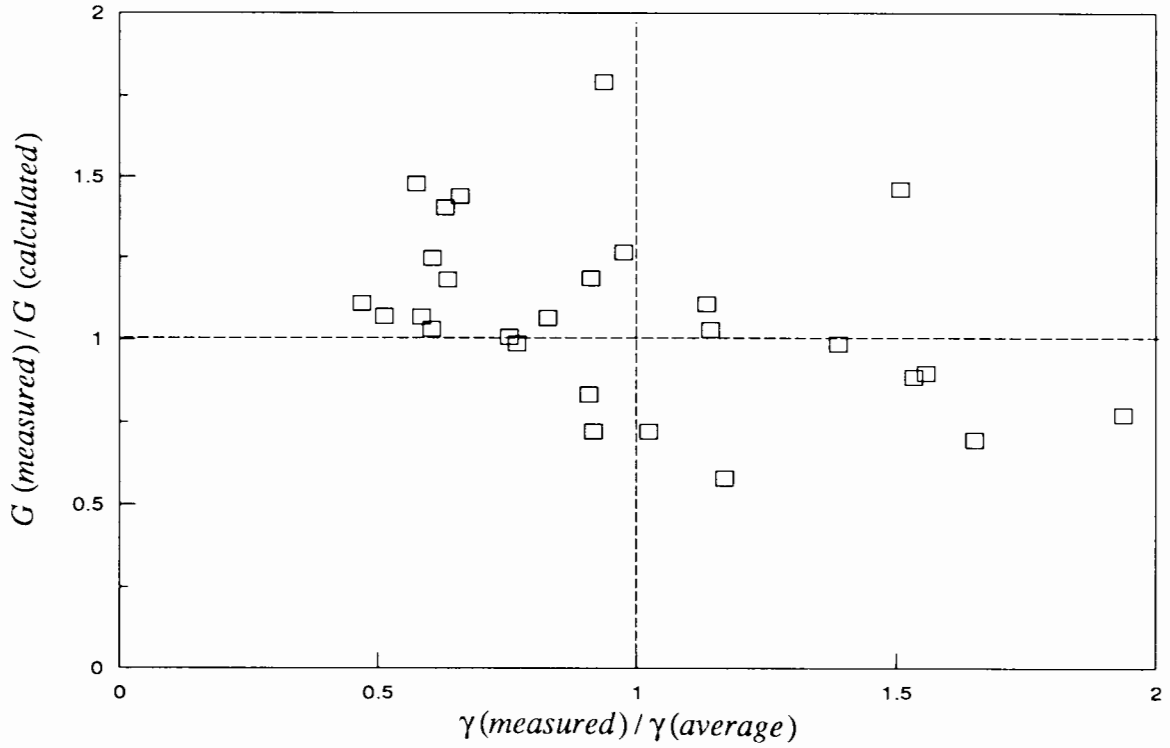

Figure 6.15 - Influence of shear strain amplitude on the shear modulus in medium sand

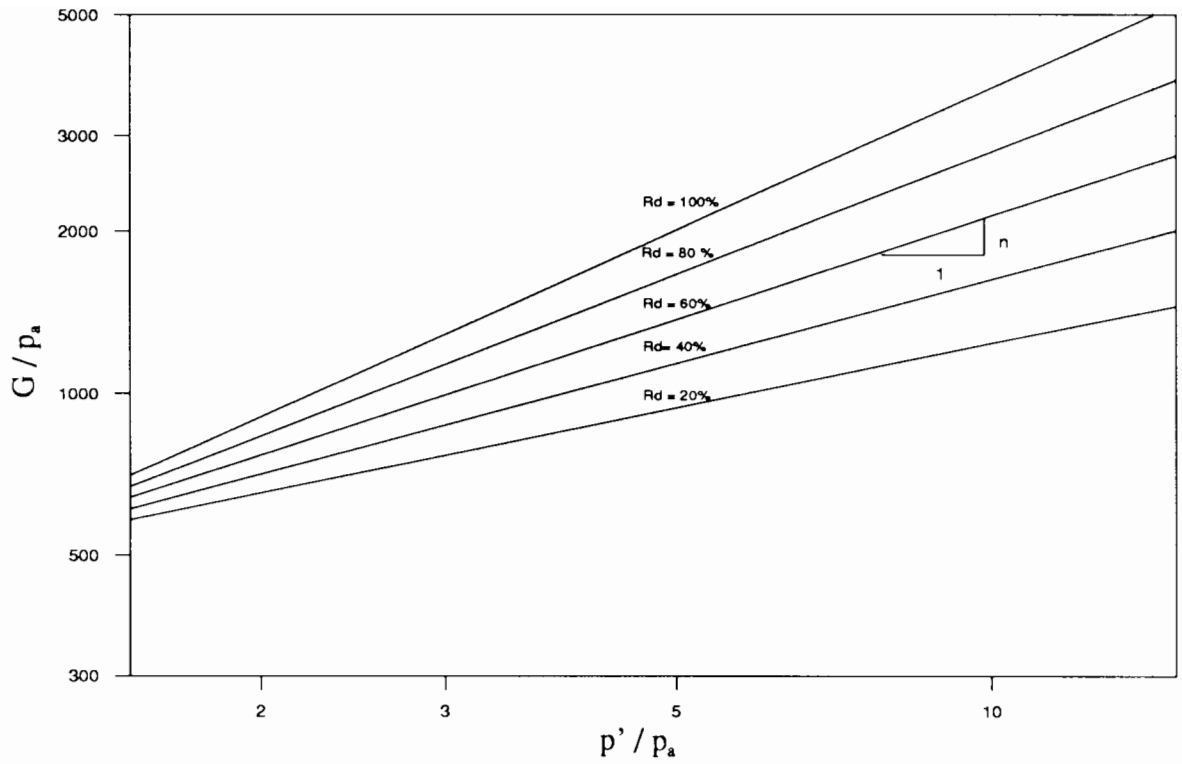

Figure 6.16 - Variation of shear moduli with mean effective stress and relative density

Improvements on both accuracy and compliance should be made to allow the variation of moduli with mean stress to be quantified.

Finally, Figure 6.17 shows a comparison between the shear modulus measured from unload-reload loops from both the cone-pressuremeter and the self-boring pressuremeter (SBP) tests in dense sand. SBP tests have been carried out at Cambridge University on Leighton Buzzard sand in a calibration chamber similar to the Oxford chamber, as reported by Fahey (1980). Values of apices moduli G_{ap} obtained from strain arm measurements were compared with the appropriate mean effective stress, according to the method proposed in this work. The moduli from cone-pressuremeter compared well with values obtained from the self-boring test. It is suggested that the scatter in results was essentially caused by the impossibility of

correcting some of the G values to account for compliance effects, since calibrations were not available for the SBP probe and the 15 cm^2 cone-pressuremeter device. The generally good agreement observed in the figure tends to confirm

a) the observation that the shear moduli obtained from unload-reload loops is not very sensitive to the initial disturbance due to the installation process (Hughes, 1982; Wroth, 1982; Hughes and Robertson, 1985; Bellotti *et al*, 1989; Withers *et al*, 1989).

b) the applicability of cylindrical cavity expansion theory to predict the elastic shear modulus of soil from cone-pressuremeter testing data.

A correct interpretation of the measured shear modulus must also account for the relevant shear strain magnitude observed during tests (Kondner, 1963; Wroth *et al*, 1979; Robertson and Hughes, 1986; Bellotti *et al*, 1986). Comparisons between the elastic moduli G_{ur} measured from pressuremeter tests and the elastic moduli G_{max} measured from downhole shear wave velocities and resonant column tests indicate a relationship between G_{ur}/G_{max} in the range 0.2 to 0.6. (Hughes and Robertson, 1985; Bellotti *et al*, 1989). This is not surprising considering that the moduli G_{max} is recorded at shear strain levels of about $1 \times 10^{-4}\%$, whereas the moduli G_{ur} is recorded at shear strain levels of about $1 \times 10^{-1}\%$. Furthermore, the reduction in shear moduli of sands with increasing shear strain amplitude has been extensively studied in laboratory tests (e.g. Iwasaki *et al*, 1978; Seed *et al*, 1986, Lo Presti, 1987). Appropriate correction for shear strain magnitudes were given by Hughes and Robertson (1985) and Bellotti *et al* (1989) to enable the modulus G obtained from pressuremeter tests to be linked to the relevant strain magnitude expected in design problems.

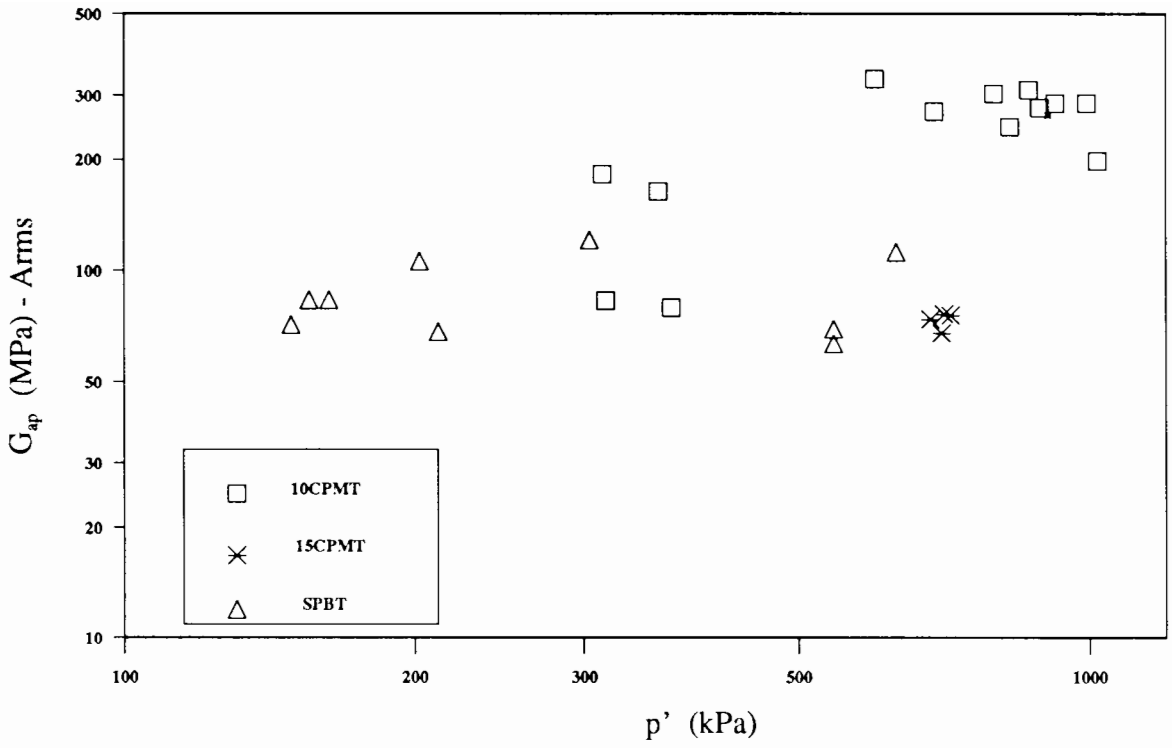

Figure 6.17 - Comparison of shear moduli from cone-pressuremeter and self-boring pressuremeter tests

CHAPTER 7

CONCLUDING REMARKS

7.1 - Introduction

The objective of the work described in this thesis is to provide a proper understanding of the cone-pressuremeter test, and in particular to establish a basic procedure to allow test data to be used to determine the engineering properties of cohesionless soils. The comments in this chapter are related to general conclusions to be drawn from the laboratory tests. These comprise a direct assessment of stress-strain and strength characteristics of sands by means of cone-pressuremeter testing results, a brief and critical appraisal of the validity of established correlations to field design problems and some suggestions for future work.

Since a limited amount of field data is available for cone-pressuremeter tests in sand, a comprehensive testing programme was carried out before a rational framework for the interpretation of the new device could be developed. Laboratory chamber tests performed in a carefully controlled and repeatable fashion were selected to provide the experimental database. Chamber tests were carried out in a known material in a well defined programme of calibration, providing a systematic examination of the effects of relative density, stress level and stress ratio on cone-pressuremeter testing results. Data from 34 tests were used to measure the elastic shear modulus and to estimate relative density, friction angle and horizontal stress.

Equipment was designed and constructed specifically to carry out this investigation. The main item was a stress controlled testing chamber which allowed independent application of horizontal and vertical confining stresses to a test sample. A driving mechanism and a

pressurisation system, to control pressuremeter tests, have been developed to support the experiments. Three devices with cross-sectional areas corresponding to 15 cm^2, 10 cm^2 and 5 cm^2 were tested in the calibration chamber.

7.2 - Interpretation of chamber tests

Calibration chamber tests on the cone-pressuremeter give measurements of limit pressure ψ_l and cone resistance q_c under conditions of controlled density, vertical stress and horizontal stress. Limit pressure was easily and accurately derived from a well-defined plateau in the pressuremeter pressure-expansion curve. A value of cone resistance measured at the same depth as the centre of the pressuremeter module was extracted from each cone profile.

Test results showed that, for each of the densities tested, there was an almost unique relationship between cone resistance and horizontal stress, in spite of the factor of 4 covering the range of σ'_h/σ'_v applied to the boundary of the sample. By comparison, values of cone resistance plotted against vertical stress showed no reasonable relationship for any of the three densities tested. A similar pattern was observed for the pressuremeter data, where a clear relationship was found between limit pressure and horizontal stress. No connection was observed between limit pressure and vertical stress.

These results suggested that both cone resistance and limit pressure depend primarily on density and horizontal stress. A direct correlation between cone resistance and limit pressure was explored, and the ratio $(q_c - \sigma_h)/(\psi_l - \sigma_h)$ was found to be essentially dependent on relative density and not on stress level and stress ratio. The ratio $(q_c - \sigma_h)/(\psi_l - \sigma_h)$ was identified as a useful variable for deriving soil parameters, in particular the density.

A linear relationship between the ratio $(q_c - \sigma_h)/(\psi_l - \sigma_h)$ and relative density was obtained from chamber tests, which is applicable to Leighton Buzzard sand with values of $(q_c - \sigma_h)/(\psi_l - \sigma_h)$ in the range of 6 to 14. It was suggested that practical benefits can be obtained from this correlation as it depends only on the measured values of cone resistance and limit pressure, since the subtraction of σ_h from both quantities represents a small correction for sands, and derived values of density are insensitive to poor estimates of σ_h.

Having established a relationship to predict relative density, it is then possible to make an estimate of the angle of friction. The use of Bolton's empirical formula (Bolton, 1986), in which density and stress level are combined to express shear strength properties of sand, is recommended, as it fitted angles of friction obtained form triaxial tests carried out on Leighton Buzzard sand within a margin of about 2°. As an alternative, it is also possible to establish a direct correlation between results of cone-pressuremeter tests and friction angles. For consistency with the analysis proposed for deriving relative density, the friction angle was predicted as a function of the ratio $(q_c - \sigma_h)/(\psi_l - \sigma_h)$. Results were fitted to a linear equation, and friction angles were predicted within approximately 1° to 2°. Predictions were considered fairly good as they reflected the same accuracy as that obtained in the laboratory triaxial tests.

An alternative method to the conventional practice of assessing horizontal stress from lift-off pressure was developed, based on the measurements obtained with the cone-pressuremeter. As previously mentioned, for a given density both cone resistance and limit pressure are controlled by the horizontal effective stress. An alternative approach is to reverse the process to estimate σ'_h as a direct function of q_c and ψ_l, with σ'_h being expressed as the root of a quadratic equation. Predicted values were compared to values applied in the calibration chamber. A generally good agreement was observed in the predictions for the range of stress tested. The horizontal stress was estimated within a factor of approximately 1.3, but with a tendency of underestimating the horizontal stress at high horizontal stress values.

Cone-pressuremeter results were used to estimate relative density, friction angle and horizontal stress. The application of the proposed empirical relationships to field problems must be considered with caution. The values of cone resistance and limit pressure measured in the calibration chamber are expected to be influenced by the size of the chamber. The influence of sand type and stress history on the test results are still to be assessed.

7.3 - Shear modulus

The pressuremeter is a unique method for assessing directly the *in situ* shear stiffness of soils. Current practice for measuring shear modulus applies small strain elastic theory to small unload-reload loops. The corrected interpretation and application of the modulus measured from cone-pressuremeter tests was investigated.

Calibrations were essential to obtain the corrected pressuremeter pressure-expansion curve, and they had an appreciable influence on the measurement of the shear modulus. A procedure is recommended to obtain the best possible estimation of the shear modulus from unload-reload loops. The inflation pressure recorded during the test was first corrected by subtracting the "membrane stiffness", which was undertaken by inflating the pressuremeter in air. The corrected pressure-expansion curve was used for calculating the shear modulus. The calculated value was corrected to account for compliance effects and then further corrected to account for the finite length of the pressuremeter probe. The strain amplitude observed during an unload-reload loop was very small, and inaccuracies in the measuring system due to compliance effects resulted in large errors. The shear moduli measured by the central deflection of the membrane by strain gauged arms were corrected by a factor of approximately 1.2, whereas the shear moduli measured from volume changes of the pressuremeter probe were corrected by a factor of approximately 1.5. The need for careful calibrations to account for compliance

effects was emphasized and the adoption of corrected factors to account for the finite length of the pressuremeter probe was recommended, especially if volume measurements are to be used.

In carrying out small unload-reload loops, care was taken not to exceed the elastic limit of the soil during the unload phase (Wroth, 1982). Nevertheless the unload-reload loops exhibited a non-linear hysteretic behaviour even for a test procedure in which creep strains were allowed to occur before the loop was performed and no excess pore pressure was generated during inflation. To assess the influence of non-linearity of a loop on the measured shear modulus two procedures for calculating the slope of the loops were examined. A procedure of drawing a single line between the two apices of the loop (to calculate G_{ap}) produced values systematically greater than a procedure of performing a linear regression analysis based on the least square fit of all points included between the two apices of loop (to calculate G_{sq}). On average the ratio G_{sq}/G_{ap} was about 0.80 for strain arm measurements and about 0.70 for volume change measurements. Since a simple change in the definition used for G led to average changes of about 20% to 30% on G values calculated from small unload-reload loops, a recommendation was made to calculate both G_{ap} and G_{sq} for every loop. Further comparisons are needed to advance the understanding of these observations to evaluate the influence of sand type and test procedure on the ratio G_{sq}/G_{ap}.

The influence of large creep strains on the shear modulus obtained from unload-reload loops was not investigated, and a sensible explanation for this effect still needs to be developed. It was suggested that creep strains may affect the values of G_{ap} and G_{sq}, as well as ratio G_{sq}/G_{ap}, and therefore any test procedure should be designed to allow creep displacements to occur before an unload-reload loop is carried out.

Comparisons between the shear moduli calculated from strain arm measurements G^a and the shear moduli calculated from volume change measurements G^v were established for the

10 cm^2 cone-pressuremeter prototype. A reasonably good agreement was observed between the two moduli. The ratio G^v/G^a fell within a range of 0.5 to 2.0, suggesting that volume change measurements can produce G values of the same order of magnitude as G values calculated from strain arm measurements.

The application of the measured shear modulus to engineering design must account for the relevant stress and strain acting around the pressuremeter during the test. A method to calculate the mean stress level at the pressuremeter-soil interface was proposed, in which a fully associated flow rule was used to compute the intermediate principal stress from Matsuoka's plastic model (Matsuoka, 1976). The measured values of shear modulus were related to the mean effective stress by a power expression similar to that suggested by Janbu (1963). Despite the scatter, relationships between G and mean stress produced consistent values for strain arm measurements. The modulus exponent n was found to increase with increasing density, in the range of 0.4 to 0.8, whereas the modulus number K_G remained approximately constant ($K_G \sim 480$). The resolution of the available data obtained from volume change measurements was not sufficiently accurate to quantify the variation of the shear modulus with stress.

Finally, the shear moduli obtained with the cone-pressuremeter produced values in good agreement with those obtained from the self-boring pressuremeter. Comparisons were based on calibration tests performed in similar chambers in dense sand.

7.4 - Additional studies

Calibration chamber tests were carried out to establish a basic procedure for the interpretation of the cone-pressuremeter test in cohesionless soils. Additional investigation was conducted in two other areas, which were relevant to the applicability of cone-pressuremeter data to engineering design problems. An assessment of chamber size effects is examined in

Appendix I, in which the variables that affect calibration chamber test derived correlations were identified and discussed. Comparisons of results obtained with the 15 cm^2, 10 cm^2 and 5 cm^2 are presented. In Appendix II a study of length to diameter ratio effects on the 5 cm^2 pressuremeter probe is presented. This work is to provide experimental support to standardize equipment dimensions in order to compare properly data from different soils. The main conclusions in these two areas are identified below.

- Chamber size effects

A method has been developed to determine the engineering properties of soil using the cone-pressuremeter, which depends essentially on the ratio $(q_c - \sigma_h)/(\psi_l - \sigma_h)$. A series of comparative tests was performed using three cone-pressuremeter prototypes with diameters of 25.2 mm, 35.7 mm and 43.7 mm to study the influence of chamber size effects on the ratio $(q_c - \sigma_h)/(\psi_l - \sigma_h)$, as well as on the independent values of cone resistance and limit pressure.

The proximity of the physical boundaries of the chamber had significant influence on the measured values of cone resistance and limit pressure, but the ratio of $(q_c - \sigma_h)/(\psi_l - \sigma_h)$ was found not to be greatly affected by the chamber size. It is recommended that correlations derived from calibration chamber tests for the interpretation of the cone-pressuremeter in sand, which are essentially dependent on the ratio $(q_c - \sigma_h)/(\psi_l - \sigma_h)$, could be applied to field conditions without any correction to account for chamber size effects.

Values of cone resistance are closely linked to values of limit pressure within the framework provided from the database obtained from cone-pressuremeter tests. It is suggested that cone resistance is controlled by a cavity expansion process, and that cavity expansion theory could satisfactorily explain observed chamber size effects. A large database of approximately 400

cone penetrometer tests using different cone sizes, chamber sizes, sands, densities, stress levels and stress ratio were examined. Loose sand was found to represent field conditions reasonably accurately, but dense and medium sand were affected by chamber size effects.

A comparison between pressuremeter test data and a one dimensional finite element analysis was performed, and the influence of shear strength, soil stiffness and chamber size effects on limit pressure was evaluated. For the three densities tested, measured and calculated values of limit pressure increase with increasing chamber to probe diameter ratio. This effect is quite considerable for loose sand and significantly more so for both medium and dense sand.

- Length to diameter ratio

A limited number of tests was performed to investigate the effect of the finite length of the pressuremeter probe on limit pressure. The scope of the work consisted of testing a 5 cm^2 cone-pressuremeter prototype with three different length to diameter ratios, corresponding to L/D equal to 5, 10 and 20. A trend of increasing limit pressure with decreasing L/D ratio was clearly observed for the conditions tested in the calibration chamber. It was suggested that any theoretical interpretation of limit pressure based on an infinitely long cylindrical cavity but using data from a finite length pressuremeter probe requires correction for L/D ratio effects. A correction factor to convert measured limit pressure to a limit pressure equivalent to a L/D = 10 probe was presented, and used successfully in preliminary comparisons between results of cone-pressuremeter tests and self-boring pressuremeter tests.

7.5 - Recommendations for future work

Preliminary cone-pressuremeter tests were carried out to stimulate the development of methods to evaluate soil properties. Tests in stiff clay (Houlsby and Withers, 1988) and sand (Hughes

and Robertson, 1985; Withers *et al*, 1989; Schnaid and Houlsby, 1990) are reported, but further work is needed to advance understanding of the cone-pressuremeter test. There are three broad areas where there is considerable scope for development.

Firstly it is proposed that the calibration chamber should continue to be used to calibrate the cone-pressuremeter. A series of tests in calcareous soils has already been initiated and, by using the same methodology adopted in this work, it will be possible to evaluate the influence of sand type on the correlations proposed in this research. Additional tests using the 5 cm^2 prototype are essential for building up an experimental database to develop a better understanding of chamber size effects on the ratio $(q_c - \sigma_h)/(\psi_l - \sigma_h)$ and to permit a more detailed examination of length to diameter effects.

The second area concerns the development of analytical and numerical solutions for the interpretation of the cone-pressuremeter. An analytical interpretation method for the test in sands is being developed by Yu (1990), and is similar to that proposed for clay by Houlsby and Withers (1988). The analytical methods must be checked by calibration against measurements with the cone-pressuremeter in the calibration chamber, in a similar way to that presented by Houlsby and Yu (1990).

The third area concerns the necessity of carrying out field tests at different sites, which should be selected to include deposits of sand and soft clay. Experience should be gained from comparisons of soil properties derived from cone-pressuremeter data and those obtained from other tests to verify the validity of the relationships developed from this series of chamber tests.

APPENDIX I

AN ASSESSMENT OF CHAMBER SIZE EFFECTS IN SAND

Calibration chamber tests have been carried out to study the cone-pressuremeter test in sand. An assumption inherent in the chamber testing approach is that measurements of an *in situ* device in the chamber would be the same as in the field, provided that the material is identical and the *in situ* stresses are reproduced. This assumption is not strictly valid, since a large body of sand has to be modelled in the laboratory as a cylinder restrained by physical boundaries at some finite radius.

The influence of chamber size effects and boundary conditions on values of cone resistance and limit pressure has been recognized for some time. This subject has been addressed by researches at informal seminars in Southampton (1984), Milan (1986), Oslo (1988) and Grenoble (1990), and relevant data has been published by Fahey (1980), Last (1982), Parkin and Lunne (1982), Bellotti (1984) and Parkin (1988). While some controversy exists, there seems to be agreement that tests on loose sand represent field conditions reasonably well, whereas tests on dense sand are significantly affected by the proximity of the chamber boundary. No systematic examination of test data has been performed to assess chamber size effects at intermediate densities. Neglecting the effects of chamber size leads to an overestimation of density (and friction angle) in the field, especially when constant stress radial boundary conditions are used in the chamber.

In the present research programme the sample surface was restrained by flexible membranes to investigate the independent effect of vertical and horizontal stress on cone-pressuremeter test data. Therefore, the present discussion is concentrated on chamber size effects for tests carried out under stress controlled boundary conditions.

New evidence regarding the interpretation of chamber size effects emerged from results of cone-pressuremeter tests. The device enables cone resistance q_c and limit pressure ψ_l to be measured independently at the same location in the ground under the same test conditions. Results presented in Chapter 5 show clearly that for a given density of sand both cone resistance and limit pressure are primarily dependent on the effective horizontal stress and not on the vertical stress. This suggests that a similar mechanism is developed during cone penetration and pressuremeter expansion. Such a mechanism might be closely related to cylindrical cavity expansion, which explains why q_c and ψ_l are governed strongly by the horizontal stress.

Further support for the hypothesis that cone resistance is controlled by a cavity expansion process is provided by a direct comparison between limit pressure and cone resistance (see Chapter 5, Figure 5.4). As previously shown, for any given density of sand there is a constant ratio between ψ_l and q_c, and the ratio $(q_c - \sigma_h)/(\psi_l - \sigma_h)$ was found to be a useful variable for deriving soil parameters, particularly density. As cavity expansion is thought to control both q_c and ψ_l, it is suggested that the ratio of q_c to ψ_l is not as sensitive to chamber size effects as the independent measurements of cone resistance and limit pressure.

A number of comparative tests was then carried out using three cone-pressuremeter prototypes (15 cm^2, 10 cm^2 and 5 cm^2) to assess the influence of chamber size effects on cone-pressuremeter data. An attempt was made to quantify this effect on measured values of limit pressure and cone resistance, and on the ratio $(q_c - \sigma_h)/(\psi_l - \sigma_h)$. A parametric study was performed using a one-dimensional cavity expansion analysis to support some of the evidence observed in the interpretation of the experimental data.

AI.1 - Experimental data

Three cone-pressuremeter prototypes with diameters of 25.2 mm, 35.7 mm and 43.7 mm, which correspond to chamber to probe diameter ratios of approximately 38, 27 and 22 respectively, were tested in the calibration chamber. Data are available for three relative densities (loose (Rd ~ 30%), medium (Rd ~ 65%) and dense sand (Rd ~ 90%)), from tests carried out at mean effective stress of 100 kPa and stress ratios of 0.5 and 1.0. The results are presented in Figure AI.1, in which normalised limit pressure $(\psi_l - \sigma_h)/\sigma'_h$ is plotted against chamber to probe diameter ratio R_{cc}/R_o. A trend of increasing normalised limit pressure with increasing chamber to probe diameter ratio is clear. For loose sand, chamber size effects are not significant, whereas for medium and dense sand limit pressure is highly affected by the proximity of the chamber boundary. For dense sand when R_{cc}/R_o ratio is increased by a factor of 1.7 the normalised limit pressure is increased by a factor of about 1.9, whereas for medium sand limit pressure is increased by a factor of approximately 1.7.

A similar plot is presented in Figure AI.2, in which normalised cone resistance $(q_c - \sigma_h)/\sigma'_h$ is plotted against chamber to probe diameter ratio. For medium and dense sand a trend of increasing normalised cone resistance with increasing chamber to probe diameter ratio is clearly observed. For dense sand, when R_{cc}/R_o ratio is increased by a factor of 1.4 the normalised cone resistance is increased by a factor of about 1.6. For medium sand, an increase on R_{cc}/R_o ratio also by a factor of 1.4 corresponds to an increase of normalised cone resistance by a factor of approximately 1.3. Chamber size effects for loose sand were not investigated in this series of tests.

For the densities tested, the increase in limit pressure with increasing R_{cc}/R_o ratio is remarkably similar to the increase in cone resistance with increasing R_{cc}/R_o ratio. Although the

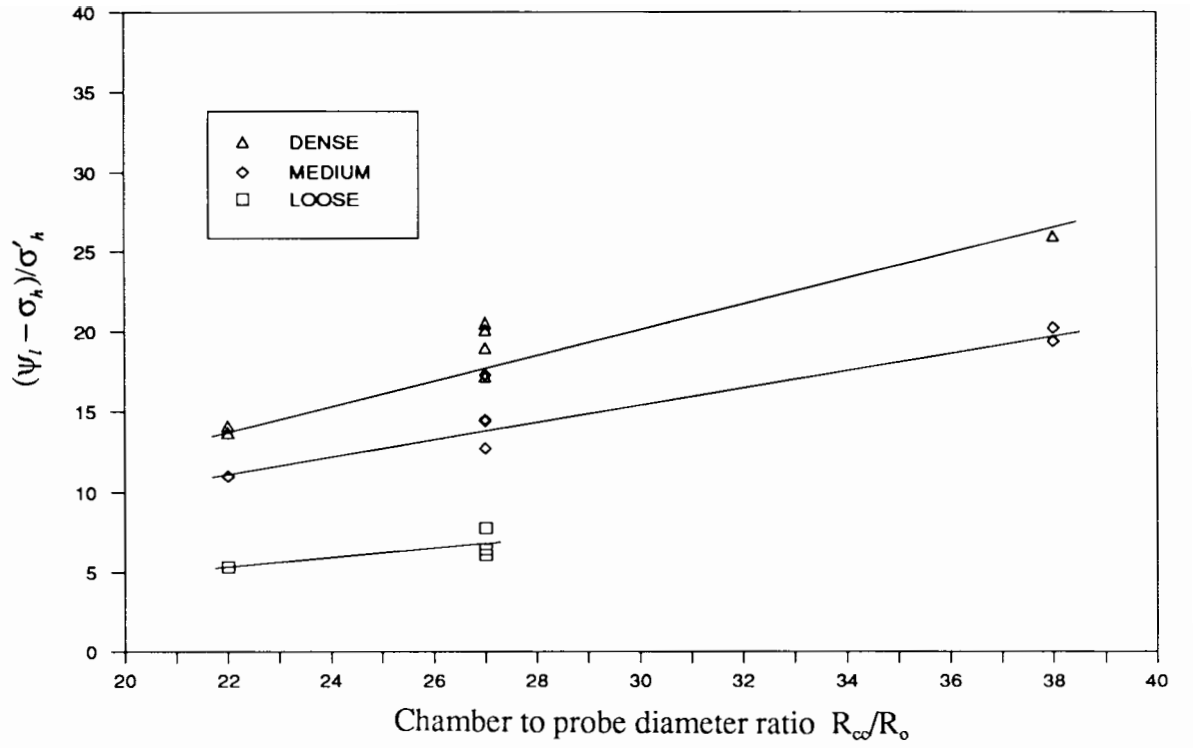

Figure AI.1 - Chamber size effects on limit pressure obtained from cone-pressuremeter tests

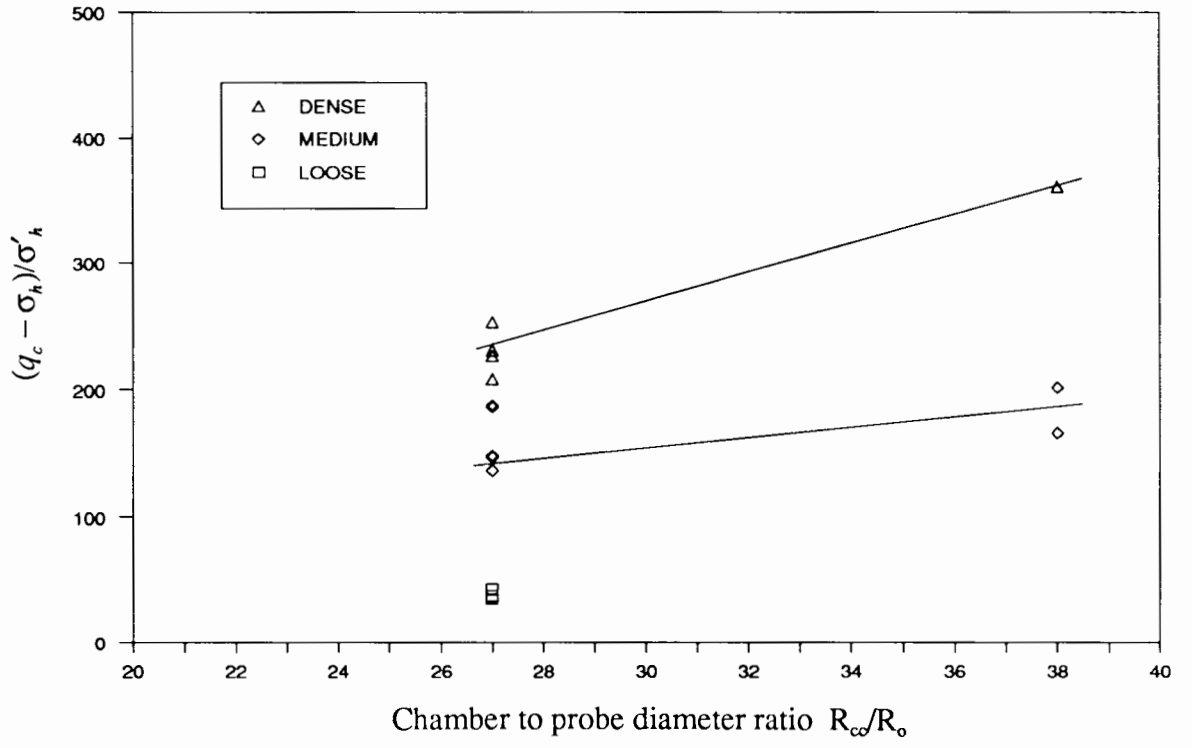

Figure AI.2 - Chamber size effects on cone resistance obtained from cone-pressuremeter tests

independent measurements of cone resistance and limit pressure are highly affected by the proximity of the chamber boundary, the ratio $(q_c - \sigma_h)/(\psi_l - \sigma_h)$ shows only small variations. This ratio is about 5.5, 10 and 12.5 for loose, medium and dense sand respectively. On the basis of this evidence, the following may be concluded:

a) the ratio $(q_c - \sigma_h)/(\psi_l - \sigma_h)$ is not significantly affected by chamber size effects for chamber to probe diameter ratios in the range of 22 to 38. More study would be required to validate this finding in different sands, but it is suggested that correlations derived from calibration chamber tests from cone-pressuremeter data can be applied to field conditions without any correction to account for chamber size effects. This finding is of critical importance to the work carried out with the cone-pressuremeter test, since assessment of soil properties is essentially dependent on the ratio $(q_c - \sigma_h)/(\psi_l - \sigma_h)$.

b) cone resistance has been closely linked to limit pressure within the framework provided by the database obtained from cone-pressuremeter tests. These results not only suggest that cone resistance is controlled, at least in part, by a cavity expansion process, but also support the hypothesis that cavity expansion theory can satisfactorily explain observed chamber size effects on cone penetrometer testing data.

AI.1.1 - Cone penetrometer tests

A comprehensive and well-documented database of calibration chamber tests using the cone penetrometer is available in the literature. Approximately 400 laboratory tests using different cone and tank sizes, densities, stress levels and stress ratios on Leighton Buzzard sand (Houlsby and Hitchman, 1988), Hokksund sand (Last *et al*, 1987) and Ticino sand (Baldi *et al*, 1986) have been examined to assess the influence of chamber size effects on tip cone resistance q_c.

Chamber tests were performed under different combinations of boundary conditions, where stress controlled or strain controlled boundaries were imposed on the sample. But, as with the analysis on the cone-pressuremeter, this discussion is concerned only with stress controlled boundary conditions.

Chamber test results are presented in Figure AI.3 in a plot of $\log((q_c - \sigma_h)/\sigma'_h)$ against $\log(\sigma'_h/p_a)$. Although the scatter of the test data is evident, for each density a trend exists of decreasing normalised cone resistance with increasing horizontal effective stress. The significant reduction of values of the ratio of q_c/σ'_h with increasing stress level is thought to be a result of reduction of peak friction angle with increasing stress level (as discussed in Chapter 5).

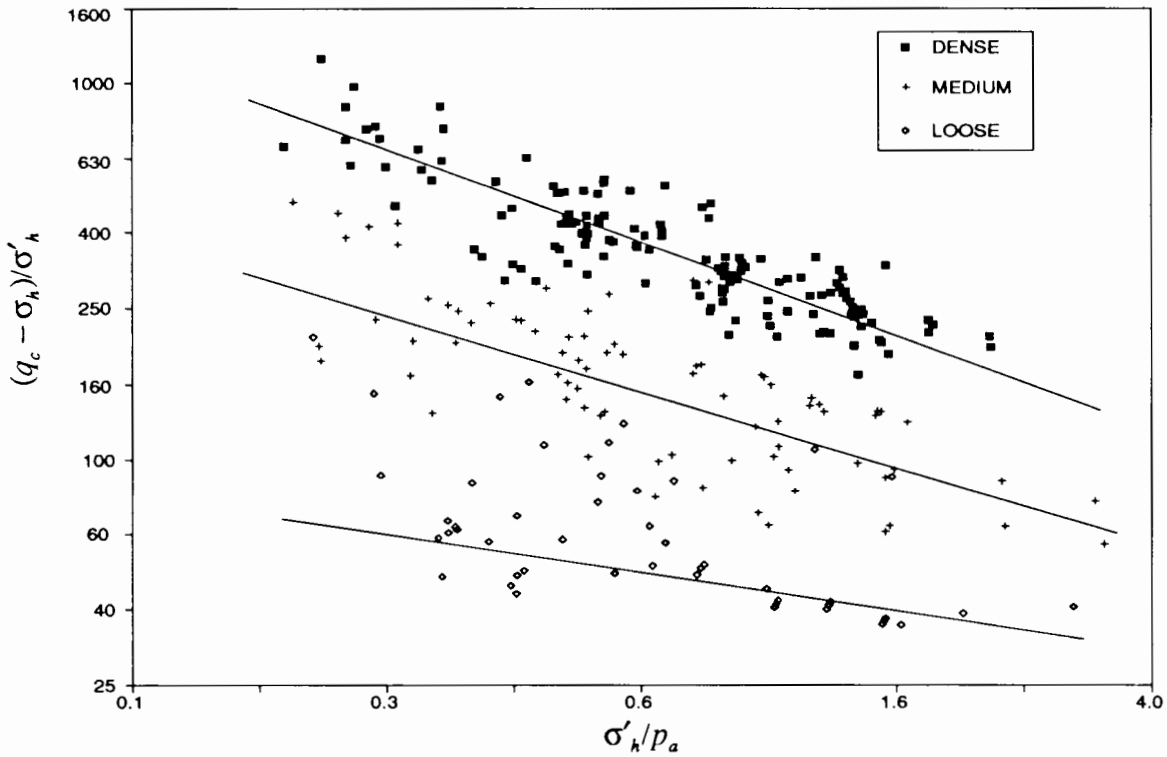

Figure AI.3 - Effects of stress level on cone resistance

Some scatter was expected to be observed in Figure AI.3, due to one or more of the following effects: chamber to probe diameter ratio, probe to particle diameter ratio, soil type (mineralogy, grading, shape of grains) and stiffness.

In attempting to assess the influence of chamber size effects on dense sand, Figure AI.3 has been redrawn in Figure AI.4 on a much large scale and showing only tests in dense sand. A clear trend of increasing cone resistance with increasing chamber to probe diameter ratio is observed in the figure. Some scatter is still evident, which suggests that other parameters should also been taken into account to understand fully the relationship between q_c and σ'_h and to evaluate correctly the influence of chamber size effects.

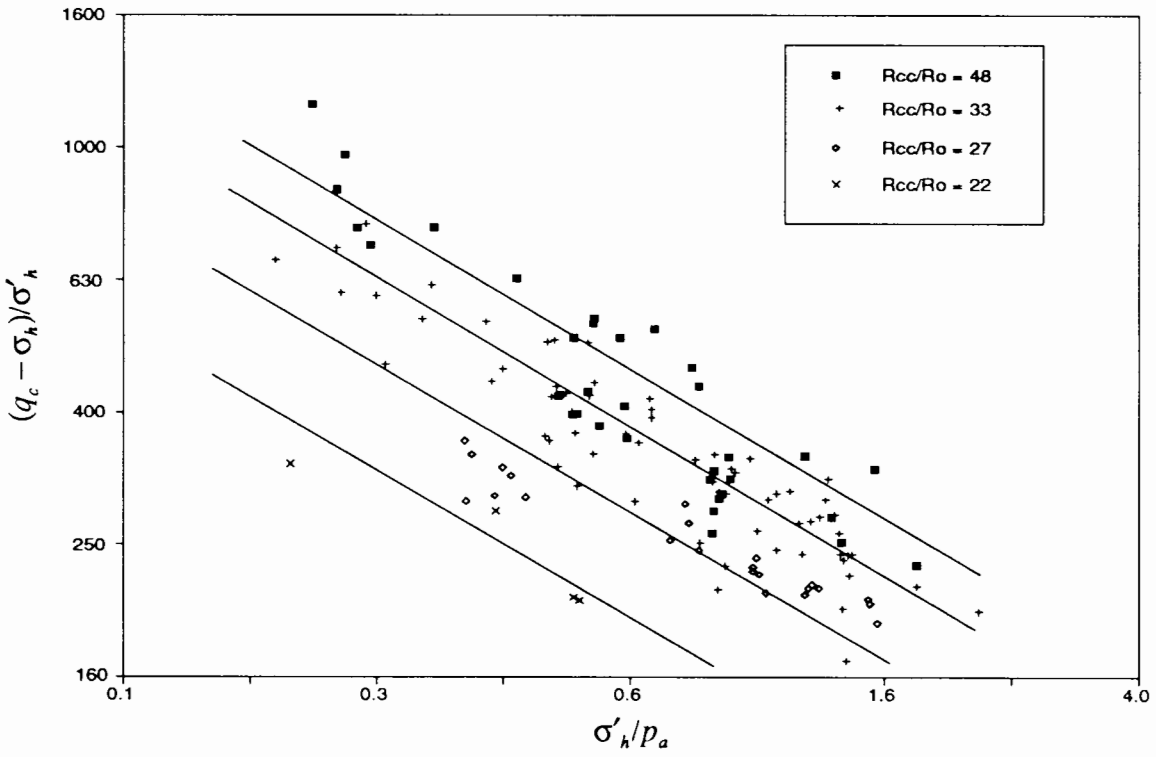

Figure AI.4 - Chamber size effects on cone resistance for dense sand

It is difficult to separate the effects of chamber to probe diameter ratio and probe to particle diameter ratio, but taking all the tests together some conclusions can be drawn. Cone resistance is substantially dependent on density and stress level. For dense sand, chamber to probe

diameter ratio also has a significant effect on the measured q_c, with a chamber of 25 probe diameters resulting in approximately half the cone resistance of one of 50 diameters. For medium sand the scatter obscures any possible trends in the test data, and no clear evidence of chamber size effects is observed. However, it is important to note that by considering the measured values of cone resistance from only the test data obtained with the cone-pressuremeter in Leighton Buzzard sand, the effect of the finite boundary is apparent (see Figure AI.2). For loose sand, measured cone resistance seems not to be affected significantly by chamber size effects. These findings are in general agreement with previous work reported by Parkin and Lunne (1982) and Parkin (1988).

AI.2 - Numerical interpretation

The interpretation of pressuremeter tests and cone penetration tests has showed that tip cone resistance, as well as limit pressure, are strongly influenced by chamber size effects. However, it is difficult to quantify the dependency of q_c and ψ_l on chamber to probe diameter ratio, since a degree of uncertainty exists due to the effect of other variables such as stiffness and soil type.

In order to assess the independent influence of chamber to probe diameter ratio, shear strength and soil stiffness on calibration chamber testing data, a numerical analysis was carried out using a one-dimensional finite element program. The program is available at Oxford University and has been developed by Yu (1990). An axysymmetric plane strain analysis was used to simulate the geometry and boundary conditions applied to the chamber (lateral pressure control). Large strain finite element analysis with a frictional model with dilation was used. An expansion ratio of four was applied to the radius of the cavity, which may be assumed to model numerically the installation of the cone-pressuremeter and the subsequent expansion of the pressuremeter probe (Houlsby and Withers, 1988; Houlsby and Yu, 1990).

The analysis was carried out using an elastic-plastic model based upon the Mohr-Coulomb criterion. The parameters for the model were determined from triaxial tests and cone-pressuremeter tests on Leighton Buzzard sand, as described in this dissertation. The elastic component is described by the shear modulus using a combination of equations [6.12] and [6.13], which is reproduced here for clarification

$$G/p_a = 480(p'/p_a)^{0.28+0.59R_d} \qquad [AI.1]$$

The strength parameters were defined by making use of Bolton's empirical formula

$$(\phi'_p - \phi'_{cv}) = 5\left[R_d\left(Q - \ln\frac{p'}{kPa}\right) - 1\right] \qquad [AI.2]$$

adopting $\phi'_{cv} = 34.3°$ and Q = 9.9 (see Chapter 3 for details).

Calculations were carried out to model as closely as possible the conditions of each test. Experimental data obtained with the 15 cm^2, 10 cm^2 and 5 cm^2 devices were used to support numerical observations. Figure AI.5 shows a comparison between measured and predicted values of limit pressure. The general agreement was considered fairly good, considering the simplicity of the theoretical model. For dense and medium sand the ratio $\psi_{l(predicted)}/\psi_{l(measured)}$ was on average 1.03 and 0.94 respectively. For loose sand an overprediction of the measured values of limit pressure was observed ($\psi_{l(predicted)}/\psi_{l(measured)}$ = 1.42). This overprediction may be due to a slightly too high friction angle being adopted in the calculations. The geometry of the problem did not significantly affect the accuracy of the predictions, i.e. the ratio $\psi_{l(predicted)}/\psi_{l(measured)}$ was found to be independent of the ratio R_c/R_o.

The agreement between measured and predicted values of limit pressure is encouraging, indicating that a simple one-dimension program can satisfactorily explain the influence of chamber size effects on limit pressure. A parametric study was then carried out, in which the effects of shear strength, stiffness and chamber to probe diameter ratio R_{cc}/R_o were examined. Strength and stiffness were chosen within the range of values predicted from equations [AI.1] and [AI.2]. Chamber to probe diameter ratios ranging from 20 to 50 were selected, as they cover most of the experimental work carried out in calibration chambers. However, even the ratio $R_{cc}/R_o = 50$ is not necessarily representative of field conditions.

The influence of the stiffness index ($I_s = G/p_o$) on limit pressure is presented in Figure AI.6, in which the ratio ψ_{150} calculated for a calibration tank of 50 probe diameters to ψ_l calculated for smaller tanks of different diameters is plotted against chamber to probe diameter ratios. For loose sand, the calculations indicate that limit pressure is controlled significantly by the stiffness index. An increase in the ratio ψ_{150}/ψ_l of about 16% is observed with increasing I_s values (from 500 to 3000). However, for medium and dense sand (ϕ'_{ps} from approximately 40° to 55°) the ratio ψ_{150}/ψ_l is virtually independent of stiffness. For the three densities tested, the ratio ψ_{150}/ψ_l increases with increasing chamber to probe diameter ratio. This effect is quite considerable for loose sand, and significantly more so for both medium and dense sands.

A similar approach has been used to assess the influence of shear strength on limit pressure. For a given stiffness index ($I_s = 500$), ratios of ψ_{150}/ψ_l were calculated for different friction angles and chamber to probe diameter ratios (see Figure AI.7). Peak friction angles were related to dilation angles by making use of the correlation suggested by Bolton (1986). For loose sand, the ratio ψ_{150}/ψ_l is sensitive to variations on friction angle. An increase in the ratio ψ_{150}/ψ_l of up to 8% is produced when the friction angle is increased from 33° to 34°. For higher values of friction angle (medium and dense sand) this effect is less significant, so that small variabilities in sand density do not produce major changes on the measured limit pressure.

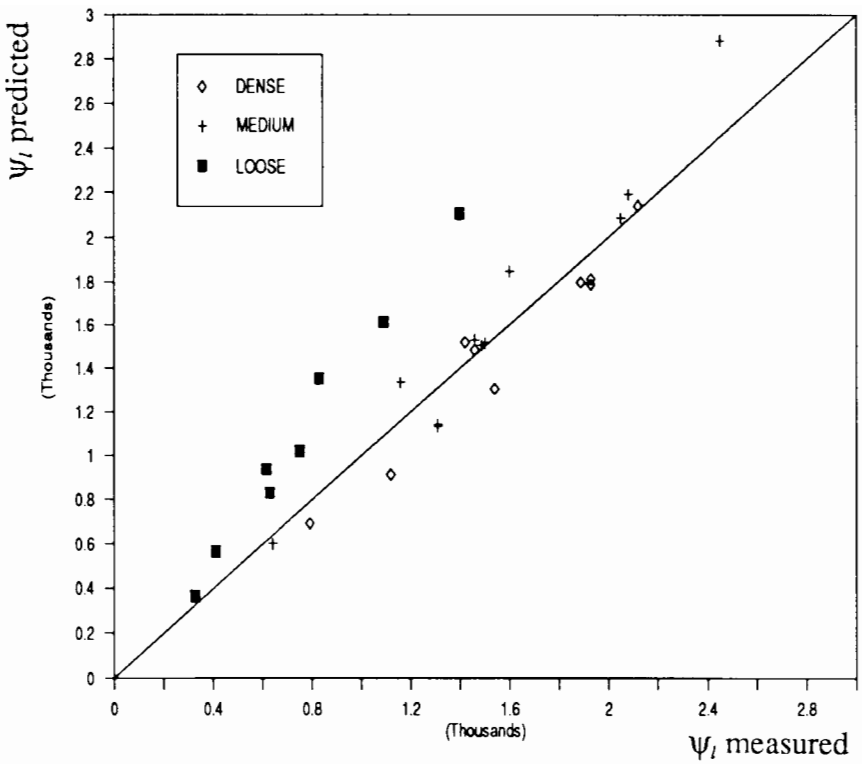

Figure AI.5 - Comparison between measured and calculated limit pressure (modified from Houlsby and Yu (1990))

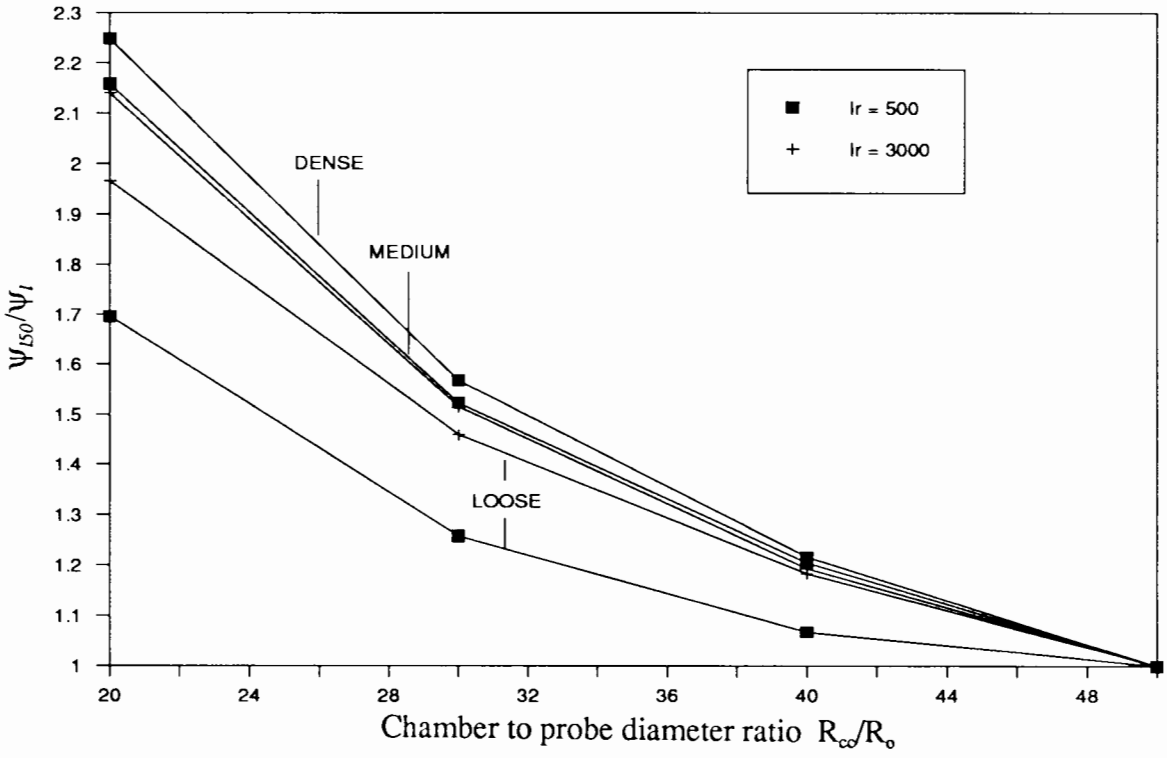

Figure AI.6 - Effect of stiffness index I_s on limit pressure

Finally, the analysis of cavity expansion in a finite cylinder was applied to account directly for chamber size effects in the calibration chamber. The value of ψ_{t27} calculated for a tank 27 probe diameters was used as a reference value for this study, since most experimental data was obtained with a 10 cm^2 device ($R_\infty/R_o = 27$). The results are presented in Figure AI.8, in which the ratio ψ_{t27}/ψ_t is plotted against chamber to probe diameter ratio[1]. A comparison is made between numerical predictions and experimental observations of chamber size effects on limit pressure. For the experimental data, ψ_{t27} was calculated as the average value of limit pressure obtained from all tests carried out at the same density.

Hypothesizing that cone resistance is controlled, at least partially, by a cavity expansion mechanism, observations based on Figure AI.8 are relevant to tip cone resistance, as well as limit pressure.

For dense sand, the measured limit pressure is considerably affected by chamber size effects. The numerical prediction estimates measured ψ_{t27}/ψ_t values with reasonable accuracy for chamber to probe diameter ratios in the range of 25 to 40, but underestimates the effect for small chambers. Experimental data indicate that the magnitude of chamber size effects for dense sand is very similar to that suggested by Parkin and Lunne (1982).

For medium sand ($R_d \sim 65\%$) the factor ψ_{t27}/ψ_t is also significantly affected by the proximity of the chamber boundary. Calculations, as well as experimental data, suggest that the effect on medium sand is almost as high as that observed for dense sand. The current interpretation of chamber size effects on medium sand had failed to identify the underlying trend, possibly because of substantial scatter of data that occurs as a result of sample variability at intermediate densities (which is evident in Figures AI.3 and AI.8). Scatter is thought to be a result of the

---

1 *This plot has been produced adopting $\phi'_{cv} = 33°$ to enable direct comparisons with the numerical solution presented by Houlsby and Yu (1990) and Yu (1990).*

influence of friction angle on limit pressure. Since test results are grouped together according to density (usually within ± 5% average relative density), it seems reasonable to suggest that the absolute increase in the values of limit pressure is of the same order of magnitude as the increase due to chamber size effects.

For loose sand, both the limited experimental and more extensive numerical data suggest that some effect due to the proximity of the boundary exists. As for medium sands, scatter is usually observed and is likely to be a result of the combined effects of variations on friction angle and soil stiffness.

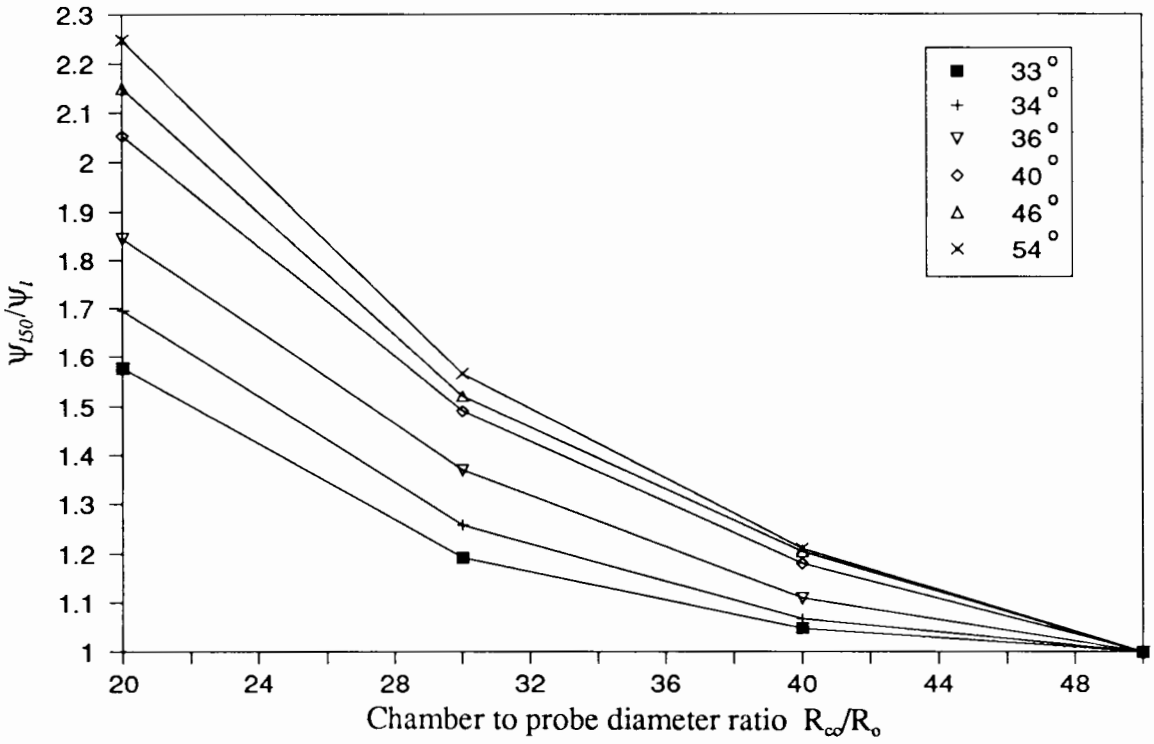

Figure AI.7 - Effect of friction angle on limit pressure

The comparison between analysis and experimental data encourages the use of cavity expansion theory to assess the influence of chamber size effects on measured values of limit pressure and cone resistance. The interpretation presented above is not, however, absolutely conclusive. Further research is necessary to quantify accurately these effects on different

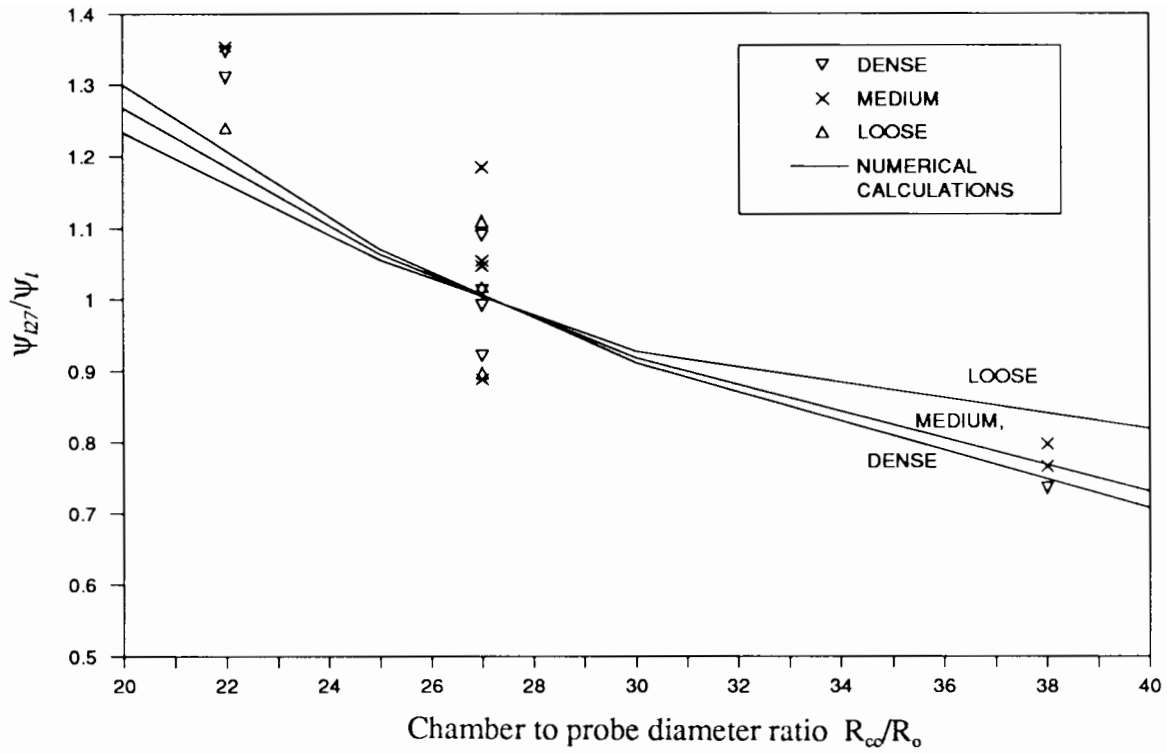

Figure AI.8 - Comparison between experimental and numerical predictions of chamber size effects

materials at different densities. Attention must be paid to intermediate states of density, since the current methods of interpretation seem to underestimate the magnitude of corrections necessary due to the physical proximity of the chamber boundary.

APPENDIX II

LENGTH TO DIAMETER RATIO EFFECTS ON LIMIT PRESSURE

The cone-pressuremeter is one of the recent advances in *in situ* testing equipment, and standardized equipment dimensions are highly desirable to allow adequate comparison of data from different soils. To the author's knowledge, three cone-pressuremeter devices have been previously used in preliminary field trials - the Fugro-McClelland probe (Withers *et al*, 1986), the Laboratoire Central des Ponts et Chaussées LPC probe (Baguelin and Jezequel, 1986) and most recently the University of British Columbia UBC probe (Campanella *et al*, 1990). The Fugro, UBC and LPC devices have length to diameter ratios of 10, 5 and 4 respectively, which anticipate the necessity of studying the possible effects of geometry on data obtained from cone-pressuremeter tests.

The results obtained from a series of chamber tests carried out to investigate the influence of length to diameter ratio, L/D, on cone-pressuremeter data is given in this appendix. An attempt to quantify the magnitude of L/D effects on measured limit pressure is presented.

AII.1 - Background

Cavity expansion theory allows closed form solutions to be obtained for pressure-expansion curves in pressuremeter tests, so that soil strength and stiffness may be obtained from back analysis of real tests. Several analyses applicable to the pressuremeter have been developed during recent decades (e.g. Gibson and Anderson, 1961; Ladanyi, 1963; Vesic, 1972; Palmer,

1972; Hughes *et al*, 1977; Houlsby *et al*, 1986). The analysis developed by Gibson and Anderson (1961) has been widely used to interpret self-boring pressuremeter tests in clay. For the derivation of the undrained shear strength, the clay is assumed to undergo zero volume change and to behave as an elastic, perfectly plastic material. For cohesionless material, the analysis has been modified by Hughes *et al* (1977) to account for volume changes that occur when the soil is subject to shear.

The relevance of both of these analyses has been confirmed in a CIRIA report on pressuremeter testing (Mair and Wood, 1987), but some results indicate considerable discrepancies between soil parameters obtained from pressuremeters and those obtained from laboratory tests or other *in situ* tests. Experience in clay has shown that the undrained strength derived from the pressuremeter is generally above values obtained from laboratory triaxial compression, field vane and cone penetrometer tests (Baguelin *et al*, 1972; Eden and Law, 1980; Ghionna *et al*, 1981; Clough *et al*, 1990; Lacasse *et al*, 1990). In cohesionless soil, friction angles derived from pressuremeter tests are occasionally higher, for example, than those obtained from cone penetrometer tests (Hughes *et al*, 1977; Jamiolkowski *et al*, 1986). Differences are partially explained by different soil stress path generated by cone tests and pressuremeter tests. The accuracy of the predictions may also depend on the validity of the assumptions regarding geometry (in particular the finite length of the pressuremeter).

An analysis of the cone-pressuremeter test in clay was presented by Houlsby and Withers (1988) using large strain cavity expansion theory. The solution of cylindrical case was successfully used for deriving undrained strength and shear modulus. In theory horizontal stress can also be derived, but excessively high values of K_o were obtained. It was then suggested that expansion pressures were somewhere between the cylindrical and the spherical cases, although a Fugro device (L/D = 10) was used in the trial tests.

An equivalent approach for test interpretation in sand has been developed by Yu (1990), in which the initial installation of the device is modelled as the expansion of a cylindrical cavity within the soil. A one dimensional finite element analysis of the test was presented, and was applied successfully to the results of calibration chamber tests. A comparison between measured and calculated limit pressures has been presented in Appendix I (see Figure AI.5). Considering the simplicity of the theoretical model, the analysis was found to predict well the measured values of limit pressure, particularly in medium and dense sand.

Most recently, this approach has been extended to a two dimensional finite element analysis (Yu, 1990) to investigate length to diameter ratio effects on self-boring pressuremeter tests in both clay and sand. The clay was modelled as an incompressible linear elastic, perfectly plastic (von Mises) material. Matsuoka's yield criterion was used to model the behaviour of granular soils, in which dilatancy was taken into account. A series of parametric studies has been carried out to examine L/D effects on undrained strength, stiffness and friction angles. Comparisons were presented between pressuremeter tests with an infinity long probe and pressuremeter tests with L/D = 6 (which is used in the Cambridge Self-Boring Pressuremeter). The effect of L/D on shear modulus was considered negligible for radial expansion calculated from central displacements of the pressuremeter probe. This finding is supported by experimental evidence reported by Laier *et al* (1975) and Briaud *et al* (1986). An overestimation of shear modulus of approximately 13% was observed for volumetric strain measurements. For L/D = 6 undrained strength values were overestimated by about 10% to 17%, with an increasing effect of length to diameter ratio on s_u with increasing rigidity index, G/s_u (for G/s_u in the range of 50 to 500). Friction angles were overestimated by approximately 10% to 17%, with an increasing effect of L/D with increasing stiffness index, G/p_o (for G/p_o in the range of 200 to 1000). This analysis is currently being extended for the interpretation of the cone-pressuremeter test in clay (Yu, 1990), but is has not yet been developed for sand.

This discussion aims to emphasise the need to develop a better understanding of length to diameter ratio effects before comparing data from different studies. Some of the difficulties in dealing theoretically with L/D effects are also highlighted, especially for cone-pressuremeter tests in sand, which indicate that an assessment of the finite length of the probe on pressuremeter data has still to be made in a purely empirical fashion.

AII.2 - Interpretation

The comparative study presented in this section is concerned only with the effect of length to diameter ratio on the measured limit pressures. There are two main reasons for this:

a) limit pressure is, in general, an easily and well defined quantity obtained from a cone-pressuremeter pressure-expansion curve. For the self-boring pressuremeter, in conditions where cavity strain is too small for a reliable estimation of limit pressure, procedures to assess ψ_l of expanding cylindrical cavities in purely friction materials are also available (Ghionna *et al*, 1989).

b) the measured limit pressure is a key factor in the interpretation of pressuremeter data, used in engineering practice either for deriving soil parameters such as friction angle and undrained shear strength (e.g. Gibson and Anderson, 1961; Marsland and Randolph, 1977) or for an estimation of bearing capacity of deep foundations (e.g. Baguelin *et al*, 1978), penetration resistance of driven piles (e.g. Randolph *et al*, 1979) and laterally loaded driven piles (e.g. Robertson *et al*; 1983, 1986).

The literature contains several well-documented reports on pressuremeter tests in both sand and clay. However, it is difficult to obtain comparative plots of expansion curves for tests carried out using different pressuremeter probes under the same soil conditions. Whenever possible, test results exhibited scatter due to the natural heterogeneity of the soil, and no definite

trend between limit pressure and L/D is observed (Briaud *et al*, 1986). One exception is the calibration chamber testing programme performed by Fahey (1980) using a self-boring pressuremeter. A limited number of comparative tests was carried out on dense sand, in which tightly fitting thin-walled brass sleeves were fixed over the ends of the membrane, reducing the length of the expanding section of the pressuremeter from 500 mm (L/D =6.2) to 322 mm (L/D = 4). The horizontal stress applied during all the tests was 90 kPa, but three stress ratios were used, corresponding to K values equal to 2, 1 and 0.45.

Using the data produced by Fahey (1980), a comparison is made between the measured values of limit pressure ψ_l and the values of limit pressure calculated for the cylindrical expansion of an infinitely long probe $\psi_{lcylinder}$. A small strain solution proposed by Fahey (1980), which accounts for the effects of the finite outside diameter of the calibration chamber, can be used to calculate $\psi_{lcylinder}$

$$\left\{\frac{\psi_{lcylinder}}{\sigma_h}\right\} = \frac{(1+\sin\phi')}{1+\left\{\frac{R_e}{R_{cc}}\right\}^2 \sin\phi'}\left\{\frac{R_e}{R}\right\}^{1-N} \qquad [AII.1]$$

in which

σ_h = horizontal stress applied to the sample boundary

R_e = radius of the elastic-plastic interface

R_{cc} = radius of the chamber

R = radius of the pressuremeter probe

$N = \frac{1-\sin\phi'}{1+\sin\phi'}$

For all tests carried out in the calibration chamber, cavity pressure reached a maximum when the plastic zone eventually reached the chamber outer boundary ($\frac{R_e}{R_{cc}} = 1$ and $\frac{R_e}{R} = \frac{R_{cc}}{R}$). Under this condition, equation [AII.1] can be re-written as:

$$\left\{\frac{\psi_{lcylinder}}{\sigma_h}\right\} = \left\{\frac{R_{cc}}{R}\right\}^{1-N} \qquad [AII.2]$$

Equation [AII.2] was then used to calculate $\psi_{lcylinder}$, which was applied to the interpretation of L/D effects using a self-boring pressuremeter. The results of chamber tests are shown in Figure AII.1, in which the ratio $\psi_l/\psi_{lcylinder}$ is plotted against the ratio L/D. Note that the horizontal axis is plotted as 1/(L/D), because it enables results to be expressed in a more convenient way within the range of 0 to 1 (instead of 0 to infinity). Although some scatter is observed, a trend exists of an increase in the ratio $\psi_l/\psi_{lcylinder}$ with decreasing L/D ratio. When L/D is decreased by a factor of 1.55 the ratio $\psi_l/\psi_{lcylinder}$ is increased on average by a factor of approximately 1.23. No influence of K values on the ratio $\psi_l/\psi_{lcylinder}$ was observed, but this may be due to the scatter in the test data.

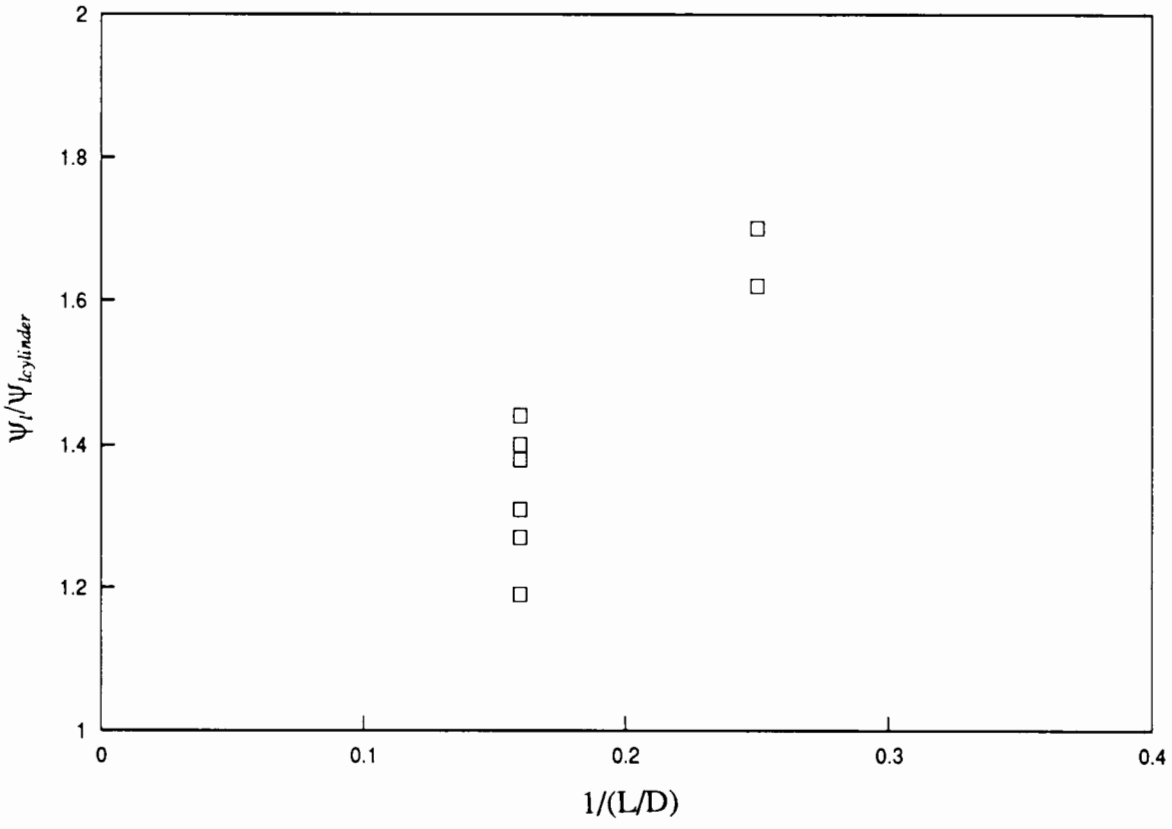

Figure AII.1 - Length to diameter ratio effect (from self-boring pressuremeter tests)

The results reported by Fahey (1980) give experimental evidence of the influence of the geometry on self-boring pressuremeter data. However, it is not possible to quantify the magnitude of L/D effects on limit pressure, due to the limited range of L/D ratios tested (L/D from 6.2 to 4) and the scatter observed in the test data.

Calibration chamber tests carried out with a pre-bored pressuremeter (Laier *et al*, 1975) have also indicated a marked effect of pressuremeter length on measured limit pressure. Three probes were tested by Laier in a chamber, each probe having three cells (one measuring cell between two guard cells). The length of the measuring cell changed from 152 mm to 475 mm in order to produce L/D ratios of 14, 29 and 38. Test results indicated that when L/D ratio is decreased by a factor of 2, the limit pressure is increased by a factor of 1.28. There is also evidence that the ratio $\psi_l/\psi_{lcylinder}$ appears to be independent of density and overconsolidation ratio.

This information was useful when establishing a test programme to evaluate length to diameter ratio effects on cone-pressuremeter limit pressure. The 5 cm^2 prototype was used, as it is provided with various adapters enabling L/D ratios of 5, 10 and 20 to be tested. Ratios in the range of 5 to 10 are commonly adopted in the design of pressuremeter probes, whereas a ratio of 20 was chosen to produce a device of maximum feasible length in order to reduce L/D effects to a minimum. All tests were carried out in medium sand, combining a mean effective stress of 100 kPa with K values of 0.5 and 1.0.

Pressure-expansion curves for six calibration chamber tests are presented in Figure AII.2. The curves are present in groups of three, so that the influence of L/D can be seen separately from that of K. A limit pressure was reached in tests carried out with L/D ratios of 20 and 10 at a cavity strain of 10% to 20%. For L/D ratios of 5, cavity strain was not sufficient for a reliable estimation of limit pressure. The effects of varying L/D ratio are as expected: a trend of increasing limit pressure as L/D decreases is evident.

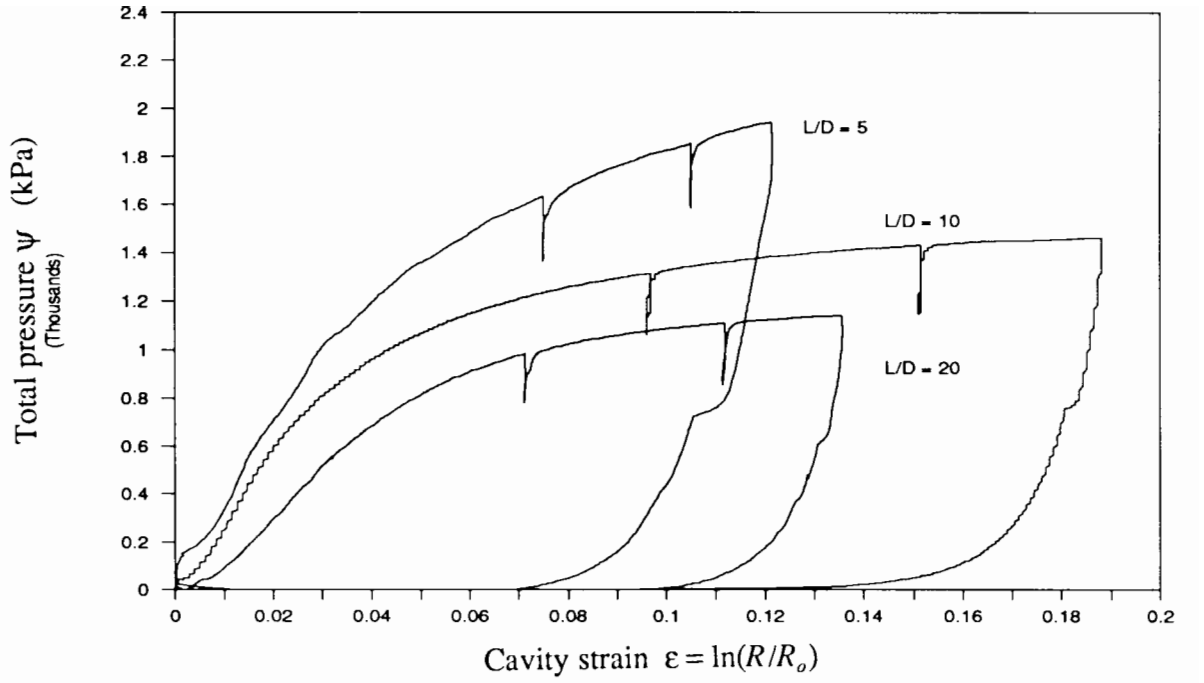

(a) K = 0.5

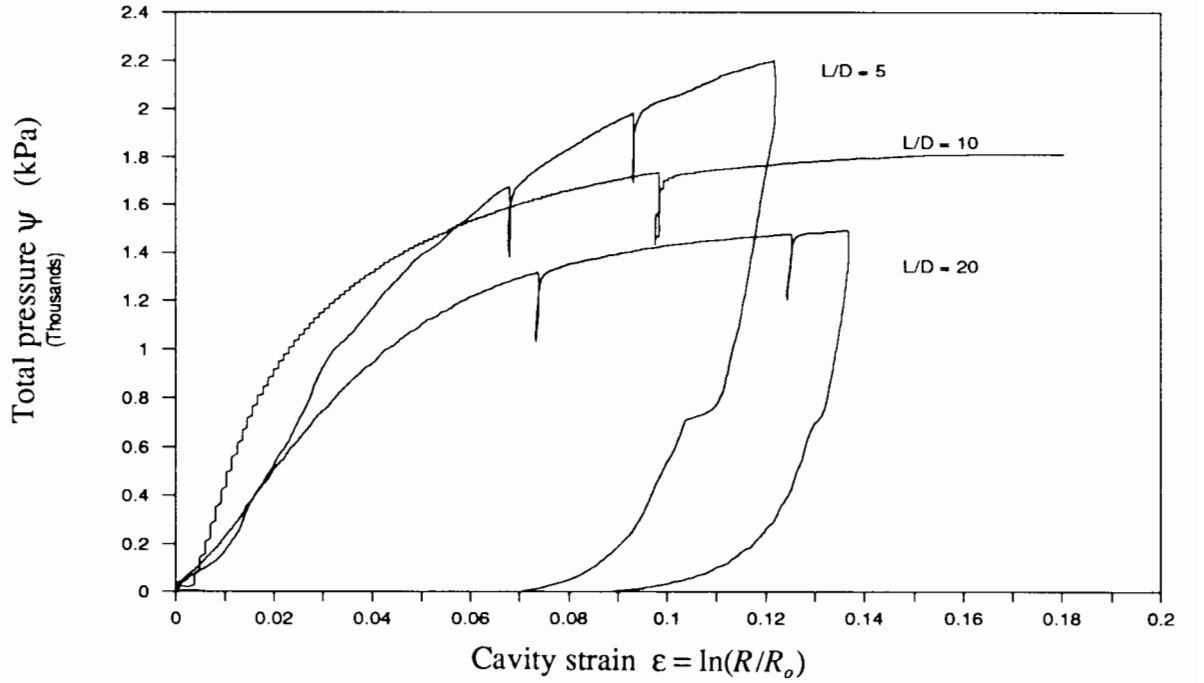

(a) K = 1.0

Figure AII.2 - Cone-pressuremeter pressure-expansion curves for tests carried out using different L/D ratios (tests on medium sand - p' = 100 kPa)

In order to compare the pressure-expansion curves presented in Figure AII.2, a value of cavity pressure corresponding to 10% cavity strain was selected from each curve. This criterion was necessary since a value of limit pressure was clearly not observed for tests carried out with L/D equal to 5. Such a comparison is presented in Figure AII.3, in which the measured values of cavity pressures $\psi^{10\%}$ are plotted against L/D ratio. Since there is no analytical solution to predict accurately the limit pressure measured with the cone-pressuremeter in the calibration chamber, values of $\psi^{10\%}$ were arbitrarily normalised by the cavity pressure (at 10% cavity strain) measured with L/D equal to 10, $\psi^{10\%}_{L/D=10}$. [1]

A clear trend of increasing limit pressure with decreasing L/D is observed in Figure AII.3. The variation of the ratio $\psi^{10\%}/\psi^{10\%}_{L/D=10}$ with 1/(L/D) can be approximated by a linear equation:

$$\frac{\psi^{10\%}}{\psi^{10\%}_{L/D=10}} = 0.69 + \frac{3.05}{(L/D)} \qquad [AII.3]$$

for the range of L/D between 5 to 20. When L/D ratio decreases by a factor of 2 the pressure $\psi^{10\%}$ is expected to increase by a factor of 1.3, which should be taken into account when comparing results from Fugro probes (L/D = 10) with results from LPC probes (L/D = 5). The experimental results also suggest that even very long probes (L/D = 20) may be sensitive to end effects, and the measured pressures do not necessarily correspond to cylindrical cavity expansion pressures.

A recent work presented by Lancellotta (1990), based on calibration chamber test data published by Ghionna *et al* (1990), provides an interesting application of equation [AII.3]. An

---

1 *Note that values of* $\psi^{10\%}_{L/D=10}$ *correspond to the "true" limit pressure measured in the tests, as they were determined from a well-defined plateau observed in the pressure-expansion curves.*

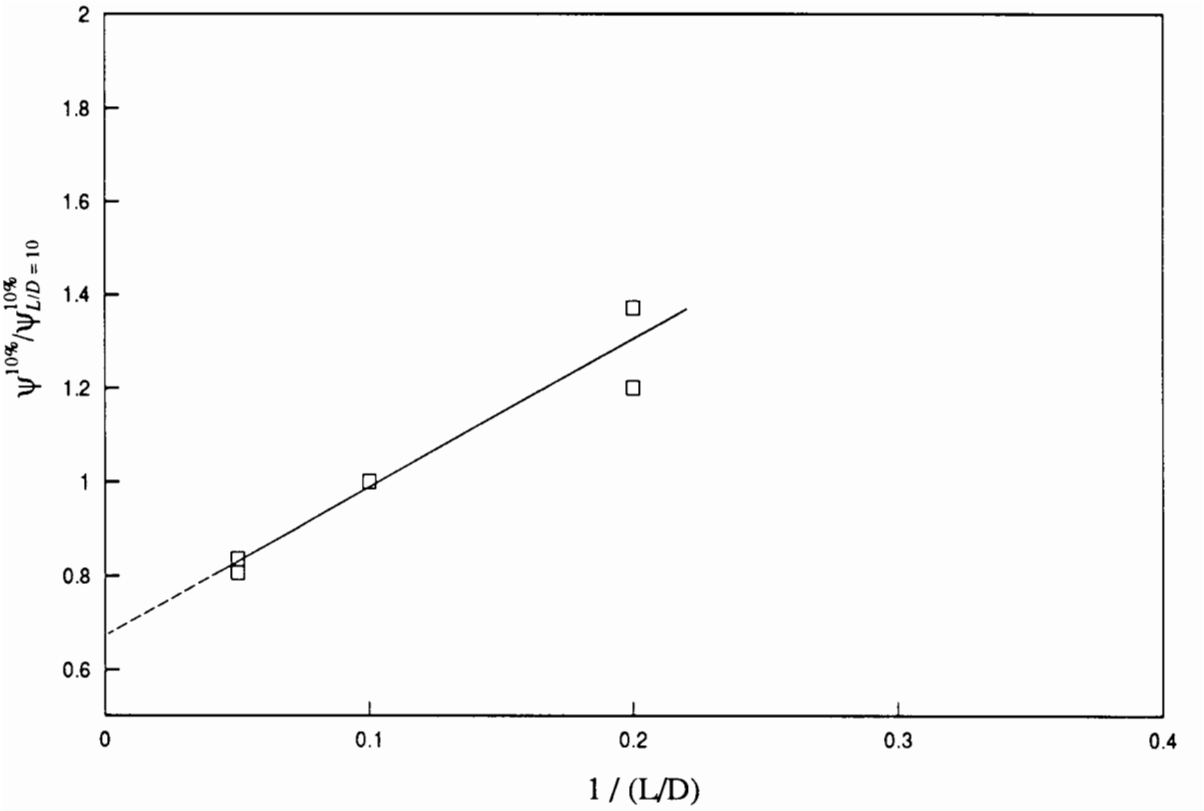

Figure AII.3 - Length to diameter ratio effects (from cone-pressuremeter tests)

attempt was made to predict relative density R_d using equation [5.1] (see Chapter 5), in which R_d is expressed as a function of the ratio $(q_c - \sigma_h)/(\psi_l - \sigma_h)$. Equation [5.1] is here reproduced for the sake of clarification

$$R_d = 9.0\frac{(q_c - \sigma_h)}{(\psi_l - \sigma_h)} - 30 \qquad [AII.4]$$

Instead of cone-pressuremeter data, the author combined values of self-boring limit pressure with independent measurements of cone resistance (tests were carried out on Ticino sand under the same stress conditions and about same density). Equation [AII.4] was found to underestimate relative density by about 20%. By making use of equation [AII.3], it is possible to correct the measured values of limit pressure obtained from self-boring pressuremeter

(L/D = 6.2), and then compare the corrected values to the expression obtained from cone-pressuremeter tests (L/D = 10). Such a comparison is presented in Figure AII.4, in which expression [AII.4] produces a generally good agreement with data obtained from Ticino sand.

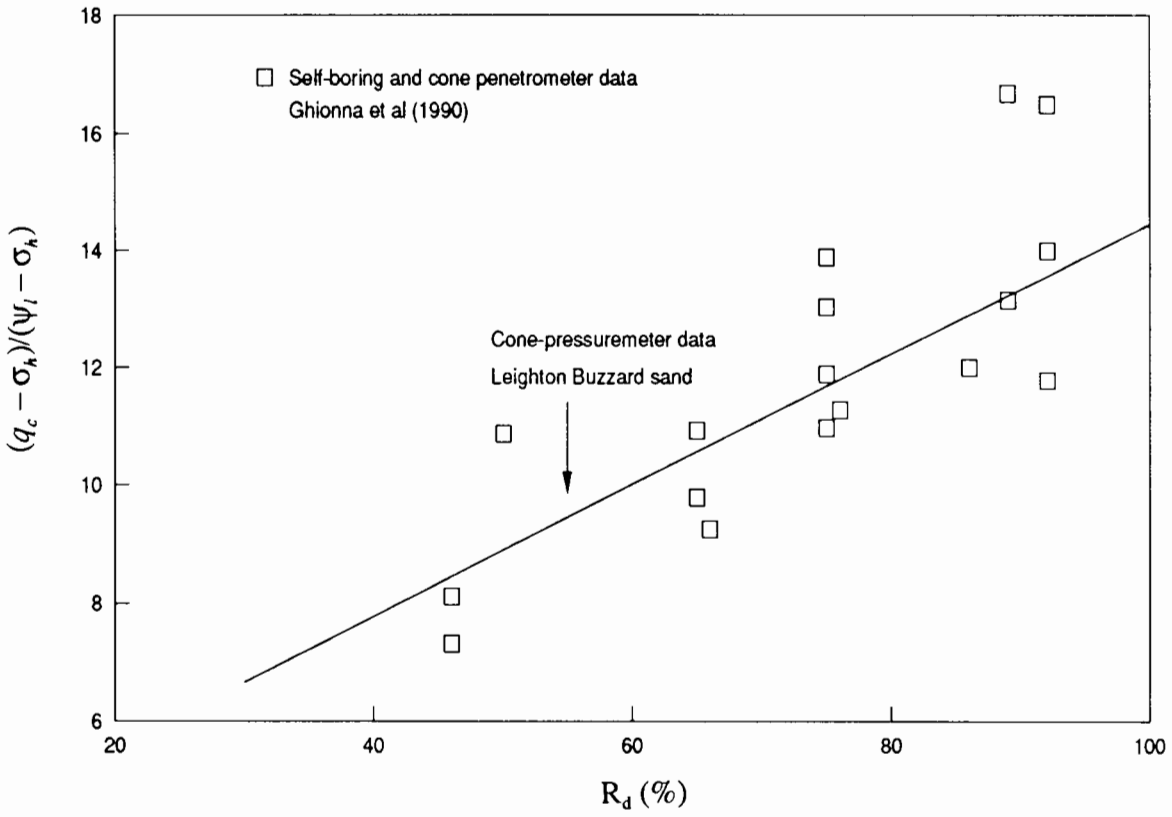

Figure AII.4 - Ratio of cone resistance to limit pressure against relative density (Ticino sand)

AII.3 - Final remarks

Despite the limited amount of experimental data presented in this appendix and the lack of a theoretical framework to support a more rigorous analysis, the influence of length to diameter ratio effects on measured limit pressure has been demonstrated. This effect should be taken

into account in order to understand correctly the results of studies and tests obtained from different pressuremeter probes. At the moment, however, it is not possible to quantify the influence of L/D effects for general engineering applications.

As far as limit pressure is concerned, some comments are necessary. The need to standardize equipment dimensions is important, but it is necessary to acknowledge that any choice of dimensions would require corrections to account for L/D effects. From the experimental point of view, short probes (L/D = 5) have the disadvantage of requiring larger expansion strains than that of a long probe (L/D from 10 to 20) for a reliable evaluation of limit pressure. From the existing evidence, it is questionable whether a long probe is more convenient than a short one, and whether cylindrical expansion is more appropriate than spherical cavity expansion theory. There seems to be no single answer, since a choice of geometry depends on which soil parameter the test aims to provide. This discussion confirms the difficulties of dealing with a complex boundary problem in purely empirical fashion. Further research is necessary to quantify L/D effects, and an extension of the analysis developed by Yu (1990) for the cone-pressuremeter test in cohesionless material may provide the answer to this problem.

REFERENCES

Al-Hussaini, M. (1980) - Comparison of various methods for determining K_o. *Proc. Symp. of Laboratory Shear Strength of Soil.* ASTM, University of Florida, 78-93.

Al-Hussaini, M. and Townsend, F.C. (1975) - Stress deformation of sand under K_o conditions. *Proc. 5th Panamerican Conf. on Soil Mech. and Fdn Engng,* Vol. 1, Buenos Aires, Argentina, 129-136.

Arthur, J.R.F. and Dunstan, T. (1988) - The engineering application of direct shear testing. Sixth Géotechnique Symp. in Print, *Géotechnique,* Vol. 38, No.1, 139-154.

American Society for Testing Materials (1982) - Designation D2049-69. Standard method of test for relative density of cohesionless soil. *ASTM,* Philadelphia.

Baguelin, F., Jézéquel, J.F., Le Mee, H. and Le Mehaute, A. (1972) - Expansion of Cylindrical probes in cohesive soils. *Jour. of Soil Mech. Fdn Div.,* ASCE, Vol. 98, SM11, 1129-1142.

Baguelin, F., Jézéquel, J.F. and Shields, D.H. (1978) - The pressuremeter and foundation engineering. *Trans. Tech. Publications,* Clausthall.

Baguelin, F. and Jézéquel, J.F. (1986) - The LPC pressiopenetrometer. Proc. *Symp. on Offshore Engng Practice,* 203-219.

Baldi, G., Bellotti, R., Ghionna, N., Jamiolkowski, M. and Pasqualini, E. (1982) - Design parameters for sands from CPT. *Proc. 2nd European Symp. Penetration Testing,* Amsterdam, Vol. 2, 425-432.

Baldi, G., Bellotti, R., Ghionna, N., Jamiolkowski, M. and Pasqualini, E. (1986) - Interpretation of CPT's and CPTU's, 2nd Part: Drained Penetration of sands. *Proc. 4th Int. Geotech. Seminar,* Singapore.

Baligh, M.M. (1985) - Strain path method. *Jour. Geotech. Engng Div.,* ASCE, Vol. 111, 1108-1136.

Baligh, M.M. (1986) - Undrained deep penetration, I: Shear stresses. *Géotechnique,* Vol. 36, No.4, 471-485.

Battaglio, M., Bellotti, R. and Pasqualini, E. (1979) - La deposizione pluviali come mezzo per la preparazione di provini di sabbia. *Revista Italiana di Geotecnica,* Anno XIII, No. 2.

Been, K. and Jefferies, M.G. (1985) - A state parameter for sands. *Géotechnique,* Vol. 35, No. 2, 99-112.

Been, K., Crooks, J.H.A., Becker, D.A. and Jefferies, M.G. (1986) - The cone penetration test in sands, Part 1: State parameter and interpretation. *Géotechnique,* Vol. 36, No.2, 239-249.

Been, K., Jefferies, M.G., Crooks, J.H.A. and Rothenburg, L. (1987) - The cone penetration test in sands, Part 2: General influence of state. *Géotechnique,* Vol. 37, No.3, 285-299.

Been, K., Horsfield, D. and Jefferies, M.G. (1989) - Discussion paper - Calibration tests of a cone penetrometer in sand. *Géotechnique,* Vol. 39, No. 4, 727-731.

Bellotti, R. (1984) - Chamber size effects and boundary conditions effects. *Seminar of Cone Penetration Testing in the Laboratory*. University of Southampton.

Bellotti, R., Bizzi, G. and Ghionna, V. (1982) - Design, construction and use of a calibration chamber. *Proc. 2nd European Symp. Penetration Testing,* Amsterdam, Vol. 2, 439-446.

Bellotti, R., Ghionna, V., Jamiolkowski, M., Lancellotta, R. and Manfredini, G. (1986) - Deformation characteristics of cohesionless soils from *in situ* tests. *In situ' 86. Spec. Conf. In Situ,* ASCE, Virginia Tech., Blackburg.

Bellotti, R., Crippa, V., Pedroni, S. and Ghionna, V.N. (1988) - Saturation of sand specimen for calibration chamber tests. *Proc. First Int. Symp. on Penetration Testing,* ISOP-1, Orlando, Vol. 2, 661-672.

Bellotti, R., Ghionna, V., Jamiolkowski, M., Robertson, P.K. and Peterson, R.W. (1989) - Interpretation of moduli from self-boring pressuremeter tests in sand. *Géotechnique,* Vol. 39, No. 2, 269-292.

Bhudu, M. (1979) - Simple shear deformation of sands. *Ph.D. Thesis,* University of Cambridge.

Bishop, A.W. (1971) - Shear strength parameters for undisturbed and remolded soil specimens. *Proc. Roscoe Memorial Symposium,* Ed. R.H.G. Parry, Foulis, 3-58.

Bishop, A.W. and Henkel, D.J. (1957) - The measurement of soil properties in the triaxial test. *Edward Arnold Ltd.,* London.

Bolton, M.D. (1986) - The strength and dilatancy of sands. *Géotechnique,* Vol. 36, No. 1, 65-78.

Bolton, M.D. (1987) - Discussion paper: The strength and dilatancy of sands. *Géotechnique,* Vol. 37, No.2, 219-226.

Briaud, J.L., Tucker, L.M. and Makarim, C.A. (1986) - Pressuremeter standards and pressuremeter parameters. *Proc. 2nd Symp. on Pressuremeter and its Marine Applications*. ASTM SPT 950, 303-323.

Bruzzi, D., Ghionna, V.N., Jamiolkowski, M., Lancellotta, R. and Manfredini, G. (1986) - Self-boring pressuremeter in Po River sand. *Proc. 2nd Symp. on Pressuremeter and its Marine Applications*. ASTM SPT 950, 57-73.

Burd, H.J. (1986) - A large displacement finite element analysis of a reinforced unpaved road. *D.Phil. Thesis,* Oxford University.

Campanella, R.G., Howie, J.A., Sully, J.P., Hers, I. and Robertson, P.K. (1990) - Evaluation of cone pressuremeter tests in soft cohesive soils. *Proc. of the Third Int. Symp. on Pressuremeters,* British Geotechnical Society, Oxford, 125-136.

Chapman, G.A. (1974) - A calibration chamber for field test equipment. *Proc. European Symp. Penetration Testing,* Stockholm, Vol. 2.2, 59-65.

Clarke, B.G. (1981) - In situ testing of Clays using the Cambridge Self-Boring Pressuremeter. *Ph.D. Thesis,* University of Cambridge.

Clarke, B.G., Carter, J.P. and Wroth, C.P. (1979) - *In situ* determination of the consolidation characteristics of saturated clays. *Proc. 7th European Conf. on Soil Mech. and Fdn Engng,* Brigton, Vol. 2, 207-211.

Clough, G.H., Briaud, J.L. and Hughes, J.M.O. (1990) - The development of pressuremeter testing. *Proc. of the Third Int. Symp. on Pressuremeters,* British Geotechnical Society, Oxford, 25-46.

Cole, E.R.L. (1967) - The behaviour of soils in the simple shear apparatus. *Ph.D. Thesis,* University of Cambridge.

Duncan, J.M. and Chang, C.Y. (1970) - Non-linear analysis of stress-strain in soils. *Jour. Soil Mech. Fdn Engng Div.,* ASCE, Vol. 96, No. SM5., 1629-1654.

De Beer, E.E. (1965) - Influence of mean normal stress on the shear strength of sands. *Proc. 6th Int. Conf. on Soil Mech. and Fdn Engng,* Montreal.

De Beer, E.E. (1974) - Interpretation of the results of static penetration tests. *Proc. European Symp. Penetration Testing,* Stockholm, Vol. 2.1.

De Beer, E.E., Goelen, E., Heynen, W.J. and Joustra, K. (1988) - Cone penetration test (CPT): International reference test procedure. *Proc. First Int. Symp. on Penetration Testing,* ISOP-1, Orlando, 27-52.

Dobry, R., Powell, D.J., Yokel, F.Y. and Ladd, R.S. (1980) - Liquefaction potential of saturated sand - the stiffness method. *Proc. 7th Wld. Conf. Earthquake Engng,* Instanbul, Vol. 3, 25-32.

Durgunoglu, H.T. and Mitchell, J.K. (1975) - Static penetration resistance of soils. *ASCE Specialty Conf. on In Situ Measurement of Soil Properties,* Vol. 1., 151-189.

Eden, W.J. and Law, K.J. (1986) - Comparison of undrained shear strength results obtained by different test methods in soft clays. *Canadian Geotech. Jour.,* Vol. 17, 369-382.

Fahey, M. (1980) - A study of the pressuremeter test in dense sand. *Ph.D. Thesis,* University of Cambridge.

Fahey, M. and Randolph, M.F. (1984) - Effect of disturbance on parameters derived from self-boring pressuremeter tests in sand. *Géotechnique,* Vol. 34, No. 1, 81-97.

Fahey, M. and Jewell, R.J. (1990) - Effect of pressuremeter compliance on measurement of shear modulus. *Proc. of the Third Int. Symp. on Pressuremeters,* British Geotechnical Society, Oxford, 115-124.

Frank, R. (1985) - Recent developments in the prediction of pile behaviour from pressuremeter results. *Symp. From Theory to Practice on Deep Foundations*. Porto Alegre, RS, Brazil, Vol. 2, 69-100.

Ghionna, V.N., Jamiolkowski, M., Lancellotta, R., Tordella, M.L. and Ladd, C.C. (1981) - Performance of self-boring pressuremeter tests in cohesive deposits. *M.I.T. Report,* Cambridge, Mass.

Ghionna, V.N., Jamiolkowski, M., Lancellotta, R. and Manassero, M. (1989) - Limit pressure of pressuremeter tests. *Proc. 12th Int. Conf. on Soil Mech. and Fdn Engng,* Rio de Janeiro, Vol. 1, 223-226.

Ghionna, V.N., Jamiolkowski, M. and Manassero, M. (1990) - Limit pressure in expansion of cylindrical cavity in sand. *Proc. of the Third Int. Symp. on Pressuremeters,* British Geotechnical Society, Oxford, 149-158.

Gibson, R.E. and Anderson, W.F. (1961) - *In situ* measurement of soil properties with the pressuremeter. *Civ. Engng and Public Works Review,* Vol. 56, 615-618.

Green, G.E. (1971) - Small scale laboratory measurement of stress-strain parameters. *Proc. Roscoe Memorial Symposium,* Ed. R.H.G. Parry, Foulis, 285-323.

Green, G.E. and Bishop, A.W. (1969) - A note on the drained strength of sand under generalised strain conditions. *Géotechnique,* Vol.19, 144-149.

Hardin B.O. and Drnevich, V.P. (1972) - Shear modulus and damping in soils: design equations and curves. *Jour. Soil Mech. Div.,* ASCE, Vol. 98, No. SM7, 667-692.

Head, K.H. (1986) - Manual of soil laboratory testing. *ELE International Ltd.,* Pentech Press, London.

Henderson, G., Smith, P.D.K. and St. John, H.D. (1979) - The development of the push-in pressuremeter for offshore site investigation. *Proc. Conf. on Offshore Site Investigation,* Society for Underwater Technology, London, 159-167.

Holden, J.C. (1971) - Laboratory research on static cone penetrometers. *Report No. CE-SM-71-1,* Dept. of Civil Engng, University of Florida.

Houlsby, G.T (1988) - Introduction to papers - Session 3. Piezocone penetration test. *Proc. Penetration Testing in the UK,* Institution of Civil Engineers, Birmingham, 141-146.

Houlsby, G.T (1988) - Methods of interpretation of *in situ* tests. *Modern in situ testing of soil,* Lecture 2, Course at Oxford University.

Houlsby, G.T., Clarke, B.G. and Wroth, C.P. (1986) - Analysis of the unloading of a pressuremeter in sand. *Proc. 2nd Symp. on Pressuremeter and its Marine Applications.* ASTM SPT 950, 245-262.

Houlsby, G.T. and Hitchman, R.C. (1988) - Calibration tests of a cone penetrometer in sand. *Géotechnique,* Vol. 38, No. 1, 39-44.

Houlsby, G.T. and Withers, N.J. (1988) - Analysis of the cone pressuremeter test in clay. *Géotechnique,* Vol. 38, No. 4, 575-587.

Houlsby, G.T. and Hitchman, R.C. (1989) - Replay to Discussion - Calibration tests of a cone penetrometer in sand. *Géotechnique,* Vol. 39, No. 4, 727-731.

Houlsby, G.T. and Carter, J.P. (1990) - The effects of pressuremeter geometry on the results of tests in clay. *Submitted to Géotechnique.*

Houlsby, G.T. and Yu, H.S. (1990) - Finite element analysis of the cone-pressuremeter test. *Proc. of the Third Int. Symp. on Pressuremeters,* British Geotechnical Society, Oxford, 221-230.

Hughes, J.M.O. (1982) - Interpretation of pressuremeter tests for the determination of elastic shear modulus. *Proc. Engng Fdn Conf. Updating Subsurface Sampling of Soils and Rocks and their In Situ Testing.* Santa Barbara, 279-289.

Hughes, J.M.O., Wroth C.P. and Windle, D. (1977) - Pressuremeter tests in sands. *Géotechnique*, Vol. 27, No. 4, 455-477.

Hughes, J.M.O. and Robertson, P.K. (1985) - Full displacement pressuremeter testing in sand. *Canadian Geotech. Jour.*, No. 22, 298-307.

Huntsman, S.R. (1985) - Determination of *in situ* lateral pressure of cohesionless soils by static cone penetrometer. *Ph.D. Thesis*. University of California, Berkeley.

Huntsman, S.R., Mitchell, J.K., Klejbuk, L.W. and Shinde, S.B. (1986) - Lateral stress measurement during cone penetration. *In situ' 86. Spec. Conf. In Situ.* ASCE, Virginia Tech., Blackburg, 618-634.

Iwasaki, T., Tatsuoka, F. and Yoshikau, T. (1978) - Shear moduli of sands under cyclic torsional shear loading. *Soils and Foundation*, Vol. 18, No. 1, 40-56.

Jáky, J. (1944) - The coefficient of earth pressure at rest. *Jour. of Soc. of Hungarian Architects and Engineers*, Budapest, Hungary, 355-358.

Jamiolkowski, M., Ladd, C.C., Germaine, J.T. and Lancellotta, R. (1985) - New developments in field and laboratory testing of soils. *Proc. 11th Int. Conf. on Soil Mech. and Fdn Engng*, San Francisco, Vol. 1, 57-154.

Jamiolkowski, M. and Robertson, P.K. (1988) - Closing address: Future trends for penetration testing. *Proc. Penetration Testing in the UK*, Institution of Civil Engineers, Birmingham, 321-342.

Jamiolkowski, M., Ghionna, V.N., Lancellotta, R. and Pasqualini, E. (1988) - New correlations of penetration tests for design practice. *Proc. First Int. Symp. on Penetration Testing*, ISOP-1, Orlando, Vol. 1, 263-296.

Janbu, N. (1963) - Soil compressibility as determined by oedometer and triaxial tests. *European Conf. on Soil Mech. and Fdn Engng*, Neisbaden, Germany, Vol 1.

Janbu, N. and Senneset, K. (1974) - Effective stress interpretation on *in situ* static penetrometer tests. *Proc. European Symp. Penetration Testing*, Stockholm, Vol. 2.1.

Jefferies, N.G. and Jonsson, L. (1987) - The cone penetration test in sands - Part 3: Horizontal geostatic stress measurements during cone penetration. *Géotechnique,* Vol. 37, No. 4, 483-498.

Jewell, R.A. (1980) - Some effects of reinforcement on the mechanical behaviour of soils. *Ph.D. Thesis,* University of Cambridge.

Kolbuszewski, J.J. (1948) - An experimental study of the maximum and minimum porosities of sands. *Proc. 2dn Int. Conf. on Soil Mech. and Fdn Engng,* 158-165.

Kolbuszewski, J.J. and Jones, R.H. (1961) - The preparation of sand samples for laboratory testing. *Proc. Midland Soil Mech. and Fdn Engng Soc.,* Vol.4, 108-123.

Kondner, R.L. (1963) - Hyperbolic stress-strain response: cohesive soils. *Jour. Soil Mech. Fdn Div.,* ASCE, Vol. 89, No. SM1., 115-144.

Lacasse, S., D'orazio, T.B. and Bandis, C. (1990) - Interpretation of self-boring and push-in pressuremeter tests. *Proc. of the Third Int. Symp. on Pressuremeters,* British Geotechnical Society, Oxford, 273-285.

Ladanyi, B. (1963) - Evaluation of pressuremeter tests in granular soils. *Proc. 2dn Panamerican Conf. on Soil Mech. and Fdn Engng,* Vol. 1, 3-20.

Ladanyi, B. (1972) - *In situ* determination of undrained stress-strain behaviour of sensitive clays with the pressuremeter. *Canadian Geotech. Jour.,* Vol. 9, No. 3, 313-319.

Lade, P.V. and Duncan, J.M. (1975) - Elastoplastic stress-strain theory for cohesionless soil. *Jour. Geotech. Engng Div.,* ASCE, Vol. 101, No. GT10, 1037-1054.

Laier, J.E. - Effects of pressuremeter probe length/diameter ratio and borehole disturbance on pressuremeter test results in dry sand. *Ph.D. Thesis,* University of Florida.

Laier, J.E., Schmertmann, J.H. and Schaub, J.H. (1975) - Effect of finite pressuremeter length in dry sand. *Proc. Conf. In Situ Measurement of Soil Properties.* ASCE, Raleigh, North Caroline, 241-259.

Lancellotta, R. (1983) - Analisi di affidabilita in ingegneria geotecnica. *Atti Insituto Scienza Costruzioni,* No. 625, Politecnico di Torino.

Lancellotta, R. (1990) - General Report. Session II: Analysis and Interpretation. *Proc. of the Third Int. Symp. on Pressuremeters,* British Geotechnical Society, Oxford.

Last, N.C. (1982) - The cone penetration test in granular materials. *Ph.D. Thesis,* University of London.

Last, N.C., Butterfield, R. and Harkness, R.M. (1987) - An investigation of full scale penetrometers in a large triaxial calibration chamber. *Internal report, University of Southampton.*

Lee, K.L. and Seed, H.B. (1967) - Drained strength characteristics of sands. *Jour. of the Soil Mech. Fdn Div.,* ASCE, Vol. 93, No. SM6, 117-141.

Lo Presti, D. (1987) - Mechanical behaviour of Ticino sand from resonant column tests. *Ph.D. Thesis,* Politechnico di Torino.

Lunne, T. and Christoffersen, H.P. (1983) - Interpretation of cone penetrometer data for offshore sands. *Offshore Technology Conf.,* 181-192.

Mair R.J. and Wood, D.M. (1987) - Pressuremeter testing - Methods and interpretation. *CIRIA Ground Engineering Report: In Situ Testing.* Butterworths, London.

Marchetti, S. (1985) - On the field determination of K_o in sand. Panel discussion Session 2A, *Proc. 11th Int. Conf. on Soil Mech. and Fdn Engng,* San Francisco.

Marsland, A. and Randolph, M.F. (1977) - Comparisons of the results from pressuremeter tests and large *in situ* plate tests in London clay. *Géotechnique,* Vol. 27, No. 2, 217-243.

Matsuoka, H. (1976) - On the significance of the spatial mobilised plane. *Soils and Foundations,* Vol. 16, No. 1, 91-100.

Mayne, P.W. and Kulhawy, F.H. (1982) - K_o-OCR relationships in soil. *Jour. of the Geotech. Engng Div.,* ASCE, Vol. 108, GT6, 851-872.

Meyerhof G.G. (1974) - Penetration testing outside Europe. *Proc. European Symp. Penetration Testing,* Stockholm, Vol. 2.1.

Miura, S. and Toki, S. (1983) - A sample preparation method and its effects on static and cyclic deformation-strength properties of sand. *Soils and Foundations,* Vol. 22, No. 1, 61-77.

Oda, M., Moishikawa, I. and Higuchi, T. (1978) - Experimental study of anisotropic shear strength of sand by plane strain test. *Soils and Foundations,* Vol. 18, No. 1, 25-38.

Palmeira, E.M. (1987) - A study of soil-reinforcement interaction by means of large scale laboratory tests. *D.Phil. Thesis,* University of Oxford.

Palmer, A.C. (1972) - Undrained plane-strain expansion of a cylindrical cavity in clay. *Proc. Roscoe Memorial Symp.,* Ed. R.H.G. Parry, Foulis, 588-599.

Parkin, A.K. (1988) - The calibration of cone penetrometers. *Proc. First Int. Symp. on Penetration Testing,* ISOP-1, Orlando, Vol. 1, 221-244.

Parkin, A.K. and Lunne, T. (1982) - Boundary effects in the laboratory calibration of a cone penetrometer for sand. *Proc. 2nd European Symp. Penetration Testing,* Amsterdam, Vol. 2, 761-768.

Pedley, M.J. (1990) - A study of soil reinforcement interaction. *D.Phil. Thesis,* University of Oxford. In preparation.

Powell, J.J.M. (1990) - A comparison of four different pressuremeters and their methods of interpretation in a stiff heavily overconsolidated clay. *Proc. of the Third Int. Symp. on Pressuremeters,* British Geotechnical Society, Oxford, 287-298.

Powell, J.J.M. and Uglow, I.M. (1985) - A comparison of Ménard, self-boring pressuremeter and push-in pressuremeter tests in a stiff clay till. *Proc. Conf. on Advances in Underwater Technology and Offshore Engng,* London, Vol. 3, Offshore Site Investigation, 201-217.

Rad, N.S. and Tumay, M.T. (1987) - Factors affecting sand specimen preparation by raining. *Geotech. Testing Jour.,* Vol. 10, No. 1, 31-37.

Randolph, M.F., Carter, J.P. and Wroth C.P. (1979) - Driven piles in clay - the effects of installation and subsequent consolidation. *Géotechnique,* Vol. 29, No. 4, 361-393.

Reid, W.M., St. John, H.D., Fyffe, S. and Rigden W.J. (1982) - The push-in pressuremeter. Proc. Symp. on The Pressuremeter and its Marine Applications, *Institut du Petrole, Laboratoires des Ponts et Chaussées,* Paris, Editions Technip, Collection Colloques et Seminaires 37, 247-261.

Robertson, P.K. (1982) - *In situ* testing of soil with emphasis on its application to liquefaction assessment. *Ph.D. Thesis,* University of British Columbia.

Robertson, P.K. and Campanella, R.G. (1983) - Interpretation of cone penetration tests, Part 1: sand. *Canadian Geotech. Jour.,* Vol. 20, No. 4, 718-733.

Robertson, P.K., Hughes, J.M.O., Campanella, R.G. and Sy, A. (1983) - Design of laterally loaded displacement piles using driven pressuremeter. *Proc. Int. Symp. Design and Performance of Laterally Loaded Piles and Pile Groups.* Special Technical Publication 835, New York, ASCE.

Robertson, P.K. and Hughes J.M.O. (1986) - Determination of properties of sand from self-boring pressuremeter tests. *Proc. 2nd Symp. on Pressuremeter and its Marine Applications.* ASTM SPT 950, 283-302.

Robertson, P.K., Hughes, J.M.O., Campanella, R.G., Brown, P. and McKeown, S. (1986) - Design of laterally loaded piles using the pressuremeter. *Proc. 2dn Int. Symp. The Pressuremeter and its Marine Applications.* ASTM SPT 950, 443-457.

Roscoe, K.H., Schofield, A.N. and Wroth, C.P. (1958) - On the yielding of soils. *Géotechnique,* Vol. 8, 22-53.

Rowe, P.W. (1962) - The stress-dilatancy relation for static equilibrium of an assembly of particles in contact. *Proc. Royal Soc.,* A 269, 500-527.

Schmertmann, J. (1976) - An updated correlation between relative density, Dr, and Fugro-type electric cone bearing, q_c. *Waterways Experimental Station,* Contract Report DACW 39-76M6646.

Schmertmann, J. (1978) - Guidelines for cone penetration test performance and design. Report No. FHWA-TS-78-209, U.S., *Department of Transportation, Federal Highway Administration,* Washington, D.C.

Schmidt, B. (1966) - Discussion paper - Earth pressures at rest related to stress history. *Canadian Geotech. Jour.,* Vol. 3, No. 4, 239-242.

Schnaid, F. (1988) - A calibration chamber at Oxford University for testing granular materials. *Proc. Seminar on Calibration of In Situ Tests in Laboratory and Field,* Session 2, Oslo.

Schnaid, F. and Houlsby, G.T. (1990) - Calibration chamber tests of the cone-pressuremeter in sand. *Proc. of the Third Int. Symp. on Pressuremeters,* British Geotechnical Society, Oxford, 263-272.

Schofield, A.N. and Wroth, C.P. (1968) - Critical state soil mechanics. *McGraw Hill,* London.

Seed, H.B., Wong, R.T., Idriss, I.M. and Tokimatsu, K. (1986) - Moduli and damping factors for dynamic analyses of cohesionless soils. *Jour. of Geotch. Engng,* ASCE, Vol. 12, No. GT11., 1016-1032.

Senneset, K., Janbu, N. and Svano, G. (1982) - Strength and deformation parameters from cone penetrometer tests. *Proc. 2nd European Symp. Penetration Testing,* Amsterdam, Vol. 2., 863-870.

Sherif, M.A., Ishibashi, I. and Ryden, D.E. (1974) - Coefficient of lateral earth pressure at rest in cohesionless soils. *Soil Engng Research Report No. 10, University of Washington,* Wash..

Sladen, J.A., D'Hollander, R.D.D. and Krahn, J. (1985) - The liquefaction of sands, a collapse surface approach. *Canadian Geotech. Jour.,* Vol. 22, No. 4, 564-578.

Stroud, M.A. (1971) - Sand at low stress levels in the simple shear apparatus. *Ph.D. Thesis,* University of Cambridge.

Teh, C.I. (1987) - An analytical study of the cone penetration test. *D.Phil. Thesis,* University of Oxford.

Teh, C.I. and Houlsby, G.T. (1988) - Analysis of the cone penetration test by the stress path method. *Proc. 6th Int. Conf. Num. and Analy. Meth. in Geomech.,* Innsbruck, Vol. 1, 397- 402.

Terzaghi, K. (1943) - Theoretical Soil Mechanics. *Wiley,* New York.

Veismanis, A. (1974) - Laboratory investigation of electrical friction cone penetrometers in sands. *Proc. European Symp. Penetration Testing,* Stockholm, Vol. 2.2, 407-419.

Vesic, A.S. (1963) - Bearing capacity of deep foundations in sand. *Highway Research Board Record No.39,* 112-153.

Vesic, A.S. (1972) - Expansion of cavities in infinite soil mass. *Jour. of Soil Mech. Fdn Div.,* ASCE, Vol. 98, SM3, 265-290.

Vesic, A.S. (1977) - Design of pile foundations. National co-operative highway research programme. *Synthesis of Highway Practice No. 42,* National Research Council, Washington D.C..

Vesic, A.S. and Clough, G.W. (1968) - Behaviour of granular materials under high stresses. *Jour. Soil Mech. Fdn Div.,* ASCE, Vol. 94, No. SM3, 661-688.

Villet, W.C.B. and Mitchell, J.K. (1981) - Cone resistance, relative density and friction angle. Cone penetration testing and experience. *Proc. ASCE National Convention,* St. Louis, 178-208.

Windle, D. (1976) - *In situ* testing of soils with a self-boring pressuremeter. *Ph.D. Thesis,* University of Cambridge.

Withers, N.J., Schaap, L.H.J. and Dalton, C.P. (1986) - The development of a full displacement pressuremeter. *Proc. Symp. on Pressuremeter and its Marine Applications*. ASTM SPT 950, 38-56.

Withers, N.J., Howie, J., Hughes, J.M.O. and Robertson, P.K. (1989) - Performance and analysis of cone pressuremeter tests in sands. *Géotechnique,* Vol. 39. No. 3, 433-454.